Manganese Homeostasis in Bacterial-Host Interactions

By

Lillian Johnson Juttukonda

Dissertation
Submitted to the Faculty of the
Graduate School of Vanderbilt University
in partial fulfillment of the requirements
for the degree of

DOCTOR OF PHILOSOPHY
in

Microbiology and Immunology
August 31, 2017
Nashville, Tennessee

Approved:

David M. Aronoff, M.D.
Aaron B. Bowman, Ph.D.
Maria Hadjifrangiskou, Ph.D.
Richard M. Peek, Jr, M.D.
Eric P. Skaar, Ph.D.

ACKNOWLEDGEMENTS

I would like to thank my thesis advisor, Eric Skaar, for his support over the past four years. Eric, I know that I have been intense at times and silly at others, and I appreciate you taking my concerns seriously and patiently answering question after question. Thank you for being an amazing role model, both as a person and as a scientist. Thank you for allowing me to pursue projects in directions that interested me, and thank you for your many ideas. Thank you for trusting me to do expensive experiments, and for understanding when I made expensive mistakes. Thank you for helping me to become a better writer, speaker, scientist, and critical thinker. The last four years have been a blast.

To all the members of the Skaar laboratory over the past four years, I heartily thank you. You are incredibly supportive, challenging, helpful, and fun colleagues, and I am grateful to call you friends. Every member of the laboratory has intellectually contributed to my dissertation research and helped by thoughtfully proof-reading my manuscripts and grant submissions. Specifically, thank you to Julie Lemen and Nichole Lobdell for keeping the laboratory running and helping me to obtain supplies for experiments. Thank you to Billy Burns, Ashley Jordan, Nikesh Dahal, Nichole Maloney, Audra Fullen, and Jocelyn Simpson for preparing media for me and helping me when I needed an extra pair of hands. I thank my post-doctoral bay-mates Mike Noto, Neal Hammer, and Will Beavers for being patient with me, listening to me every day, and setting excellent examples of efficiency and curiosity in the lab. Jacob Choby, Cathy Wakeman, Lisa Lojek and Joe Zackular: thank you for helping me out by checking my mice, streaking strains and other miscellaneous items, especially during my travel. To team *Acinetobacter*: Brittany Nairn nee Mortensen,

Lauren Palmer, and Zach Lonergan: I couldn't have done much of the work in my dissertation without your experimental and intellectual contributions. Finally, I am grateful to new Skaar lab members Jessica Sheldon, Erin Green and Andrew Monteith for continuing the studies that I have not completed.

I have been blessed with incredible collaborators. Walter Chazin and Ben Gilston provided recombinant calprotectin for multiple projects. Zach Lonergan performed the hydrogen peroxide imaging experiments. Many individuals contributed to the project presented in Chapter IV. Joe Zackular performed microbiota analyses and *Clostridium difficile* infections. Jessica Moore cryosectioned samples for imaging mass spectrometry and performed MALDI-IMS. Yaofang Zhang performed LA-ICP-MS. Chris Wijers and Will Beavers were helpful with growth assays and western blot analyses. Jonathan Schmitz provided staphylococcal endocarditis isolates. Jim Atkinson and Kay Washington analyzed pathology in histologic sections. Evelien Berends and Victor Torres performed neutrophil killing assays. Matthew Stier and Stokes Peebles were immensely helpful in performing and interpreting the bone marrow chimera experiments in Chapter V. Margaret Allaman and staff at the Flow Cytometry Shared Resource provided technical assistance for the immunology assays in Chapter V. I thank Aaron Bowman and his graduate student Kyle Horning for initiating the studies on small molecule VU0026921 and appreciate their insightful comments as this project as progressed. Daisy Unsihuay, an undergraduate summer student in the Skaar laboratory, was very helpful with the VU0026921 project. Maria Hadjifrangiskou and Allison Eberly, Kirsten Guckes and Kyle Floyd in her laboratory dedicated significant time to our attempt to establish a urinary tract infection model for *A. baumannii.* Henry Ong spent many hours collecting head MRIs on *S. aureus*-

infected mice. Many individuals in the Skaar laboratory helped me with large animal experiments, including Brittany Nairn, Cathy Wakeman, Neal Hammer, Eric Skaar, Jake Choby, Joe Zackular, Mike Noto, and Lauren Palmer.

I thank the Vanderbilt Medical Scientist Training Program for its support over the past six years. Former Director Terry Dermody and current Director Chris Williams have been important mentors to me, and I am grateful for the opportunities they have given me within the MSTP. I am grateful to Melissa Krasnove for her administrative support – whenever a situation gets really confusing and I don't know how to handle it, Melissa always seems to find a way to make everything work out.

I also thank my Ph.D. Thesis Committee, including Committee Chair David Aronoff, Aaron Bowman, Maria Hadjifrangiskou, and Richard Peek. You have been incredibly supportive and encouraging to me. I thank you for your challenging questions during my committee meetings and the interest you have taken in my projects, and I particularly appreciate the time you have taken to meet with me one-on-one over the past few years.

I also am grateful for the financial support that made these studies possible. The research reported in this dissertation were supported by grants award to Eric Skaar, including Public Health Service Grants AI101171, AI107233, AI069233, and AI073843, Veterans Affairs grant INFB-024-13F, Vanderbilt Digestive Disease Research Center (VDDRC) (grant no. P30DK058404), and the Defense Advanced Research Projects Agency (DARPA). Experiments reported in Chapter IV were supported by Public Health Service Grant 6P41 GM103391-06 awarded to Richard Caprioli. L.J.J. was supported by American Heart Association Grant 15PRE25060007 and Public Health Service award T32

GM07347 from the National Institute of General Medical Studies for the Vanderbilt Medical-Scientist Training Program.

Finally, I thank my friends and family for supporting me during my Ph.D. studies. You mean the world to me, and I owe everything to you.

TABLE OF CONTENTS

LIST OF TABLES

LIST OF FIGURES

CHAPTER I

INTRODUCTION

Bacterial infections are a significant cause of morbidity and mortality worldwide, but sepsis, pneumonia, meningitis and endocarditis are no longer the death sentences they were at the turn of the 20th century (Aminov, 2010). Effective vaccine and the discovery of antibiotics have made it possible to prevent or cure acute bacterial infections (Aminov, 2010). Unfortunately, antibiotic resistance has emerged amongst many common pathogens amidst a decades-long drought in antibiotic development (Luepke et al., 2017). Because of these confluence of factors, management, containment, and therapeutic development for antibiotic resistant bacterial pathogens has been named a priority by numerous public health organizations. This Dissertation focuses on understanding the mechanisms driving the pathogenesis of infections caused by two organisms that have been highlighted as particular threats, namely *Acinetobacter baumannii* and *Staphylococcus aureus*. Both *A. baumannii* and *S. aureus* have been labeled ESKAPE pathogens (*Enterococcus faecium, S. aureus, Klebsiella pneumoniae, Acinetobacter, Pseudomonas aeruginosa,* and *Enterobacter*) by the Infectious Diseases Society of America, listed as 'serious threats' by the Centers for Disease Control, and more recently highlighted by the World Health Organization (Boucher et al., 2009; CDC, 2013; WHO, 2017).

A. baumannii is a Gram-negative opportunistic pathogen that most commonly infects the respiratory tract and the bloodstream (Dijkshoorn et al., 2007). Carbapenem-resistant *A. baumannii* was categorized by the World Health Organization (WHO) in

February, 2017 as the top 'critical' priority for research and discovery of new antibiotics (WHO, 2017). While *A. baumannii* mechanisms of drug resistance have been studied extensively, understanding of the pathogenesis of infections has lagged behind. As of yet, no classical virulence factors have been identified for *A. baumannii* (Antunes et al., 2014). Perhaps even more importantly, the genetic manipulation tools for the study of this organism have also been limited, although recent advances spearheaded by basic scientific research have improved the situation (Gallagher et al., 2015; Kumar et al., 2010; Tucker et al., 2014). Taken together, these facts illustrate the importance of understanding the molecular mechanisms by which *A. baumannii* persists within the host.

S. aureus is a Gram-positive facultative anaerobe that colonizes about one third of adult humans (Wertheim et al., 2005). *S. aureus* has substantial virulence potential when physical barriers are breached and staphylococci gain access to visceral tissues (Tong et al., 2015). Methicillin-resistant *S. aureus* and vancomycin-resistant *S. aureus* were named as a 'high priority' for the development of new antibiotics by the WHO (WHO, 2017). This prioritization underscores the importance of improving understanding of *S. aureus* infections, both to develop new antimicrobial strategies and to decrease the burden of disease.

The research questions outlined in this Dissertation focus on the utilization of nutrient manganese (Mn) by bacterial pathogens during infection, the role of host Mn-binding proteins in defense against infection, and the development of novel therapeutics that target bacterial Mn homeostasis. Chapter I (Introduction) summarizes the known mechanisms of Mn homeostasis in bacteria, the role of Mn in bacterial physiology, and the importance of Mn during infection, together providing the rationale for the studies

described herein. Chapter I also includes a literature review regarding host mechanisms to restrict Mn during infection and outlines areas requiring future research.

In this Dissertation, I address several unanswered questions regarding Mn and bacterial infection. First, no mechanisms for Mn import had been identified in *A. baumannii.* Chapter II defines the Nramp-family transporter MumT as a Mn acquisition system in *A. baumannii* that contributes to infection in the lung. Similarly, the mechanisms regulating Mn import were unknown. Chapters II presents data that the transcriptional regulator MumR activates transcription of Mn import machinery, and Chapter III delineates the role of MumR in hydrogen peroxide stress resistance. Second, the importance of dietary Mn in bacterial infections has not been interrogated. The consequences of excess dietary Mn intake on *S. aureus* infections are addressed in Chapter IV. Data presented in Chapter IV also revealed that the host protein calprotectin promotes *S. aureus* infection of the heart, but the mechanism for this was unknown and is explored in Chapter V. Finally, the question of whether Mn homeostasis can be targeted with a small molecule antibiotic is confronted in Chapter VI. Together, this Thesis establishes a role for Mn during *A. baumannii* infection, defines dietary Mn intake as a critical factor modulating *S. aureus* virulence, and presents a potential therapeutic targeting Mn homeostasis.

A version of the following section (*Chapter I, Manganese homeostasis and utilization in pathogenic bacteria*) was previously published in Molecular Microbiology 97(2), 216-228 (July 2015) | doi:10.1111/mmi.13034

A version of the following section (*Chapter I, Manganese homeostasis and utilization in pathogenic bacteria*) was previously published in Molecular, Genetic, and Nutritional Aspects of Major and Trace Minerals, Edited by James Collins, 377-387 (2016).

Manganese homeostasis and utilization in pathogenic bacteria

Introduction

Transition metals are required for life. Bacteria require transition metals to fulfill specific physiological requirements. Metals stabilize the structure of proteins, nucleic acids, and small molecules, donate and accept electrons in oxidation/reduction chemistry, and form electrostatic interactions during enzymatic catalysis (Hood and Skaar, 2012). Because metal is essential for bacterial survival and replication, bacterial pathogens must acquire metals during infection in order to cause disease (Hood and Skaar, 2012). Vertebrate hosts, including humans, are a reservoir of essential nutrients, as they are required for eukaryotic cell function. To prevent bacterial acquisition of metals during invasive infections, vertebrates have evolved mechanisms to manipulate metal levels as a component of the immune response (Hood and Skaar, 2012). Hosts deplete infection sites of essential metals to 'starve' pathogens, while directing an influx of highly reactive (and therefore highly toxic) metals to the same sites (Hood and Skaar, 2012). Host redirection of essential metals as an antibacterial strategy is known as nutritional immunity (Hood and Skaar, 2012). Nutritional immunity was originally used to describe host restriction of iron. However, it is now known that other metals are also sequestered during infection, including manganese (Mn).

Mn is an essential nutrient for organisms in all domains of life. Mn is a first-row transition metal most commonly in a +2 charge state. Mn has a notable role in oxidative stress resistance. Like iron, Mn is capable of redox cycling; however, Mn is much less susceptible than iron to toxic Fenton chemistry when exposed to hydrogen peroxide

(Aguirre and Culotta, 2012; Lisher and Giedroc, 2013). Therefore, Mn serves as an antioxidant instead of promoting the toxicity of reactive oxygen species (Aguirre and Culotta, 2012).

Mn is a cofactor for many enzymes. In humans, Mn is a required cofactor for superoxide dismutase, pyruvate carboxylase and arginase (Bowman et al., 2011, Horning et al., 2015). Mn also less-specifically activates hydrolases, phosphatases, transferases, dehydrogenases, kinases, peptidases, decarboxylases, and sugar transferases (Aschner and Aschner, 2005). As a result, Mn is important for bone formation, fat and carbohydrate metabolism, and blood sugar regulation (Bowman et al., 2011). In bacteria, Mn can serve as a cofactor for specific superoxide dismutases, ribonucleotide reductases, adhesion proteins, and antibiotic resistance enzymes amongst others (Lin et al., 2011; Papp-Wallace and Maguire, 2006; Thompson et al., 2014). Mn therefore confers activity to several important physiological processes in both the host and microbial invaders. In this section, bacterial mechanisms of Mn homeostasis, the known roles of Mn transport and regulation in pathogenesis, and Mn utilization in oxidative stress responses and DNA synthesis will be introduced (**Figure 1**).

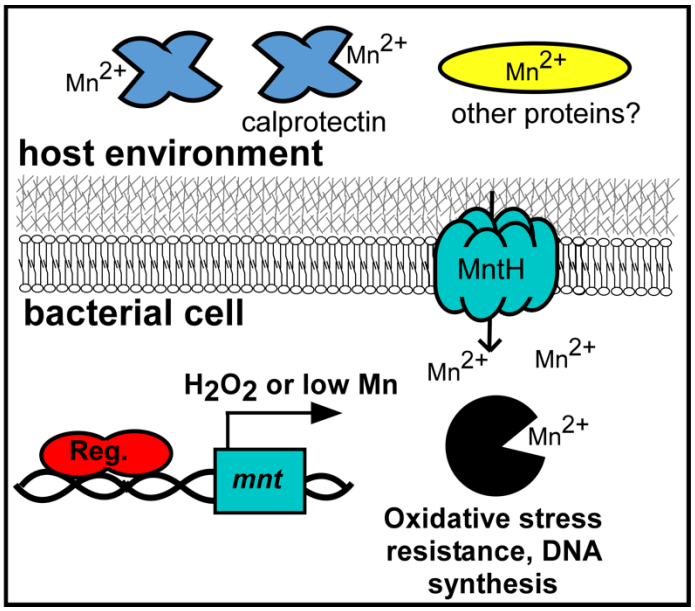

Figure 1: Overview of Mn homeostasis and utilization during infection.
During infection, the host restricts pathogen access to Mn through a variety of mechanisms, including calprotectin-mediated Mn sequestration and Mn-binding by additional proteins/factors that have not yet been identified. The bacterial cell responds to Mn restriction via transcriptional regulators that upregulate Mn import systems. Mn import can also be activated by transcriptional regulators that sense reactive oxygen species such as hydrogen peroxide. Intracellular Mn is utilized by bacteria for processes essential for survival within the host, including oxidative stress resistance and DNA synthesis.

Bacterial Mn importers: acquiring Mn during infection

Vertebrate hosts have multiple strategies that limit the concentration of available manganese for an invading bacterium. In a process termed nutritional immunity, mammalian hosts restrict access of nutrient metals to invading pathogens as a defense mechanism to prevent microbial acquisition of these essential nutrients. Vertebrates restrict Mn from bacteria using several strategies. First, extracellular Mn concentrations are kept low, ranging from < 10 nM in serum (Keen *et al.*, 2000) to ~10 μM in the liver in humans (Rahil-Khazen *et al.*, 2002); similar concentrations are seen in mouse organs (Kehl-Fie *et al.*, 2013). During bacterial infection, liver and kidney Mn levels are further decreased, suggesting the existence of additional global mechanisms that starve microbes during inflammation. Notably, the host proteins responsible for this redistribution of Mn during infection have not been identified (Kehl-Fie *et al.*, 2013, Pompilio *et al.*, 2014). Second, the host possesses mechanisms to restrict Mn within the intracellular phagosomal compartment as well as in the extracellular environment. To combat these host sequestration strategies, bacterial pathogens utilize Mn import systems to successfully compete for Mn in Mn-restricted environments during infection (Diaz-Ochoa *et al.*, 2014) (Porcheron *et al.*, 2013) (Kehl-Fie & Skaar, 2010). The mechanisms for bacterial acquisition of Mn are presented herein.

Bacteria possess high affinity manganese importers that allow them to combat host nutritional immunity. Bacterial manganese importers are essentially ubiquitous as they allow cells to survive in low manganese environments or conditions that require high amounts of manganese, such as oxidative stress (Juttukonda and Skaar, 2015). Because of its ionic nature, manganese cannot pass through membranes via diffusion; instead, a pore

must be formed in the membrane (Ferguson and Deisenhofer, 2004). To import manganese, Gram-positive bacteria must transport this cation across a single lipid bilayer while Gram-negative bacteria must transport the metal across two lipid bilayers. Transport mechanisms across the Gram-negative inner membrane and Gram-positive cytoplasmic membrane are homologous and are generally well understood. Manganese transport mechanisms across the Gram-negative outer membrane are poorly defined. Manganese requirements vary drastically between species. For instance, *Borrelia burgdorferi,* the causative agent of Lyme Disease, has tremendously high requirements for manganese as it uses manganese in the place of iron (Posey and Gherardini, 2000). In contrast, *Escherichia coli* has very low levels of manganese and only expresses a single manganese importer under conditions of oxidative stress (Anjem et al., 2009). In the following sections, competition with the host for Mn will be discussed in two sections: intracellular competition and extracellular competition. In addition to a broad overview as to how bacteria utilize manganese transporters compete with the host for Mn, two pathogens will be discussed in depth: *S. aureus* and *Salmonella enterica* sv. Typhimurium.

Intracellular host-microbe interactions for Mn

Host-mediated restriction: NRAMP

The macrophage phagolysosome is depleted of Mn through the actions of the natural resistance-associated macrophage protein (NRAMP)-family member, NRAMP1. Encoded by *SLC11A1* in humans, NRAMP1 transports Fe, Mn, and Co and depletes the phagolysosome of divalent cations (Forbes & Gros, 2003, Jabado *et al.*, 2000). Furthermore, *SLC11A1* polymorphisms are associated with increased risk of infectious disease in humans, including pulmonary tuberculosis, emphasizing the clinical importance

of NRAMP1 (Blackwell *et al.*, 2003, Li *et al.*, 2011). More detailed information regarding NRAMP1 can be found in the next section of the Introduction.

ii. Bacterial acquisition systems: MntH and ABC-family transporters

Bacterial pathogens have evolved dedicated import machinery that allows them to compete with host NRAMP1 for Mn within the phagosome. For details regarding the biophysical characteristics of the proteins involved in this process, see the review by Lisher and Giedroc (Lisher & Giedroc, 2013). Bacteria encode several broadly conserved classes of importers. One major family of Mn importers is the NRAMP family of metal cation transporters. The NRAMP family of proton-powered Mn importers is conserved across all domains of life and is usually named MntH in bacteria (manganese transporter, H^+-dependent) (Makui *et al.*, 2000, Que & Helmann, 2000). The NRAMP-family of manganese transporters in bacteria is homologous to the SLC11 family of transporters previously discussed in eukaryotes. This family of transporters possesses 10-12 transmembrane domains and utilizes proton gradients to provide the energy needed to transport manganese against a concentration gradient (Ehrnstorfer et al., 2014). Many NRAMP-family transporters in bacteria are somewhat promiscuous, transporting multiple divalent cations with different affinities (Ehrnstorfer et al., 2014). An excellent analysis of the structure and function of the NRAMP family was recently published (Ehrnstorfer *et al.*, 2014). The crystal structure of the *Staphylococcus capitis* NRAMP-family protein, named DMT in this case, was solved as a truncated protein without the first 41-amino acids, and the binding of numerous metals including Mn was evaluated (Ehrnstorfer *et al.*, 2014). The observation that many NRAMP-family proteins transport multiple metals was corroborated by this crystal structure, showing Fe^{2+}, Mn^{2+}, Co^{2+}, and Ni^{2+} coordinated by the same four

residues in a pocket formed by transmembrane helices 1 and 6 (Ehrnstorfer *et al.*, 2014). Zn, Ca, and Mg, which are not known to be transported by NRAMP, either do not bind the same pocket or do not bind at all (Ehrnstorfer *et al.*, 2014). The authors verified DMT-mediated Mn transport by employing a fluorescent dye that is quenched by Mn in a proteoliposome system, with quenching only occurring when the liposome contains the NRAMP protein (Ehrnstorfer *et al.*, 2014). Finally, the authors evaluated the importance of each of the four metal binding residues identified in the crystal structure to Mn binding; introducing single point mutations in the Mn-coordinating site lowers the Mn-binding affinity from 29 μM to 400-929 μM, depending on the mutation (Ehrnstorfer *et al.*, 2014). With the solved crystal structure as a template, site-directed mutagenesis can now be used to query the importance of Mn-binding by NRAMP to the ability of a bacterium to cause disease in the host.

Another major family of Mn import proteins is the ABC-type transport family. The ABC-transport family in bacteria is a broad family of transporters with many different substrates. Typical ABC-transporters consist of a substrate-binding subunit that coordinates Mn on the surface of the cytoplasmic membrane in gram-positives or in the periplasm of gram-negatives, two hydrophobic permease subunits (or one fused subunit) that are embedded within the membrane and facilitate passage of Mn through the lipid bilayer, and a catalytic subunit on the cytoplasmic side of the membrane that hydrolyzes ATP to provide the energy required for transport (Higgins, 1992). Unlike siderophore systems for transport of Fe (Guerinot, 1994) or Zn (Bobrov *et al.*, 2014), no small molecule metal-binding system has been defined as a Mn scavenger. Given the finding that at least one siderophore is able to bind a metal other than Fe (Bobrov *et al.*, 2014), their ability to

scavenge Mn should be assessed. Additionally, only one Mn-specific outer membrane porin in gram-negatives has been identified. This porin was discovered in the non-pathogenic bacterium *Bradyrhizobium japonicum* through a transcriptional screen for genes up-regulated in a Mn-limiting environment that are regulated by the Mn-dependent transcription factor Mur (Hohle *et al.*, 2011). A similar screening approach of identifying mutants that are up-regulated in conditions of Mn limitation may lead to the identification of Mn-specific outer membrane proteins in pathogenic bacteria.

iii. Importance of Mn import during infection by intracellular pathogens

Studies investigating the role of Mn transporters in virulence have been spearheaded by work in obligate or facultative intracellular pathogens. **Figure 2A** depicts the competition for Mn during infection of a phagocytic cell. For a detailed introduction to Mn transport and the original studies into the contribution of Mn importers to the virulence of intracellular pathogens, see previous reviews (Papp-Wallace & Maguire, 2006, Kehres & Maguire, 2003).

S. Typhimurium is a Gram-negative organism that causes food poisoning in humans and a mouse disease that mimics Typhoid fever in humans (House et al., 2001). Typhoid fever is a life-threatening illness caused by systemic spread of *Salmonella* from the gut, causing high fever and abdominal pain (House et al., 2001). To cause Typhoid fever, *Salmonella* subverts the antibacterial functions of macrophages, surviving within the macrophage to be carried from the gut to the liver, spleen, bone marrow, and lymph nodes (House et al., 2001). Therefore, surviving within the macrophage is critical to macrophage pathogenesis. Macrophage NRAMP1 depletes the phagosome of Mn to starve bacteria. In fact, the presence of a functional NRAMP1 is required for mice to survive *S.* Typhimurium

infection (Govoni et al., 1996). *S.* Typhimurium expresses two Mn importers, MntH and SitABCD (Boyer et al., 2002). MntH is an NRAMP-family transporter and SitABCD is an ABC-family Mn transporter, and both of these proteins exhibit higher affinity for Mn than Fe in vitro (Boyer et al., 2002). Confirming their importance in the virulence of *Salmonella,* inactivation of *mntH, sitABCD,* or both decreases virulence of the bacterium in *SLC11A1* congenic mice (Zaharik et al., 2004). However, MntH is not important in mice that lack functional NRAMP1 (Boyer et al., 2002). This establishes that *Salmonella* importers are required to combat nutritional immunity of the macrophage imposed by NRAMP1.

Mn acquisition systems may be nearly universally required for complete fitness of intracellular bacteria in the host. In addition to *Salmonella,* Mn import by MntH-family or ABC-family Mn importers is required for full virulence of *S.* Typhimurium during intraperitoneal murine infection, *Brucella abortus* in mice, *Yersinia pseudotuberculosis* in a *Galleria mellonella* larvae infection, *Yersinia pestis* in murine bubonic plague, and *Shigella flexneri* in macrophages and non-phagocytic cells (Champion *et al.*, 2011, Ouyang *et al.*, 2009, Anderson *et al.*, 2009, Perry *et al.*, 2012, Runyen-Janecky *et al.*, 2006, Fetherston *et al.*, 2012). Furthermore, Mn import by BmtA, a ZIP family homolog and the only known metal transporter in *Borrelia*, is required for virulence of *B. burgdorferi* in ticks (Ouyang *et al.*, 2009). In *Y. pestis* as well as *S.* Typhimurium, multiple import systems must be inactivated to reduce virulence in murine models of infection, which correlates well with *in vitro* evidence suggesting that Mn acquisition systems are functionally redundant in these organisms (Perry *et al.*, 2012, Boyer *et al.*, 2002). Interestingly, *Y. pestis* inactivated for both *feo* and *yfe* is fully virulent in a murine pneumonic plague model, but a 90-fold increase in dose is required to cause mortality in a murine bubonic plague model

(Fetherston *et al.*, 2012, Perry *et al.*, 2012). This suggests that Mn-importers have varying roles in different infection models. This variation could be due to differences in Mn availability or oxidative stress levels throughout the host. In summary, these studies illustrate that some intracellular bacteria require Mn importers to survive in metal-depleted phagosomes, and several of these bacterial species have redundant metal acquisition systems in order to fulfill this Mn requirement.

Extracellular host-microbe interactions for Mn

i. Host-mediated restriction: Calprotectin

Calprotectin is a Mn-chelating protein that contributes to antibacterial host defense (Corbin *et al.*, 2008). Calprotectin (CP) is a protein heterodimer of S100A8 and S100A9, is highly abundant in the cytoplasm of neutrophils, and is expressed by multiple cell types under inflammatory conditions and at sites of infection (Goyette & Geczy, 2011, Moore *et al.*, 2014, Marionnet *et al.*, 2003, Boyd *et al.*, 2008, Uhlen *et al.*, 2015). Calprotectin is antibacterial against a wide range of Gram-positive and Gram-negative bacteria, and this activity is dependent on the ability of calprotectin to chelate Mn and Zn; additionally, this is thought to occur only in the extracellular environment because Ca is required for high-affinity metal chelation (Steinbakk *et al.*, 1990, Lusitani *et al.*, 2003, Corbin *et al.*, 2008, Damo *et al.*, 2013, Brophy *et al.*, 2013). Therefore, metal binding by calprotectin is a mechanism by which the host restricts bacterial access to Mn in the extracellular environment during infection. Calprotectin will be reviewed in detail in the next section of the Introduction.

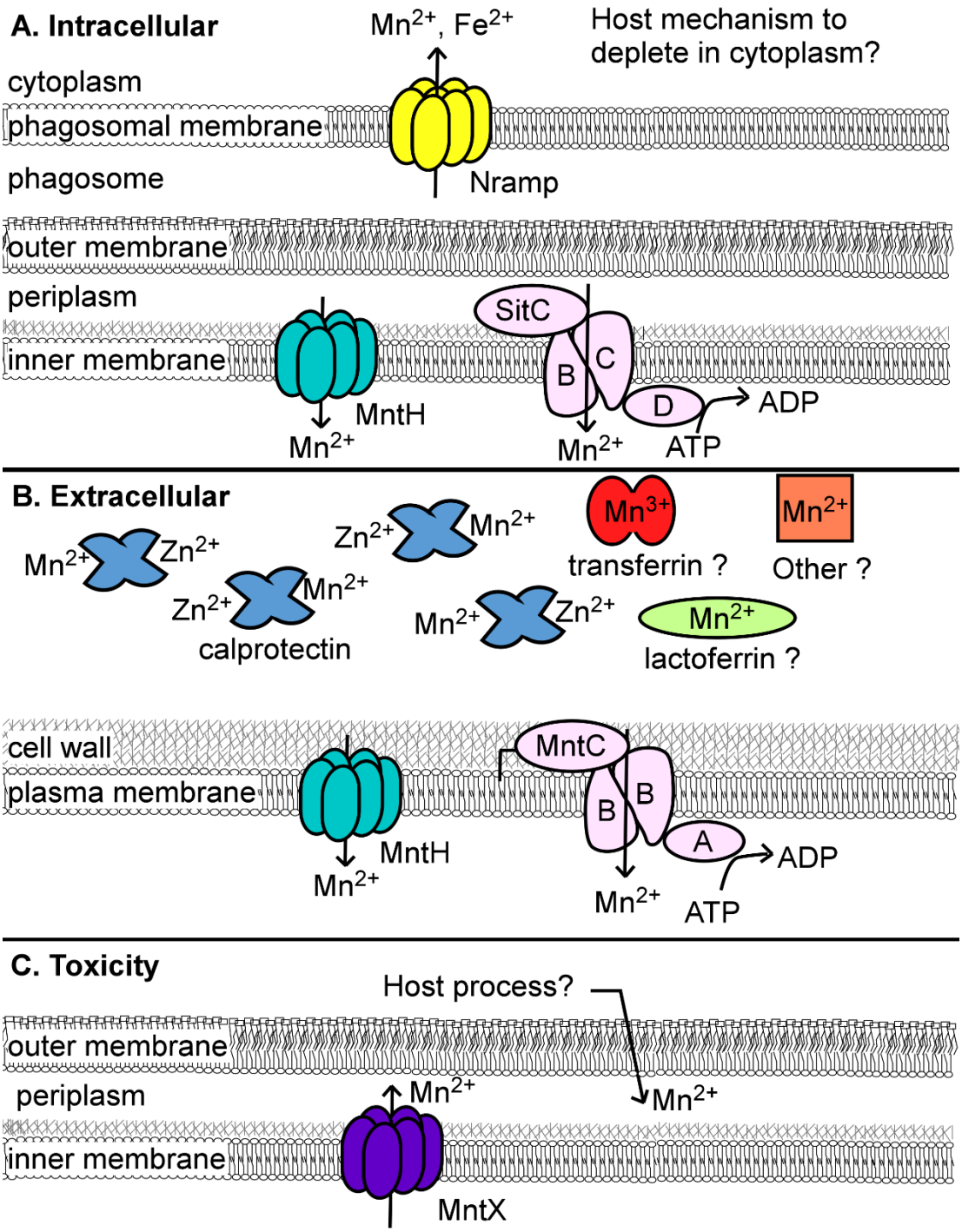

Figure 2. The battle for Mn at the pathogen-host interface.
(A) Intracellular pathogens such as *S.* Typhimurium that reside within the phagosome of macrophages must survive a Mn deplete environment. Mn and Fe are actively removed from the phagosome by the eukaryotic NRAMP1 protein. Host processes to restrict microbial access to Mn within other cellular compartments, including the cytoplasm, have not yet been identified. To acquire Mn in this restricted environment, *Salmonella* utilizes MntH and SitABCD, an ABC-family transporter, to acquire Mn and possibly Fe. MntH

consists of a single integral membrane protein, whereas ABC-type transporters are made up of a substrate-binding domain, a permease domain, and an ATP-hydrolyzing domain. **(B)** Extracellular Mn is sequestered by calprotectin, which is released by neutrophils actively or through cell lysis. Other proteins, including lactoferrin and transferrin, have been shown to bind to Mn in plasma or other tissues, but whether Mn-binding by these or as-yet identified extracellular chelators contributes to host nutritional immunity is unknown. To combat this sequestration, extracellular *S. aureus* also utilizes MntH and ABC-type Mn importers. **(C)** In contrast, *Neisseria meningitidis* requires Mn export through MntX for virulence, presumably to prevent Mn toxicity during infection**.** Host mechanisms to intoxicate bacteria with Mn have not yet been identified.

ii. Bacterial acquisition systems in extracellular bacteria

S. aureus is a Gram-positive pathogen that is a leading cause of skin and soft-tissue infection, endocarditis, osteomyelitis and bacteremia in the United States and throughout the world (Tong et al., 2015). *S. aureus* asymptomatically colonizes the anterior nares (nose) of many adults but is able to infect nearly any organ in the body if the physical or immunological barriers to infection are breached (Tong et al., 2015). This pathogen causes invasive infections because of numerous virulence factors and nutrient acquisition systems (Tong et al., 2015). *S. aureus* expresses two manganese transporters, an NRAMP-family importer and an ABC-family importer (Horsburgh et al., 2002). In *S. aureus*, the NRAMP-family transporter is named MntH (Horsburgh et al., 2002) and the manganese ABC transporter is named MntABC; the genes *mntABC* are transcribed as an operon but translated into three separate proteins with three separate functions (Kehl-Fie et al., 2013). MntB forms the transmembrane channel that permits passage of manganese across the cytoplasmic membrane (Kehl-Fie et al., 2013). MntA is a cytoplasmic protein that hydrolyzes ATP to generate the energy required for transport against a concentration gradient (Kehl-Fie et al., 2013). Finally, MntC is a substrate binding protein that is on the extracellular side of the cytoplasmic membrane (Kehl-Fie et al., 2013). MntC binds manganese and transfers manganese to MntB for transport (Kehl-Fie et al., 2013). It is thought that the substrate binding protein confers metal ion selectivity to manganese ABC transporters (Counago et al., 2014). Interestingly, *S. aureus* expresses the MntH and MntABC transporters at slightly different times. *mntH* is expressed constitutively and may be responsible for basal manganese transport (Horsburgh et al., 2002). On the other hand, *mntABC* is only expressed when manganese is low, as the gene is regulated by a

manganese-binding transcriptional repressor (Horsburgh et al., 2002). Therefore, MntABC may be more important for manganese import under conditions of host nutritional immunity.

S. aureus relies on MntH and MntABC for subversion of calprotectin-mediated nutritional immunity. In liquid growth, inactivation of *mntH, mntC,* or both *mntH* and *mntC* causes *S. aureus* to be more susceptible to calprotectin (Kehl-Fie et al., 2013). In a mouse model of systemic *S. aureus* infection, inactivation of both *mntH* and *mntC* decreases the ability of *S. aureus* to colonize the kidney and the liver (Kehl-Fie et al., 2013). Interestingly, this is only true for mice that express calprotectin, as calprotectin deficient animals have similar numbers of wild-type bacteria and the *mntH*/*mntC* mutant strain recovered (Kehl-Fie et al., 2013). This suggests that calprotectin is required to manganese starve *S. aureus,* and the MntH and MntABC transporters combat manganese starvation.

Beyond *S. aureus,* bacterial Mn import systems are important for the virulence of some, but not all tested, extracellular pathogens. **Figure 2B** depicts the competition for Mn between bacterial and host proteins. *Streptococcus mutans*, *Streptococcus suis*, *Streptococcus sanguinis*, and *Streptococcus uberis* require Mn import for full virulence as measured by murine survival and bacterial burdens in models of rat endocarditis, murine peritoneal-induced systemic infection, rabbit endocarditis, and bovine mammary gland infection, respectively (Paik *et al.*, 2003, Wichgers Schreur *et al.*, 2011). In contrast, inactivation of the Mn importers *mntH* and *zupT* has no effect on *E. coli* colonization of C57BL/6 mice or gnotobiotic mice (Kupz *et al.*, 2013), and inactivation of *mntH* alone in avian pathogenic *E. coli* does not alter colonization of chicks (Sabri *et al.*, 2008). For avian pathogenic *E. coli* and *S. aureus,* simultaneous inactivation of two Mn transporters

decreases colonization in a chick air sac infection model (Sabri *et al.,* 2008, Kehl-Fie *et al.,* 2013). Together, these data suggest that Mn import is required for several extracellular pathogens, but redundant metal cation transporters can rescue single mutants and inactivation of multiple transport systems may be required to impair fitness within the host. Furthermore, Mn import systems have only been described and investigated in a minority of pathogens and only a few sites of infection. Chapter II will address this question in the opportunistic pathogen *A. baumannii* and interrogate the role for Mn uptake during lung infection.

Mn import systems are thus important for pathogenesis of multiple organisms. However, the cellular requirement for Mn import during infection is not understood. Bacteria with mutated Mn transport proteins may have decreased fitness in the host because of gross dysregulation of metal homeostasis, toxicity of Mn-requiring enzymes incorrectly populated with other metals, or loss of specific enzyme function. RNA sequencing analysis during infection comparing WT strains and strains lacking Mn import proteins may identify differentially regulated genes for further study. Similarly, recent advances such as Tn-Seq (van Opijnen & Camilli, 2013) could be utilized for *in vivo* selection of bacterial mutants with relative fitness advantages in calprotectin- or NRAMP1- deficient mice. By comparing this selected mutant pool with the pool selected in WT mice, genes important for growth in metal restricted environments could be compared to genes required for other processes.

Bacterial processes that require Mn during infection

The necessity for bacterial acquisition systems during infection demonstrates that Mn is required for pathogenesis, but the requirement for Mn during infection is not completely understood. Intracellular concentrations of Mn vary dramatically between bacterial species and growth conditions, which may reflect vastly different requirements for Mn (Anjem *et al.*, 2009, Jacobsen *et al.*, 2011, Rolfe *et al.*, 2012, Outten & O'Halloran, 2001, Posey & Gherardini, 2000). In the following section, the role of Mn in protection from reactive oxygen species and DNA synthesis will be described in some detail (**Figure 3**), but it is important to note that Mn is important for diverse processes in bacteria. Certain proteins important for cell signaling utilize Mn, including phosphodiesterases and ppGpp hydrolases (Papp-Wallace and Maguire, 2006). *Clostridium difficile* encodes a fibronectin-binding protein, Fbp68, that requires Mn for the conformational change that stabilizes binding (Lin et al., 2011). The *S. aureus* fosfomycin resistance protein FosB is activated by manganese (Roberts et al., 2013; Thompson et al., 2014). Therefore, Mn contributes to multiple cellular processes in an organism-specific manner.

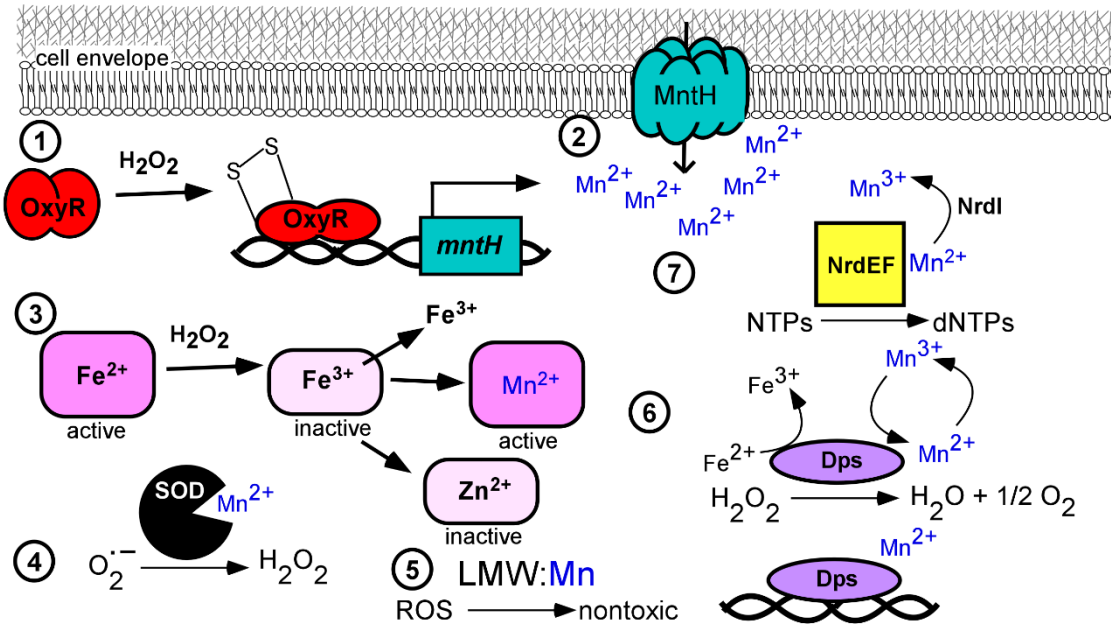

Figure 3. Intracellular utilization of Mn in the oxidative stress response and DNA synthesis. (1) In the presence of hydrogen peroxide, the transcriptional regulator OxyR is oxidized to form an intramolecular disulfide bind that alters the binding affinity of OxyR to the *mntH* promoter, leading to the activation of *mntH* transcription. (2) *mntH* transcription upregulates MntH expression at the cell membrane, increasing Mn import into the cytoplasm where it can be utilized in various processes. (3) Fe-mononuclear enzymes are inactivated by hydrogen peroxide via oxidation of Fe(II) to Fe(III) and dissolution of Fe(III) from the enzyme; Zn can then be incorporated into the enzyme but does not confer enzymatic activity. In the presence of increased Mn either through supplementation or MntH-mediated import, Mn can be incorporated into the mononuclear enzyme and restore enzymatic activity while remaining nonsusceptible to hydrogen peroxide-mediated oxidation. (4) Superoxide anion is dismutased to hydrogen peroxide through the activity of Mn-superoxide dismutase (SOD). (5) Low molecular weight Mn complexes (LMW:Mn), such as Mn-phosphate and Mn-lactate, are capable of detoxifying reactive oxygen species (ROS) in a protein-independent manner. (6) Dps is an Fe-storage protein that protects against hydrogen peroxide through several Mn-requiring activities. First, when Mn is bound to a regulatory site near the N-terminus of the protein, Dps binds to and protects DNA from oxidative damage. Second, Dps ferroxidase activity oxidizes Fe(II) to Fe(III) at the metal-binding site B while reducing hydrogen peroxide, avoiding toxic Fenton chemistry. The ferroxidase activity requires redox cycling of Mn at metal-binding site A. (7) Ribonucleotide reductase NrdEF utilizes a Mn cofactor to reduce ribonucleotides (NTPs) to deoxyribonucleotides (dNTPs). The active cofactor form (Mn(III)-thiyl radical) is derived by the flavodoxin NrdI.

Another interesting concept that requires further investigation is the utilization of Mn for metabolism during infection. A number of metabolic enzymes in bacteria require Mn, but the implications for pathogenesis have not been explored (Kehres & Maguire, 2003, Jakubovics & Jenkinson, 2001). Mn-activated or requiring metabolic enzymes include phosphoglyceromutase, enolase, pyruvate kinase, phosphoenolpyruvate carboxylase and phosphoenolpyruvate carboxykinase (Papp-Wallace and Maguire, 2006). Further analysis of these metabolic processes may reveal Mn-requiring enzymes that represent candidate therapeutic targets. Assessing the function of Mn-requiring metabolic pathways in cells following calprotectin treatment, for instance, may provide intriguing information about the effect of host-mediated Mn chelation on the ability of cells to generate energy and synthesize micro- and macro-molecules. Chapter II and IV includes investigation into urea metabolism as a potential Mn-requiring metabolic process that is important when the host is imposing Mn restriction during infection.

i. Resistance to oxidative stress

The most well-known purpose of Mn is in the oxidative stress response (Aguirre & Culotta, 2012, Lisher & Giedroc, 2013). Reactive oxygen species are chemically reactive molecules containing oxygen that cause cellular damage, in part by participating in the Fenton Reaction with Fe and oxidizing Fe in Fe-mononuclear enzymes, rendering the enzymes non-functional (Sobota and Imlay, 2011). Reactive oxygen species include hydroxyl radical, hydrogen peroxide, and superoxide anion, and there is evidence that Mn is important for detoxification of several of these reactive compounds.

Mn is important for detoxification of hydrogen peroxide via multiple mechanisms. Mn is important for the function of Dps, a protein that protects against hydrogen peroxide

via DNA-binding, Fe sequestration, and ferroxidase-activity that reduces H_2O_2 to H_2O (Anjem & Imlay, 2012, Almiron *et al.*, 1992, Martinez & Kolter, 1997, Su *et al.*, 2005) (Zhao *et al.*, 2002, Ardini *et al.*, 2013). Mn binds to a regulatory site within Dps to permit DNA-binding activity and inhibit ferroxidase activity, which serves as a regulatory mechanism that physically separates the two activities such that hydroxide radicals are not produced directly adjacent to DNA (Nguyen & Grove, 2012). A distinct, high-affinity Mn-binding site is required for ferroxidase activity (Ardini *et al.*, 2013); thus, Mn is essential for the full repertoire of Dps function. There is also substantial *in vitro* evidence that Mn can replace Fe cofactors in mononuclear enzymes, maintaining enzyme function when the Fe cofactor has been oxidized by hydrogen peroxide (Anjem & Imlay, 2012, Sobota & Imlay, 2011, Sobota *et al.*, 2014, Imlay, 2014). In sum, Mn has multiple links to survival under hydrogen peroxide stress.

Mn is also important for other antioxidant functions. Mn serves as a cofactor for Mn-Superoxide Dismutase (Mn-SOD), an enzyme that detoxifies superoxide into water and hydrogen peroxide. SOD activity in *S. aureus* is significantly diminished in the presence of the host Mn chelator calprotectin and following deletion of the *S. aureus* Mn importers, *mntABC* and *mntH*, supporting the idea that Mn is the Mn-SOD cofactor *in vivo* (Kehl-Fie *et al.,* 2013, Kehl-Fie *et al.,* 2011). In addition to its contributions as an enzymatic cofactor, Mn also functions as an antioxidant in a protein-independent mechanism (Culotta & Daly, 2013, Chang & Kosman, 1989, Tseng *et al.*, 2001, Tabares & Un, 2013, Ardini *et al.*, 2013, Inaoka *et al.*, 1999, Daly *et al.*, 2010, Seib *et al.*, 2004, Archibald & Fridovich, 1981, Barnese *et al.*, 2012, Sharma *et al.*, 2013). Taken together, these findings illustrate the importance of Mn in detoxification of ROS; however, the role

of Mn in ROS detoxification *in vivo* has not been established and will be subject of Chapter V.

ii. DNA replication

Ribonucleotide reductase (RNR) enzymes are required for the synthesis of deoxyribonucleotides from ribonucleotides and have been used to decipher whether Mn is a preferred enzyme cofactor during infection. In bacteria, Class Ib aerobic RNRs can utilize Mn or Fe as a cofactor (Makhlynets *et al.*, 2014, Stubbe & Cotruvo, 2011, Zhang & Stubbe, 2011, Cotruvo & Stubbe, 2011, Martin & Imlay, 2011). *S. sanguinis* NrdEF, which is required for virulence of this organism in a rabbit catheter-associated endocarditis model, can utilize Mn^{3+} or Fe^{3+} in aerobic environments (Makhlynets *et al.*, 2014). NrdI, a flavodoxin, is required for oxidizing Mn^{2+} bound to NrdE to the Mn^{3+}-thiyl radical required for catalysis, but NrdI is not used in the formation of the Fe^{3+}-thiyl radical (Rhodes *et al.*, 2014, Cotruvo *et al.*, 2013). Inactivation of NrdI completely abolishes virulence, similar to inactivation of NrdEF, suggesting that the Mn cofactor is required *in vivo* (Rhodes *et al.*, 2014). These observations fit well with an earlier report that SsaB, a putative Mn transporter, is required for virulence of *S. sanguinis* in a competitive infection (Das *et al.*, 2009). Together, these findings suggest that the cofactor preference of NrdEF *in vivo* is Mn.

iii. Areas for future study

Many questions remain about the subcellular localization and utilization of Mn within bacteria. The intracellular location of Mn has yet to be elucidated and the predominant reservoir of Mn within the cell has not been identified. This reservoir could be ‘free’ Mn in soluble salt complexes, membrane bound, nonspecifically bound to

macromolecules, or integrated into Mn-specific proteins. It is also not known if Mn atoms are shuttled within the cell by Mn chaperones or freely diffuse. Furthermore, the fate of Mn-requiring enzymes when intracellular Mn is low should be interrogated as well as the effect of high intracellular Mn on non-cognate metalloproteins.

Transcriptional regulation of Mn transporters

Bacteria have evolved regulatory mechanisms to ensure that Mn import systems are appropriately expressed during times of need. Although many levels of regulation of the Mn import systems may be at work, the best studied regulatory mechanisms involve protein transcriptional regulators that repress or activate transcription of Mn import systems (**Figure 4**). There are three main classes of transcriptional regulators of Mn import systems: (1) dedicated Mn-binding transcriptional repressors, (2) Fe-binding transcriptional repressors, and (3) regulators that sense oxidative stress.

Mn-binding metalloregulators prototypically fall either into the MntR family (Merchant & Spatafora, 2014) or the Mur family (Lee & Helmann, 2007). Both MntR and Mur function by binding to specific sequences in the promoters of their regulated genes and blocking transcription; this only occurs when the regulatory protein is bound to Mn, which induces a conformational change permissive to DNA binding (Kliegman *et al.*, 2006, Schmitt, 2002, Guedon *et al.*, 2003). Since the regulon typically includes Mn import machinery, this mechanism ensures that the importers are not expressed when intracellular Mn levels are already adequate, and de-represses transcription when intracellular Mn levels are low (Golynskiy *et al.*, 2005).

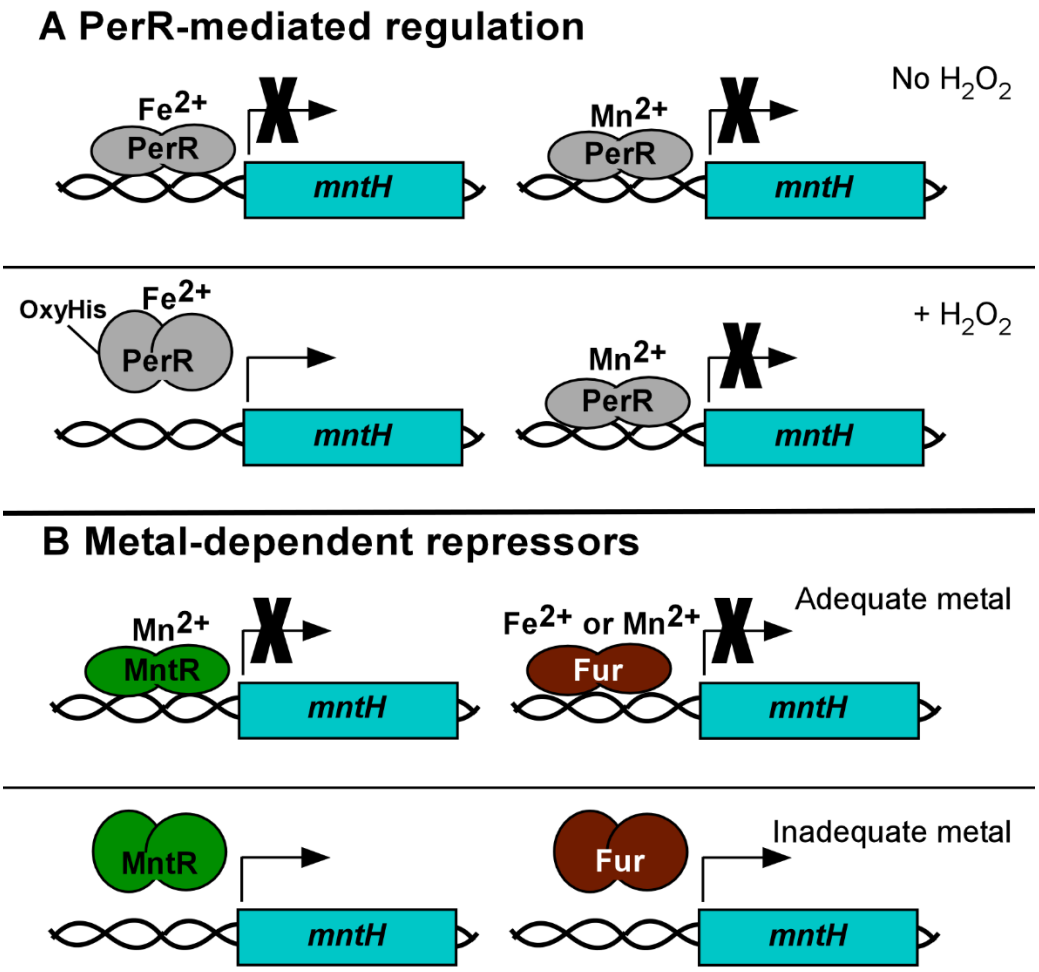

Figure 4: **Regulation of Mn import. (A)** PerR-mediated derepression of *mnt* expression is dependent on metal cofactor binding. PerR:Fe is highly susceptible to peroxide-induced oxidation of one of two histidine residues within PerR, which causes PerR to release from the *mnt* promoter. However, PerR:Mn is not susceptible to oxidation and remains bound. Presumably, when the Mn:Fe ratio is high enough for Mn to populate the PerR regulatory site, Mn levels are also sufficiently high to protect the cell from peroxide stress. **(B)** MntR and Fur both function as metal-dependent repressors of Mn transport genes in some bacteria. MntR:Mn represses transcription when Mn levels are adequate, but repression is relieved when Mn levels are not sufficient for MntR to be bound to Mn. Fur can repress Mn transport genes either when bound to Fe or Mn.

Fur is a Fe-binding repressor that senses and responds to Fe levels. Fur also binds a structural Zn atom and a Zn atom important for dimerization (Fillat M.F. 2014). However, in *S.* Typhimurium, *E. coli,* and *Y. pestis,* Fur represses Mn uptake systems (Ikeda *et al.*, 2005, Patzer & Hantke, 2001). Fur-repression of Mn importers is mediated both by Fe-bound Fur and Mn-bound Fur (Ikeda *et al.*, 2005, Patzer & Hantke, 2001). In *Y. pestis,* the Mn-bound isoform of Fur only represses *mntH* and *yfeABC*, while other Fur regulon members are exclusively repressed by Fe-bound Fur (Perry *et al.*, 2012). The use of Fur to repress Mn import systems demonstrates that the requirement for Mn is partially determined by Fe availability within the cell, emphasizing the importance of the Mn:Fe ratio within the cell. The regulatory crosstalk between Mn and Fe metalloregulators enables this ratio to be sensed without any additional machinery.

Mn importer expression is also modulated via the oxidative stress sensors PerR in gram-positive bacteria and OxyR in gram-negative bacteria. PerR binds to either Mn or Fe at a regulatory site (Lee & Helmann, 2006, Makthal *et al.*, 2013). Fe-PerR is oxidized at a histidine residue in the presence of hydrogen peroxide and no longer binds DNA, whereas Mn-bound PerR is not oxidatively modified by low levels of hydrogen peroxide (Lee & Helmann, 2006, Makthal *et al.*, 2013). Thus, PerR acts as a dual sensor of both the Mn:Fe ratio and peroxide stress. In *S. aureus*, PerR represses *mntABC*; when PerR is inactivated by peroxide stress, repression of *mntABC* is relieved and the operon is transcribed (Horsburgh *et al.*, 2002). In *E. coli, S. enterica*, and *Shigella flexneri,* OxyR acts as a transcriptional activator of *mntH* transcription when OxyR is activated by hydrogen peroxide through the formation of an intramolecular disulfide bond (Anjem *et al.*, 2009, Kehres *et al.*, 2002, Runyen-Janecky *et al.*, 2006). PerR and OxyR ensure that Mn

importers are expressed when oxidative stress response systems are activated, which is essential because Mn serves as a necessary cofactor for some peroxide detoxification machinery.

Bacterial response to Mn toxicity during infection

Mn levels are variable in human and mouse tissues, and bacterial intracellular requirements for Mn are also quite diverse. It is not surprising that some bacterial pathogens experience conditions of Mn toxicity during infection (**Figure 2C**). In *Neisseria meningitidis*, inactivation of the Mn exporter *mntX* decreases survival of the bacterium in human serum and mouse blood following intraperitoneal inoculation (Veyrier *et al.*, 2011). Additional experiments suggest that when Mn becomes more abundant than Fe, Mn populates enzymes that require Fe for function (Veyrier *et al.*, 2011). Because other *Neisseria* species do not harbor a functional *mntX* gene, it is possible that MntX may contribute to the unique tissue niche of *N. meningitidis* (Veyrier *et al.*, 2011). MntE is a cation diffusion facilitator (CDF) protein that exports Mn in *Streptococcus pneumoniae,* and inactivation of *mntE* reduces *S. pneumoniae* virulence in a murine model of pneumonia (Rosch *et al.*, 2009). Decreased virulence in a strain with presumably high Mn levels is consistent with the phenotype of the Mn-dependent repressor *psaR* deletion strain, which also is impaired in colonization of the murine lung (Johnston *et al.*, 2006). However, this evidence for excess Mn levels in the lung is somewhat in contrast with the finding that deletion of *S. pneumoniae psaBCA*, which encodes a Mn ABC-type importer, also impairs virulence in multiple infection models (Marra *et al.*, 2002). The two findings together reveal that *S. pneumoniae* must balance both influx and efflux of Mn for full virulence.

It would be intriguing to investigate whether *S. pneumoniae* experiences limitation and toxicity differentially throughout infection. One straightforward approach would be to engineer *S. pneumoniae* to co-express different fluorescent reporters that are driven either by the *psaBCA* promoter or the *mntE* promoter. Information about cell and location specificity of high or low Mn stress could be gleaned by collecting tissues and imaging the fluorescence. Further study is warranted to understand how Mn availability in host niches and species-specific bacterial requirements for intracellular Mn (balanced with the intracellular metal pool as a whole) alter the balance of Mn import and Mn efflux during infection. Finally, the possibility of Mn toxicity as a host-mediated immune defense is an intriguing avenue of exploration.

Conclusions

Appropriate Mn homeostasis is important for the pathogenesis of many bacterial pathogens. Mn is restricted from intracellular phagosomes by NRAMP1 and from the extracellular space by calprotectin. Bacteria combat Mn sequestration with high affinity Mn import systems and Mn toxicity with Mn export systems, and these transporters are required for full virulence of some pathogens. Within the bacterial cell, Mn is utilized in oxidative stress tolerance and DNA replication. The expression of Mn import systems is regulated by several classes of transcriptional regulators. These findings have garnered excitement about the possibility of Mn homeostasis proteins being suitable targets for vaccines or new antibiotics, and also reveal important gaps in knowledge that are addressed in this Dissertation.

A version of the following section (*Chapter I, Manganese and Nutritional Immunity*) was previously published in Molecular Microbiology 97(2), 216-228 (July 2015) | doi:10.1111/mmi.13034

A version of the following section (*Chapter I, Manganese and Nutritional Immunity*) was previously published in Molecular, Genetic, and Nutritional Aspects of Major and Trace Minerals, Edited by James Collins, 377-387 (2016).

Manganese and Nutritional Immunity

Introduction

Nutritional immunity of Mn refers to host mechanisms to deplete manganese at the site of infection to starve pathogens for this nutrient. Successful pathogens have developed mechanisms that allow them to compete for Mn even when it is scarce and therefore subvert nutritional immunity. In this section, host mechanisms of Mn nutritional immunity are described and areas of future interest to the field of Mn nutritional immunity are proposed.

Mn distribution in mammals

Mn primarily enters the body through the gastrointestinal tract following ingestion of the metal in food or drink (**Figure 5**) (Aschner and Aschner, 2005). Absorption occurs predominantly in the duodenum of the proximal small intestine. An average of 2-4 mg of Mn is eaten by humans on a daily basis, but only 1-3.5% is absorbed (Bowman et al., 2011). Mn is absorbed by enterocytes via the divalent metal transporter-1 (DMT-1) (Aschner and Aschner, 2005). Following absorption, manganese is transported to the liver where a small percent is oxidized to Mn^{3+} and bound to transferrin for serum transport to other tissues (Aschner and Aschner, 2005). The majority of Mn in plasma is complexed to beta-1 microglobulin and albumin (Bowman et al., 2011). Cells throughout the body take up Mn utilizing several different transport mechanisms. These include DMT-1, transferrin receptor-mediated endocytosis, zinc-interacting proteins (ZIP) ZIP8 and ZIP14, the transient receptor potential melastatin 7 (TRPM7), and the solute carrier-39 (SLC39) family of zinc (Zn) transporters (Bowman et al., 2011). All of these transporters have

numerous metal substrates, with Mn being intermediate in affinity. Within cells, Mn is concentrated in the mitochondria by the Ca uniporter (Bowman et al., 2011). Finally, Mn is excreted in bile and removed from the body in the stool (Bowman et al., 2011). It is notable that no mechanisms have been identified for Mn-specific transport or storage throughout the body; instead, it appears that Mn usurps Fe, Zn, Ca, and magnesium (Mg) transport strategies. Whether any of these strategies alter nutritional immunity pertaining to manganese remains unclear. Given the importance of Mn in the host-pathogen interaction, future work should investigate whether any of these transport mechanisms are altered by cytokine signaling and serve to redistribute Mn as an antibacterial strategy.

It is unclear whether global mechanisms exist to redistribute Mn during infection. Fe and Zn are redistributed during infection and this is thought to serve a functional role in nutritional immunity (King, 2011; Nairz et al., 2014). In a healthy adult, Mn levels vary somewhat based on tissue, with relatively low levels in muscle, heart, and brain and higher levels in the pancreas and the liver, both organs that participate in bile production and Mn excretion (Schroeder et al., 1966). The distribution of Mn in the mouse appears to be similar (Kehl-Fie et al., 2013). Intriguingly, infection with *S. aureus* leads to dramatic rearrangements of Mn in the mouse kidney (Kehl-Fie et al., 2013). This finding suggests that mechanisms exist to restructure tissue and body Mn during an acute inflammatory response. However, the specific mechanisms remain obscure and should be a focus of future research.

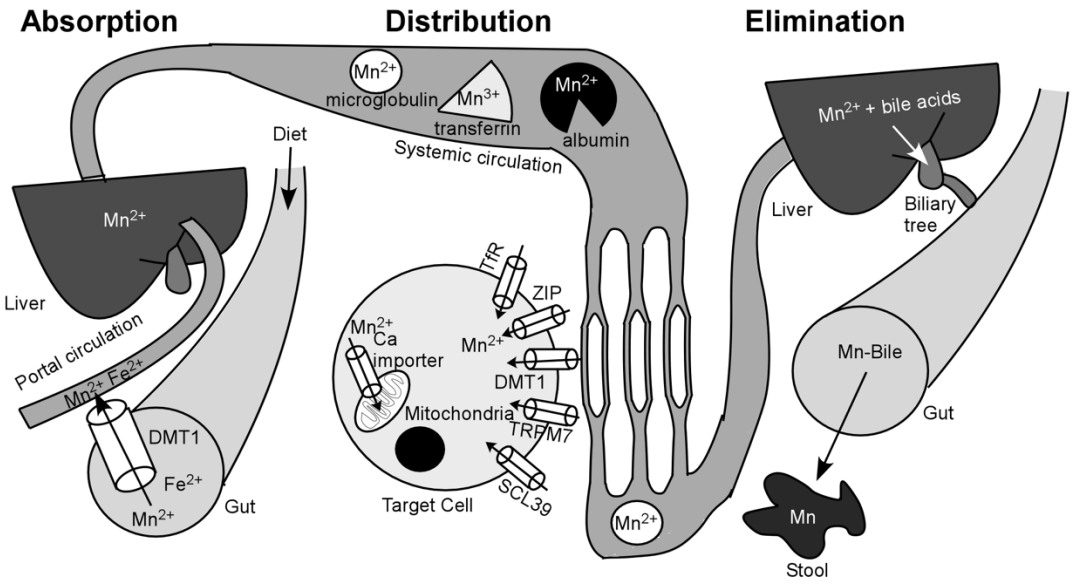

Figure 5: **Mn homeostasis in vertebrates.** Mn is absorbed in the gut by DMT-1 and transported to the liver. From the liver, Mn is distributed to the body in the bloodstream, where it is carried bound to beta-1 microglobulin, albumin, and transferrin. Mn is brought into cells by various transporters throughout the body and sequestered in the mitochondria. Mn is excreted from the body in bile, which is produced in the liver and released into the gut for removal in feces.

Calprotectin: chelating Mn and Zn at the site of infection

Upon entering the host, most bacterial pathogens elicit an inflammatory response that attempts to kill or restrict growth of the invading pathogen and quell the infection. One component of this inflammatory response are cells and products of the innate immune system. Neutrophils are an essential component of the innate immune response to extracellular bacteria (Mantovani et al., 2011). Following rapid recruitment to the site of bacterial invasion, neutrophils kill bacteria via phagocytosis and release of antibacterial cellular contents (Mantovani et al., 2011). These contents include proteases, reactive oxygen species, histones, and metal sequestering proteins (Mantovani et al., 2011). One such metal-binding protein is calprotectin, an extracellular chelator of Mn and Zn that is highly antimicrobial (Zackular et al., 2015). Because of its abundance at the site of infection and its high-affinity Mn-binding properties, calprotectin is an important component of Mn nutritional immunity (**Figure 6**).

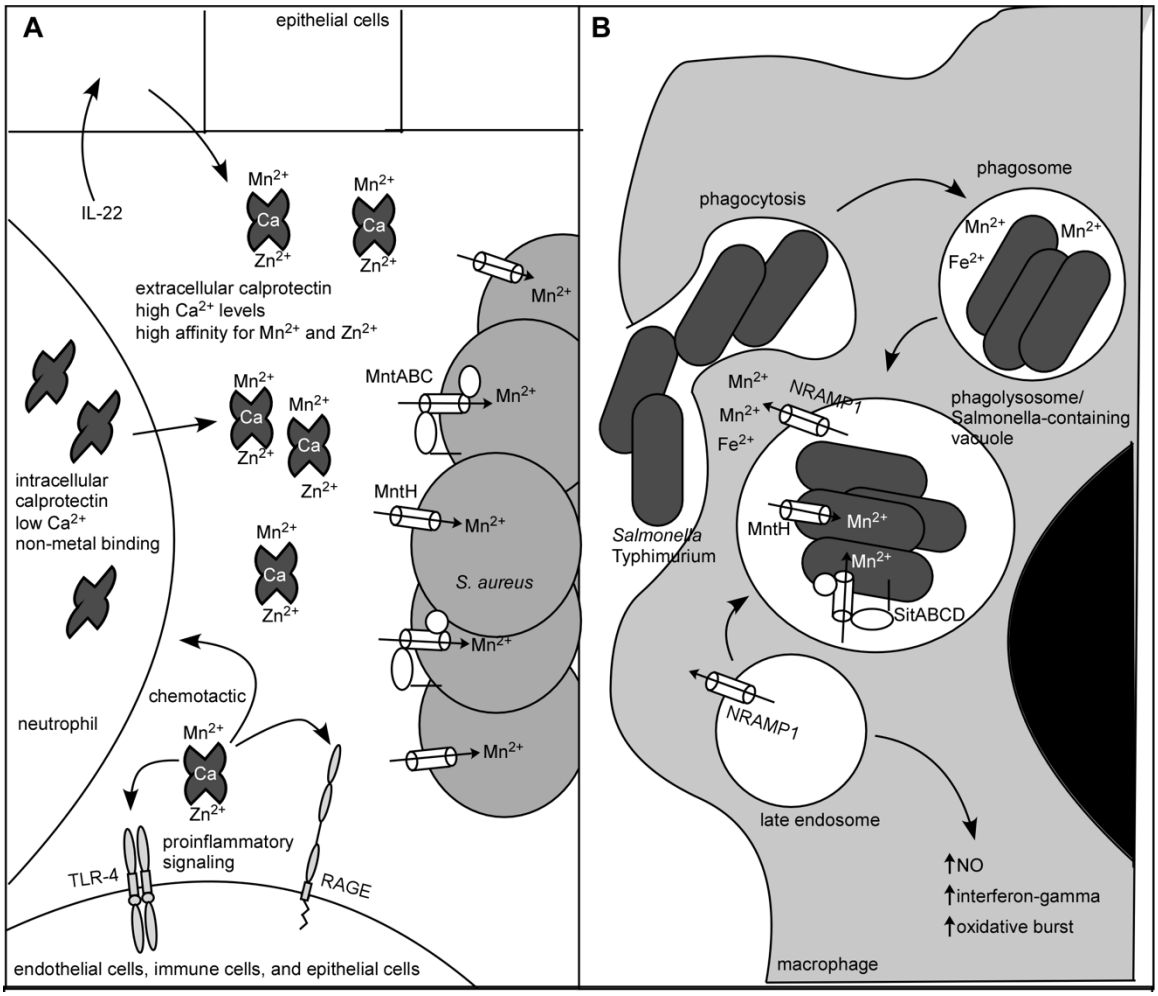

Figure 6: Calprotectin, NRAMP1, and nutritional immunity. (**A**) Calprotectin (CP) is produced by neutrophils constitutively or induced in epithelial cells by inflammatory stimuli. After being released from the cell, calprotectin binds calcium (Ca) to become activated. Calprotectin then binds manganese (Mn) and zinc (Zn), sequestering these metals during infection. Calprotectin also promotes the pro-inflammatory response by binding to various receptors. *S. aureus* imports manganese through MntH and MntABC. This allows *S. aureus* to compete with calprotectin for manganese in the liver and the kidney. **(B)** NRAMP1 is expressed in late endosomes and lysosomes in macrophages. After a pathogen is phagocytosed, NRAMP1 is recruited to the phagosome where it serves to deplete the phagosome of manganese and other metals. This causes phagocytosed bacteria to be manganese starved and more susceptible to other macrophage killing strategies. NRAMP1 also promotes antibacterial functions of macrophages. *S.* Typhimurium imports manganese through MntH and SitABCD. This permits *S.* Typhimurium to compete with NRAMP1 for manganese in the salmonella-containing vacuole within macrophages and disseminate throughout the body.

A major advancement in the field of Mn nutritional immunity was made with the discovery that calprotectin is a Mn-chelating protein that contributes to antibacterial host defense (Corbin *et al.*, 2008). Calprotectin (CP) is a protein heterodimer of S100A8 and S100A9. The S100 family of proteins is found in vertebrates and characterized by two helix-loop-helix (EF-hand) Ca-binding domains (Zackular et al., 2015). While the majority of S100 proteins form homodimers, S100A8 and S100A9 (also known as MRP8/14 and calgranulin A/B) instead form the heterodimer calprotectin (Zackular et al., 2015). Calprotectin is highly abundant in the cytoplasm of neutrophils and is expressed by multiple cell types including monocytes, endothelial cells, and keratinocytes (Goyette & Geczy, 2011, Moore *et al.*, 2014, Marionnet *et al.*, 2003, Boyd *et al.*, 2008, Uhlen *et al.*, 2015).

Calprotectin makes up approximately 40% of the protein content in the cytoplasm of neutrophils, where it is constitutively produced (Zackular et al., 2015). In a mouse model of *S. aureus* infection, neutrophils are required for calprotectin accumulation in staphylococcal lesions in the liver (Corbin et al., 2008). *S100a8* and *S100a9* gene expression is constitutive in neutrophils but induced by pro-inflammatory stimuli in various epithelial cell lines. Inducers include bacterial flagella, lipopolysaccharide, IL-6, IL-1 alpha, and IL-22 (Behnsen et al., 2014; Goyette and Geczy, 2011). It is an intriguing possibility that calprotectin may be produced by epithelial cells or endothelial cells to chelate Mn and Zn very early in infection before neutrophils have accumulated at an infectious site, but this has not been investigated. In sum, calprotectin is produced in high amounts by inflammatory cells as part of the innate immune response.

Calprotectin has two transition-metal binding sites, site 1 (S1) and site 2 (S2). S2 is an S100 protein canonical metal binding site that coordinates Zn (K_d = 8.2 nM) by three histidines and an aspartate (Damo et al., 2013). S1 is a non-canonical binding site that consists of six histidines, two from S100A8 and four from S100A9 (Damo et al., 2013). S1 is capable of binding Zn (K_d = 3.4 nM) or Mn (K_d = 5.8 nM) (Damo et al., 2013). Thus, calprotectin is capable of binding two Zn atoms or one Zn and one Mn atom simultaneously. In 2013, two independent groups demonstrated Mn-binding by calprotectin through isothermal titration calorimetry (Damo *et al.*, 2013) and competition binding experiments (Brophy *et al.*, 2013).

Both the S100A8 and S100A9 protomers of calprotectin contain EF-hand Ca-binding domains, which are conserved in the S100 protein family (Leukert *et al.*, 2006, Korndorfer *et al.*, 2007, Vogl *et al.*, 2006). Ca binding to calprotectin's EF hands is required for high-affinity Mn binding (Hayden *et al.,* 2013), which has important functional implications *in vivo*. Presumably, the low concentration of cytoplasmic Ca (Srikanth & Gwack, 2013) prevents calprotectin from binding Mn until it is released into the extracellular environment upon neutrophil lysis or possibly through active secretion (Rammes *et al.*, 1997). Thus, the requirement for Ca to trigger the high affinity Mn binding state of calprotectin suggests that calprotectin is an extracellular Mn chelator.

It is now appreciated that calprotectin inhibits growth of diverse microbial species. This has been demonstrated by experiments in liquid and solid culture where microbes are grown in the presence of purified recombinant human calprotectin. These experiments have shown that calprotectin inhibits growth of the human bacterial pathogens *S. aureus, A. baumannii, Helicobacter pylori, Salmonella enterica, Staphylococcus epidermidis,*

Staphylococcus lugdunensis, Enterococcus faecalis, P. aeruginosa, and *S. flexneri,* as well as the fungal pathogens *Candida albicans, Aspergillus fumigatus,* and *Cryptococcus neoformans* (Amich et al., 2014; Damo et al., 2013; Gaddy et al., 2014; Liu et al., 2012; Mambula et al., 2000; Sohnle et al., 2000). In order to determine whether the antibacterial properties of calprotectin require the Mn or Zn binding sites, point mutations were introduced in SI or SII and the resulting metal-binding deficient forms of calprotectin were tested for antimicrobial activity (Damo et al., 2013; Kehl-Fie et al., 2011). Calprotectin that cannot bind metal loses all antimicrobial capabilities in liquid culture growth, proving that growth inhibition by calprotectin is due to metal chelation (Damo et al., 2013). Strikingly, calprotectin deficient for binding at the Mn/Zn-binding SI is highly attenuated for antimicrobial activity (Damo et al., 2013). In contrast, the calprotectin mutant deficient for binding at the Zn-binding SII still inhibits growth, underscoring the physiological importance of Mn chelation as an antibacterial strategy (Damo et al., 2013). Indeed, calprotectin inhibits Mn-dependent superoxide dismutase activity in *S. aureus* (Kehl-Fie et al., 2011) In conclusion, calprotectin inhibits bacterial growth via Mn and Zn limitation, but mutational analysis suggests that Mn binding is more important than Zn binding for the antibacterial functions of calprotectin,

Mice that are calprotectin-deficient (*S100a9* constitutive knockout; hereafter $CP^{-/-}$) are more susceptible to infection with a range of bacterial pathogens. $CP^{-/-}$ mice have higher bacterial burdens in the liver following intravenous *S. aureus* infection (Corbin et al., 2008), higher bacterial burdens in the lung and liver following *A. baumannii* intranasal infection (Hood et al., 2012), decreased survival and increased bacterial dissemination in a *K. pneumoniae* pneumonia model (Achouiti et al., 2012), and higher fungal burdens and

decreased survival in a subcutaneous *C. albicans* model (Urban et al., 2009). These findings imply that calprotectin-mediated metal sequestration may play an important part in extracellular pathogen defense in vivo. In contrast to this, some mouse infection models are protected by calprotectin deficiency, including *S.* Typhimurium infection (Liu et al., 2012), *S. pneumoniae* intranasal inoculation (Achouiti et al., 2014), and *H. pylori* gastric infection (Gaddy et al., 2014). For *Salmonella,* the presence of calprotectin allows *Salmonella* to outcompete gut microbes because *Salmonella* possesses a high-affinity zinc importer (Liu et al., 2012). For *H. pylori,* calprotectin activates a virulence program of gene expression that includes the T4SS (Gaddy et al., 2014). These findings indicate that calprotectin metal-sequestration contributes to nutritional immunity, but that some pathogens have adaptive responses to metal limitation that increase virulence.

Calprotectin also contributes to alterations in tissue metal distribution that are dramatically evident following infection. Infection with *S. aureus* leads to dramatic alterations in the distribution of Mn and other metals in the liver and kidney (Corbin et al., 2008; Kehl-Fie et al., 2013). *S. aureus* infection causes visible lesions that contain bacterial microcolonies surrounded by immune cells. In the kidneys and livers of wild-type mice, *S. aureus* lesions are devoid of Mn and zinc relative to the surrounding tissue (Corbin et al., 2008; Kehl-Fie et al., 2013). On the other hand, *S. aureus* lesions in calprotectin-deficient mice contain levels of Mn consistent with surrounding healthy tissuee (Corbin et al., 2008; Kehl-Fie et al., 2013). Therefore, calprotectin is an important factor in producing a Mn-depleted *S. aureus* lesion.

In addition to the metal-sequestering properties of calprotectin, calprotectin has at least two other functions. Calprotectin serves as a proinflammatory molecule, activating

the transcription factor NF-kappa B by acting as an agonist for the receptor for advanced glycation end products (RAGE) and toll-like receptor 4 (TLR-4) (Ibrahim et al., 2013). Calprotectin is also predicted to serve as an oxidant sink, as the S100A8 protomer of calprotectin isolated from asthmatic sputa exhibits oxidative modifications on cysteine residues, methionine residues and a tryptophan residue (Gomes et al., 2013). These proposed functions for calprotectin may or may not intersect with its function as a metal chelating protein.

Several aspects regarding the contribution of calprotectin to defense against infection remain unknown. Single-nucleotide polymorphisms (SNPs) in calprotectin have been identified and correlated with severity of periodontitis in a Chinese population (Li *et al.*, 2007, Sun *et al.*, 2011), but the small-scale studies focused on two specific marker SNPs and did not include sequencing of the locus or identification of the specific residue linked to the phenotype. Further investigation of allelic variation in calprotectin is warranted, including in-depth exploration of whether any alleles have altered metal-binding properties. Patients with hypercalprotectinemia (overexpression of CP due to an unknown etiology) have gross dysregulation of Zn levels (Sampson *et al.*, 2002, Gustafsson *et al.*, 2012) suggesting that CP has a role in metal homeostasis beyond sequestering metals during infection; however, the role of CP in Mn homeostasis has not been interrogated. Calprotectin also has documented signaling activity, and the relative contributions of this signaling and metal restriction to *in vivo* bacterial defense remain to be defined (Moisan *et al.*, 2006, Gomez *et al.*, 2007, Ehrchen *et al.*, 2009, Hofmann *et al.*, 1999). Furthermore, it is not understood whether the processes are interdependent, i.e. if Mn binding is required for calprotectin's signaling properties.

It is likely that additional vertebrate proteins are involved in Mn chelation during infection. This contention is supported by LA-ICP-MS analysis of *S. aureus* lesions in the kidney of infected mice, which, in contrast to *S. aureus* liver lesions (Corbin *et al.*, 2008), remain Mn-depleted in calprotectin-deficient mice (Kehl-Fie *et al*., 2013). Thus, other unidentified factor(s) are responsible for removing Mn from sites of infection in the kidney. Several Fe-binding proteins have also been shown to bind Mn, and these proteins may play a role in Mn sequestration during infection. Transferrin is the major Mn-binding protein in plasma (Davidsson *et al.*, 1989, Scheuhammer & Cherian, 1985, Critchfield & Keen, 1992), binding Mn exclusively as an oxidized trivalent cation (Gibbons *et al.*, 1976). Transferrin facilitates receptor-mediated transport of Mn into target tissues such as the mammary gland and the CNS and should be investigated for antimicrobial roles in these tissues (Aschner & Gannon, 1994, Moutafchiev *et al.*, 1998). Similarly, lactoferrin binds Mn in human breast milk (Lonnerdal *et al.*, 1985). *In vitro* studies utilizing purified lactoferrin and transferrin will be useful for determining whether these proteins bind Mn with sufficient affinity to restrict microbial access to this metal. However, these studies will have to be carefully designed to parse the antimicrobial effects of Fe-binding vs. Mn-binding to any observed phenotypes.

NRAMP1/*Slc11a1*: starving bacteria in macrophages

The previous section detailed a mechanism for starving extracellular bacteria of Mn. A distinct mechanism also exists for depleting the phagolysosome of Mn. Phagolysosomal depletion is carried out by NRAMP1, encoded by the gene *Slc11a1*, which is a member of the solute carrier family of transporters. NRAMP1 is a phagocyte specific

protein that is only expressed in late endosomes, lysosomes and phagolysosomes, where it transports metals to the cytoplasm. NRAMP1 function is important for the defense against several pathogens in mice and humans, including *Mycobacterium* species.

NRAMP1 expression patterns suggest that its functional role is limited to classically activated, M1-type macrophages and neutrophils; both of these cell types have vital roles in antibacterial defense (Italiani and Boraschi, 2014; Mantovani et al., 2011). Classically activated macrophage subsets are important for antibacterial defense and are categorized by production of nitric oxide (Italiani and Boraschi, 2014). In neutrophils, NRAMP1 is limited to gelatinase-positive tertiary granules, but its function in this cell type is not understood (Canonne-Hergaux et al., 2002). However, NRAMP1 function in macrophages has been extensively characterized. NRAMP1 encodes a conserved N-terminal lysosomal targeting motif and is expressed in late endosomes and lysosomes of resting macrophages (Lam-Yuk-Tseung et al., 2006). The cellular targeting of NRAMP1 to the lysosome was confirmed by co-localization with the lysosomal marker Lamp1 (Cellier et al., 2007). Following phagocytosis, NRAMP1 is recruited to the membrane of phagosomes as the phagolysosome is formed (Cellier et al., 2007). This expression pattern poises NRAMP1 to antagonize bacteria contained within the vacuole. NRAMP1 expression is induced by macrophage classical activators, including interferon-gamma, IL-1, IL-6, IL-10, TNF-alpha and exposure to bacteria or bacterial products such as LPS (Cellier et al., 2007). Together, the expression patterns of NRAMP1 place NRAMP1 in a suitable position to aid in macrophage killing of phagocytosed bacteria.

NRAMP1 transports divalent cations across the phagosomal membrane (Lam-Yuk-Tseung et al., 2006). Much of what is known about NRAMP1 metal transport has been

inferred by comparison with the other SLC11 transporter in humans, DMT1 (also called SLC11A2 and NRAMP2), which is ubiquitously expressed (Gruenheid et al., 1999). NRAMP1 and DMT1 are highly similar, with twelve predicted transmembrane domains and 78% amino acid identity across the hydrophobic core (Gruenheid et al., 1999). DMT1 is responsible for Fe uptake at the duodenum and iron import at the plasma membrane in peripheral tissues, as well as for Fe transport in transferrin-recycling endosomes (Nevo and Nelson, 2006; Shawki et al., 2012). *In vitro* studies have demonstrated DMT1 transport of Fe and Mn (as well as other divalent cations) in a pH-dependent fashion, symporting the metals with protons (Nevo and Nelson, 2006; Shawki et al., 2012). Based on the discovery that DMT1 transports metals, it was hypothesized that NRAMP1 also functions as a metal transporter. Indeed, NRAMP1 pH-dependent metal transport has been confirmed by studies utilizing isolated oocytes and peritoneal macrophages (Goswami et al., 2001; Jabado et al., 2000). Similar to DMT1, NRAMP1 also transports other divalent cations (Forbes and Gros, 2003; Goswami et al., 2001; Nevo and Nelson, 2006). However, unlike DMT1, NRAMP1 transports Mn preferentially over Fe (Forbes and Gros, 2003). In sum, NRAMP1 is a divalent cation transporter with a wide range of metal substrates but a preference for Mn.

While the transport properties of NRAMP1 are largely agreed upon, the direction of NRAMP1 transport has been more difficult to establish. Some arguments have been made that NRAMP1 imports metals into the phagosome to intoxicate bacteria via the Fenton and Haber-Weiss reactions (Nairz et al., 2014). However, the majority of evidence suggests that NRAMP1 depletes the phagolysosome of divalent cations (Nairz et al., 2014). Expression of NRAMP1 decreases phagosome Mn levels as measured by a fluorescent

probe that is quenched by Mn (Forbes and Gros, 2003; Jabado et al., 2000). When NRAMP1 is engineered to be expressed at the plasma membrane, it inserts in the membrane in the same orientation and transports metals in the same direction as DMT1 (Forbes and Gros, 2003). Macrophages expressing NRAMP1 starve *S.* Typhimurium for Fe, whereas macrophages expressing nonfunctional NRAMP1 do not Fe starve the bacterium (Nairz et al., 2009). Finally, functional NRAMP1 expression in peritoneal macrophage enhances killing of *S.* Typhimurium defective for Mn transport; the same *S.* Typhimurium strain is not killed by macrophages with a nonfunctional NRAMP1 (Zaharik and Finlay, 2004). Taken together, these results support a model whereby the antibacterial mechanism of NRAMP1 is metal depletion, not metal intoxication. It is now generally accepted that NRAMP1 transports metals out of the phagosome, depleting the phagosomal environment. NRAMP1 has a function during nutritional immunity: to starve bacteria that have been phagocytosed so they are more susceptible to macrophage killing mechanisms.

The nutritional immunity imposed by NRAMP1 governs resistance to numerous pathogens in mice. This list includes the bacterial pathogens *S. typhimurium, Mycobacterium bovis, Mycobacterium intracellulare, Mycobacterium lepraemurium,* and *Campylobacter jejuni* as well as the parasites *Leishmania donovani* and *L. infantum* (Bradley, 1977; Brown et al., 1982; Champion et al., 2008; Goto et al., 1984; Govoni et al., 1996; Leclercq et al., 1996). In fact, NRAMP1 was discovered as the locus that determines susceptibility of different inbred mouse strains to specific infections. Many common mouse lines, including C57BL/6 and BALB/C, encode an *Slc11a1* allele (the gene encoding NRAMP1) with an amino acid substitution, G169D (Vidal et al., 1996). This mutation occurs in the fourth transmembrane domain, and the addition of the negatively

charged aspartate causes a nonfunctional protein that is rapidly degraded (Vidal et al., 1996). Mouse strains expressing the nonfunctional Asp169 allele are susceptible to a number of intracellular pathogens, meaning that the pathogens grow to high numbers in the liver and spleen early in infection (Govoni et al., 1996). For *S.* Typhimurium infection, susceptible mice are unable to clear the bacterium and will succumb to disease (Govoni et al., 1996). To demonstrate that susceptibility is due to the *Slc11a1* allele specifically, congenic mouse lines that express the functional Gly169 *Slc11a1* allele were engineered and found to be protected from *S.* Typhimurium and *M. bovis* (Govoni et al., 1996). Therefore, NRAMP1 is a vital component of the immune response to certain bacteria.

There is additional evidence demonstrating that the role of NRAMP1 in defense against intracellular pathogens is due to nutritional immunity. Mice expressing nonfunctional NRAMP1 or the functional NRAMP1 allele were infected with *S.* Typhimurium strains with different inactivating mutations in metal transport systems (Boyer et al., 2002). *S.* Typhimurium has two divalent transporters, MntH and SitABCD, both of which exhibit higher affinity for Mn than Fe in vitro (Boyer et al., 2002). Mice with the nonfunctional Asp169 NRAMP1 are equally susceptible to wild-type bacteria and a strain lacking *mntH,* and deletion of *sitABCD* modestly decreases virulence (Boyer et al., 2002). However, when mice express functional Gly169 NRAMP1 both single and double knockouts of *mntH* and *sitABCD* exhibit decreased virulence relative to wild-type bacteria (Zaharik and Finlay, 2004). This establishes that host NRAMP1 is required to stress the bacterium by metal depletion during intracellular infection.

Slc11a1 promoter alleles are linked with human disease susceptibility. Sequencing analysis identified four promoter alleles for *Slc11a1,* two of which are extremely rare

(Blackwell et al., 2000). Allele three is highly active and is present in approximately three-quarters of the population (Blackwell et al., 2000). Allele two is a very low expressing promoter and is present in approximately one quarter of the population (Blackwell et al., 2000). Intriguingly, the high-expressing allele 3 is associated with autoimmunity and poor infectious disease outcomes when the disease is driven by immune-mediated pathology, i.e. meningococcal meningitis (Blackwell et al., 2003). In contrast, the low-expressing allele 2 is associated with diseases that require activated macrophages for clearance, i.e. *Mycobacterium tuberculosis* (Blackwell et al., 2003). *Slc11a1* haplotypes are also associated with HIV, leprosy, and protozoal infections (Blackwell et al., 2003). The genetic associations between *Slc11a1* and infectious disease susceptibility in humans support an important role for NRAMP1 in nutritional immunity.

The role for NRAMP1 in immunity is not limited to metal deprivation. NRAMP1 also influences production of a number of important macrophage molecules, including nitric oxide, interferon-gamma, interleukin-6, interleukin-1 beta, major histocompatability complex II, and tumor necrosis factor-alpha (Blackwell et al., 2000). NRAMP1 also alters L-arginine flux, oxidative burst, and processing of antigen (Blackwell et al., 2000). As a result, expression of the functional Gly169 NRAMP1 allele biases the immune response towards a Th1-type response, whereas expression of the nonfunctional Asp169 allele biases the immune response towards a Th2-type response (Blackwell et al., 2000). The mechanistic basis for the differences in macrophage function is not understood, but it is an intriguing idea to presume that metal flux from the phagosome is an intracellular stimulus that alters gene expression or gene stability.

In summary, NRAMP1 is important for nutritional immunity in the phagosome. NRAMP1 localizes to lysosomes and phagolysosomes within macrophages and neutrophils where phagocytosed bacteria are subjected to intense stressors, including reactive oxygen species and proteases. NRAMP1 depletes the phagolysosome of essential metals, especially Mn. Mn starvation renders bacteria susceptible to the onslaught of reactive oxygen species, as many antioxidant mechanisms require Mn for function. NRAMP1 is an essential component of macrophage defense during bacterial infection.

Intersection of Mn nutritional immunity with other minerals

Nutritional immunity of Mn intersects with the homeostasis of many other minerals. First, this occurs in mechanisms of Mn homeostasis. Absorption and distribution of Mn exploits transport mechanisms for Fe, Ca and Mg. This may mean that intake of high amounts of Mn could cause Mn to outcompete Fe, causing functional Fe deficiency. Second, interactions with other metals occur because the proteins involved in nutritional immunity of Mn also bind other metals. For instance, the Mn chelating protein calprotectin binds Zn at the same site as Mn and also serves as a Zn chelator; binding affinities for either metal are much higher when Ca is at high levels. Therefore, high concentrations of Zn or low concentrations of Ca could alter the Mn binding potential of calprotectin. In another example, NRAMP1 depletes the phagosome of Mn, but also transports Fe, cadmium, and cobalt. It is likely that starving phagocytosed bacteria of multiple metals is a better antibacterial strategy than removing one metal alone. Third, Mn import proteins in bacteria may be promiscuous, transporting multiple metals in addition to Mn. The potential consequences of this remain unclear. In sum, the Mn handling mechanisms described in

this chapter certainly do not exist in a vacuum devoid of other metals; rather, the relative levels of each metal and their interactions with each other is an important component of nutritional immunity.

Areas for future study

Nutritional immunity of Mn is an important aspect of the host-pathogen dynamic, but many questions remain regarding Mn restriction during infection. Besides calprotectin and NRAMP1, what other host mechanisms exist to limit Mn during infection? What are the mechanisms permitting global tissue redistribution in Mn levels during infection? Do alterations in Mn status caused by variations in dietary Mn intake alter the risk of bacterial infectious disease (see Chapter IV)? How does the microbiota shape Mn homeostasis? Does restriction of Mn have a functional consequence in viral infection? Better understanding vertebrate Mn homeostasis will shape our understanding of these processes during infection. On the bacterial side, several important questions remain to be answered. What are the subcellular destinations of Mn in the bacterial cell? How is Mn trafficked within the cell? What speciation does excess or stored Mn take within the cell? Improved identification of bacterial Mn-binding proteins and small molecules will aid in answering these questions.

One important long-term goal for the field of nutritional immunity is to use this knowledge to guide therapeutic interventions. Before any such therapies may be derived based on NRAMP1 and calprotectin, several unanswered mechanistic questions should be answered. NRAMP1 has a well-understood role in macrophages, but is also expressed in neutrophils; what is the function of NRAMP1 in nutritional immunity of neutrophils?

Similarly, while calprotectin is produced in high levels in neutrophils, it is produced by many other cell types upon inflammatory stimulation. Is calprotectin produced in high enough quantities from these cells to sequester Mn? Additionally, both calprotectin and NRAMP1 have roles in proinflammatory cytokine production; is this tied to the metal handling properties of these proteins? Can these two functions be distinguished in vivo? Finally, calprotectin and NRAMP1 both have significant associations with autoimmune and allergic disease; do the metal binding properties of these proteins promote the generation of autoreactive cells or inhibit immune tolerance mechanisms? It is intriguing to hypothesize that Mn levels and/or flux may be key signal for orchestrating inflammatory responses.

Conclusions

Manganese is an essential nutrient for bacteria as it serves as a cofactor for numerous cellular processes. When a pathogen enters a vertebrate host, it faces a hostile environment with minimal bioavailable manganese. The host accomplishes this by sequestering manganese at the focus of the infection. Calprotectin, a protein produced by neutrophils, tightly binds manganese to inhibit growth of extracellular bacteria. NRAMP1 is a transporter expressed in the phagosomes of macrophages, where it transports manganese out into the cytosol, starving bacteria within the vacuole and contributing to intracellular killing. To combat these strategies, pathogenic bacteria express high-affinity manganese importers that are important for the virulence of numerous bacteria. In sum, the host-pathogen interface is a battle for nutrient manganese, and the outcome determines the pathogenesis of infection.

References

Achouiti, A., Vogl, T., Urban, C.F., Rohm, M., Hommes, T.J., van Zoelen, M.A.*, et al.* (2012) Myeloid-related protein-14 contributes to protective immunity in gram-negative pneumonia derived sepsis. PLOS Pathog. *8*: e1002987.

Achouiti, A., Vogl, T., Endeman, H., Mortensen, B.L., Laterre, P.F., Wittebole, X.*, et al.* (2014) Myeloid-related protein-8/14 facilitates bacterial growth during pneumococcal pneumonia. Thorax *69*: 1034-1042.

Aguirre, J.D. & Culotta, V.C. (2012) Battles with iron: manganese in oxidative stress protection. J. Biol. Chem. *287*: 13541-13548.

Almiron, M., Link, A.J., Furlong, D. & Kolter, R. (1992) A novel DNA-binding protein with regulatory and protective roles in starved *Escherichia coli*. Genes Dev. *6*: 2646-2654.

Amich, J., Vicentefranqueira, R., Mellado, E., Ruiz-Carmuega, A., Leal, F., Calera, J.A. (2014). The ZrfC alkaline zinc transporter is required for *Aspergillus fumigatus* virulence and its growth in the presence of the Zn/Mn-chelating protein calprotectin. Cell. Microbiol. *16*: 548-564.

Aminov, R.I. (2010). A brief history of the antibiotic era: lessons learned and challenges for the future. Front. Microbiol. *1*, 134.

Anderson, E.S., Paulley, J.T., Gaines, J.M., Valderas, M.W., Martin, D.W., Menscher, E.*, et al.* (2009) The manganese transporter MntH is a critical virulence determinant for *Brucella abortus* 2308 in experimentally infected mice. Infect. Immun. *77*: 3466-3474.

Anjem, A. & Imlay, J.A. (2012) Mononuclear iron enzymes are primary targets of hydrogen peroxide stress. J. Biol. Chem. *287*: 15544-15556.

Anjem, A., Varghese, S. & Imlay, J.A. (2009) Manganese import is a key element of the OxyR response to hydrogen peroxide in *Escherichia coli*. Mol. Microbiol. *72*: 844-858.

Antunes, L.C., Visca, P., and Towner, K.J. (2014). *Acinetobacter baumannii:* evolution of a global pathogen. Pathog. Dis. *71*, 292-301.

Archibald, F.S. & Fridovich, I. (1981) Manganese and defenses against oxygen toxicity in *Lactobacillus plantarum*. J. Bacteriol. *145*: 442-451.

Ardini, M., Fiorillo, A., Fittipaldi, M., Stefanini, S., Gatteschi, D., Ilari, A. & Chiancone, E. (2013) *Kineococcus radiotolerans* Dps forms a heteronuclear Mn-Fe ferroxidase center that may explain the Mn-dependent protection against oxidative stress. Biochim. Biophys. Acta *1830*: 3745-3755.

Aschner, J.L., Aschner, M. (2005). Nutritional aspects of manganese homeostasis. Mol. Aspects Medd *26*, 353-362.

Aschner, M. & Gannon, M. (1994) Manganese (Mn) transport across the rat blood-brain barrier: saturable and transferrin-dependent transport mechanisms. Brain Res. Bull. *33*: 345-349.

Barnese, K., Gralla, E.B., Valentine, J.S. & Cabelli, D.E. (2012) Biologically relevant mechanism for catalytic superoxide removal by simple manganese compounds. Proc. Natl. Acad. Sci. *109*: 6892-6897.

Behnsen, J., Jellbauer, S., Wong, C.P., Edwards, R.A., George, M.D., Ouyang, W., Raffatellu, M. (2014). The cytokine IL-22 promotes pathogen colonization by suppressing related commensal bacteria. Immunity *40*, 262-273.

Blackwell, J.M., Searle, S., Goswami, T., Miller, E.N., 2000. Understanding the multiple functions of Nramp1. Microbes Infect. *2*, 317-321.

Blackwell, J.M., Searle, S., Mohamed, H. & White, J.K. (2003) Divalent cation transport and susceptibility to infectious and autoimmune disease: continuation of the *Ity/Lsh/Bcg/Nramp1/Slc11a1* gene story. Immunol. Lett. *85*: 197-203.

Bobrov, A.G., Kirillina, O., Fetherston, J.D., Miller, M.C., Burlison, J.A. & Perry, R.D. (2014) The *Yersinia pestis* siderophore, yersiniabactin, and the ZnuABC system both contribute to zinc acquisition and the development of lethal septicaemic plague in mice. Mol. Microbiol. *93*: 759-775.

Boucher, H.W., Talbot, G.H., Bradley, J.S., Edwards, J.E., Gilbert, D., Rice, L.B., Scheld, M., Spellberg, B., and Bartlett, J. (2009). Bad bugs, no drugs: no ESKAPE! An update from the Infectious Diseases Society of America. Clin. Infect. Dis. *48*, 1-12.

Bowman, A.B., Kwakye, G.F., Herrero Hernandez, E., Aschner, M. (2011). Role of manganese in neurodegenerative diseases. J. Trace Elem. Med. Biol. *25*, 191-203.

Boyd, J.H., Kan, B., Roberts, H., Wang, Y. & Walley, K.R. (2008) S100A8 and S100A9 mediate endotoxin-induced cardiomyocyte dysfunction via the receptor for advanced glycation end products. Circ. Res. *102*: 1239-1246.

Boyer, E., Bergevin, I., Malo, D., Gros, P. & Cellier, M.F. (2002) Acquisition of Mn(II) in addition to Fe(II) is required for full virulence of *Salmonella enterica* serovar Typhimurium. Infect. Immun. *70*: 6032-6042.

Bradley, D.J. (1977). Regulation of Leishmania populations within the host. II. genetic control of acute susceptibility of mice to *Leishmania donovani* infection. Clin. Exp. Immunol. *30*, 130-140.

Brophy, M.B., Nakashige, T.G., Gaillard, A. & Nolan, E.M. (2013) Contributions of the S100A9 C-terminal tail to high-affinity Mn(II) chelation by the host-defense protein human calprotectin. J. Am. Chem. Soc. *135*: 17804-17817.

Brophy, M.B. & Nolan, E.M. (2015) Manganese and Microbial Pathogenesis: Sequestration by the Mammalian Immune System and Utilization by Microorganisms. ACS Chem. Biol. *10:* 641-651.

Brown, I.N., Glynn, A.A., Plant, J. (1982) Inbred mouse strain resistance to *Mycobacterium lepraemurium* follows the Ity/Lsh pattern. Immunology *47*, 149-156.

Canonne-Hergaux, F., Calafat, J., Richer, E., Cellier, M., Grinstein, S., Borregaard, N., Gros, P. (2002). Expression and subcellular localization of NRAMP1 in human neutrophil granules. Blood *100*, 268-275.

CDC (2013). Antibiotic resistance threats in the United States, 2013. https://www.cdc.gov/drugresistance/pdf/ar-threats-2013-508.pdf.

Cellier, M.F., Courville, P. & Campion, C. (2007) Nramp1 phagocyte intracellular metal withdrawal defense. Microbes Infect. *9*: 1662-1670.

Champion, O.L., Karlyshev, A., Cooper, I.A., Ford, D.C., Wren, B.W., Duffield, M.*, et al.* (2011) *Yersinia pseudotuberculosis mntH* functions in intracellular manganese accumulation, which is essential for virulence and survival in cells expressing functional Nramp1. Microbiology *157*: 1115-1122.

Champion, O.L., Valdez, Y., Thorson, L., Guttman, J.A., Menendez, A., Gaynor, E.C., Finlay, B.B. (2008). A murine intraperitoneal infection model reveals that host resistance to *Campylobacter jejuni* is Nramp1 dependent. Microbes Infect. *10*, 922-927.

Chang, E.C. & Kosman, D.J. (1989) Intracellular Mn (II)-associated superoxide scavenging activity protects Cu,Zn superoxide dismutase-deficient *Saccharomyces cerevisiae* against dioxygen stress. J. Biol. Chem. *264*: 12172-12178.

Corbin, B.D., Seeley, E.H., Raab, A., Feldmann, J., Miller, M.R., Torres, V.J.*, et al.* (2008) Metal chelation and inhibition of bacterial growth in tissue abscesses. Science *319*: 962-965.

Cotruvo, J.A., Jr., Stich, T.A., Britt, R.D. & Stubbe, J. (2013) Mechanism of assembly of the dimanganese-tyrosyl radical cofactor of class Ib ribonucleotide reductase: enzymatic generation of superoxide is required for tyrosine oxidation via a Mn(III)Mn(IV) intermediate. J. Am. Chem. Soc. *135*: 4027-4039.

Cotruvo, J.A. & Stubbe, J. (2011) *Escherichia coli* class Ib ribonucleotide reductase contains a dimanganese(III)-tyrosyl radical cofactor in vivo. Biochemistry *50*: 1672-1681.

Counago, R.M., Ween, M.P., Begg, S.L., Bajaj, M., Zuegg, J., O'Mara, M.L., Cooper, M.A., McEwan, A.G., Paton, J.C., Kobe, B., McDevitt, C.A. (2014). Imperfect coordination chemistry facilitates metal ion release in the Psa permease. Nat. Chem. Biol. *10*, 35-41.

Critchfield, J.W. & Keen, C.L. (1992) Manganese + 2 exhibits dynamic binding to multiple ligands in human plasma. Metabolism *41*: 1087-1092.

Culotta, V.C. & Daly, M.J. (2013) Manganese complexes: diverse metabolic routes to oxidative stress resistance in prokaryotes and yeast. Antioxid. Redox Signal. *19*: 933-944.

Daly, M.J., Gaidamakova, E.K., Matrosova, V.Y., Kiang, J.G., Fukumoto, R., Lee, D.Y.*, et al.* (2010) Small-molecule antioxidant proteome-shields in *Deinococcus radiodurans*. PLOS One *5*: e12570.

Damo, S.M., Kehl-Fie, T.E., Sugitani, N., Holt, M.E., Rathi, S., Murphy, W.J.*, et al.* (2013) Molecular basis for manganese sequestration by calprotectin and roles in the innate immune response to invading bacterial pathogens. Proc. Natl. Acad. Sci. *110*: 3841-3846.

Das, S., Kanamoto, T., Ge, X., Xu, P., Unoki, T., Munro, C.L. & Kitten, T. (2009) Contribution of lipoproteins and lipoprotein processing to endocarditis virulence in *Streptococcus sanguinis*. J. Bacteriol. *191*: 4166-4179.

Davidsson, L., Lonnerdal, B., Sandstrom, B., Kunz, C. & Keen, C.L. (1989) Identification of transferrin as the major plasma carrier protein for manganese introduced orally or intravenously or after in vitro addition in the rat. J. Nutr. *119*: 1461-1464.

Diaz-Ochoa, V.E., Jellbauer, S., Klaus, S. & Raffatellu, M. (2014) Transition metal ions at the crossroads of mucosal immunity and microbial pathogenesis. Front. Cell. Infect. Microbiol. *4*: 2.

Ding, H. & Demple, B. (1997) *In vivo* kinetics of a redox-regulated transcriptional switch. Proc. Natl. Acad. Sci. *94*: 8445-8449.

Dijkshoorn, L., Nemec, A., and Seifert, H. (2007). An increasing threat in hospitals: multidrug-resistant *Acinetobacter baumannii*. Nat. Rev. Microbiol. *5*, 939-951.

Ehrchen, J.M., Sunderkotter, C., Foell, D., Vogl, T. & Roth, J. (2009) The endogenous Toll-like receptor 4 agonist S100A8/S100A9 (calprotectin) as innate amplifier of infection, autoimmunity, and cancer. J. Leukoc. Biol. *86*: 557-566.

Ehrnstorfer, I.A., Geertsma, E.R., Pardon, E., Steyaert, J. & Dutzler, R. (2014) Crystal structure of a SLC11 (NRAMP) transporter reveals the basis for transition-metal ion transport. Nat. Struct. Mol. Biol. *21*: 990-996.

Fetherston, J.D., Mier, I., Jr., Truszczynska, H. & Perry, R.D. (2012) The Yfe and Feo transporters are involved in microaerobic growth and virulence of *Yersinia pestis* in bubonic plague. Infect. Immun. *80*: 3880-3891.

Ferguson, A.D., Deisenhofer, J. (2004). Metal import through microbial membranes. Cell *116*, 15-24.

Fillat, M.F. (2014) The FUR (ferric uptake regulator) superfamily: Diversity and versatility of key transcriptional regulators. Arch. Biochem. Biophys. *546*: 41-52.

Forbes, J.R. & Gros, P. (2003) Iron, manganese, and cobalt transport by Nramp1 (Slc11a1) and Nramp2 (Slc11a2) expressed at the plasma membrane. Blood *102*: 1884-1892.

Gaddy, J.A., Radin, J.N., Loh, J.T., Piazuelo, M.B., Kehl-Fie, T.E., Delgado, A.G., Ilca, F.T., Peek, R.M., Cover, T.L., Chazin, W.J., Skaar, E.P., Scott Algood, H.M. (2014) The host protein calprotectin modulates the *Helicobacter pylori cag* type IV secretion system via zinc sequestration. PLOS Pathog. *10*, e1004450.

Gallagher, L.A., Ramage, E., Weiss, E.J., Radey, M., Hayden, H.S., Held, K.G., Huse, H.K., Zurawski, D.V., Brittnacher, M.J., and Manoil, C. (2015). Resources for genetic and genomic analysis of emerging pathogen *Acinetobacter baumannii*. J. Bacteriol. *197*, 2027-2035.

Gaudu, P., Moon, N. & Weiss, B. (1997) Regulation of the *soxRS* oxidative stress regulon. Reversible oxidation of the Fe-S centers of SoxR *in vivo*. J. Biol. Chem. *272*: 5082-5086.

Gibbons, R.A., Dixon, S.N., Hallis, K., Russell, A.M., Sansom, B.F. & Symonds, H.W. (1976) Manganese metabolism in cows and goats. Biochim. Biophys. Acta. *444*: 1-10.

Golynskiy, M.V., Davis, T.C., Helmann, J.D. & Cohen, S.M. (2005) Metal-induced structural organization and stabilization of the metalloregulatory protein MntR. Biochemistry *44:* 3380-3389.

Gomes, L.H., Raftery, M.J., Yan, W.X., Goyette, J.D., Thomas, P.S., Geczy, C.L. (2013). S100A8 and S100A9-oxidant scavengers in inflammation. Free Radical Biol. Med. *58*, 170-186.

Gomez, M.A., Li, S., Tremblay, M.L. & Olivier, M. (2007) NRAMP-1 expression modulates protein-tyrosine phosphatase activity in macrophages: impact on host cell signaling and functions. J. Biol. Chem. *282*: 36190-36198.

Goswami, T., Bhattacharjee, A., Babal, P., Searle, S., Moore, E., Li, M., Blackwell, J.M. (2001). Natural-resistance-associated macrophage protein 1 is an H+/bivalent cation antiporter. Biochem. J. *354*, 511-519.

Goto, Y., Nakamura, R.M., Takahashi, H., Tokunaga, T. (1984). Genetic control of resistance to *Mycobacterium intracellulare* infection in mice. Infect. Immun. *46*, 135-140.

Govoni, G., Vidal, S., Gauthier, S., Skamene, E., Malo, D., Gros, P. (1996). The Bcg/Ity/Lsh locus: genetic transfer of resistance to infections in C57BL/6J mice transgenic for the Nramp1 Gly169 allele. Infect. Immun. *64*, 2923-2929.

Goyette, J. & Geczy, C.L. (2011) Inflammation-associated S100 proteins: new mechanisms that regulate function. Amino Acids *41*: 821-842.

Greenberg, J.T., Monach, P., Chou, J.H., Josephy, P.D. & Demple, B. (1990) Positive control of a global antioxidant defense regulon activated by superoxide-generating agents in *Escherichia coli*. Proc. Natl. Acad. Sci. *87*: 6181-6185.

Gruenheid, S., Canonne-Hergaux, F., Gauthier, S., Hackam, D.J., Grinstein, S., Gros, P. (1999). The iron transport protein NRAMP2 is an integral membrane glycoprotein that colocalizes with transferrin in recycling endosomes. J. Ex. Med. *189*, 831-841.

Gu, M. & Imlay, J.A. (2011) The SoxRS response of *Escherichia coli* is directly activated by redox-cycling drugs rather than by superoxide. Mol. Microbiol. *79*: 1136-1150.

Guedon, E., Moore, C.M., Que, Q., Wang, T., Ye, R.W. & Helmann, J.D. (2003) The global transcriptional response of *Bacillus subtilis* to manganese involves the MntR, Fur, TnrA and sigmaB regulons. Mol. Microbiol. *49*: 1477-1491.

Guerinot, M.L. (1994) Microbial iron transport. Annu. Rev. Microbiol. *48*: 743-772.

Gustafsson, D., Breimer, L.H., Isaksson, H.S. & Nilsson, T.K. (2012) Tissue zinc levels in a child with hypercalprotectinaemia and hyperzincaemia: A case report and a review of the literature. Scand. J. Clin. Lab. Invest. *72*: 34-38.

Hayden, J.A., Brophy, M.B., Cunden, L.S., Nolan, E.M. (2013). High-affinity manganese coordination by human calprotectin is calcium-dependent and requires the histidine-rich site formed at the dimer interface. J. Am. Chem. Soc. *135*, 775-787.

Helmann, J.D. (2014) Specificity of metal sensing: iron and manganese homeostasis in *Bacillus subtilis*. J. Biol. Chem. *289*: 28112-28120.

Hidalgo, E., Ding, H. & Demple, B. (1997) Redox signal transduction: mutations shifting [2Fe-2S] centers of the SoxR sensor-regulator to the oxidized form. Cell *88*: 121-129.

Higgins, C.F. (1992) ABC transporters: from microorganisms to man. Annu. Rev. Cell. Biol. *8*: 67-113.

Hofmann, M.A., Drury, S., Fu, C., Qu, W., Taguchi, A., Lu, Y.*, et al.* (1999) RAGE mediates a novel proinflammatory axis: a central cell surface receptor for S100/calgranulin polypeptides. Cell *97*: 889-901.

Hohle, T.H., Franck, W.L., Stacey, G. & O'Brian, M.R. (2011) Bacterial outer membrane channel for divalent metal ion acquisition. Proc. Natl. Acad. Sci. *108*: 15390-15395.

Hood, M.I., Mortensen, B.L., Moore, J.L., Zhang, Y., Kehl-Fie, T.E., Sugitani, N.*, et al.* (2012) Identification of an *Acinetobacter baumannii* zinc acquisition system that facilitates resistance to calprotectin-mediated zinc sequestration. PLOS Pathog. *8*: e1003068.

Hood, M.I., Skaar, E.P. (2012). Nutritional immunity: transition metals at the pathogen-host interface. Nat. Rev. Micrbiol. *10,* 525-537.

Horsburgh, M.J., Wharton, S.J., Cox, A.G., Ingham, E., Peacock, S. & Foster, S.J. (2002) MntR modulates expression of the PerR regulon and superoxide resistance in *Staphylococcus aureus* through control of manganese uptake. Mol. Microbiol. *44:* 1269-1286.

Horning, K.J., Caito, S.W., Tipps, K.G., Bowman, A.B., Aschner, M. (2015) Manganese is essential for neuronal health. Ann. Rev. Nutr. *35*, 71-108.

House, D., Bishop, A., Parry, C., Dougan, G., Wain, J. (2001). Typhoid fever: pathogenesis and disease. Curr. Opin. Infect. Dis. *14*, 573-578.

Ibrahim, Z.A., Armour, C.L., Phipps, S., Sukkar, M.B. (2013). RAGE and TLRs: relatives, friends or neighbours? Mol. Immunol. *56*, 739-744.

Ikeda, J.S., Janakiraman, A., Kehres, D.G., Maguire, M.E. & Slauch, J.M. (2005) Transcriptional regulation of *sitABCD* of *Salmonella enterica* serovar Typhimurium by MntR and Fur. J. Bacteriol. *187*: 912-922.

Imlay, J.A. (2014) The mismetallation of enzymes during oxidative stress. J. Biol. Chem. *289*: 28121-28128.

Inaoka, T., Matsumura, Y. & Tsuchido, T. (1999) SodA and manganese are essential for resistance to oxidative stress in growing and sporulating cells of *Bacillus subtilis*. J. Bacteriol. *181*: 1939-1943.

Italiani, P., Boraschi, D. (2014). From monocytes to M1/M2 macrophages: phenotypical vs. functional differentiation. Front. Immunol. *5*, 514.

Jabado, N., Jankowski, A., Dougaparsad, S., Picard, V., Grinstein, S. & Gros, P. (2000) Natural resistance to intracellular infections: natural resistance-associated macrophage protein 1 (Nramp1) functions as a pH-dependent manganese transporter at the phagosomal membrane. J. Exp. Med. *192*: 1237-1248.

Jacobsen, F.E., Kazmierczak, K.M., Lisher, J.P., Winkler, M.E. & Giedroc, D.P. (2011) Interplay between manganese and zinc homeostasis in the human pathogen *Streptococcus pneumoniae*. Metallomics *3*: 38-41.

Jakubovics, N.S. & Jenkinson, H.F. (2001) Out of the iron age: new insights into the critical role of manganese homeostasis in bacteria. Microbiology *147:* 1709-1718.

Johnston, J.W., Briles, D.E., Myers, L.E. & Hollingshead, S.K. (2006) Mn2+-dependent regulation of multiple genes in *Streptococcus pneumoniae* through PsaR and the resultant impact on virulence. Infect. Immun. *74*: 1171-1180.

Juttukonda, L.J., and Skaar, E.P. (2015). Manganese homeostasis and utilization in pathogenic bacteria. Mol. Microbiol. *97*, 216-228.

Keen, C.L., Ensunsa, J.L. & Clegg, M.S. (2000) Manganese metabolism in animals and humans including the toxicity of manganese. Met. Ions. Biol. Syst. *37*: 89-121.

Kehl-Fie, T.E. & Skaar, E.P. (2010) Nutritional immunity beyond iron: a role for manganese and zinc. Curr. Opin. Chem. Biol. *14*: 218-224.

Kehl-Fie, T.E., Chitayat, S., Hood, M.I., Damo, S., Restrepo, N., Garcia, C., Munro, K.A., Chazin, W.J., and Skaar, E.P. (2011). Nutrient metal sequestration by calprotectin inhibits bacterial superoxide defense, enhancing neutrophil killing of *Staphylococcus aureus*. Cell Host Microbe *10*, 158-164.

Kehl-Fie, T.E., Zhang, Y., Moore, J.L., Farrand, A.J., Hood, M.I., Rathi, S.*, et al.* (2013) MntABC and MntH contribute to systemic *Staphylococcus aureus* infection by competing with calprotectin for nutrient manganese. Infect. Immun. *81*: 3395-3405.

Kehres, D.G., Janakiraman, A., Slauch, J.M. & Maguire, M.E. (2002) Regulation of *Salmonella enterica* serovar Typhimurium *mntH* transcription by H(2)O(2), Fe(2+), and Mn(2+). J. Bacteriol. *184*: 3151-3158.

Kehres, D.G. & Maguire, M.E. (2003) Emerging themes in manganese transport, biochemistry and pathogenesis in bacteria. FEMS Microbiol. Rev. *27*: 263-290.

King, J.C. (2011). Zinc: an essential but elusive nutrient. Am. J. Clin. Nutr. *94,* 679S-684S.

Kliegman, J.I., Griner, S.L., Helmann, J.D., Brennan, R.G. & Glasfeld, A. (2006) Structural basis for the metal-selective activation of the manganese transport regulator of *Bacillus subtilis*. *Biochemistry* **45**: 3493-3505.

Korndorfer, I.P., Brueckner, F. & Skerra, A. (2007) The crystal structure of the human (S100A8/S100A9)2 heterotetramer, calprotectin, illustrates how conformational changes of interacting alpha-helices can determine specific association of two EF-hand proteins. J. Mol. Biol. *370*: 887-898.

Kumar, A., Dalton, C., Cortez-Cordova, J., and Schweizer, H.P. (2010). Mini-Tn7 vectors as genetic tools for single copy gene cloning in *Acinetobacter baumannii*. J. Microbiol. Methods. *82*, 296-300.

Kupz, A., Fischer, A., Nies, D.H., Grass, G., Gobel, U.B., Bereswill, S. & Heimesaat, M.M. (2013) Impact of metal ion homeostasis of genetically modified *Escherichia coli* Nissle 1917 and K12 (W3110) strains on colonization properties in the murine intestinal tract. Eur. J. Microbiol. Immunol. *3*: 229-235.

Lam-Yuk-Tseung, S., Picard, V., Gros, P. (2006). Identification of a tyrosine-based motif (YGSI) in the amino terminus of Nramp1 (Slc11a1) that is important for lysosomal targeting. J. Biol. Chem. *281*, 31677-31688.

Leclercq, V., Lebastard, M., Belkaid, Y., Louis, J., Milon, G. (1996). The outcome of the parasitic process initiated by *Leishmania infantum* in laboratory mice: a tissue-dependent pattern controlled by the Lsh and MHC loci. J. Immunol. *157*, 4537-4545.

Lee, J.W. & Helmann, J.D. (2006) The PerR transcription factor senses H2O2 by metal-catalysed histidine oxidation. Nature *440*: 363-367.

Lee, J.W. & Helmann, J.D. (2007) Functional specialization within the Fur family of metalloregulators. Biometals *20*: 485-499.

Leukert, N., Vogl, T., Strupat, K., Reichelt, R., Sorg, C. & Roth, J. (2006) Calcium-dependent tetramer formation of S100A8 and S100A9 is essential for biological activity. J. Mol. Biol. *359*: 961-972.

Li, Q., Meng, H., Zhang, L., Xu, L., Chen, Z., Shi, D.*, et al.* (2007) Correlation between single nucleotide polymorphisms in a calprotectin subunit gene and risk of periodontitis in a Chinese population. Ann. Hum. Genet. *71*: 312-324.

Li, X., Yang, Y., Zhou, F., Zhang, Y., Lu, H., Jin, Q. & Gao, L. (2011) *SLC11A1* (NRAMP1) polymorphisms and tuberculosis susceptibility: updated systematic review and meta-analysis. PLOS One *6*: e15831.

Lin, Y.P., Kuo, C.J., Koleci, X., McDonough, S.P., Chang, Y.F., 2011. Manganese binds to Clostridium difficile Fbp68 and is essential for fibronectin binding. J. Biol. Chem. *286*, 3957-3969.

Lisher, J.P. & Giedroc, D.P. (2013) Manganese acquisition and homeostasis at the host-pathogen interface. Front. Cell. Infect. Microbiol. *3*: 91.

Liu, J.Z., Jellbauer, S., Poe, A.J., Ton, V., Pesciaroli, M., Kehl-Fie, T.E., Restrepo, N.A., Hosking, M.P., Edwards, R.A., Battistoni, A., Pasquali, P., Lane, T.E., Chazin, W.J., Vogl, T., Roth, J., Skaar, E.P., Raffatellu, M. (2012). Zinc sequestration by the neutrophil protein calprotectin enhances *Salmonella* growth in the inflamed gut. Cell Host Microbe *11*, 227-239.

Lonnerdal, B., Keen, C.L. & Hurley, L.S. (1985) Manganese binding proteins in human and cow's milk. Am. J. Clin. Nutr. *41*: 550-559.

Luepke, K.H., Suda, K.J., Boucher, H., Russo, R.L., Bonney, M.W., Hunt, T.D., and Mohr, J.F., 3rd (2017). Past, present, and future of antibacterial economics: increasing bacterial resistance, limited antibiotic pipeline, and societal implications. Pharmacotherapy *37*, 71-84.

Lusitani, D., Malawista, S.E. & Montgomery, R.R. (2003) Calprotectin, an abundant cytosolic protein from human polymorphonuclear leukocytes, inhibits the growth of *Borrelia burgdorferi*. Infect. Immun. *71*: 4711-4716.

Makhlynets, O., Boal, A.K., Rhodes, D.V., Kitten, T., Rosenzweig, A.C. & Stubbe, J. (2014) *Streptococcus sanguinis* Class Ib Ribonucleotide Reductase: high activity with both iron and manganese cofactors and structural insights. J. Biol. Chem. *289*: 6259-6272.

Makthal, N., Rastegari, S., Sanson, M., Ma, Z., Olsen, R.J., Helmann, J.D.*, et al.* (2013) Crystal structure of peroxide stress regulator from *Streptococcus pyogenes* provides functional insights into the mechanism of oxidative stress sensing. J. Biol. Chem. *288*: 18311-18324.

Makui, H., Roig, E., Cole, S.T., Helmann, J.D., Gros, P. & Cellier, M.F. (2000) Identification of the *Escherichia coli* K-12 Nramp orthologue (MntH) as a selective divalent metal ion transporter. Mol. Microbiol. *35*: 1065-1078.

Mambula, S.S., Simons, E.R., Hastey, R., Selsted, M.E., Levitz, S.M. (2000). Human neutrophil-mediated nonoxidative antifungal activity against *Cryptococcus neoformans*. Infect. Immun. *68*, 6257-6264.

Mantovani, A., Cassatella, M.A., Costantini, C., Jaillon, S. (2011). Neutrophils in the activation and regulation of innate and adaptive immunity. Nat. Rev. Immunol. *11*, 519-531.

Marionnet, C., Bernerd, F., Dumas, A., Verrecchia, F., Mollier, K., Compan, D.*, et al.* (2003) Modulation of gene expression induced in human epidermis by environmental stress *in vivo*. J. Invest. Dermatol. *121*: 1447-1458.

Marra, A., Lawson, S., Asundi, J.S., Brigham, D. & Hromockyj, A.E. (2002) *In vivo* characterization of the *psa* genes from *Streptococcus pneumoniae* in multiple models of infection. Microbiology *148:* 1483-1491.

Martin, J.E. & Imlay, J.A. (2011) The alternative aerobic ribonucleotide reductase of *Escherichia coli*, NrdEF, is a manganese-dependent enzyme that enables cell replication during periods of iron starvation. Mol. Microbiol. *80*: 319-334.

Martinez, A. & Kolter, R. (1997) Protection of DNA during oxidative stress by the nonspecific DNA-binding protein Dps. J. Bacteriol. *179*: 5188-5194.

Merchant, A.T. & Spatafora, G.A. (2014) A role for the DtxR family of metalloregulators in gram-positive pathogenesis. Mol. Oral. Microbiol. *29:* 1-10.

Moisan, J., Thuraisingam, T., Henault, J., De Sanctis, J. & Radzioch, D. (2006) Role of SLC11A1 (formerly NRAMP1) in regulation of signal transduction induced by Toll-like receptor 7 ligands. FEMS. Immunol. Med. Microbiol. *47:* 138-147.

Moore, J.L., Becker, K.W., Nicklay, J.J., Boyd, K.L., Skaar, E.P. & Caprioli, R.M. (2014) Imaging mass spectrometry for assessing temporal proteomics: analysis of calprotectin in *Acinetobacter baumannii* pulmonary infection. Proteomics *14:* 820-828.

Moutafchiev, D., Sirakov, L. & Bontchev, P. (1998) The competition between transferrins labeled with 59Fe, 65Zn, and 54Mn for the binding sites on lactating mouse mammary gland cells. Biol. Trace. Elem. Res. *61*: 181-191.

Nairz, M., Fritsche, G., Crouch, M.L., Barton, H.C., Fang, F.C., Weiss, G. (2009). Slc11a1 limits intracellular growth of *Salmonella enterica* sv. Typhimurium by promoting macrophage immune effector functions and impairing bacterial iron acquisition. Cell. Microbiol. *11*, 1365-1381

Nairz, M., Haschka, D., Demetz, E., Weiss, G. (2014). Iron at the interface of immunity and infection. Front. Pharmacol. *5*, 152.

Nevo, Y., Nelson, N. (2006). The NRAMP family of metal-ion transporters. Biochim. Biophys. Acta *1763*, 609-620.

Nguyen, K.H. & Grove, A. (2012) Metal binding at the *Deinococcus radiodurans* Dps-1 N-terminal metal site controls dodecameric assembly and DNA binding. Biochemistry *51*: 6679-6689.

Outten, C.E. & O'Halloran, T.V. (2001) Femtomolar sensitivity of metalloregulatory proteins controlling zinc homeostasis. Science *292*: 2488-2492.

Ouyang, Z., He, M., Oman, T., Yang, X.F. & Norgard, M.V. (2009) A manganese transporter, BB0219 (BmtA), is required for virulence by the Lyme disease spirochete, *Borrelia burgdorferi*. Proc. Natl. Acad. Sci. *106*: 3449-3454.

Paik, S., Brown, A., Munro, C.L., Cornelissen, C.N. & Kitten, T. (2003) The *sloABCR* operon of *Streptococcus mutans* encodes an Mn and Fe transport system required for endocarditis virulence and its Mn-dependent repressor. J. Bacteriol. *185*: 5967-5975.

Papp-Wallace, K.M. & Maguire, M.E. (2006) Manganese transport and the role of manganese in virulence. Annu. Rev. Microbiol. *60*: 187-209.

Patzer, S.I. & Hantke, K. (2001) Dual repression by Fe(2+)-Fur and Mn(2+)-MntR of the *mntH* gene, encoding an NRAMP-like Mn(2+) transporter in *Escherichia coli*. J. Bacteriol**.** *183:* 4806-4813.

Perry, R.D., Craig, S.K., Abney, J., Bobrov, A.G., Kirillina, O., Mier, I., Jr*., et al.* (2012) Manganese transporters Yfe and MntH are Fur-regulated and important for the virulence of *Yersinia pestis*. Microbiology *158*: 804-815.

Pompilio, A., Ciavardelli, D., Crocetta, V., Consalvo, A., Zappacosta, R., Di Ilio, C. & Di Bonaventura, G. (2014) *Stenotrophomonas maltophilia* virulence and specific variations in trace elements during acute lung infection: implications in cystic fibrosis. PLOS On*e 9*: e88769.

Porcheron, G., Garenaux, A., Proulx, J., Sabri, M. & Dozois, C.M. (2013) Iron, copper, zinc, and manganese transport and regulation in pathogenic Enterobacteria: correlations between strains, site of infection and the relative importance of the different metal transport systems for virulence. Front. Cell. Infect. Microbiol. *3*: 90.

Posey, J.E. & Gherardini, F.C. (2000) Lack of a role for iron in the Lyme disease pathogen. Science *288*: 1651-1653.

Que, Q. & Helmann, J.D. (2000) Manganese homeostasis in *Bacillus subtilis* is regulated by MntR, a bifunctional regulator related to the diphtheria toxin repressor family of proteins. Mol. Microbiol. *35*: 1454-1468.

Rahil-Khazen, R., Bolann, B.J., Myking, A. & Ulvik, R.J. (2002) Multi-element analysis of trace element levels in human autopsy tissues by using inductively coupled atomic emission spectrometry technique (ICP-AES). J. Trace Elem. Med. Biol. *16*: 15-25.

Rammes, A., Roth, J., Goebeler, M., Klempt, M., Hartmann, M. & Sorg, C. (1997) Myeloid-related protein (MRP) 8 and MRP14, calcium-binding proteins of the S100 family, are secreted by activated monocytes via a novel, tubulin-dependent pathway. J. Biol. Chem. *272*: 9496-9502.

Rhodes, D.V., Crump, K.E., Makhlynets, O., Snyder, M., Ge, X., Xu, P*., et al.* (2014) Genetic Characterization and Role in Virulence of the Ribonucleotide Reductases of *Streptococcus sanguinis*. J. Biol. Chem. *289*: 6273-6287.

Roberts, A.A., Sharma, S.V., Strankman, A.W., Duran, S.R., Rawat, M., Hamilton, C.J. (2013) Mechanistic studies of FosB: a divalent-metal-dependent bacillithiol-S-transferase that mediates fosfomycin resistance in *Staphylococcus aureus.* Biochem. J. *451,* 69-79.

Rolfe, M.D., Rice, C.J., Lucchini, S., Pin, C., Thompson, A., Cameron, A.D*., et al*. (2012) Lag phase is a distinct growth phase that prepares bacteria for exponential growth and involves transient metal accumulation. J. Bacteriol. *194:* 686-701.

Rosch, J.W., Gao, G., Ridout, G., Wang, Y.D. & Tuomanen, E.I. (2009) Role of the manganese efflux system mntE for signalling and pathogenesis in *Streptococcus pneumoniae*. Mol. Microbiol. *72*: 12-25.

Runyen-Janecky, L., Dazenski, E., Hawkins, S. & Warner, L. (2006) Role and regulation of the *Shigella flexneri sit* and MntH systems. Infect. Immun. *74*: 4666-4672.

Sabri, M., Caza, M., Proulx, J., Lymberopoulos, M.H., Bree, A., Moulin-Schouleur, M*., et al.* (2008) Contribution of the SitABCD, MntH, and FeoB metal transporters to the virulence of avian pathogenic *Escherichia coli* O78 strain chi7122. Infect. Immun. *76:* 601-611.

Sampson, B., Fagerhol, M.K., Sunderkotter, C., Golden, B.E., Richmond, P., Klein, N*., et al.* (2002) Hyperzincaemia and hypercalprotectinaemia: a new disorder of zinc metabolism. Lancet *360*: 1742-1745.

Scheuhammer, A.M. & Cherian, M.G. (1985) Binding of manganese in human and rat plasma. Biochim. Biophys. Acta *840*: 163-169.

Schmitt, M.P. (2002) Analysis of a DtxR-like metalloregulatory protein, MntR, from *Corynebacterium diphtheriae* that controls expression of an ABC metal transporter by an Mn(2+)-dependent mechanism. J. Bacteriol. *184*: 6882-6892.

Schroeder, H.A., Balassa, J.J., Tipton, I.H. (1966) Essential trace metals in man: manganese. A study in homeostasis. J. Chronic. Dis. *19*, 545-571.

Seib, K.L., Tseng, H.J., McEwan, A.G., Apicella, M.A. & Jennings, M.P. (2004) Defenses against oxidative stress in *Neisseria gonorrhoeae* and *Neisseria meningitidis*: distinctive systems for different lifestyles. J. Infect. Dis. *190*: 136-147.

Sharma, A., Gaidamakova, E.K., Matrosova, V.Y., Bennett, B., Daly, M.J. & Hoffman, B.M. (2013) Responses of Mn2+ speciation in *Deinococcus radiodurans* and *Escherichia coli* to gamma-radiation by advanced paramagnetic resonance methods. Proc. Natl. Acad. Sci. *110*: 5945-5950.

Shawki, A., Knight, P.B., Maliken, B.D., Niespodzany, E.J., Mackenzie, B. (2012) H(+)-coupled divalent metal-ion transporter-1: functional properties, physiological roles and therapeutics. Curr. Top. Mem. *70*, 169-214.

Sobota, J.M., Gu, M. & Imlay, J.A. (2014) Intracellular hydrogen peroxide and superoxide poison 3-deoxy-D-arabinoheptulosonate 7-phosphate synthase, the first committed enzyme in the aromatic biosynthetic pathway of *Escherichia coli*. J. Bacteriol. *196*: 1980-1991.

Sobota, J.M. & Imlay, J.A. (2011) Iron enzyme ribulose-5-phosphate 3-epimerase in *Escherichia coli* is rapidly damaged by hydrogen peroxide but can be protected by manganese. Proc. Natl. Acad. Sci. *108*: 5402-5407.

Sohnle, P.G., Collins-Lech, C. & Wiessner, J.H. (1991) The zinc-reversible antimicrobial activity of neutrophil lysates and abscess fluid supernatants. J. Infect. Dis. *164*: 137-142.

Sohnle, P.G., Hunter, M.J., Hahn, B., Chazin, W.J. (2000) Zinc-reversible antimicrobial activity of recombinant calprotectin (migration inhibitory factor-related proteins 8 and 14). J. Infect. Dis. *182*, 1272-1275.

Srikanth, S. & Gwack, Y. (2013) Measurement of intracellular Ca2+ concentration in single cells using ratiometric calcium dyes. Methods Mol. Biol. *963*: 3-14.

Steinbakk, M., Naess-Andresen, C.F., Lingaas, E., Dale, I., Brandtzaeg, P. & Fagerhol, M.K. (1990) Antimicrobial actions of calcium binding leucocyte L1 protein, calprotectin. Lancet *336*: 763-765.

Stubbe, J. & Cotruvo, J.A., Jr. (2011) Control of metallation and active cofactor assembly in the class Ia and Ib ribonucleotide reductases: diiron or dimanganese? Curr. Opin. Chem. Biol. *15*: 284-290.

Su, M., Cavallo, S., Stefanini, S., Chiancone, E. & Chasteen, N.D. (2005) The so-called Listeria innocua ferritin is a Dps protein. Iron incorporation, detoxification, and DNA protection properties. Biochemistry *44:* 5572-5578.

Sun, X., Meng, H., Shi, D., Xu, L., Zhang, L., Chen, Z.*, et al.* (2011) Analysis of plasma calprotectin and polymorphisms of S100A8 in patients with aggressive periodontitis. J. Periodontal Res. *46:* 354-360.

Tabares, L.C. & Un, S. (2013) In situ determination of manganese(II) speciation in *Deinococcus radiodurans* by high magnetic field EPR: detection of high levels of Mn(II) bound to proteins. J. Biol. Chem. *288*: 5050-5055.

Thompson, M.K., Keithly, M.E., Goodman, M.C., Hammer, N.D., Cook, P.D., Jagessar, K.L., Harp, J., Skaar, E.P., Armstrong, R.N. (2014). Structure and function of the genomically encoded fosfomycin resistance enzyme, FosB, from *Staphylococcus aureus*. Biochemistry *53*, 755-765.

Tong, S.Y., Davis, J.S., Eichenberger, E., Holland, T.L., Fowler, V.G., Jr. (2015) *Staphylococcus aureus* infections: epidemiology, pathophysiology, clinical manifestations, and management. Clin. Microbiol. Rev. *28*, 603-661.

Troxell, B. & Yang, X.F. (2013) Metal-dependent gene regulation in the causative agent of Lyme disease. Front. Cell. Infect. Microbiol. *3*: 79.

Tsaneva, I.R. & Weiss, B. (1990) *soxR*, a locus governing a superoxide response regulon in *Escherichia coli* K-12. J. Bacteriol. *172*: 4197-4205.

Tseng, H.J., Srikhanta, Y., McEwan, A.G. & Jennings, M.P. (2001) Accumulation of manganese in *Neisseria gonorrhoeae* correlates with resistance to oxidative killing by superoxide anion and is independent of superoxide dismutase activity. Mol. Microbiol. *40:* 1175-1186.

Tucker, A.T., Nowicki, E.M., Boll, J.M., Knauf, G.A., Burdis, N.C., Trent, M.S., and Davies, B.W. (2014). Defining gene-phenotype relationships in *Acinetobacter baumannii* through one-step chromosomal gene inactivation. mBio *5*, e01313-01314.

Uhlen, M., Fagerberg, L., Hallstrom, B.M., Lindskog, C., Oksvold, P., Mardinoglu, A.*, et al.* (2015) Proteomics. Tissue-based map of the human proteome. Science *347:* 1260419.

Urban, C.F., Ermert, D., Schmid, M., Abu-Abed, U., Goosmann, C., Nacken, W., Brinkmann, V., Jungblut, P.R., Zychlinsky, A. (2009) Neutrophil extracellular traps contain calprotectin, a cytosolic protein complex involved in host defense against *Candida albicans*. PLOS Pathog. *5,* e1000639.

van Opijnen, T. & Camilli, A. (2013) Transposon insertion sequencing: a new tool for systems-level analysis of microorganisms. Nat. Rev. Microbiol. *11*: 435-442.

Vidal, S.M., Pinner, E., Lepage, P., Gauthier, S., Gros, P. (1996) Natural resistance to intracellular infections: Nramp1 encodes a membrane phosphoglycoprotein absent in macrophages from susceptible (Nramp1 D169) mouse strains. J. Immunol. *157*, 3559-3568.

Veyrier, F.J., Boneca, I.G., Cellier, M.F. & Taha, M.K. (2011) A novel metal transporter mediating manganese export (MntX) regulates the Mn to Fe intracellular ratio and *Neisseria meningitidis* virulence. PLOS Pathog. *7*: e1002261.

Vogl, T., Leukert, N., Barczyk, K., Strupat, K. & Roth, J. (2006) Biophysical characterization of S100A8 and S100A9 in the absence and presence of bivalent cations. Biochim. Biophys. Acta *1763:* 1298-1306.

Wertheim, H.F., Melles, D.C., Vos, M.C., van Leeuwen, W., van Belkum, A., Verbrugh, H.A., and Nouwen, J.L. (2005). The role of nasal carriage in *Staphylococcus aureus* infections. Lancet Infect. Dis. *5*, 751-762.

WHO (2017). Global priority list of antibiotic-resistant bacteria to guide research, discovery, and development of new antibiotics. http://www.who.int/medicines/publications/WHO-PPL-Short_Summary_25Feb-ET_NM_WHO.pdf.

Wichgers Schreur, P.J., Rebel, J.M., Smits, M.A., van Putten, J.P. & Smith, H.E. (2011) TroA of *Streptococcus suis* is required for manganese acquisition and full virulence. J. Bacteriol. *193:* 5073-5080.

Zackular, J.P., Chazin, W.J., Skaar, E.P. (2015) Nutritional Immunity: S100 Proteins at the Host-Pathogen Interface. J. Biol. Chem. *31*: 18991-18998.

Zaharik, M.L., Cullen, V.L., Fung, A.M., Libby, S.J., Kujat Choy, S.L., Coburn, B., Kehres, D.G., Maguire, M.E., Fang, F.C., Finlay, B.B. (2004) The *Salmonella enterica* serovar typhimurium divalent cation transport systems MntH and SitABCD are essential for virulence in an Nramp1G169 murine typhoid model. Infect. Immun. *72*, 5522-5525.

Zaharik, M.L. & Finlay, B.B. (2004) Mn2+ and bacterial pathogenesis. Front. Biosci. *9:* 1035-1042.

Zhang, Y. & Stubbe, J. (2011) *Bacillus subtilis* class Ib ribonucleotide reductase is a dimanganese(III)-tyrosyl radical enzyme. Biochemistry *50*: 5615-5623.

Zhao, G., Ceci, P., Ilari, A., Giangiacomo, L., Laue, T.M., Chiancone, E. & Chasteen, N.D. (2002) Iron and hydrogen peroxide detoxification properties of DNA-binding protein from starved cells. A ferritin-like DNA-binding protein of *Escherichia coli*. J. Biol. Chem. *277*: 27689-27696.

A version of the following section (*Chapter II, Acinetobacter baumannii coordinates urea metabolism with metal import to resist host-mediated metal limitation*) was previously published in mBio 7(5), e01475-16 (September 2016) | doi:10.1128/mBio.01475-16.

CHAPTER II

ACINETOBACTER BAUMANNII COORDINATES UREA METABOLISM WITH METAL IMPORT TO RESIST HOST-MEDIATED METAL LIMITATION

Introduction

During infection, bacterial pathogens must adapt to a nutrient metal-limited environment that is imposed by the host. The innate immune protein calprotectin inhibits bacterial growth *in vitro* by chelating the divalent metal ions zinc (Zn^{2+}, Zn) and manganese (Mn^{2+}, Mn), but pathogenic bacteria are able to cause disease in the presence of this antimicrobial protein *in vivo.* One such pathogen is *A. baumannii,* a Gram-negative bacterium that causes pneumonia and bloodstream infections complicated by resistance to multiple antibiotics. *A. baumannii* inhibition by calprotectin is dependent on calprotectin Mn binding, but the mechanisms employed by *A. baumannii* to overcome Mn limitation have not been identified. The work described in this Chapter demonstrates that *A. baumannii* coordinates transcription of an NRAMP-family Mn transporter and a urea carboxylase to resist the antimicrobial activities of calprotectin. This NRAMP-family transporter facilitates Mn accumulation and growth of *A. baumannii* in the presence of calprotectin. *A. baumannii* is found to utilize urea as a sole nitrogen source, and urea utilization requires the urea carboxylase encoded in an operon with the NRAMP-family transporter. Moreover, urea carboxylase activity is essential for calprotectin resistance in *A. baumannii.* Finally, evidence is provided that this system combats calprotectin *in vivo,* as deletion of the transporter impairs *A. baumannii* fitness in a mouse model of pneumonia

and this fitness defect is modulated by the presence of calprotectin. These findings reveal that *A. baumannii* has evolved mechanisms to subvert host-mediated metal sequestration and uncover a connection between metal starvation and metabolic stress.

A. baumannii is a Gram-negative bacterium and an opportunistic pathogen that has emerged as an important cause of infection, especially in critically ill patients (Dexter et al., 2015; Peleg and Hooper, 2010). While *A. baumannii* is capable of infecting many organs in the human body, this bacterium is most commonly associated with infections of the lung, accounting for 7% of ventilator-associated pneumonias (Sievert et al., 2013). Most *A. baumannii* infections are caused by strains that are resistant to at least three classes of antibiotics, rendering treatment of *A. baumannii* infections challenging (Kaye and Pogue, 2015). Due to the threat posed by *A. baumannii* to human health, it is of paramount importance to improve the current understanding of *A. baumannii* pathogenesis, particularly of the bacterial response to antimicrobial strategies of the host.

A key aspect of host defense against bacterial infection is termed 'nutritional immunity', which includes sequestration of nutrient metals (Hood and Skaar, 2012). Host-mediated bacterial metal starvation was first described for iron (Fe), but has now been extended to zinc and manganese following the discovery of the multiple metal chelating properties of the S100 protein calprotectin (Corbin et al., 2008). Calprotectin is a heterodimer of S100A8 and S100A9 (also known as calgranulin A and B or MRP8 and MRP14) that binds Zn^{2+} (Zn), Mn^{2+} (Mn), and Fe^{2+} ions *in vitro* with high affinity at the dimer interface (Brophy et al., 2013; Damo et al., 2013; Nakashige et al., 2015).

Calprotectin is important for host defense against *A. baumannii* in the lung. Calprotectin comprises 45% of the cytoplasmic protein in neutrophils (Edgeworth et al.,

1991), and *A. baumannii* infection of the murine lung leads to robust recruitment of neutrophils, which are necessary for bacterial clearance (van Faassen et al., 2007). Neutrophil recruitment causes a dramatic accumulation of calprotectin that co-localizes with sites of lobar inflammation and *A. baumannii* colonization (Moore et al., 2014). Calprotectin-deficient mice have increased bacterial burdens and mortality from *A. baumannii* pneumonia (Hood et al., 2012). Finally, recombinant calprotectin inhibits *A. baumannii* growth *in vitro*, and this is dependent on an intact hexahistidine Mn binding site within calprotectin; this finding suggests that *A. baumannii* requires Mn for full fitness (Damo et al., 2013; Hood et al., 2012).

Mn is an essential cofactor for life and is predominantly utilized as a redox-active cofactor for enzymes, including superoxide dismutase and ribonucleotide reductase (Juttukonda and Skaar, 2015). Several families of Mn transporters have been identified in bacteria. The most widely conserved of these are Mn ATP-binding cassette (ABC) transporters and the natural resistance-associated macrophage protein (NRAMP) family of Mn transporters, which are important for the virulence of many bacterial pathogens (Juttukonda and Skaar, 2015). NRAMP family transporters are transmembrane proteins that utilize the proton-motive force as an energy source for transport (Juttukonda and Skaar, 2015). In the pathogen *S. aureus*, both an NRAMP family transporter and an ABC family Mn transporter are important for bacterial resistance to calprotectin (Kehl-Fie et al., 2013). To date, no Mn transporters have been characterized in *A. baumannii.*

Calprotectin-mediated Mn deprivation restricts *A. baumannii* growth presumably because Mn-dependent bacterial processes are rendered inactive without their cognate cofactor. However, exactly which bacterial processes are inhibited and how the bacterium

responds to these alterations in physiology remain unknown. For instance, multiple metabolic enzymes involved in carbon metabolism, including phosphoglyceromutase (Fraser et al., 1999) and pyruvate carboxylase (Milrad de Forchetti and Cazzulo, 1976), require Mn or are activated by Mn, but whether central metabolic processes are altered by calprotectin-mediated Mn sequestration is unclear. We hypothesized that understanding the effects of calprotectin exposure on *A. baumannii* physiology *in vitro* may uncover bacterial processes essential for infection in niches where calprotectin is abundant.

The overall goal of this study was to identify mechanisms by which *A. baumannii* overcomes calprotectin-based nutritional immunity. An operon that contains a putative Mn transporter and urea catabolism enzymes from the urea amidolyase family was identified. Based on transcriptional regulation, we hypothesized that urea amidolyase is a component of the *A. baumannii* response to calprotectin-mediated Mn sequestration. Mn transport was demonstrated to be important for growth in the presence of calprotectin and colonization of the murine lung. Urea catabolism was found to be vital for growth in the presence of calprotectin and functionally linked to Mn acquisition in *A. baumannii*. Taken together, these results uncover that host-mediated metal sequestration restricts metabolism in bacterial pathogens and broaden the understanding of the bacterial factors required to survive this restriction.

Materials and Methods

Bacterial strains and reagents. The strains used in this study are described in **Table 1**. All strains are derivatives of the human clinical isolate *A. baumannii* ATCC 17978. Cloning was performed in *E. coli* DH5α. Bacteria were routinely grown in lysogeny broth

(LB) at 37°C unless otherwise noted. Solid medium contained 1.5% agar. Antibiotics were added at the following concentrations for *A. baumannii* and *E. coli*, respectively: 500 μg mL^{-1} and 100 μg mL^{-1} ampicillin, 40 μg mL^{-1} kanamycin, 10 μg mL^{-1} and 5 μg mL^{-1} tetracycline. All antibiotics were purchased from Sigma (St. Louis, MO). In-frame deletion strains (Δ*mumR,* Δ*mumT,* Δ*mumL,* Δ*mumU,* Δ*mumH,* and Δ*mumC*) were generated via homologous recombination utilizing the suicide plasmid pFLP2 and screened by PCR and Southern blot as previously described (Mortensen et al., 2014); some constructs were generated by ligating the stitched PCR directly into pFLP2 (Δ*mumR,* Δ*mumT*) or using Gibson recombineering (Δ*mumL,* Δ*mumU,* Δ*mumH,* and Δ*mumC*) (New England Biolabs, Ipswich, MA). Primers used to generate in-frame deletion strains, complementation plasmids and reporter plasmids are listed in **Table 2**. Complementation vectors for the Δ*mumT* and Δ*mumC* strain were constructed in pWH1266 under the control of the 16S promoter (*r01*) as previously described (Mortensen et al., 2014), except that complementation vectors did not include a cMyc tag and the *mumC* complementation vector was cloned between EcoRV and BamH1. p.*r01.WH1266* was used as the empty vector control. Antibiotic selection of strains containing the pWH1266 plasmid used 500 μg ml^{-1} ampicillin. Luciferase promoter reporter constructs were generated in pMU368 and derivatives (Dorsey et al., 2006). The *Photorhabdus luminescens* luciferase operon *luxABCDE* was PCR amplified from pXen1 (Francis et al., 2000) with primers including 5' BamHI and 3' SpeI restriction sites, digested, and ligated into pMU368 to generate p.*luxABCDE.*MU368. To permit selection of the pMU368 plasmid in kanamycin-resistant deletion strains, a tetracycline-resistance cassette was PCR amplified from AB0057 genomic DNA and ligated into p.*luxABCDE.*MU368 at the KpnI restriction site to create

p.*luxABCDE*.MU368.*tet*. The ligation product was transformed into DH5α, selected on 5 μg mL^{-1} tetracycline LB agar, and plasmid was purified. An approximately 300 basepair segment of the *mumT* promoter was PCR amplified with primers including 5' SacI and 3' BamHI restriction sites, restriction digested, and ligated into p.*lux.ABCDE.*MU368.*tet* to generate p.P_{mumT}.*luxABCDE*.MU368.*tet.* The ligation product was transformed in DH5α, plasmid purified by miniprep and transformed into wild-type *A. baumannii* or Δ*mumR*. Antibiotic selection of strains containing the p.MU368.*tet* plasmid was achieved by using 10 μg ml^{-1} tetracycline. Recombinant human calprotectin was expressed and purified as previously described (35).

Table 1: Bacterial strains used in Chapter II.

Strain	Relevant characteristics	Reference or source
17978	Wild-type	ATCC
Δ*znuB*	In-frame Δ*znuB::aphA*	(Hood et al., 2012)
Δ*mumT*	In-frame Δ*mumT::aphA*	This study
Δ*mumR*	In-frame Δ*mumR::aphA*	This study
Δ*mumL*	In-frame Δ*mumL::aphA*	This study
Δ*mumU*	In-frame Δ*mumU::aphA*	This study
Δ*mumH*	In-frame Δ*mumH::aphA*	This study
Δ*mumC*	In-frame Δ*mumC::aphA*	This study
Δ*mumT* pWH1266	Empty vector control	This study
17978 pWH1266	Empty vector control	(Hood et al., 2012)
Δ*mumT* p.*mumT*	Complementation strain containing plasmid p.P_{r01}.*mumT*.WH1266	This study
Δ*mumC* pWH1266	Empty vector control (p.P_{r01}.WH1266)	This study
Δ*mumC* p.*mumC*	Complementation strain containing plasmid p.P_{r01}.*mumC*.WH1266	This study
17978 p.P_{mumT}.*lux*	Reporter strain containing plasmid p.P_{mumT}.*luxABCDE*.MU368.*tet*	This study
Δ*mum*R p.P_{mumT}.*lux*	Reporter strain containing plasmid p.P_{mumT}.*luxABCDE*.MU368.*tet*	This study
Escherichia coli DH5α pFLP2	Cloning strain containing *A. baumannii* suicide vector	(Hoang et al., 1998)
Escherichia coli DH5α p.*mumT::aphA*.FLP2	Cloning strain containing *mumT* knockout vector	This study
Escherichia coli DH5α p.*mumR::aphA*.FLP2	Cloning strain containing *mumR* knockout vector	This study
Escherichia coli DH5α p.*mumL::aphA*.FLP2	Cloning strain containing *mumL* knockout vector	This study
Escherichia coli DH5α p.*mumU::aphA*.FLP2	Cloning strain containing *mumU* knockout vector	This study
Escherichia coli DH5α p.*mumH::aphA*.FLP2	Cloning strain containing *mumH* knockout vector	This study
Escherichia coli DH5α p.*mumC::aphA*.FLP2	Cloning strain containing *mumC* knockout vector	This study
Escherichia coli DH5α p.P_{r01}.WH1266	Cloning strain containing plasmid p.P_{r01}.WH1266	(46)
Escherichia coli DH5α p.*mumT*	Cloning strain containing plasmid p.P_{r01}.*mumT*.WH1266	This study

Escherichia coli DH5α p.*mumC*	Cloning strain containing plasmid p.P_{r01}.*mumC*.WH1266	This study
Escherichia coli DH5α p.P_{mumT}.*lux*	Cloning strain containing plasmid p.P_{mumT}.*lux*	This study
Escherichia coli DH5α pMU368	Cloning strain containing plasmid pMU368	(47)
Escherichia coli DH5α pXen1	Cloning strain containing plasmid pXen1	(48)
Escherichia coli DH5α p.*luxABCDE*.MU368	Cloning strain containing plasmid p.*luxABCDE*.MU368	This study
Escherichia coli DH5α p.*luxABCDE*.MU368.*tet*	Cloning strain containing plasmid p.*luxABCDE*.MU368.*tet*	This study

Table 2: Primers used in Chapter II.

Primer	Primer Sequence	Primer description
1265_FL1F	ATA TAA GGA TCC GGC AGA AGA AAC AGA AAA ATA T	5' primer for amplifying upstream flanking region for *mumR* knockout construct
1265_FL1R	CTAGTTAGTCACATATG GCCTTTATGGGTC	3' primer for amplifying upstream flanking region for *mumR* knockout construct
1265_FL2F	GAGGGAATAATGACATA TGGCTATTTCTTGAATG	5' primer for amplifying downstream flanking region for *mumR* knockout construct
1265_FL2R	CAT TAT TCT AGA TCC GGC ATA ACA GAT ATA ACC AC	3' primer for amplifying downstream flanking region for *mumR* knockout construct
1265_K1F	GACCCATAAAGGCCATA TGTGACTAACTAG	5' primer for amplifying *aphA* for *mumR* knockout construct
1265_K1R	CATTCAAGAAATAGCCA TATGTCATTATTCCCTC	3' primer for amplifying *aphA* for *mumR* knockout construct
1266_FL1F	atataaGGATCCCAACAGG AATTCCCAAAA	5' primer for amplifying upstream flanking region for *mumT* knockout construct
1266_FL1R	CCTCCTAGTTAGTCACA TATGAAAAATTGAGGC	3' primer for amplifying upstream flanking region for *mumT* knockout construct
1266_FL2F	TGGAGGGAATAATGACA TATGGGGTAATTATAAC TA	5' primer for amplifying downstream flanking region for *mumT* knockout construct
1266_FL2R	ctatgtTCTAGAAAACCTGC ACGGATTTTTAAAC	3' primer for amplifying downstream flanking region for *mumT* knockout construct
1266_K1F	GCCTCAATTTTTCATATG TGACTAACTAGGAGG	5' primer for amplifying *aphA* for *mumT* knockout construct
1266_K1R	TAGTTATAATTACCCCA TATGTCATTATTCCCTCC A	3' primer for amplifying *aphA* for *mumT* knockout construct
LEJ_54	aagttcctattctctaggggGGCAT GACTGTACATTTTG	5' primer for amplifying upstream flanking region for *mumC* knockout construct
LEJ_55	tagttagtcaTTCATTCTCAAA ATCTGTAAATTCG	3' primer for amplifying upstream flanking region for *mumC* knockout construct
LEJ_56	tgagaatgaaTGACTAACTAG GAGGAATAAATG	5' primer for amplifying *aphA* for *mumC* knockout construct
LEJ_57	gttcaaagctTCATTATTCCCT CCAGGTAC	3' primer for amplifying *aphA* for *mumC* knockout construct

LEJ_58	ggaataatgaAGCTTTGAACT GTTTTAAATTG	5’ primer for amplifying downstream flanking region for *mumC* knockout construct
LEJ_59	ggttaaaaaggatcgatcctCGCAA CTAAACCAAAGATC	3’ primer for amplifying downstream flanking region for *mumC* knockout construct
LEJ_116	AATATAGGATCCTACTG GCATTTCTGGTGATT	5’ primer for amplifying upstream flanking region for *mumL* knockout construct
LEJ_117	CCTCCTAGTTAGTCAGG CATTATCCCTTTATCAA	3’ primer for amplifying upstream flanking region for *mumL* knockout construct
LEJ_118	TTGATAAAGGGATAATG CCTGACTAACTAGGAGG	5’ primer for amplifying *aphA* for *mumL* knockout construct
LEJ_119	ATACATTGCGCTCTTCCT CATTATTCCCTC	3’ primer for amplifying *aphA* for *mumL* knockout construct
LEJ_120	GAG GGA ATA ATG AGG AAG AGC GCA ATG TAT	5’ primer for amplifying downstream flanking region for *mumL* knockout construct
LEJ_121	ataatatctagaAAAAAAACCA AAATTGTTTTTGCAGCG	3’ primer for amplifying downstream flanking region for *mumL* knockout construct
LEJ_77	aagttcctattctctaggggTTTAA CGGATTGGTGTTG	5’ primer for amplifying upstream flanking region for *mumU* knockout construct
LEJ_78	tagttagtcaTGCGCTCTTCCT TATGCT	3’ primer for amplifying upstream flanking region for *mumU* knockout construct
LEJ_79	gaagagcgcaTGACTAACTA GGAGGAATAAATG	5’ primer for amplifying *aphA* for *mumU* knockout construct
LEJ_80	tttagctattTCATTATTCCCT CCAGGTAC	3’ primer for amplifying *aphA* for *mumU* knockout construct
LEJ_81	ggaataatgaAATAGCTAAA GAAGAATTAAAAAGG	5’ primer for amplifying downstream flanking region for *mumU* knockout construct
LEJ_82	ggttaaaaaggatcgatcctTTGAT AGCTTGCAAAGTCC	3’ primer for amplifying downstream flanking region for *mumU* knockout construct
LEJ_88	aagttcctattctctaggggCAATT GATGGTGTATTTACCC	5’ primer for amplifying upstream flanking region for *mumH* knockout construct
LEJ_89	tagttagtcaTTGCTTATCCTT TTTAATTCTTC	3’ primer for amplifying upstream flanking region for *mumH* knockout construct
LEJ_90	ggataagcaaTGACTAACTA GGAGGAATAAATG	5’ primer for amplifying *aphA* for *mumH* knockout construct

LEJ_91	tctgtattcaTCATTATTCCCT CCAGGTAC	3’ primer for amplifying *aphA* for *mumH* knockout construct
LEJ_92	ggaataatgaTGAATACAGA AAAATTATTGATTG	5’ primer for amplifying downstream flanking region for *mumH* knockout construct
LEJ_93	ggttaaaaaggatcgatcctGACCT TGAGCTTTCGGTG	3’ primer for amplifying downstream flanking region for *mumH* knockout construct
LEJ_140	actcaGATATCatgatgaatacag aaaaattattgattg	5’ primer for cloning *mumC* into complementation plasmid
LEJ_141	aataaGGATCCttagtgaatactcg caatagca	3’ primer for cloning *mumC* into complementation plasmid
1266_16S_ pWH_F	atataaGGATCCGCTCAAAT GGATGAGG	5’ primer for cloning *mumT* into complementation plasmid
1266_pWH _R	AGT GTG TCG ACT TAA AGC TTG GTC AAA TAA TTA	3’ primer for cloning *mumT* into complementation plasmid
1266_pro_S ac1	ataattGAGCTCAAAGCTGT TTTGTAGGTAAAAC	5’ primer for cloning *mumT* promoter into luminescence reporter construct
1266_pro_ BamH1	aattctGGATCCTTAACAAC GCTATTTTCAAATTG	3’ primer for cloning *mumT* promoter into luminescence reporter construct
lux368For	TTA GGA TCC TGC AGA TGA AGC AAG AGG	5’ primer for cloning *luxABCDE* from pXen1 into luminescence reporter construct
lux368Rev	GGC ACT AGT GTC GAC TCA ACT ATC AAA	3’ primer for cloning *luxABCDE* from pXen1 into luminescence reporter construct
tetF	ATT AGC GGT ACC CGC TCG AAC AAG AGG ATG	5’ primer for cloning *tet* cassette into luminescence reporter construct
tetR	TAA ATA GGT ACC GCG CCG TCC CGA TAA GAG A	3’ primer for cloning *tet* cassette into luminescence reporter construct
1266f	GGC CTA GAC ACA AAG TGG GG	*mumT* 5’ qRT-PCR primer
1266r	AGC AAT CCC AAC ACG ATC ATG C	*mumT* 3’ qRT-PCR primer
r01RTf	CTGTAGCGGGTCTGAGA GGAT	*r01* 5’ qRT-PCR primer
r01RTr	CCATAAGGCCTTCTTCA CAC	*r01* 3’ qRT-PCR primer
LEJ_23	GAACCGGCAGGGCGTAT TTC	*mumU* 5’ qRT-PCR primer
LEJ_24	TACACTTGGCATACGCG CTG	*mumU* 3’ qRT-PCR primer
LEJ_27	AGTGGCAGGCTCAAAAG TGC	*mumL* 5’ qRT-PCR primer

LEJ_28	GCATCAATTACGGCTGCTGC	*mumL* 3’ qRT-PCR primer
LEJ_29	AAAGACAGTCCGGGTGGTTG	*mumH* 5’ qRT-PCR primer
LEJ_30	CCCGGTAACAGCAATGCAGG	*mumH* 3’ qRT-PCR primer
LEJ_31	TAAAGCCGCGTTTGGTGGTG	*mumC* 5’ qRT-PCR primer
LEJ_32	TGCTTCACGTACTGCCGACT	*mumC* 3’ qRT-PCR primer
LEJ_25	GAAGGGGTACGTACAGGCGA	5’ *mumR* primer for Supplemental Fig 2A
LEJ_34	GCAATCAGCGCCGACACAAA	3’ *A1S_1271* primer for Supplemental Fig 2A

Bacterial growth assays. Unless otherwise stated, all growth assays were carried out in 96-well flat-bottomed plates in 100 µL volume following inoculation with 1 µL overnight culture. Optical density absorbance at 600 nm was measured as a proxy for growth. *Urea and metal toxicity assays:* All toxicity assays were carried out in LB medium with the addition of freshly prepared, sterile metal or urea stocks. Ten M urea stocks were prepared in LB and the final volume of each well was 90 µL. One hundred mM $MnCl_2$, 100 mM $ZnCl_2$, and 100 mM $FeSO_4$ stocks were prepared in water, filter sterilized, and used immediately. *Calprotectin antimicrobial growth assays:* Calprotectin antimicrobial growth assays were performed using methods similar to those previously described (Damo et al., 2013). Briefly, overnight cultures were sub-cultured 1:50 in LB for one hour prior to 1:100 inoculation of 40% LB and 60% calprotectin buffer (100 mM NaCl, 3 mM $CaCl_2$, 5 mM β-mercaptoethanol, 20 mM Tris, pH 7.5) and a titration of calprotectin with or without supplementation of $MnCl_2$ at the indicated concentrations. *mumT-reporter luminescence assay: A. baumannii* strains harboring luminescence reporter plasmids were grown in medium containing a titration of calprotectin in 60% LB and 40% calprotectin buffer. Cultures were grown in black-sided 96-well plates (Corning) and luminescence was measured using a plate reader (BioTek, Winooski, VT). *Sole-nitrogen source growth assays:* Assays were performed in modified E medium lacking nitrogen sources (Vogel and Bonner, 1956): 28 mM K_2HPO_4, 28 mM KH_2PO_4, 1 mM $MgSO_4$, 50 mM acetate (carbon source) and a modified Vishniac's trace minerals mix (650 µM Na_2EDTA, 90 µM $FeSO_4$, 13 µM $MnCl_2$, 8 µM $CuCl_2$, 4.5 µM Na_2MoO_4, 33.5 µM $CoCl_2$, 68 µM $ZnCl_2$) (Vishniac and Santer, 1957). Urea was added at the indicated concentrations.

Mouse infections. A mouse pneumonia model of *A. baumannii* infection was employed as previously described (Hood et al., 2012). Briefly, wild-type *A. baumannii* or Δ*mumT* was freshly streaked from frozen stocks onto LB agar or LB agar containing 40 μg mL^{-1} kanamycin, respectively, two days prior to infection. Overnight cultures were grown in LB without antibiotic selection. On the day of the infection, overnight cultures were sub-cultured 1:1,000 in 10 mL of LB and grown to mid-exponential phase. Cells were then harvested by centrifugation, washed twice in PBS, and resuspended in PBS to a final concentration of 1 x 10^{10} CFU mL^{-1}. Wild-type and Δ*mumT* suspensions were then combined in a 1:1 ratio, mixed thoroughly, and immediately utilized for infection. Mice were anesthetized with intraperitoneal injection of 2,2,2-tribromoethanol diluted in PBS. Anesthetized mice were inoculated intranasally with 5 x 10^8 CFU in 50 microliter volume. Infection proceeded for 36 hours. Mice were then euthanized with CO_2 and lungs and livers removed and placed on ice. Organs were homogenized in 1 mL PBS, serially diluted in PBS, and dilutions were spot-plated onto LB agar and LB agar containing 40 μg mL^{-1} kanamycin. Δ*mumT* burdens were enumerated by counting colonies recovered on kanamycin-containing plates. Infections were performed at the Vanderbilt University Medical Center under the principles and guidelines described in the *Guide for the Care and Use of Laboratory Animals* using Institutional Animal Care and Use Committee (IACUC)-approved protocol M/10/165. Vanderbilt University Medical Center is an American Association for Laboratory Animal Science (AALAS)-accredited facility. The Vanderbilt University Medical Center is registered with the Office of Laboratory Animal Welfare (OLAW), assurance number A-3227-01.

Inductively-coupled plasma mass spectrometry. To prepare bacterial samples for ICP-MS analysis, bacterial cultures were grown overnight in LB containing 500 μg mL^{-1} ampicillin, sub-cultured 1:50 in LB containing 500 μg mL^{-1} ampicillin. Bacteria were sub-cultured 1:50 for one hour and then cultures were diluted 1:100 into 10 mLs of 60% LB / 40% calprotectin buffer containing 500 μg mL^{-1} ampicillin and grown for eight hours. Bacterial cultures were then transferred to pre-weighed metal-free 15 mL conical tubes (VWR, Radnor, PA). Pellets were harvested by centrifugation, washed twice with MilliQ deionized water, and dried. The pellet weight was then recorded using an analytical balance (Mettler Toledo, Columbus, OH). Pellets were digested with 1 mL 50% HNO_3 (Optima grade metal-free; Fisher, Waltham, MA) at 50°C overnight, diluted with 9 mL MilliQ deionized water, weighed using an analytical balance, and subjected to mass spectrometry. Whole organs from *A. baumannii*-infected mice were homogenized in 1 mL PBS and digested in 2 mL HNO_3 and 500 μL H_2O_2 (Optima grade metal-free; Fisher, Waltham, MA) at 90 °C overnight in metal-free Teflon jars for digestion. Digested samples were then diluted with 9 mL MilliQ deionized water and submitted for inductively coupled plasma mass spectrometry (ICP-MS) analysis at the Vanderbilt Mass Spectrometry Research Center. Levels of ^{66}Zn, ^{55}Mn, and ^{56}Fe were measured, concentrations were determined utilizing a standard curve for each metal, and results were normalized by dilution factor.

Determining the conservation of the *mum* operon *in silico.* The 'compare region' feature of the SEED viewer (Overbeek et al., 2005) was used to identify genomic regions similar to the *mum* operon, with *mumT* set as the focus gene. From the 58 archaea, 962 bacteria, and 562 eukaryota genomes in the SEED database at the time of query, 88 were found to include sets of genes with similar sequences. Genomic regions from eleven organisms were

selected for protein alignments. Protein sequences were downloaded from the SEED and aligned by ClustalW2 (Goujon et al., 2010; Larkin et al., 2007) to the 17978 homologue.

Quantitative RT-PCR. RNA isolation from *A. baumannii*, cDNA generation, and qRT-PCR using SYBR green (BIO-RAD) was performed as previously described (Mortensen et al., 2014). CT values for each transcript were normalized by *16s.*

Statistical analyses. All raw numerical data were saved in Excel files and imported into GraphPad Prism for statistical analysis. Specific statistical tests employed each experiment are outlined in the figure legends.

Results

A. baumannii encodes an NRAMP-family transporter that mediates resistance to calprotectin

I hypothesized that *A. baumannii* is able to overcome calprotectin-mediated Mn chelation by utilizing a metal transporter system that has high affinity for Mn. To identify predicted Mn transporters in *A. baumannii*, the KEGG database (Kanehisa and Goto, 2000; Kanehisa et al., 2016) was searched for Mn transporter orthologs in the *A. baumannii* ATCC 17978 genome. This search identified only one gene encoding a protein with similarity to NRAMP or ABC family Mn transporters, the gene *A1S_1266. A1S_1266* encodes a potential NRAMP-family member. NRAMP-family members are integral membrane proteins that transport divalent cations, often having specificity for Mn(II) (Juttukonda and Skaar, 2015). *A1S_1266* is in a predicted operon containing genes that catabolize urea to ammonia, which I named the manganese and urea metabolism (*mum*)

operon (**Figure 7A**). As *A1S_1266* is predicted to encode a transporter, this gene was named *mumT* (**Figure 7A**).

I hypothesized that *mumT* encodes a Mn importer that is important for growth in Mn-restricted conditions, such as upon exposure to calprotectin. Consistent with this, normalized *mumT* transcript abundance increases upon calprotectin treatment (**Figure 7B**). Genetic deletion of *mumT* delays *A. baumannii* growth in the presence of recombinant calprotectin, as does deletion of the Zn import gene *znuB* (**Figure 7C & D**). This growth lag can be complemented by the expression of *mumT* from a plasmid or by the addition of excess Mn (**Figure 7E-G**). Importantly, Δ*znuB* growth inhibition in the presence of calprotectin is only fully rescued by the addition of excess Zn and is not rescued by excess Mn alone (Nairn et al., 2016). We hypothesized that if *mumT* preferentially imports Mn, loss of *mumT* would increase resistance to toxic levels of Mn but not other divalent cations. In support of this, Δ*mumT* is able to grow in 3 mM Mn, which is highly toxic to wild-type *A. baumannii* (**Figure 8A & B**), whereas Δ*mumT* is more sensitive than wild-type *A. baumannii* to Fe toxicity and has similar sensitivity to Zn toxicity (**Figure 8C & D**). Finally, to determine whether *mumT* is required for Mn acquisition, cellular Mn concentrations were measured by inductively coupled plasma mass spectrometry (ICP-MS) (**Figure 8E**). Δ*mumT* has lower Mn levels in cell pellets than wild-type *A. baumannii,* and this defect is complemented by expression of *mumT in trans*. In contrast, cellular Zn and Fe levels in Δ*mumT* were not significantly different than wild-type *A. baumannii* levels (**Figure 8F**). Together, these results demonstrate that *A. baumannii mumT* is important for growth in Mn restricted conditions and accumulation of cellular Mn.

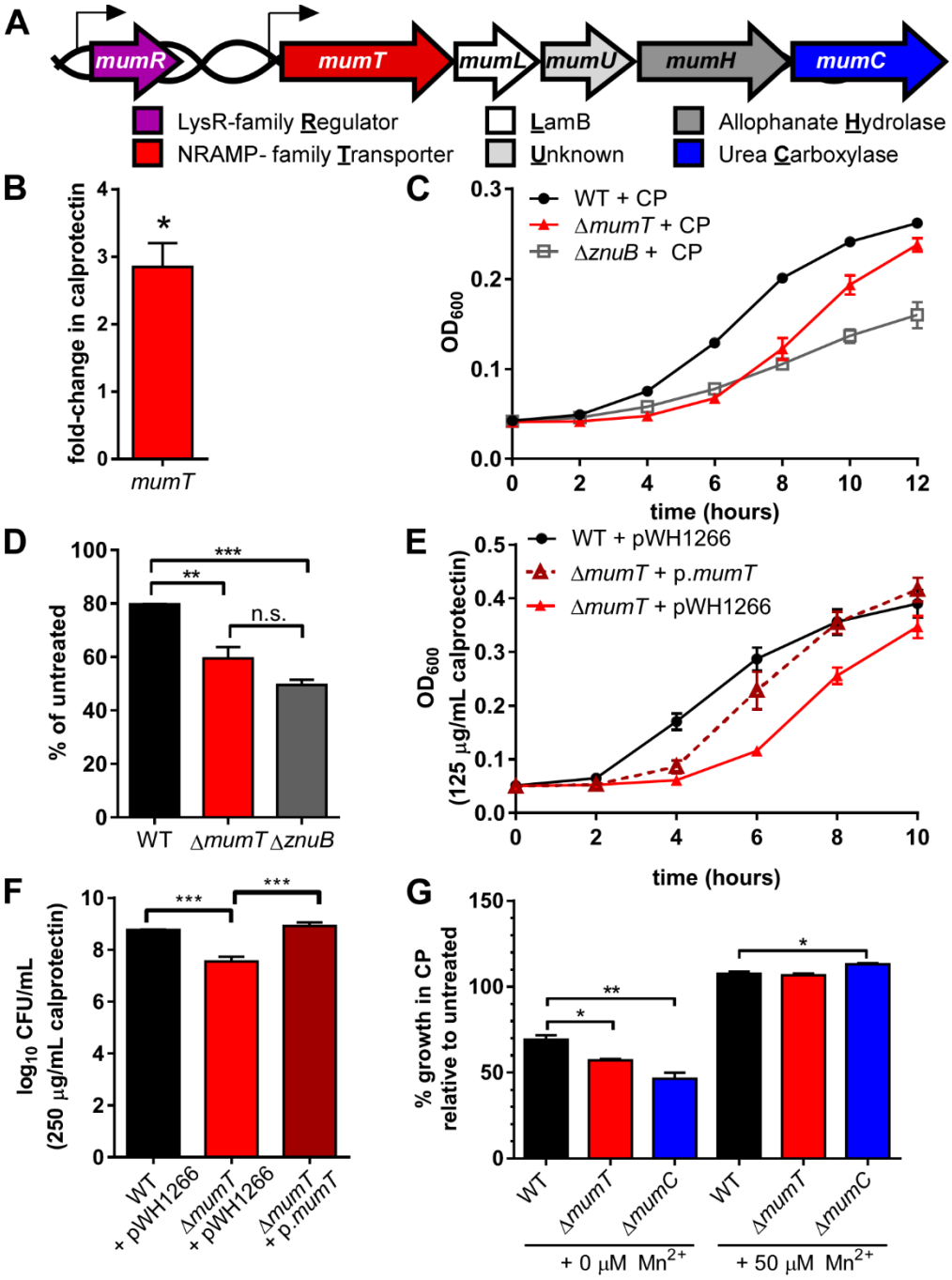

Figure 7: *Acinetobacter baumannii* encodes an NRAMP-family Mn importer that mediates resistance to calprotectin. (A) Schematic of *mum* locus with gene names and predicted protein functions labeled. (B) *mumT* transcription by quantitative real-time polymerase chain reaction (qRT-PCR). cDNA was reverse transcribed from RNA harvested from wild-type *A. baumannii* in the presence of 125 μg/mL calprotectin. Transcription is graphed as fold-change over untreated cells. Data are combined from three independent experiments each performed in technical triplicate with the mean and S.E.M. graphed. Statistical significance was determined by a Student's *t* test using a reference value of 1.0. (C) Growth of wild-type *A. baumannii*, Δ*mumT*, and Δ*znuB* treated with 125

μg/mL calprotectin over time. (D) Growth of *A. baumannii*, Δ*mumT*, and Δ*znuB* treated with 125 μg/mL calprotectin relative to untreated cells at 8 hours. For C and D, data are combined from three independent experiments each performed in technical triplicate with the mean and S.E.M. graphed. Significance was calculated using a one-way analysis of variance with Tukey's multiple comparisons. (E) Growth over time in the presence of 125 μg/mL calprotectin. Wild-type and Δ*mumT* harbor an empty plasmid, whereas Δ*mumT* p*mumT* expresses *mumT* from a constitutive promoter. (F) Colony forming units recovered following eight hours of growth in the presence of 250 μg/mL calprotectin. (G) Calprotectin growth inhibition of Δ*mumT* and Δ*mumC* is complemented by excess Mn. Percent growth of *A. baumannii* strains treated with 125 μg/mL calprotectin with or without the addition of 50 μM $MnCl_2$ to the media. Growth relative to buffer alone is shown at 8 hours. Experiments in F & G are combined from three independent experiments with three technical replicates each and the mean and S.E.M. is graphed. Statistical significance for F and G was determined using a one-way analysis of variance with Dunnet's multiple comparisons test. *, $p < 0.05$; **, $p < 0.01$; ***, $p < 0.001$; n.s. not significant.

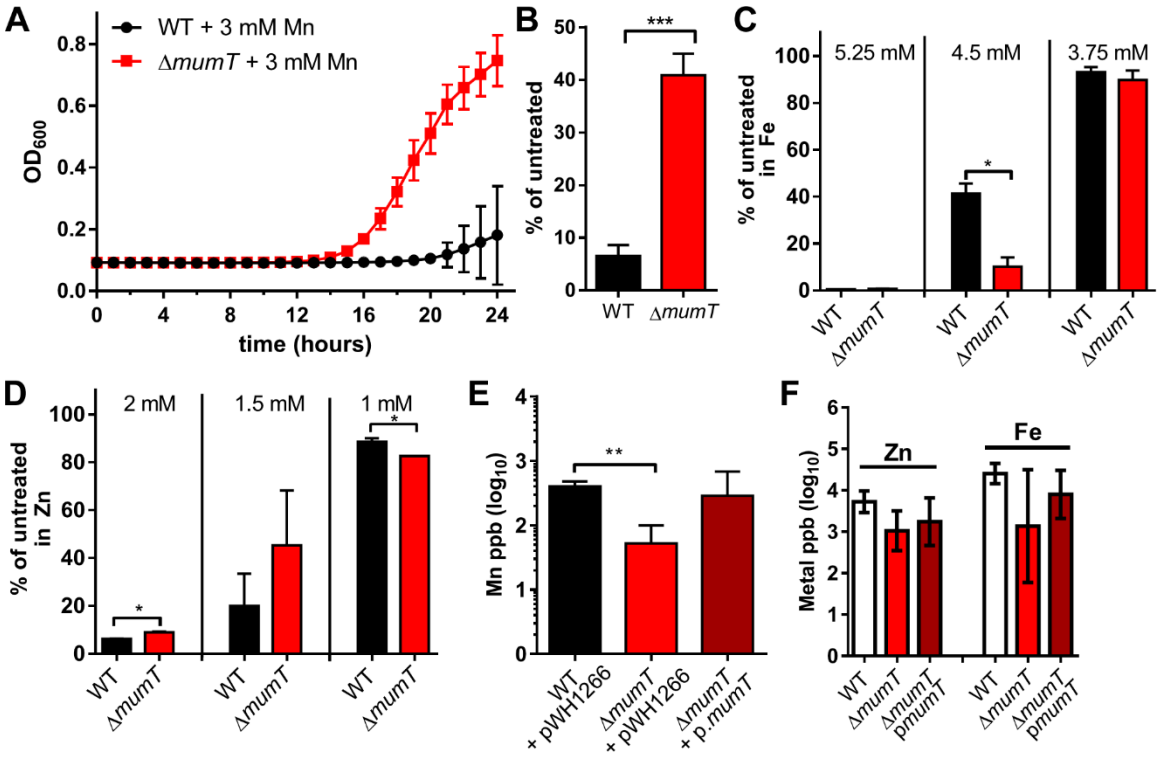

Figure 8: Resistance of Δ*mumT* to toxic Mn concentrations correlates with decreased cellular Mn levels. (A) Growth of *A. baumannii* and Δ*mumT* in LB supplemented with 3 mM $MnCl_2$ over time. (B) Growth of *A. baumannii* and Δ*mumT* in 3 mM $MnCl_2$ relative to LB alone at 20 hours. For E & F, data are combined from a single experiment performed with three biological replicates with the mean and standard deviation graphed. Data are representative of multiple independent experiments. Significance was calculated using a Student's *t* test. (C-D) Growth of wild-type *A. baumannii* and Δ*mumT* in toxic concentrations of (C) Fe, and (D) Zn graphed as percent of untreated cells at 8 hours. Experiments in C & D are combined from three independent experiments with three technical replicates each and the mean and S.E.M. is graphed. Significance for each condition (WT vs. Δ*mumT*) were determined using a Student's *t* test. (E) Mn levels of WT *A. baumannii* with empty vector, Δ*mumT* with empty vector, and Δ*mumT* with a vector containing *mumT* under the control of the 16S promoter grown to mid-log phase. Cells were digested in metal-free nitric acid and analyzed by inductively-coupled plasma mass spectrometry. Data are combined from three biological replicates that were measured in technical triplicate, with the mean and standard deviation graphed. Significance was calculated using a Student's *t* test. (F) Zn and Fe levels of WT *A. baumannii* with an empty vector, Δ*mumT* with an empty vector, and Δ*mumT* with a vector containing *mumT* under the control of the 16S promoter grown to mid-log phase. Cells were digested in metal-free nitric acid and analyzed by inductively-coupled plasma mass spectrometry. Data are combined from three biological replicates that were measured in technical triplicate. The differences in mean values (WT vs. Δ*mumT*) for each metal were not significant using a Student's *t* test. *, $p < 0.05$; **, $p < 0.01$ ***, $p < 0.001$.

mumT upregulation in the presence of calprotectin requires the LysR-family transcriptional regulator MumR

mumT is encoded immediately downstream from a gene encoding a predicted LysR family transcriptional regulator, *mumR* (**Figure 7A**). I hypothesized that *mumR* is required for transcriptional control of *mumT*. To understand the contributions of *mumR* to *mumT* regulation, a strain containing an in-frame deletion of *mumR* was generated. The abundance of *mumT* transcript is significantly decreased in Δ*mumR* relative to wild-type *A. baumannii* (**Figure 9A**). This suggests that MumR activates *mumT* expression. To confirm this finding, activity of the *mumT* promoter was investigated using a reporter system. The *mumT* promoter was cloned into a plasmid harboring the *Photorhabdus luminescens* luciferase operon, *luxABCDE,* such that activity of the *mumT* promoter results in luminescence. This vector was transformed into wild-type *A. baumannii* and Δ*mumR,* and luminescence was measured in various growth conditions. In rich medium, the *mumT* promoter is active in wild-type *A. baumannii* but not Δ*mumR* (**Figure 9B**). When incubated with 125 μg/mL calprotectin, the activity of the *mumT* promoter is significantly enhanced in wild-type *A. baumannii* and this is dependent on *mumR.* This result demonstrates that calprotectin exposure induces expression from the *mumT* promoter. Furthermore, it shows that *mumR* is required for upregulation of *mumT* in the presence of calprotectin.

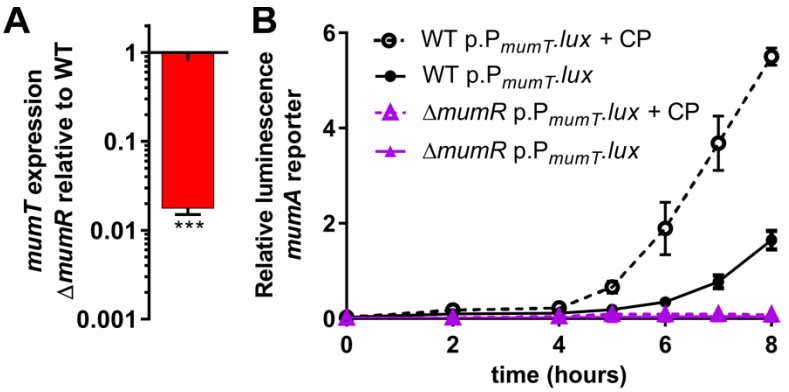

Figure 9: *mumT* is upregulated in the presence of calprotectin by *mumR*. (A) *mumT* transcription in Δ*mumR*, measured by qRT-PCR. cDNA was reverse transcribed from RNA harvested from cells grown in LB. Transcription is graphed as fold-change relative to wild-type *A. baumannii*. Data are combined from three biological replicates that were analyzed in technical triplicate. Statistical significance was determined by a Student's *t* test using a reference value of 1.0. ***, $p < 0.001$. (B) The *mumT* promoter was cloned in front of the luciferase operon *luxABCDE*. The *mumT* promoter reporter construct was transformed into wild-type *A. baumannii* or Δ*mumR*. Luminescence was recorded in cells treated with 125 µg/mL calprotectin as well as untreated cells. Data are combined from one biological replicate for each strain grown in four technical replicates. The mean and standard deviation for one representative experiment (of >4) are graphed.

***mumT* is in an operon with *mumE,* a urea carboxylase that contributes to *A. baumannii* urea utilization**

Based on the small intergenic distances between the open reading frames (ORFs) for *mumT* (*A1S_1266*) through *mumC* (*A1S_1270*), I predicted that these genes constitute an operon. This was confirmed by performing polymerase chain reaction (PCR) on cDNA prepared using RNA isolated from wild-type *A. baumannii* (**Figure 10A**). PCR products were amplified across adjacent ORFs for *mumT, mumL, mumU, mumH* and *mumC,* and no products were amplified for primers designed to amplify the *mumR-mumT* or *mumC-A1S_1271* junctions, demonstrating that *mumTLUHC* form an operon.

Next, I sought to identify the function of members of the *mum* operon. MumH is homologous to allophanate hydrolase and MumC is a putative member of the biotin carboxylase family. In fungi, the enzyme urea amidolyase contains urea carboxylase and allophanate hydrolase domains. Urea amidolyase converts urea first to allophanate by biotin-mediated carboxylation (urea carboxolyase domain) and then converts allophanate to carbon dioxide and ammonia via hydrolysis (allophanate hydrolase domain) (Roon et al., 1972). Because *mumH* and *mumC* are adjacent ORFs, I posited that MumC is a biotin-dependent urea carboxylase and MumH and MumC mediate urea degradation (**Figure 10B**). Urea amidolyase enzymatic activity has been characterized in enzymes cloned from *Oleomonas sagaranensis* (Kanamori et al., 2004; Kanamori et al., 2005), but the role of urea amidolyase in bacterial physiology and pathogenesis remains unknown.

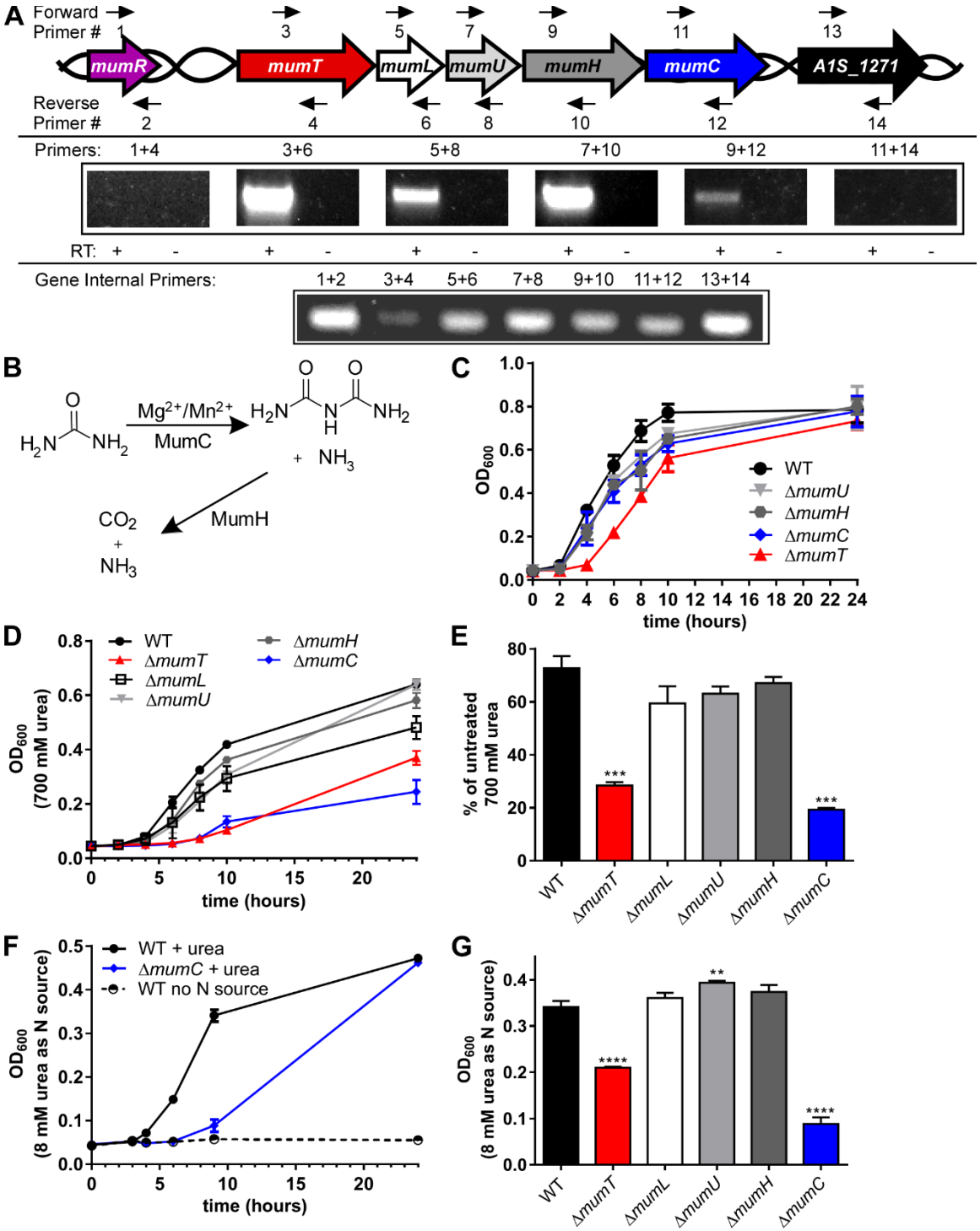

Figure 10: ***mumT* is in an operon that contributes to utilization of urea as a nitrogen source.** (A) cDNA was amplified from RNA isolated from wild-type *A. baumannii* using reverse transcriptase (RT) and random primers. Polymerase chain reaction was performed using this cDNA as template using primer pairs designed to amplify across the junctions of predicted open reading frames. Primer annealing positions are shown schematically by arrows. cDNA samples prepared without RT were included as negative controls, and gene

internal primer pairs were included as positive controls. (B) Predicted reactions catalyzed by urea carboxylase MumC and allophanate hydrolase MumH. Urea is converted to allophanate via biotin-mediated carboxylation of urea by urea carboxylase MumC in a reaction that requires Mg or Mn. Allophanate is hydrolyzed by allophanate hydrolase MumH to carbon dioxide and ammonia. (C) Wild-type *A. baumannii* and isogenic mutants Δ*mumT*, Δ*mumU*, Δ*mumH*, and Δ*mumC* were sub-cultured in LB 1:50 for one hour then inoculated 1:100 into LB for growth curve analysis. Optical density at 600 nm was monitored over time. (D) Growth of wild-type *A. baumannii*, Δ*mumT*, Δ*mumL*, Δ*mumU*, Δ*mumH*, and Δ*mumC* in 700 mM urea over time. (E) Growth of wild-type *A. baumannii*, Δ*mumT*, Δ*mumL*, Δ*mumU*, Δ*mumH*, and Δ*mumC* in 700 mM urea relative to LB alone at 24 hours. For experiments D and E, data are combined from 3 or more independent experiments performed in technical duplicate. Significance was calculated using one-way analysis of variance for each condition, comparing each strain to wild-type control with Dunnett's multiple comparisons test. (F) Growth of wild-type *A. baumannii* and Δ*mumC* with 8 mM urea as the sole nitrogen source. Wild-type grown with no nitrogen source is included as a negative control. (G) Utilization of 8 mM urea as a nitrogen source by wild-type *A. baumannii*, Δ*mumT*, Δ*mumL*, Δ*mumU*, Δ*mumH*, and Δ*mumC*. OD_{600} at nine hours is shown. Data in F and G are from a single experiment performed in biological duplicate. Data are representative of 5 independent experiments. Significance was calculated using one-way analysis of variance for each condition, comparing each strain to wild-type control with Dunnett's multiple comparisons test. ***, $p < 0.001$. ***, $p < 0.001$; ****, $p < 0.0001$.

To evaluate the importance of each *mum* gene in urea degradation, in-frame deletions of *mumL, mumU, mumH*, and *mumC* were generated and found to lack general growth defects in LB (**Figure 10C**). Inactivation of *mumC,* but not *mumH*, impaired growth in toxic levels of urea (**Figure 10D & E**). While *A. baumannii* cannot grow using urea as a sole carbon source (data not shown), *A. baumannii* can utilize urea as a sole nitrogen source in a manner dependent on the presence of *mumC* (**Figure 10F & G**). Importantly, Δ*mumH* is capable of utilizing urea as a sole nitrogen source (**Figure 10G**), which indicates that the single ammonia molecule produced by MumC-mediated urea carboxylation (**Figure 10B**) is sufficient to support *A. baumannii* growth as a sole nitrogen source.

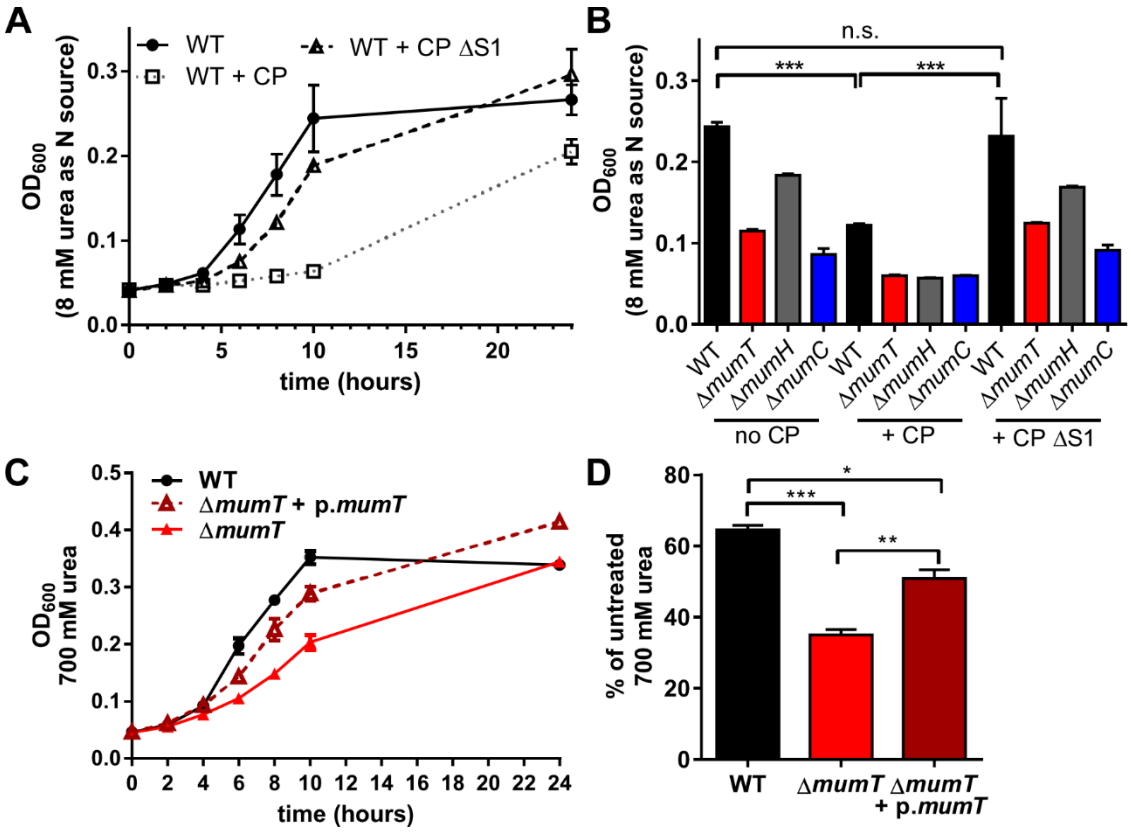

Figure 11: Calprotectin inhibits growth with urea as a sole nitrogen source. (A) Wild-type *A. baumannii* growth with urea as primary nitrogen source in the presence of 780 µg/mL calprotectin or calprotectin ΔS1, a variant of calprotectin unable to bind Mn. (B) Growth at 10 hours is shown as raw OD_{600} with urea as the primary nitrogen source with the addition of no calprotectin, 780 µg/mL calprotectin or 780 µg/mL calprotectin ΔS1, a variant of calprotectin unable to bind Mn. For experiments A and B, data are from a single experiment performed in biological triplicate and are representative of 4 independent experiments. Significance was calculated using one-way analysis of variance for each condition, comparing each strain to wild-type control with Dunnett's multiple comparisons test. (C) Growth of wild-type *A. baumannii*, Δ*mumT*, and Δ*mumT* expressing *mumT* from a constitutive promoter in trans in 700 mM urea. Optical density was monitored over time. (D) Growth of *A. baumannii*, Δ*mumT*, and Δ*mumT* p.*mumT* in 700 mM urea relative to growth in LB alone at 8 hours. Data in C, and D are combined from three separate experiments with three technical replicates each and depict the mean and S.E.M. Significance was calculated using a one-way analysis of variance with Dunnet's multiple comparisons test. *, $p < 0.05$; **, $p < 0.01$; ***, $p < 0.001$. ***, $p < 0.001$.

Urea carboxylase activity in *Oleomonas sagaranensis* and *Candida utilis* requires either Mg^{2+}, Mn^{2+} or Co^{2+} (Kanamori et al., 2004; Roon and Levenberg, 1972), suggesting that *A. baumannii* utilization of urea by MumC may require Mn^{2+}. To address this, I chelated Mn by the addition of calprotectin to medium containing urea as the sole nitrogen source. The addition of calprotectin was sufficient to substantially impair growth in urea (**Figure 11A & B**). Importantly, growth was not inhibited when a variant of calprotectin (ΔS1) that is unable to bind Mn (Damo et al., 2013) was added to the medium. Consistent with these findings, *mumT* inactivation decreased growth in high concentrations of urea, which was complemented by the expression of *mumT in trans*, demonstrating that the MumT Mn transporter is important to enable urea degradation (**Figure 11C & D**). Together, these results demonstrate that *mumC* is vital for catabolism of urea in *A. baumannii* and suggest that urea catabolism may be altered by Mn availability.

***mumC* is important for *A. baumannii* growth in calprotectin**

The entire *mum* operon is upregulated following exposure to calprotectin (**Figure 12A**). Based on this observation, I hypothesized that additional *mum* genes may be important for growth in calprotectin. The sensitivities of *A. baumannii* Δ*mumL,* Δ*mumU,* Δ*mumH,* and Δ*mumC* to calprotectin growth inhibition were evaluated (**Figure 12B**). The strains lacking *mumL* and *mumU* exhibit sensitivity to calprotectin similar to wild-type *A. baumannii* (**Figure 12C, Figure 13A**). This demonstrates that *mumL* and *mumU* are not important for growth in the presence of calprotectin. In contrast, Δ*mumH* and Δ*mumC,* strains harboring in-frame deletions of allophanate hydrolase and urea carboxylase, respectively, have increased sensitivity to calprotectin (**Figure 12B & C**). Δ*mumC* does not exhibit decreased transcription of *mumT* (**Figure 13B**). The growth deficit of Δ*mumC*

in calprotectin can be complemented by the addition of exogenous Mn to the medium (**Figure 13C**) or by providing a copy of *mumC in trans* (**Figure 13C &D**). Importantly, the Δ*mumC* strain does not exhibit resistance to Mn toxicity (**Figure 13E**), suggesting that its role in calprotectin resistance is not related to Mn transport. These data indicate that urea catabolism via *mumH* and *mumC* is important for *A. baumannii* resistance to calprotectin.

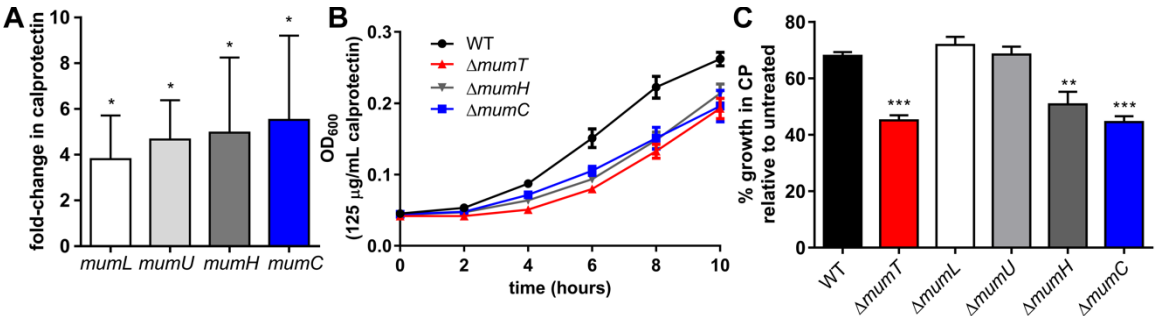

Figure 12: Urea catabolism genes *mumH* and *mumC* are important for growth in calprotectin. (A) *mumT, mumL, mumU, and mumH* transcription following treatment with 250 µg/mL calprotectin. Expression was quantified by qRT-PCR, graphed as fold-change over growth in buffer alone, and averaged from three independent experiments with qRT-PCR performed in technical triplicate. Statistical significance was determined by a Student's *t* test using a reference value of 1.0. (B) Growth of wild-type *A. baumannii*, Δ*mumT*, Δ*mumH* and Δ*mumC* in the presence of 125 µg/mL calprotectin. (C) Percent growth of *A. baumannii* strains in 125 µg/mL calprotectin relative to buffer alone is shown at 8 hours. Growth curves in B and C were carried out in rich medium (LB) mixed with calprotectin buffer. Data in B and C are combined from three independent experiments performed in technical triplicate and depict the mean and S.E.M. Significance was calculated using a one-way analysis of variance comparing each strain to wild-type control with Dunnett's multiple comparisons test. *, $p < 0.05$; **, $p < 0.01$; ***. $p < 0.001$.

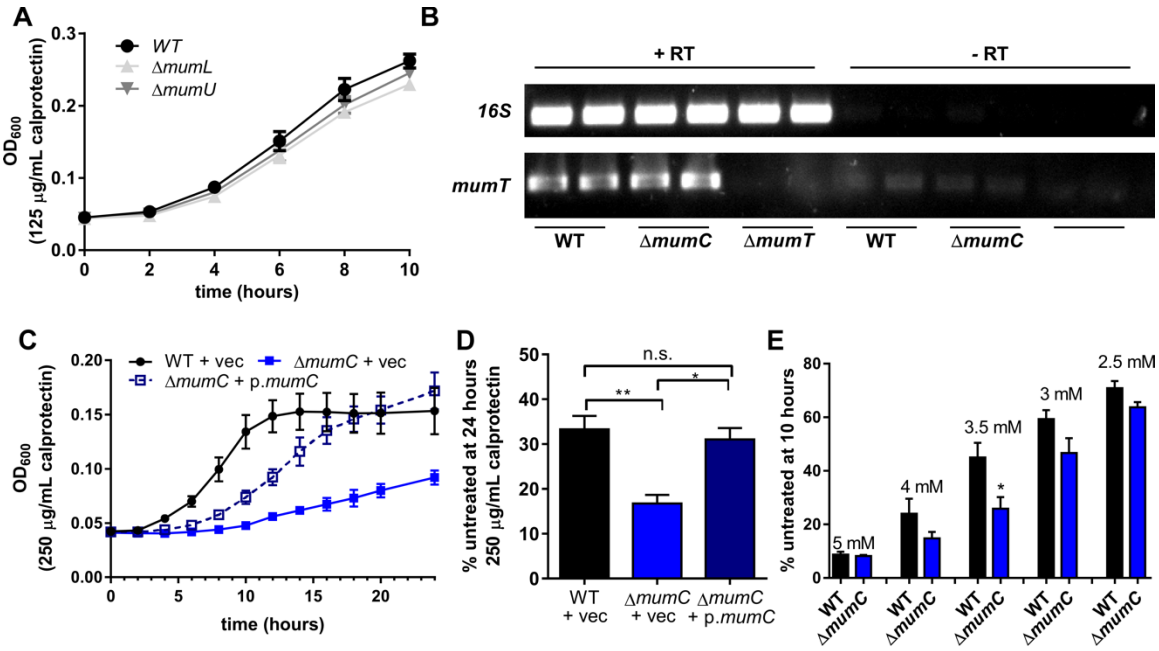

Figure 13: Complementation of Δ*mumC* growth in calprotectin. (A) Growth of wild-type *A. baumannii*, Δ*mumL* and Δ*mumU* in the presence of 125 μg/mL calprotectin. (B) PCR products amplified (35 cycles) from 1:100 dilution of cDNA synthesized from 2 μg of DNAse treated RNA. PCR products were amplified from primers specific to *mumT* or *16s*. RNA was isolated from WT *A. baumannii,* Δ*mumC*, and Δ*mumT* grown in LB to early exponential phase. No reverse transcriptase samples were included as a negative control. (C-D) The growth deficit of Δ*mumC* in calprotectin is complemented by the expression of *mumC* on a plasmid under a constitutive promoter. (C) Growth was monitored by optical density at 600 nm (OD_{600}) over time. (D) Growth relative to buffer alone is shown at 24 hours. For B & C, data are combined from three independent experiments with three technical replicates in each experiment and depict the mean and S.E.M. Significance was calculated using a one-way analysis of variance with Dunnet's multiple comparisons test. (E) Growth of wild-type *A. baumannii* and Δ*mumC* in LB supplemented with toxic concentrations of $MnCl_2$ (2.5 mM – 5 mM, as indicated on the graph). Growth relative to untreated is shown at 10 hours. Data are combined from three independent experiments with three technical replicates in each experiment and depict the mean and S.E.M. Significance was calculated using a Student's *t* test comparing two groups at each concentration of Mn. *, $p < 0.05$; **, $p < 0.01$.

mumT contributes to the fitness of *A. baumannii* in a murine pneumonia model

To investigate the contribution of *mumT* to *A. baumannii* fitness in the murine lung, C57BL/6 mice were inoculated intra-nasally with a 1:1 mixture of wild-type *A. baumannii* and Δ*mumT*. After 36 hours, bacterial burdens were quantified from the lungs and the liver, a site of systemic dissemination (**Figure 14A & B**). Δ*mumT* burdens were significantly lower than wild-type burdens in both the lungs and the livers of C57BL/6 mice, indicating that *mumT* contributes to fitness in this infection model. To define the role of calprotectin in the fitness defect of the Δ*mumT* strain, calprotectin-deficient mice (*S100a9*$^{-/-}$) were also co-infected with wild-type *A. baumannii* and Δ*mumT*. As in C57BL/6 mice, Δ*mumT* burdens were significantly lower than wild-type in the lungs of calprotectin-deficient mice. However, the fitness deficit of the Δ*mumT* strain in the liver was completely rescued in the absence of calprotectin. These findings indicate that calprotectin is vital for limiting *A. baumannii* Δ*mumT* dissemination to the liver. To elucidate whether the differential rescue of Δ*mumT* in the liver and the lung of calprotectin-deficient mice correlates with Mn concentrations, *A. baumannii*-infected livers and lungs were subjected to ICP-MS analysis. Mn abundance in the liver is over 25-fold greater than Mn abundance in the lung (**Figure 14C**). The high level of Mn in the liver correlates with increased fitness of the Δ*mumT* strain in the liver relative to the lung in calprotectin-deficient mice; this indicates that the liver of a calprotectin-deficient mouse is Mn-replete. The result that Δ*mumT* is attenuated in the livers of wild-type mice suggests that calprotectin is sufficient to Mn-starve *A. baumannii* even in the Mn-abundant liver. Taken as a whole, these data reveal that *mumT* is important for *A. baumannii* fitness during infection and demonstrate that calprotectin is important for preventing Δ*mumT* dissemination to the murine liver.

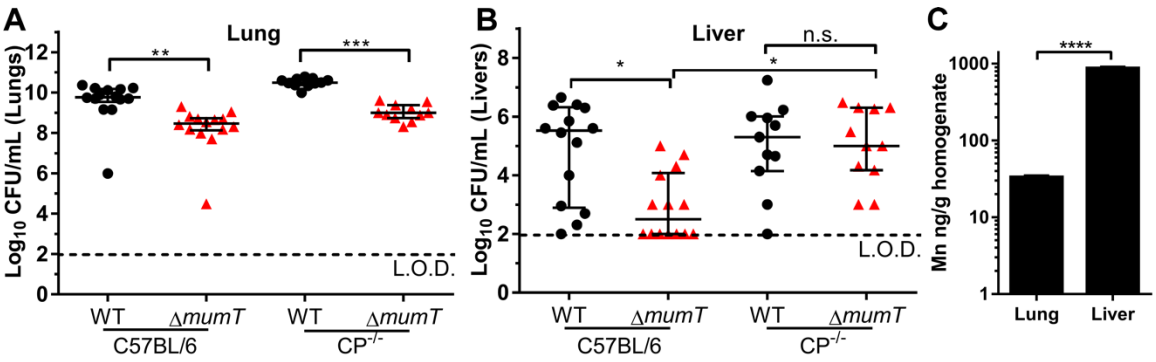

Figure 14: *mumT* contributes to the fitness of *A. baumannii* during murine pneumonia. Mice were intranasally inoculated with a 1:1 mixture of wild-type (WT) *A. baumannii* and Δ*mumT*. Following 36 hours of infection, mice were euthanized and lungs (primary infection) and livers (dissemination) were harvested and bacteria enumerated by dilution plating on non-selective medium and medium containing kanamycin. (A) Bacterial burdens of wild-type and Δ*mumT* recovered from lungs of C57BL/6 and $CP^{-/-}$ mice. The mean and standard deviation are indicated by lines. Significance was calculated using one-way ANOVA with Tukey's multiple comparisons. (B) Bacterial burdens of wild-type and Δ*mumT* recovered from livers of C57BL/6 and $CP^{-/-}$ mice. Median and interquartile range are indicated by lines. Significance was calculated using a Kruskal-Wallis test with Dunn's multiple comparisons. For A and B, each symbol represents the burdens recovered from an individual mouse, and two independent experiments are combined. The limit of detection was 100 C.F.U. per organ and is indicated by a dashed line in A and B. (C) Mn levels in *A. baumannii*-infected livers and lungs were measured by ICP-MS. Organs harvested from three mice were used for this analysis. Significance was calculated using a Student's *t* test. *, $p < 0.05$; **, $p < 0.01$; ***, $p < 0.001$; ****, $p < 0.0001$.

The *mum* system is broadly conserved across bacteria

Calprotectin is antimicrobial against numerous pathogens (Damo et al., 2013). Because of the importance of the *mum* operon in *A. baumannii* resistance to calprotectin, the conservation of this system was investigated (**Figure 15**). The *mum* operon is present in all *A. baumannii* strains queried and other *Acinetobacter* species. A *mumR* homologue is present adjacent to the *mum* operon in all *Acinetobacter* species interrogated but is not present outside of the *Acinetobacter* genus, suggesting that *Acinetobacter* have evolved a unique regulatory mechanism for this operon. The *mum* operon is present with at least four of the five genes retained in some other Gamma Proteobacteria, including the urinary pathogen *Proteus mirabilis,* and more distantly related Proteobacteria including *Agrobacterium tumafaciens.* Portions of the *mum* operon, including NRAMP-family transporters and allophanate hydrolase genes, are also present in diverse bacterial phyla, including *Actinobacteria* and *Firmicutes*. Importantly, portions of the *mum* operon are present in diverse bacterial pathogens, including *S. aureus* and *N. meningitidis*. These observations indicate that the *mum* operon is broadly conserved across bacteria but not in other domains of life.

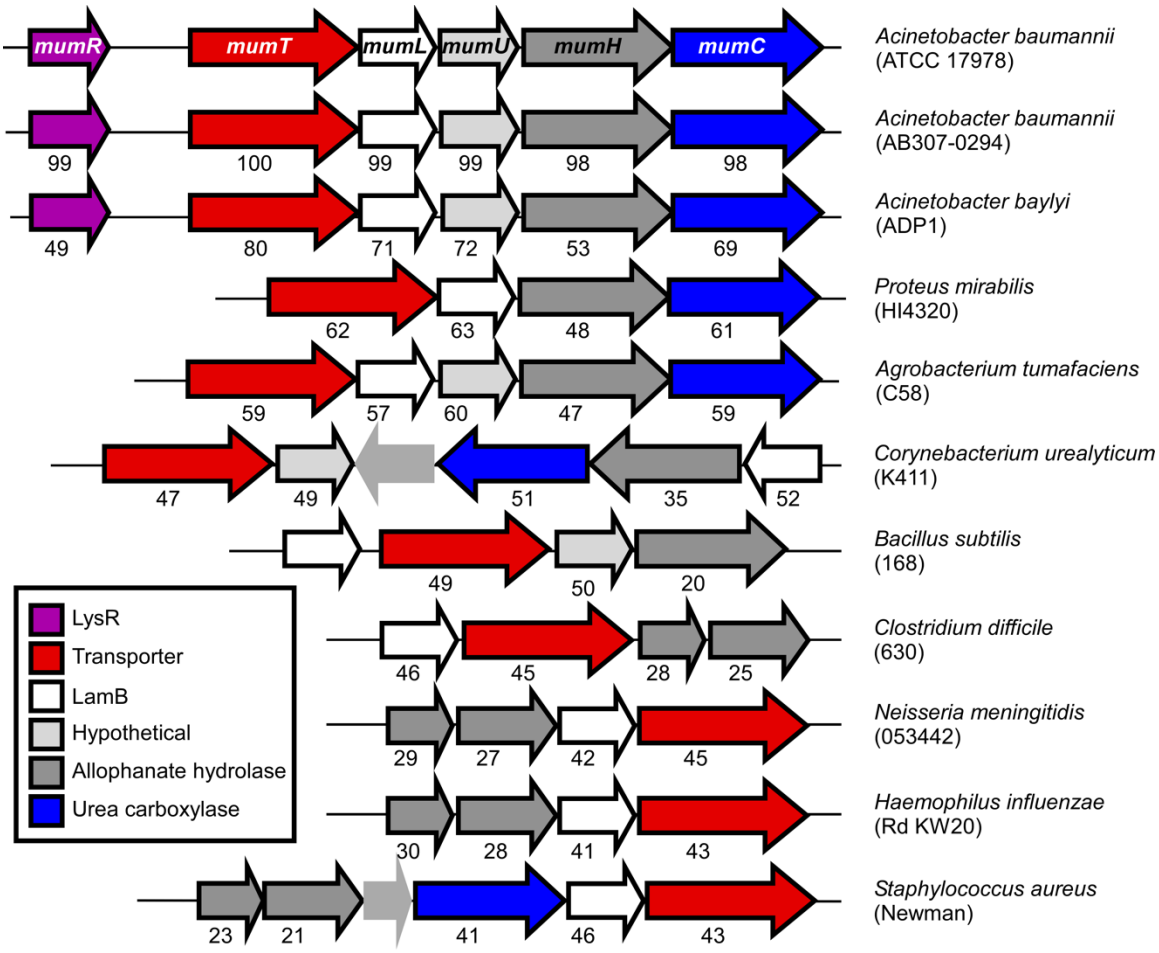

Figure 15: The *mum* system is broadly conserved across bacteria. Genetic alignments of representative organisms that are predicted to contain orthologs of the *mum* system in adjacent loci. Eleven organisms are depicted of the 88 total organisms identified in the SEED database. The numbers underneath each gene correspond to amino acid similarity based on ClustalW2 alignment to the representative *A. baumannii* genes. Genes in light grey with no outline are not part of the *A. baumannii mum* operon.

Discussion

A. baumannii colonization of the murine lung generates a robust immune response, which ultimately results in copious amounts of calprotectin being present at the host-pathogen interface (Moore et al., 2014). Here I demonstrated that the *mum* operon responds to calprotectin and contributes to *A. baumannii* calprotectin resistance (**Figure 16**). MumT was established as a Mn transporter, the unique transcriptional regulation of *mumT* by *mumR* was determined, and a link between *mumT* and urea catabolism via *mumC* was identified. Additionally, urea catabolism was identified as the first metabolic pathway linked to calprotectin resistance, an important step in identifying the mechanisms by which calprotectin disrupts bacterial physiology and inhibits bacterial growth during infection. Finally, the *mum* system was demonstrated to be important for *A. baumannii* fitness in the murine lung and liver, and calprotectin was found to be required to Mn-starve *A. baumannii* in the liver.

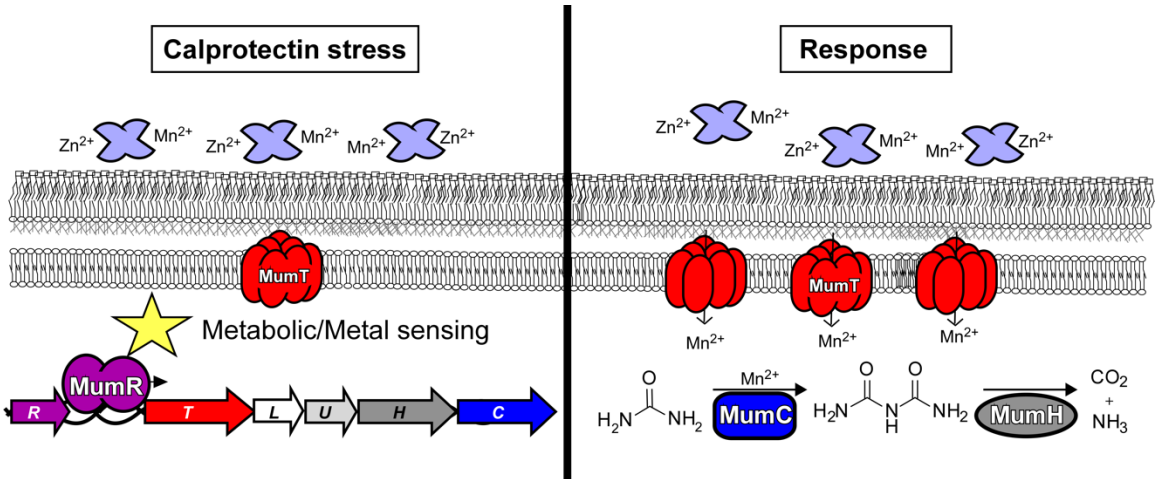

Figure 16: Model for *mum* system response to calprotectin-mediated manganese sequestration. Calprotectin induces *A. baumannii* Mn starvation and an adaptive response. *mum* activation is orchestrated by the transcriptional regulator, MumR, which enhances *mum* expression. *mumT* encodes an NRAMP-family transporter, MumT, that increases cellular Mn content by facilitating Mn import into the cytoplasm. *mumT* increases *A. baumannii* fitness in the lung presumably by providing Mn for important intracellular processes. *mumC* encodes a urea carboxylase enzyme, MumC, that likely utilizes Mn as cofactor. MumC catabolizes urea to ammonia and carbon dioxide, enables the use of urea as a sole nitrogen source, and provides resistance to calprotectin.

mumT encodes an NRAMP-family homologue. *mumT* is unique compared to previously identified NRAMPs, as MumT shares low sequence homology with reported NRAMPs (<25%) and NRAMPs are typically monocistronic (Shabayek, 2016). Inactivation of the *S. aureus* NRAMP-family member MntH increases sensitivity to calprotectin, although a second Mn-transporter (MntABC) must be deleted to see a dramatic growth difference in the presence of calprotectin (Kehl-Fie et al., 2013). Similar to this finding, deletion of *mumT* delayed *A. baumannii* growth in the presence of calprotectin, and this growth difference was reversed by the addition of excess Mn to the medium. In contrast to results obtained in *S. aureus, A. baumannii* growth was significantly decreased by inactivation of *mumT* alone, suggesting that *A. baumannii* may not encode another high-affinity Mn import system. Previously reported NRAMP-family transporters have varying specificity for Mn, Fe, and other divalent cations (Agranoff et al., 1999; Ehrnstorfer et al., 2014; Hohle and O'Brian, 2009; Kehres et al., 2000; Makui et al., 2000; Shin et al., 2014). The metal specificity of MumT was evaluated by determining sensitivity to toxic levels of Mn, Fe, and Zn. Δ*mumT* is less sensitive than WT *A. baumannii* to Mn toxicity. This is consistent with the decreased ability of this strain to accumulate Mn, as measured by ICP-MS. Together, the increased sensitivity of Δ*mumT* to calprotectin, and decreased sensitivity of Δ*mumT* to toxicity of Mn, strongly suggest that *mumT* encodes a transporter that imports Mn. Interestingly, Δ*mumT* has increased sensitivity to Fe toxicity. I hypothesize that the enhanced sensitivity of Δ*mumT* to Fe toxicity stems from disruption of the Mn:Fe ratio. This is consistent with the finding that the ratio of Mn to Fe is important for *N. meningitidis* to survive metal toxicity (Veyrier et al., 2011).

Δ*mumT* is less fit than wild-type *A. baumannii* at colonizing the lung and disseminating to the liver. Of note, Δ*mumT* is not attenuated in dissemination to the livers of mice lacking calprotectin, consistent with the model that calprotectin is required to Mn-starve *A. baumannii* and prevent colonization of the liver. *S. aureus* inactivated for Mn transporters *mntH* and *mntABC* is also attenuated in the livers of wild-type but not calprotectin-deficient mice (Kehl-Fie et al., 2013). Similarly, *A. baumannii* inactivated for the Zn transporter *znuABC* is significantly attenuated in the livers of wild-type mice but not significantly attenuated in calprotectin-deficient mice (Hood et al., 2012). Together, these findings implicate calprotectin metal sequestration as particularly important in host defense of the liver relative to other organs. The heightened efficacy of calprotectin in the liver may be because the liver, the site of Mn absorption into systemic circulation and Mn excretion into bile, is the most Mn-replete organ in the body (Rahil-Khazen et al., 2002). The concentrations of Mn in the *A. baumannii*-infected liver are approximately 25-fold higher than Mn concentrations in the *A. baumannii*-infected lung. In this setting of excess Mn, Δ*mumT* appears to be capable of importing sufficient Mn through other transport systems unless calprotectin is present to sequester Mn. Δ*mumT* is less fit than wild-type *A. baumannii* in the lungs of mice lacking calprotectin, suggesting that additional stresses beyond calprotectin exist in the lung that decrease the fitness of this strain.

Unlike other reported NRAMP-family transporters, *mumT* is in an operon. The other genes in this operon were not previously described in *A. baumannii* and lacked an obvious link to Mn homeostasis. A predicted function was not identified for *mumU* or *mumL,* but based on sequence homology *mumH* and *mumC* were predicted to encode allophanate hydrolase and urea carboxylase, enzymes that catalyze the biotin- and ATP-

dependent two-step catabolism of urea to ammonia and carbon dioxide. Homologs of these genes in *O. sagaranensis* have been cloned and their enzymatic activity verified (Kanamori et al., 2004; Kanamori et al., 2005); however, allophanate hydrolase in *Pseudomonas* functions in cyanuric acid metabolism, not urea metabolism (Cheng et al., 2005). Therefore, the physiological role of these enzymes in bacteria can vary. I found that *A. baumannii* utilizes urea as a nitrogen source but not a carbon source, and urea nitrogen utilization depends on *mumC*. These results demonstrate that urea carboxylase has a physiological role in urea catabolism in this bacterium.

Since *mumC* is in an operon with *mumT,* I investigated whether *mumC* requires *mumT*-delivered Mn for activity. Previous reports suggest that urea carboxylase activity requires divalent cations (Kanamori et al., 2004; Roon and Levenberg, 1972). A strain inactivated for *mumT* is impaired for growth in urea as a sole nitrogen source and in toxic levels of urea. Furthermore, this effect is specific to inactivation of *mumT* and does not occur when other genes in the operon are inactivated. Therefore, this finding suggests that *mumC*-mediated urea catabolism is Mn-dependent.

It is well established that calprotectin inhibits bacterial growth *in vitro* and hampers the growth of some bacteria during infection (Zackular et al., 2015). Ostensibly, calprotectin inhibits growth by suppressing metal-dependent bacterial processes. However, it is unclear what specific bacterial processes are inhibited and how this affects bacterial physiology; currently, the only bacterial process known to be inhibited by calprotectin is *S. aureus* superoxide dismutase activity (Kehl-Fie et al., 2011). Because evolutionary conservation of genomic organization can suggest similar function, I hypothesized that other genes in the *mum* operon may be important for resistance to calprotectin. In keeping

with this, inactivation of *mumC* significantly decreased growth in the presence of calprotectin. This result demonstrates that urea degradation increases the ability of *A. baumannii* to combat calprotectin metal limitation. Furthermore, calprotectin, but not calprotectin lacking the ability to tightly bind Mn, completely inhibits growth of *A. baumannii* utilizing urea as a sole nitrogen source. One interpretation of these results is that urea degradation is a Mn, Zn, or Fe dependent process that is inhibited by calprotectin.

The question remains: why is urea degradation important for growth in the presence of calprotectin? Urea is generated as a byproduct of metabolism in rich medium, and calprotectin-mediated metal starvation may cause a metabolic strain by inhibiting metal-dependent metabolic processes. This could lead to a buildup of urea that requires *mumC*-mediated breakdown. Future work to query this hypothesis will also help define metabolic pathways in *A. baumannii.* Alternatively, urea and/or ammonia could serve as a signaling molecule within the bacterial cell. Our findings emphasize the importance of improving understanding of *A. baumannii* metabolism and the role of metabolism in *A. baumannii* virulence. In this regard, we report that calprotectin-mediated metal starvation and urea catabolism are linked in *A. baumannii.*

The finding that urea carboxylase is important for defense against the antimicrobial protein calprotectin *in vitro* extends the known role of urea in microbial pathogenesis. There are two described pathways for catabolizing urea in bacteria: urease and urea amidolyase (Strope et al., 2011). Urease is a key virulence factor for *H. pylori,* as it is required for local alkalinization and chemotaxis in the stomach (Eaton et al., 1991; Huang et al., 2015; Marshall et al., 1990). *P. mirabilis* also utilizes urease as a virulence factor in the bladder, the site of host urea excretion; urease activity by *P. mirabilis* alters the pH and

causes calculus formation in urine (Schaffer and Pearson, 2015). Urease is also required for virulence of the fungal pathogens *C. neoformans* (Cox et al., 2000) and *Coccidioides posadasii* (Mirbod-Donovan et al., 2006). The only reported virulence role for urea amidolyase systems is for *C. albicans,* which uses urea-produced ammonia to regulate pH and induce the yeast-to-hyphae transition; this system is important for escape from macrophages and colonization of the kidney (Ghosh et al., 2009; Navarathna et al., 2012). The present study indicates that urea amidolyase systems are also important for defense against the human antimicrobial protein calprotectin.

The *mum* operon is conserved across many, but not all bacteria. The *mum* operon is present in many non-pathogenic organisms, including *Acinetobacter baylyi*, suggesting this operon did not evolve exclusively as a virulence factor. However, it is present in many pathogens, including *S. aureus*. Therefore, a better understanding of the genes encoded within this operon may reveal drug targets for the treatment of multi-drug resistant infections.

References

Agranoff, D., Monahan, I.M., Mangan, J.A., Butcher, P.D., and Krishna, S. (1999). *Mycobacterium tuberculosis* expresses a novel pH-dependent divalent cation transporter belonging to the Nramp family. J. Ex. Med. *190*, 717-724.

Brophy, M.B., Nakashige, T.G., Gaillard, A., and Nolan, E.M. (2013). Contributions of the S100A9 c-terminal tail to high-affinity Mn(II) chelation by the host-defense protein human calprotectin. J. Am. Chem. Soc. *135*, 17804-17817.

Cheng, G., Shapir, N., Sadowsky, M.J., and Wackett, L.P. (2005). Allophanate hydrolase, not urease, functions in bacterial cyanuric acid metabolism. Appl. Environ. Microbiol. *71*, 4437-4445.

Corbin, B.D., Seeley, E.H., Raab, A., Feldmann, J., Miller, M.R., Torres, V.J., Anderson, K.L., Dattilo, B.M., Dunman, P.M., Gerads, R.*, et al.* (2008). Metal chelation and inhibition of bacterial growth in tissue abscesses. Science *319*, 962-965.

Cox, G.M., Mukherjee, J., Cole, G.T., Casadevall, A., and Perfect, J.R. (2000). Urease as a virulence factor in experimental cryptococcosis. Infect. Immun. *68*, 443-448.

Damo, S.M., Kehl-Fie, T.E., Sugitani, N., Holt, M.E., Rathi, S., Murphy, W.J., Zhang, Y., Betz, C., Hench, L., Fritz, G.*, et al.* (2013). Molecular basis for manganese sequestration by calprotectin and roles in the innate immune response to invading bacterial pathogens. Proc. Nat. Acad. Sci. *110*, 3841-3846.

Dexter, C., Murray, G.L., Paulsen, I.T., and Peleg, A.Y. (2015). Community-acquired *Acinetobacter baumannii*: clinical characteristics, epidemiology and pathogenesis. Exp. Rev. Anti-Infect. Ther. *13*, 567-573.

Dorsey, C.W., Tomaras, A.P., and Actis, L.A. (2006). Sequence and organization of pMAC, an *Acinetobacter baumannii* plasmid harboring genes involved in organic peroxide resistance. Plasmid *56*, 112-123.

Eaton, K.A., Brooks, C.L., Morgan, D.R., and Krakowka, S. (1991). Essential role of urease in pathogenesis of gastritis induced by *Helicobacter pylori* in gnotobiotic piglets. Infect. Immun. *59*, 2470-2475.

Edgeworth, J., Gorman, M., Bennett, R., Freemont, P., and Hogg, N. (1991). Identification of p8,14 as a highly abundant heterodimeric calcium binding protein complex of myeloid cells. J. Biol. Chem. *266*, 7706-7713.

Ehrnstorfer, I.A., Geertsma, E.R., Pardon, E., Steyaert, J., and Dutzler, R. (2014). Crystal structure of a SLC11 (NRAMP) transporter reveals the basis for transition-metal ion transport. Nat. Struct. Mol. Biol. *21*, 990-996.

Francis, K.P., Joh, D., Bellinger-Kawahara, C., Hawkinson, M.J., Purchio, T.F., and Contag, P.R. (2000). Monitoring bioluminescent *Staphylococcus aureus* infections in living mice using a novel *luxABCDE* construct. Infect. Immun. *68*, 3594-3600.

Fraser, H.I., Kvaratskhelia, M., and White, M.F. (1999). The two analogous phosphoglycerate mutases of *Escherichia coli*. FEBS letters *455*, 344-348.

Ghosh, S., Navarathna, D.H., Roberts, D.D., Cooper, J.T., Atkin, A.L., Petro, T.M., and Nickerson, K.W. (2009). Arginine-induced germ tube formation in *Candida albicans* is essential for escape from murine macrophage line RAW 264.7. Infect. Immun. *77*, 1596-1605.

Goujon, M., McWilliam, H., Li, W., Valentin, F., Squizzato, S., Paern, J., and Lopez, R. (2010). A new bioinformatics analysis tools framework at EMBL-EBI. Nucleic Acids Res. *38*, W695-699.

Hoang, T.T., Karkhoff-Schweizer, R.R., Kutchma, A.J., and Schweizer, H.P. (1998). A broad-host-range Flp-FRT recombination system for site-specific excision of chromosomally-located DNA sequences: application for isolation of unmarked *Pseudomonas aeruginosa* mutants. Gene *212*, 77-86.

Hohle, T.H., and O'Brian, M.R. (2009). The mntH gene encodes the major Mn(2+) transporter in *Bradyrhizobium japonicum* and is regulated by manganese via the Fur protein. Mol. Microbiol. *72*, 399-409.

Hood, M.I., Mortensen, B.L., Moore, J.L., Zhang, Y., Kehl-Fie, T.E., Sugitani, N., Chazin, W.J., Caprioli, R.M., and Skaar, E.P. (2012). Identification of an *Acinetobacter baumannii* zinc acquisition system that facilitates resistance to calprotectin-mediated zinc sequestration. PLOS Pathog. *8*, e1003068.

Hood, M.I., and Skaar, E.P. (2012). Nutritional immunity: transition metals at the pathogen-host interface. Nat. Rev. Microbiol. *10*, 525-537.

Huang, J.Y., Sweeney, E.G., Sigal, M., Zhang, H.C., Remington, S.J., Cantrell, M.A., Kuo, C.J., Guillemin, K., and Amieva, M.R. (2015). Chemodetection and Destruction of Host Urea Allows *Helicobacter pylori* to Locate the Epithelium. Cell Host Microbe *18*, 147-156.

Juttukonda, L.J., and Skaar, E.P. (2015). Manganese homeostasis and utilization in pathogenic bacteria. Mol. Microbiol. *97*, 216-228.

Kanamori, T., Kanou, N., Atomi, H., and Imanaka, T. (2004). Enzymatic characterization of a prokaryotic urea carboxylase. J. Bacteriol. *186*, 2532-2539.

Kanamori, T., Kanou, N., Kusakabe, S., Atomi, H., and Imanaka, T. (2005). Allophanate hydrolase of *Oleomonas sagaranensis* involved in an ATP-dependent degradation pathway specific to urea. FEMS Microbiol. Let. *245*, 61-65.

Kanehisa, M., and Goto, S. (2000). KEGG: kyoto encyclopedia of genes and genomes. Nucleic Acids Res. *28*, 27-30.

Kanehisa, M., Sato, Y., Kawashima, M., Furumichi, M., and Tanabe, M. (2016). KEGG as a reference resource for gene and protein annotation. Nucleic Acids Res. *44*, D457-462.

Kaye, K.S., and Pogue, J.M. (2015). Infections Caused by Resistant Gram-Negative Bacteria: Epidemiology and Management. Pharmacotherapy *35*, 949-962.

Kehl-Fie, T.E., Chitayat, S., Hood, M.I., Damo, S., Restrepo, N., Garcia, C., Munro, K.A., Chazin, W.J., and Skaar, E.P. (2011). Nutrient metal sequestration by calprotectin inhibits bacterial superoxide defense, enhancing neutrophil killing of *Staphylococcus aureus*. Cell Host Microbe *10*, 158-164.

Kehl-Fie, T.E., Zhang, Y., Moore, J.L., Farrand, A.J., Hood, M.I., Rathi, S., Chazin, W.J., Caprioli, R.M., and Skaar, E.P. (2013). MntABC and MntH contribute to systemic *Staphylococcus aureus* infection by competing with calprotectin for nutrient manganese. Infect. Immun. *81*, 3395-3405.

Kehres, D.G., Zaharik, M.L., Finlay, B.B., and Maguire, M.E. (2000). The NRAMP proteins of *Salmonella typhimurium* and *Escherichia coli* are selective manganese transporters involved in the response to reactive oxygen. Mol. Microbiol. *36*, 1085-1100.

Larkin, M.A., Blackshields, G., Brown, N.P., Chenna, R., McGettigan, P.A., McWilliam, H., Valentin, F., Wallace, I.M., Wilm, A., Lopez, R.*, et al.* (2007). Clustal W and Clustal X version 2.0. Bioinformatics *23*, 2947-2948.

Makui, H., Roig, E., Cole, S.T., Helmann, J.D., Gros, P., and Cellier, M.F. (2000). Identification of the *Escherichia coli* K-12 Nramp orthologue (MntH) as a selective divalent metal ion transporter. Mol. Microbiol. *35*, 1065-1078.

Marshall, B.J., Barrett, L.J., Prakash, C., McCallum, R.W., and Guerrant, R.L. (1990). Urea protects *Helicobacter (Campylobacter) pylori* from the bactericidal effect of acid. Gastroenterology *99*, 697-702.

Milrad de Forchetti, S.R., and Cazzulo, J.J. (1976). Some properties of the pyruvate carboxylase from *Pseudomonas fluorescens*. J. Gen. Microbiol. *93*, 75-81.

Mirbod-Donovan, F., Schaller, R., Hung, C.Y., Xue, J., Reichard, U., and Cole, G.T. (2006). Urease produced by *Coccidioides posadasii* contributes to the virulence of this respiratory pathogen. Infect. Immun. *74*, 504-515.

Moore, J.L., Becker, K.W., Nicklay, J.J., Boyd, K.L., Skaar, E.P., and Caprioli, R.M. (2014). Imaging mass spectrometry for assessing temporal proteomics: analysis of calprotectin in *Acinetobacter baumannii* pulmonary infection. Proteomics *14*, 820-828.

Mortensen, B.L., Rathi, S., Chazin, W.J., and Skaar, E.P. (2014). *Acinetobacter baumannii* response to host-mediated zinc limitation requires the transcriptional regulator Zur. J. Bacteriol. *196*, 2616-2626.

Nairn, B.L., Lonergan, Z.R., Wang, J., Braymer, J.J., Zhang, Y., Calcutt, M.W., Lisher, J.P., Gilston, B.A., Chazin, W.J., de Crecy-Lagard, V.*, et al.* (2016). The Response of *Acinetobacter baumannii* to Zinc Starvation. Cell Host Microbe *19*, 826-836.

Nakashige, T.G., Zhang, B., Krebs, C., and Nolan, E.M. (2015). Human calprotectin is an iron-sequestering host-defense protein. Nat. Chem. Biol. *11*, 765-771.

Navarathna, D.H., Lionakis, M.S., Lizak, M.J., Munasinghe, J., Nickerson, K.W., and Roberts, D.D. (2012). Urea amidolyase (DUR1,2) contributes to virulence and kidney pathogenesis of *Candida albicans*. PlOS One *7*, e48475.

Overbeek, R., Begley, T., Butler, R.M., Choudhuri, J.V., Chuang, H.Y., Cohoon, M., de Crecy-Lagard, V., Diaz, N., Disz, T., Edwards, R.*, et al.* (2005). The subsystems approach to genome annotation and its use in the project to annotate 1000 genomes. Nucleic Acids Res. *33*, 5691-5702.

Peleg, A.Y., and Hooper, D.C. (2010). Hospital-acquired infections due to gram-negative bacteria. N. Engl. J. Med. *362*, 1804-1813.

Rahil-Khazen, R., Bolann, B.J., Myking, A., and Ulvik, R.J. (2002). Multi-element analysis of trace element levels in human autopsy tissues by using inductively coupled atomic emission spectrometry technique (ICP-AES). J. Trace. Elem. Med. Biol. *16*, 15-25.

Roon, R.J., Hampshire, J., and Levenberg, B. (1972). Urea amidolyase. The involvement of biotin in urea cleavage. J. Biol. Chem. *247*, 7539-7545.

Roon, R.J., and Levenberg, B. (1972). Urea amidolyase. I. Properties of the enzyme from *Candida utilis*. J. Biol. Chem. *247*, 4107-4113.

Schaffer, J.N., and Pearson, M.M. (2015). *Proteus mirabilis* and Urinary Tract Infections. Microbiol. Spectrum *3*.

Shabayek, S., Bauer, R., Mauerer, S., Mizaikoff, B. and Spellerberg, B. (2016). A streptococcal NRAMP homologue is crucial for the survival of *Streptococcus agalactiae* under low pH conditions. Mol. Microbiol..

Shin, J.H., Wakeman, C.A., Goodson, J.R., Rodionov, D.A., Freedman, B.G., Senger, R.S., and Winkler, W.C. (2014). Transport of magnesium by a bacterial Nramp-related gene. PLOS Genet. *10*, e1004429.

Sievert, D.M., Ricks, P., Edwards, J.R., Schneider, A., Patel, J., Srinivasan, A., Kallen, A., Limbago, B., Fridkin, S., Network, N.H.S.*, et al.* (2013). Antimicrobial-Resistant Pathogens Associated with Healthcare-Associated Infections: Summary of Data Reported to the National Healthcare Safety Network at the Centers for Disease Control and Prevention, 2009-2010. Infect. Cont. Hosp. Ep. *34*, 1-14.

Strope, P.K., Nickerson, K.W., Harris, S.D., and Moriyama, E.N. (2011). Molecular evolution of urea amidolyase and urea carboxylase in fungi. BMC Evol. Biol. *11*, 80.

van Faassen, H., KuoLee, R., Harris, G., Zhao, X., Conlan, J.W., and Chen, W. (2007). Neutrophils play an important role in host resistance to respiratory infection with *Acinetobacter baumannii* in mice. Infect. Immun. *75*, 5597-5608.

Veyrier, F.J., Boneca, I.G., Cellier, M.F., and Taha, M.K. (2011). A novel metal transporter mediating manganese export (MntX) regulates the Mn to Fe intracellular ratio and *Neisseria meningitidis* virulence. PLOS Pathog. *7*, e1002261.

Vishniac, W., and Santer, M. (1957). The thiobacilli. Bacteriol. Rev. *21*, 195-213.

Vogel, H.J., and Bonner, D.M. (1956). Acetylornithinase of *Escherichia coli*: partial purification and some properties. J. Biol. Chem. *218*, 97-106.

Zackular, J.P., Chazin, W.J., and Skaar, E.P. (2015). Nutritional Immunity: S100 Proteins at the Host-Pathogen Interface. J. Biol. Chem. *290*, 18991-18998.

CHAPTER III

THE TRANSCRIPTIONAL REGULATORS OXYR AND MUMR RESPOND TO HYDROGEN PEROXIDE IN THE LUNG DURING *ACINETOBACTER BAUMANNII* INFECTION

Introduction

A. baumannii is a Gram-negative coccobacillus and an obligate aerobe. Since the emergence of *A. baumannii* as a cause of infection decades ago, this organism has become one of the most difficult bacterial infections to treat because of extensive intrinsic and evolved antimicrobial resistance (Antunes et al., 2014; Dijkshoorn et al., 2007; Peleg et al., 2008; Perez et al., 2007; Potron et al., 2015). The increasing rates of carbapenem-resistant *A. baumannii* infections are such a threat to human health globally that the World Health Organization named carbapenem-resistant *A. baumannii* as the number one 'critical' priority for the development of new antibiotics (WHO, 2017). Therefore, research investigating basic mechanisms by which *A. baumannii* within hosts and in the environment is an urgent need.

Infections caused by *A. baumannii* are often in the context of critically ill or immunocompromised hosts, although community-acquired infections have become more common (Dexter et al., 2015). *A. baumannii* does not possess known classical virulence mechanisms such as effector toxins or immune evasion strategies (Antunes et al., 2014). Instead, *A. baumannii* utilizes genes evolved for survival in the environment to persist during infection (McConnell et al., 2013). Moreover, the ability of *A. baumannii* to survive

within the hospital environment allows this organism to cause outbreaks of hospital-associated infections that are costly to eradicate (Roca et al., 2012). We therefore predict that processes involved in sensing and responding to the environment are critical for *A. baumannii* to be a successful opportunistic pathogen.

During infection, bacteria experience numerous stresses imposed by the host. These stresses must be sensed by the bacterium in order to alter its physiological state and survive this stress. For instance, nutrient metals are limited during infection; metal starvation is sensed by transcriptional regulators and high-affinity metal importers are upregulated (Becker and Skaar, 2014). Another stress encountered during infection is reactive oxygen species produced by effector cells of the innate immune system (Hampton et al., 1998). In particular, neutrophils generate an oxidative burst that results in the production of superoxide, hydrogen peroxide, hypochlorous acid and peroxynitrate at the site of infection (Hampton et al., 1998). These molecules are highly toxic. In response, pathogens encode proteins that detoxify reactive oxygen species. Expression of detoxification proteins is controlled by transcriptional regulators that sense either the reactive molecule itself or the damage caused by reactive molecules (Demple, 1991).

The previous chapter identified the Mn transporter MumT in *A. baumannii* and demonstrated that this transporter enhances the fitness of *A. baumannii* in a murine model of pneumonia. Adjacent to the *mum* operon is a gene encoding the predicted transcriptional regulator *mumR.* Transcription of *mumT* is activated in a *mumR*-dependent fashion, but the function of MumR and role of MumR during infection was not explored in this study.

MumR is a member of the LysR family of transcriptional regulators. LysR regulators are the most common transcriptional regulator in bacteria and respond to a

variety of stimuli (Schell, 1993). A conserved helix-turn-helix DNA binding domain is found at the N-terminus of LysR regulators, followed by a dimerization interface and finally the substrate-binding C-terminal domain (Maddocks and Oyston, 2008). The substrate-binding domain is highly divergent and determines the specificity of the regulator (Maddocks and Oyston, 2008). While most LysR-family proteins regulate one locus that is often divergently transcribed from the regulator, some LysR-family regulators have large regulons (Schell, 1993). Interestingly, LysR-family regulators can be activators or repressors of gene transcription and often bind to multiple locations within a single promoter (Schell, 1993).

While carrying out the experiments of the previous study (Chapter II), I observed that *A. baumannii* genetically inactivated for *mumR* (Δ*mumR*) grows more slowly in the presence of hydrogen peroxide (unpublished work). This result suggested that MumR may have some role in responding to peroxide stress. The possibility that MumR may be important under peroxide stress is intriguing because a different LysR-family transcriptional regulator, OxyR, is the canonical orchestrator of the hydrogen peroxide detoxification response in Gram-negative bacteria (Christman et al., 1985).

OxyR is a highly conserved transcriptional regulator of the LysR-family that senses and responds to hydrogen peroxide stress (Chiang and Schellhorn, 2012; Christman et al., 1989; Tao et al., 1991). Oxidation of a conserved cysteine residue causes OxyR to undergo a conformational change and alters DNA binding activity of OxyR (Chiang and Schellhorn, 2012; Choi et al., 2001; Jo et al., 2015; Storz et al., 1990; Zheng et al., 1998). In *Escherichia coli,* OxyR serves as a transcriptional activator of genes involved in hydrogen peroxide detoxification, including alkyl hydroperoxidase, catalase, and dps (Tao et al., 1991;

Tartaglia et al., 1989). While OxyR is highly conserved, the function of this protein varies between organisms; for instance, OxyR in *Corynebacterium glutamicum* is a transcriptional repressor, and inactivation of *oxyR* enhances resistance to hydrogen peroxide (Milse et al., 2014). While *oxyR* in *A. baumannii* and other *Acinetobacter* species has been identified and shown to confer resistance to hydrogen peroxide in agar plates, the function of *A. baumannii* OxyR has not been studied (Geissdorfer et al., 1999; Longkumer et al., 2014; Tucker et al., 2014).

There are a number of interesting similarities between MumR and OxyR. Both regulators are members of the LysR family of transcriptional regulators and both proteins contain two cysteine residues in the substrate-binding domain that could serve as thiol sensors of peroxides (Hillion and Antelmann, 2015). OxyR in *E. coli* and *Salmonella* is transcriptional activator of *mntH,* which encodes the Nramp-family Mn transporter in *E. coli* (Anjem et al., 2009; Kehres et al., 2002). *A. baumannii* MumR is a transcriptional activator of *mumT*, which encodes the Nramp-family Mn transporter in *A. baumannii* (see Chapter II). It is intriguing to note that LysR family regulators bind to the relatively nonspecific motif $AN_{11}T$, and OxyR consensus binding sequences are degenerate, suggesting that promoter binding at the same site may be possible for multiple regulators (Tartaglia et al., 1992). Finally, transcriptomic analysis in *E. coli* has revealed that some genes are regulated by hydrogen peroxide in an *oxyR*-independent fashion, suggesting a role for additional peroxide-sensing regulators (Zheng et al., 2001). Therefore, I hypothesize that MumR and OxyR both regulate genes involved in the survival of hydrogen peroxide stress and that a subset of gene targets may be regulated by both MumR and

OxyR. I anticipate that this is functionally important for *A. baumannii* because of differences in the mechanism of action by MumR and OxyR.

In the study described in this Chapter, I seek to define the roles of MumR and OxyR in *A. baumannii* defense against hydrogen peroxide stress during infection. In doing this, the function of *A. baumannii* OxyR in hydrogen peroxide stress resistance and regulation of genes required for hydrogen peroxide detoxification is defined. Moreover, the contribution of the uncharacterized regulator MumR to hydrogen peroxide stress resistance is also explored. Finally, we demonstrate that hydrogen peroxide is formed *in vivo* during *A. baumannii* lung infection, and that *mumR* and *oxyR* enhance the fitness of *A. baumannii* in this infection model.

Materials and Methods

Bacterial strains and reagents. The strains used in this study are described in **Table 3**. All strains are derivatives of the human clinical isolate *A. baumannii* ATCC 17978. Cloning was performed in *E. coli* DH5α. Bacteria were routinely grown in lysogeny broth (LB) at 37°C unless otherwise noted. Solid medium contained 1.5% agar. Antibiotics were added at the following concentrations: 75 μg mL^{-1} carbenicillin, 40 μg mL^{-1} kanamycin, and 10 μg mL^{-1} tetracycline. All antibiotics were purchased from Sigma (St. Louis, MO).

Strain generation. Primers used in this Chapter are listed in **Table 4**. In-frame deletion strain Δ*oxyR* was generated via one-step recombineering as previously described. Briefly, the kanamycin resistance cassette *aph1* from pUC18K1 was amplified using primer pairs LEJ_209 and LEJ_220, which contained 120 bp regions of homology flanking the *oxyR* ORF. The PCR product was purified using column PCR purification (QIAGEN, Hilden,

DE), concentrated to >1 μg/μL, and electroporated into WT *A. baumannii* containing pATO2 (Tucker et al., 2014). Rec_{Ab} expression was induced with 2 mM isopropyl β-D-1-thiogalactopyranoxide (IPTG, Sigma, St. Louis, MO), cultures were grown at 37 °C for four hours, and half of the transformed cells were plated onto LB agar containing kanamycin. Kanamycin resistant colonies were re-streaked onto LB agar with kanamycin and screened by PCR for replacement of the *oxyR* allele with *aph1* with primer pairs LEJ_213 and LEJ_214. Clones with the correct insertion were restreaked to kanamycin and carbenicillin containing solid medium to screen for the loss of the pAT02 plasmid and kan^R $carb^S$ clones were saved at -80°C. Complementation vectors were constructed in either pWH1266 (*oxyR*) or pMU368tet (*mumR*) under the control of the 16S promoter (*r01*) by PCR amplification of the open reading frame (ORF), double digest of the vector and PCR product with the enzymes indicated in the primer list (all from New England Biolabs, Ipswich, MA), and ligation with T4 DNA ligase (Promega, Madison WI). Site-directed mutagenesis was performed by subcloning the ORF into pCRBlunt (Invitrogen, Carlsbad, CA) and amplifying the vector with Pfu Turbo polymerase (ThermoFisher, Waltham, MA) and primers as indicated in **Table 4**. The 50 μL PCR product was treated with 1.5 μL Dpn1 (New England Biolabs, Ipswich, MA) for 2 hours, transformed into DH5α, and transformants were plated onto LB agar containing kanamycin. Clones that contained the desired mutations were confirmed by Sanger sequences, pCR2.1 plasmids were miniprepped and digested, and inserts were subcloned into pP_{r01}WH1266 to generate complementation vectors with desired point mutations.

Table 3: Bacterial strains used in Chapter III.

Strain	Relevant characteristics	Reference or source
17978	Wild-type	ATCC
Δ*mumR*	In-frame Δ*mumR::aphA*	(Juttukonda et al., 2016)
Δ*oxyR*	In-frame Δ*oxyR::aphA*	This study
Δ*mumR* pMU368tet	Empty vector control	This study
17978 pMU368tet	Empty vector control	This study
17978 pP_{r01}WH1266	Empty vector control	(Hood et al., 2012)
Δ*mumR* p.P_{r01}.*mumR*.MU368tet	Complementation strain containing plasmid p.P_{r01}.*mumR*.MU368tet	This study
Δ*oxyR* pP_{r01}WH1266	Empty vector control	This study
Δ*oxyR* pP_{r01}.*oxyR*.WH1266	Complementation strain containing plasmid p.P_{r01}.*oxyR*.WH1266	This study
Δ*mumR* p.*mumR* C154S	Complementation strain containing plasmid p.P_{r01}.*mumR*.WH1266 with C154S mutation	This study
Δ*mumR* p.*mumR* C154S C160S	Complementation strain containing plasmid p.P_{r01}.*mumR*.WH1266 with C154S and C160S mutations	This study
Δ*oxyR* p.*oxyR* C202S	Complementation strain containing plasmid p.P_{r01}.*oxyR*.WH1266 with C202S mutation	This study
Δ*oxyR* p.*oxyR* C211S	Complementation strain containing plasmid p.P_{r01}.*oxyR*.WH1266 with C211S mutation	This study
Δ*oxyR* p.*oxyR* C202S C211S	Complementation strain containing plasmid p.P_{r01}.*oxyR*.WH1266 with C202S and C211S mutation	This study
17978 pAT02	WT harboring rec_{Ab} machinery for recombineering	(Tucker et al., 2014)
Escherichia coli DH5α p.*mumR*	Cloning strain containing plasmid p.P_{r01}.*mumR*.WH1266	This study
Escherichia coli DH5α p.*oxyR*	Cloning strain containing plasmid p.P_{r01}.*oxyR*.WH1266	This study
Escherichia coli DH5α p.*mumR* C154S	Cloning strain containing plasmid p.P_{r01}.*mumR*.WH1266 with C154S mutation	This study
Escherichia coli DH5α p.*mumR* C154S C160S	Cloning strain containing plasmid p.P_{r01}.*mumR*.WH1266 with C154S and C160S mutations	This study

Escherichia coli DH5α p.*oxyR* C202S	Cloning strain containing plasmid p.P_{r01}.*oxyR*.WH1266 with C202S mutation	This study
Escherichia coli DH5α p.*oxyR* C211S	Cloning strain containing plasmid p.P_{r01}.*oxyR*.WH1266 with C211S mutation	This study
Escherichia coli DH5α p.*oxyR* C202S C211S	Cloning strain containing plasmid p.P_{r01}.*oxyR*.WH1266 with C202S and C211S mutation	This study
Escherichia coli DH5α p.*mumR* pCRBlunt	Cloning strain containing *mumR* in pCRBlunt	This study
Escherichia coli DH5α p.*oxyR* pCRBlunt	Cloning strain containing *oxyR* in pCRBlunt	This study
Escherichia coli DH5α p.*mumR* C154S pCRBlunt	Cloning strain containing *mumR* with C154S mutation in pCRBlunt	This study
Escherichia coli DH5α p.*mumR* C154S C160S pCRBlunt	Cloning strain containing *mumR* with C154S and C160S mutations in pCRBlunt	This study
Escherichia coli DH5α p.*oxyR* C202S pCRBlunt	Cloning strain containing *oxyR* with C202S mutation in pCRBlunt	This study
Escherichia coli DH5α p.*oxyR* C211S pCRBlunt	Cloning strain containing *oxyR* with C211S mutation in pCRBlunt	This study
Escherichia coli DH5α p.*oxyR* C202S C211S pCRBlunt	Cloning strain containing *oxyR* with C202S and C211S mutation in pCRBlunt	This study
Escherichia coli BL21 (DE3) p.*mumR*.ET15B	Protein expressing strain for *mumR* cloned into pET15B	This study
Escherichia coli BL21 (DE3) p.*oxyR*.ET15B	Protein expressing strain for *oxyR* cloned into pET15B	This study
Escherichia coli DH5α p.*mumR*.ET15B	Cloning strain for *mumR* cloned into pET15B	This study
Escherichia coli DH5α p.*oxyR*.ET15B	Cloning strain for *oxyR* cloned into pET15B	This study

Table 4: Primers used in Chapter III.

Primer	Primer Sequence	Primer description
LEJ_27	AGTGGCAGGCTCAAAAGTGC	*mumL* 5' qRT-PCR primer
LEJ_28	GCATCAATTACGGCTGCTGC	*mumL* 3' qRT-PCR primer
LEJ_42	AGGCGTGGAAATCTACGGTG	*A1S_1205* 5' qRT-PCR primer
LEJ_43	ATCGCGTCTGAAGTGTCGTG	*A1S_1205* 3' qRT-PCR primer
LEJ_46	CGAATTTGGGTACGCCTGAGA	*A1S_3382* 5' qRT-PCR primer
LEJ_47	GCCTTGTTGAGAACGCCAGT	*A1S_3382* 3' qRT-PCR primer
LEJ_99	gcggcagccatatgctcgagAATTTAAAG AATCTTGAAGCATTTTAC	5' primer for amplifying *mumR* with BamHI site for cloning into pET15B vector
LEJ_100	tgttccaggggcccggatccAATTTAAAG AATCTTGAAGCATTTTAC	3' primer for amplifying *mumR* with XhoI 1265 for cloning into pET15B vector
LEJ_209	AAGTTTGAATTAATTGATGGAA TGGGGCATGATATCCCTGCCCA TTTTATTCCACAGCTTAGCGGT TTATTTGCGCATCATTTTAAATC ATCATACTAGGACACTATGGCT GCATTACCCTCACTATGA CTA ACT AGG AGG AATA	5' primer to amplify *aph1* kanamycin resistance cassette for *oxyR* recombineering
LEJ_220	AAAAAATAATTGCAGATGATA GCTTGGATTTGAGATCGGCTTG GGTATTTAAATGGGCTTCCCTA ACAGCACAGTAAAATAAAAAG GAGTCCGCAGACTCCTTTTTTT ATTCATGTAAGTTTGTGGT TCATTATTCCCTCCAGGTACT	3' primer to amplify *aph1* kanamycin resistance cassette for *oxyR* recombineering
LEJ_211	TAAGGATCCatggctgcattaccct	5' primer to amplify *oxyR* with BamHI cut site, for cloning into pP_{r01}WH1266 complementation vector
LEJ_212	GGAGTCGACttattcatgtaagtttgtggta	3' primer to amplify *oxyR* with SalI cut site, for cloning into pP_{r01}WH1266 complementation vector
LEJ_213	ACTGCAACTGGACCGTGAAAT	5' primer outside of *oxyR* recombineering construct to check integration
LEJ_214	GACCCTGCCAATGACTATGCA	3' primer outside of *oxyR* recombineering construct to check integration
LEJ_217	GGCCAACTTTGGCTTTTGAA AGCATTGAGCAGTCGCTTTGTA AC	Side-directed mutagenesis primer for *mumR* C154S

LEJ_218	GAATGTATTGAGCAGTCGCTT AGCAACTTTGAACTGAGTTTCT TG	Side-directed mutagenesis primer for *mumR* C160S
LEJ_219	CAACTTTGGCTTTTGAA AGC ATTGAGCAGTCGCTT AGC AACTTTGAACTGAGTTTC	Side-directed mutagenesis primer for *mumR* C154SC160S
LEJ_234	gtgatcatgtattaagtgccAGCccaattggtgag cgtaaaaac	Side-directed mutagenesis primer for *oxyR* C211S
LEJ_235	gtttttacgctcaccaattggGCTggcacttaatac atgatcac	Side-directed mutagenesis primer for *oxyR* C211S, reverse complement
LEJ_236	cattttgcttgaagaaggccacAGCttacgtgatc atgtattaag	Side-directed mutagenesis primer for *oxyR* C204S
LEJ_237	cttaatacatgatcacgtaaGCTgtggccttcttca agcaaaatg	Side-directed mutagenesis primer for *oxyR* C204S, reverse complement
LEJ_243	AGAGGGATTTAAAACTAAGTAT TCAGTAATTTCAG	5' primer for amplifying promoter of *A1S_3382*
LEJ_244	AATGTTAAATCCAAAAGTATAA ATGCCTTTCC	3' primer for amplifying promoter of *A1S_3382*
LEJ_245	GAAGCTTACCTACTAAAAATTC AAGGGTG	3' primer for amplifying promoter of *A1S_1205*
LEJ_246	GTTCAAAACGCTGTCTAACTTT TGC	5' primer for amplifying promoter of *A1S_1205*
LEJ_247	GATTATATTCTCTCTGGGTAAT ATTTATTGAGCTC	3' primer for amplifying promoter of *A1S_0412*
LEJ_248	CTTTATTCGATACGCATCATTTT TTTAACCCAG	5' primer for amplifying promoter of *A1S_0412*
LEJ_251	TAGTCGACttaTAGATCTTCTTCA GATATCAGTTTCTGTTCttcatgtaag tttgtggtaa	3' primer to amplify *oxyR* with C-terminal myc tag and SalI cut site
LEJ_252	TAGGATCCATGGAACAGAAAC TGATATCTGAAGAAGATCTAgct gcattaccctcacta	5' rimer to amplify *oxyR* with N-terminal myc tag and BamHI cut site
LEJ_253	agcaGGATCCATGAATTTAAAGA ATCTTG	5' primer for amplifying *mumR* with BamHI cut site, changing start codon to ATG, for cloning into pP_{r01}WH1266 complementation vector
LEJ_254	cagcgtGTCGACTTATTTTTTAATT TGTTCATTGAG	3' primer to amplify *mumR* with SalI site, for cloning into pP_{r01}WH1266 complementation vector
LEJ_183	tagtaatggtgcggcagcag	*A1S_1351* 5' qRT-PCR primer
LEJ_184	atctgccgcatgcggattac	*A1S_1351* 3' qRT-PCR primer
LEJ_187	ccagatttccaccgtcgtga	*A1S_1386* 5' qRT-PCR primer
LEJ_188	cggccaattggtgtaacaggaa	*A1S_1386* 3' qRT-PCR primer

LEJ_203	cgggaacatcgcacttgagtc	*A1S_0412* 5' qRT-PCR primer
LEJ_204	gcttcagagttgcgatgagct	*A1S_0412* 3' qRT-PCR primer
LEJ_205	aggcgaaacggttgaccttg	*A1S_0159* 5' qRT-PCR primer
LEJ_206	aagttgtttgcagggaagcctaag	*A1S_0159* 3' qRT-PCR primer
r01RTf	CTGTAGCGGGTCTGAGAGGAT	*r01* 5' qRT-PCR primer
r01RTr	CCATAAGGCCTTCTTCACAC	*r01* 3' qRT-PCR primer
LEJ_227	attCATATGgctgcattaccctcactaag	5' primer for amplifying *mumR* with NdeI site for cloning into pET15B vector
LEJ_228	gctGGATCCttattcatgtaagtttgtgg	3' primer for amplifying *mumR* with BamHI 1265 for cloning into pET15B vector

Hydrogen peroxide growth assays. LB was used as the growth medium for all assays and contained antibiotics as necessary for maintenance of plasmids. Bacterial strains were freshly streaked to solid agar and grown to stationary phase in 3 mL overnight cultures. Overnight cultures were sub-cultured 1:50 in LB for one hour prior to 1:100 inoculation of medium containing hydrogen peroxide (30%, EMD Millipore, Darmstadt, DE) at the indicated concentrations. All growth assays were carried out in 96-well plates in 100 μL volume, and optical density absorbance at 600 nm was measured as a proxy for growth.

Hydrogen peroxide disc diffusion assays. Disc diffusion assays were modified from published protocols (LeBlanc et al., 2008; Sund et al., 2008). Freshly streaked strains were grown to stationary phase in 3 mL overnight cultures, diluted 1:10 in in LB, and 100 μL of diluted culture was added to 4 mL of melted soft agar (0.75% agar) and immediately poured onto LB agar plates, which were allowed to dry for 5 minutes. Sterile 6-mm paper discs were placed in the center of the plate and loaded with 10 μL of 30% H_2O_2 (EMD Millipore, Darmstadt, DE). After incubation at 37°C for 20 hours, the zone of growth inhibition was determined as the mean of three separate diameter measurements.

Hydrogen peroxide killing assays. Biological triplicate overnight cultures of *A. baumannii* WT, Δ*oxyR,* and Δ*mumR* were diluted 1:1000 into 10 mL LB in 50 mL conical tubes and grown to mid-exponential phase. Cultures were treated with hydrogen peroxide (EMD Millipore, Darmstadt, DE) at the indicated concentrations for the time indicated. At each timepoint, 10 μL of culture was collected, serially diluted in PBS containing catalase (2,000 units/mL, catalase from bovine liver, Sigma, St. Louis, MO) and spot-plated to LB agar for CFU enumeration.

Purification of recombinant protein. The open reading frames of *mumR* and *oxyR* were cloned into pET15B (Novagen, EMD Millipore, Darmstadt, DE) to generate N-terminal hexahistidine-tagged constructs. ORFs were amplified primer pairs LEJ_99 and LEJ_100 (*mumR*) or LEJ_227 and LEJ_228 (*oxyR*), double digested with XhoI and BamHI-HF (*mumR*) or NdeI and BamHI-HF (*oxyR*) (New England Biolabs, Ipswich, MA), ligated into pET15B with T4 DNA ligase (Promega, Madison, WI), and transformed into DH5α. *E. coli* BL21 (DE3) was transformed with the resultant vectors and grown at 37°C to an OD_{600} of 0.4-0.6 before induction with 1 mM isopropyl β-D-1-thiogalactopyranoxide (IPTG, Sigma, St. Louis, MO). Following induction, bacteria were maintained at 30 °C for an addition 8-10 hours. Cells were harvested by centrifugation at 6000 x *g* for 10 minutes, washed once with LB, and stored at -70°C. Cells were thawed, resuspended in lysis buffer (50 mM Tris pH 8, 300 mM NaCl, 20 mM imidazole, 1 mg/mL lysozyme, protease inhibitor cocktail (Sigma, St. Louis, MO), and deoxyribonuclease (Sigma, St. Louis, MO)), dounce homogenized, and lysed at 20,000 psi for 5 minutes in an EmulsiFlex homogenizer (Aventin, Inc., Ottawa, ON). Following disruption, lysates were centrifuged at 15,000 rpm for 1 hour at 4 °C to remove the insoluble fraction. The supernatants were passed through a 45 micron filter and applied to a Ni-NTA column (Qiagen, Hilden, DE). The column was washed with 20 bed volumes of wash buffer (50 mM Tris pH 8, 300 mM NaCl, 25 mM imidazole) followed by sequential washes with increasing concentrations of imidazole (100 mM, 150 mM, 200 mM, 250 mM, 300 mM, 500 mM). OxyR eluted free of contaminating proteins at 200 mM imidazole and MumR eluted free of contaminating proteins at 150 mM imidazole. Buffer exchange was performed using PD-10 desalting columns (GE Healthcare

Life Sciences, Little Chalfont, UK) to the final buffer (20 mM tris, pH, 500 mM NaCl, 5% glycerol).

Electromobility shift assays. Promoter DNA was amplified by PCR using primer pairs outlined in **Table 4** and purified by Qiagen PCR clean up kit (Qiagen, Hilden, DE). Forty ng of promoter was incubated for 30 minutes at room temperature with freshly purified OxyR or MumR at the indicated concentrations in EMSA binding buffer (20 mM tris HCl pH 7.5, 2.5 mM $MgCl_2$, 0.45 mM EDTA, 0.05% nonidet P-40, 10% glycerol, and 0.5 mM dithiothreitol) that was modified with DTT or hydrogen peroxide as noted. Samples were separated by electrophoresis in 6% polyacrylamide 0.5X TBE gels (5X TBE contained 89 mM Tris base, 89 mM boric acid, and 1 mM EDTA) that were prerun at 100V for 20 minutes. Following electrophoresis, gels were stained with SYBR Green (Invitrogen, Carlsbad, CA) diluted 1:10,000 in 0.5X TBE for 20 minutes in the dark, washed twice with H_2O, and visualized with a gel imager (BIO-RAD, Herculues, CA).

Mouse infections. A competitive infection murine model of pneumonia was utilized. Wild-type *A. baumannii* or isogenic, kanamycin-marked strains (Δ*mumR* or Δ*oxyR*) was freshly streaked from frozen stocks onto LB agar or LB agar containing 40 μg mL^{-1} kanamycin, respectively, two days prior to infection. Overnight cultures were grown in LB without antibiotic selection. On the day of the infection, overnight cultures were sub-cultured 1:1,000 in 10 mL of LB and grown to mid-exponential phase. Cells were then harvested by centrifugation, washed twice in PBS, and resuspended in PBS to a final concentration of 1 x 10^{10} CFU mL^{-1}. Wild-type and isogenic mutant suspensions were then combined in a 1:1 ratio, mixed thoroughly, and immediately utilized for infection. Mice were anesthetized with intraperitoneal injection of 2,2,2-tribromoethanol diluted in PBS.

Anesthetized mice were inoculated intranasally with 5 x 10^8 CFU in 50 microliter volume. Infection proceeded for 36 hours. Mice were then euthanized with CO_2 and lungs and livers removed and placed on ice. Organs were homogenized in 1 mL PBS, serially diluted in PBS or PBS with catalase (for Δ*oxyR*; 2,000 units/mL, catalase from bovine liver, Sigma, St. Louis, MO), and dilutions were spot-plated onto LB agar and LB agar containing 40 μg mL^{-1} kanamycin. Isogenic mutant burdens were enumerated by counting colonies recovered on kanamycin-containing plates. Infections were performed at the Vanderbilt University Medical Center under the principles and guidelines described in the *Guide for the Care and Use of Laboratory Animals* using Institutional Animal Care and Use Committee (IACUC)-approved protocol M1600123-00. Vanderbilt University Medical Center is an American Association for Laboratory Animal Science (AALAS)-accredited facility. The Vanderbilt University Medical Center is registered with the Office of Laboratory Animal Welfare (OLAW), assurance number A-3227-01.

Imaging of hydrogen peroxide production *in vivo*. Imaging was carried out similar to published methods (Van de Bittner et al., 2013). FVB-luc^+ (FVB-Tg(CAG-luc-GFP)L2G85Chco/J) mice were infected using the protocol described above, except that only WT *A. baumannii* was included in the inoculum. FVB-luc^+ mice were a gift from Chris Chang (UC Berkeley) and were bred in-house at Vanderbilt University. After 36 hours of infection, mice were injected intraperitoneally with 0.05 μmoles Peroxy Caged Luciferin-2 (PCL-2) and 0.05 μmoles D-cysteine in 50 μL DMSO (Sigma, St. Louis, MO). Chemical probes were provided by Chris Chang (UC Berkeley). Mice were imaged 30 minutes post-injection using a Xenogen IVIS 200 (Caliper Life Sciences, Hopkinton, MA).

Mice were anesthetized prior to injection and during imaging via inhalation of isoflurane (Piramal, Bethlehem, PA).

Growth for RNASeq and RNA isolation. Biological triplicate overnight cultures of *A. baumannii* WT, Δ*oxyR,* and Δ*mumR* were diluted 1:1000 into 10 mL LB in 50 mL conical tubes and grown to mid-exponential phase. Cultures were treated with 5.65 μL of 30% H_2O_2 (EMD Millipore, Darmstadt, DE), for a final concentration of 5 mM, or untreated at 37 °C with shaking at 180 rpm for 10 minutes. Following treatment, 10 μL of cells were saved for CFU plating, while the remaining culture was immediately mixed with 10 mL 1:1 mixture of ice-cold acetone (JT Baker, Center Valley, PA) and ethanol (Sigma, St. Louis, MO) and frozen at -70 °C. CFU were enumerated by serially diluting cultures in PBS containing catalase (2,000 units/mL, catalase from bovine liver, Sigma, St. Louis, MO) and spot-plating to LB agar. For RNA purification, pellets were pelleted at 7,000 rpm for 10 minutes, supernatants were decanted, and pellets were dried on paper towels. Pellets were resuspended in LETS buffer (0.1 M LiCl, 10 mM EDTA, 10 mM Tris HCl pH 7.4, 1% SDS), homogenized in a bead beater (Fastprep-24, MP Biomedical, Santa Ana, CA) with Lysing Matrix B beads (MP Biomedicals, MP Biomedical, Santa Ana, CA) at a speed of 6 m/s for 45 seconds, heated at 55 °C for 5 minutes, and centrifuged for 10 minutes at 15,000 rpm. The upper phase was collected, mixed with 1 mL TRI Reagent (Sigma, St. Louis, MO), and incubated for 5 minutes at room temperature. Chloroform (0.2 mL, Acros Organics, Waltham, MA) was added, samples were vigorously shaken for 15 seconds, and samples were incubated at room temperature for 2 minutes. Following centrifugation at 4 °C for 15 minutes, 600 μL of the upper aqueous phase was collected and RNA was precipitated with 1 mL isopropanol (Sigma, St. Louis, MO). RNA was washed with 70%

ethanol (Sigma, St. Louis, MO) and resuspended in 100 μL DNase-Free, RNase-Free water (ThermoFisher, Waltham, MA). DNA contamination was removed by treatment with 8 μL RQ1 enzyme (Promega, Madison, WI), 12 μL 10X RQ1 buffer, and 2 μL Ribolock RNase inhibitor (ThermoFisher, Waltham, MA) for 2 hours at 37 °C. DNase was removed and samples further purified by the RNEasy kit (Qiagen, Hilden, DE) using the manufacturer's instructions and RNA was stored long-term at -80 °C.

Quantitative RT-PCR. Two μg of RNA was reverse transcribed by M-MLV reverse transcriptase (Fisher Scientific, Waltham, MA) in the presence of random hexamers (Promega, Madison, WI) and Ribolock RNase inhibitor (ThermoFisher, Waltham, MA). Reactions containing no reverse transcriptase were used to control for DNA contamination. Resultant cDNA was diluted 1:100 and subjected to qRT-PCR using iQ SYBR green supermix (BIO-RAD, Hercules, CA) with primer pairs listed in **Table 4**. Amplification was performed on a CFX96 qPCR cycler (BIO-RAD, Hercules, CA) using a 3-step melt curve program. CT values for each transcript were normalized by *16s* and fold changes were calculated using the ΔΔCT method.

Statistical analyses. All raw numerical data were saved in Excel files and imported into GraphPad Prism for statistical analysis. Specific statistical tests employed each experiment are outlined in the figure legends.

Results

mumR and *oxyR* encode LysR-family transcriptional regulators

Because *mumR* encodes a LysR-family transcriptional regulator that up-regulates transcription of the Nramp-family transporter *mumT*, the function and regulation of *mumR*

was of interest. The gene encoding MumR is located upstream of the *mum* operon, which encodes genes involved in Mn uptake and utilization (**Figure 17A**) (Juttukonda et al., 2016). Interestingly, MumR includes two cysteine residues at position 154 and 160 in the substrate binding domain of the protein, a region important for ligand recognition. Cysteines serve as sensors for oxidizing agents such as hydrogen peroxide in multiple transcriptional regulators, raising the possibility that MumR may function as an oxidative stress sensing regulator similar to the canonical OxyR regulator. *A. baumannii* also encodes an OxyR homolog that has been shown to be sensitive to hydrogen peroxide in LB agar plates (Tucker et al., 2014). *oxyR* is encoded in a predicted operon, similar to that described in *Acinetobacter* ADP1 (**Figure 17B**) (Geissdorfer et al., 1999). However, the function and regulon of OxyR in *A. baumannii* remains to be characterized.

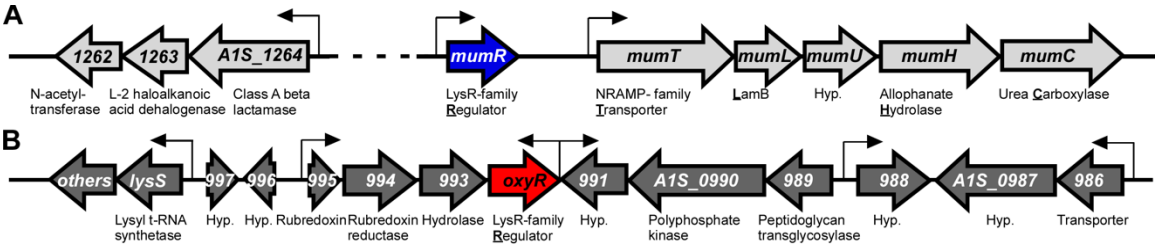

Figure 17. The genomic context of two LysR-family transcriptional regulators in *A. baumannii.* Cartoon depiction of the genetic loci surrounding (**A**) *mumR* and (**B**) *oxyR* in the *A. baumannii* ATCC 17978 genome.

***oxyR* and *mumR* differentially contribute to hydrogen peroxide stress resistance**

I hypothesized that *oxyR* and *mumR* both contribute to *A. baumannii* resistance to hydrogen peroxide. Strains with in-frame replacements of the *oxyR* and *mumR* with kanamycin resistance cassettes (Δ*oxyR,* Δ*mumR*) were interrogated for growth and survival in the presence of hydrogen peroxide. When grown in the presence of 100 μM hydrogen peroxide, lag time was increased by 6 hours in Δ*oxyR* and 2 hours in Δ*mumR* (**Figure 18A**). Growth curves with multiple concentrations of hydrogen peroxide revealed that growth of Δ*oxyR* was impaired by concentrations of hydrogen peroxide as low as 50 μM, whereas Δ*mumR* was capable in growing in up to 200 μM and WT *A. baumannii* was not fully inhibited even at 250 μM (**Figure 18B**). Similar results were obtained with hydrogen peroxide disc diffusion assays. Namely, Δ*oxyR* exhibited a substantially greater zone of inhibition by hydrogen peroxide, but Δ*mumR* also demonstrated a subtle but statistically significant increase in the zone of inhibition compared to WT *A. baumannii* (**Figure 18C&D**). Together, these results demonstrate that *oxyR* is important for growth in the presence of hydrogen peroxide, but that *mumR* also contributes in these conditions.

The importance of *mumR* and *oxyR* in the acute response to hydrogen peroxide was evaluated by assessing survival after a single bolus exposure to hydrogen peroxide was applied to exponential phase bacterial cultures. As expected, increasing concentrations of hydrogen peroxide resulted in decreased survival of WT *A. baumannii* (**Figure 18E**). Similar results were obtained for the Δ*mumR* strain (**Figure 18E**). To our surprise, Δ*oxyR* was staunchly resistant to killing by hydrogen peroxide in these conditions, with no decrease in survival until 40 mM hydrogen peroxide was applied (**Figure 18E**).

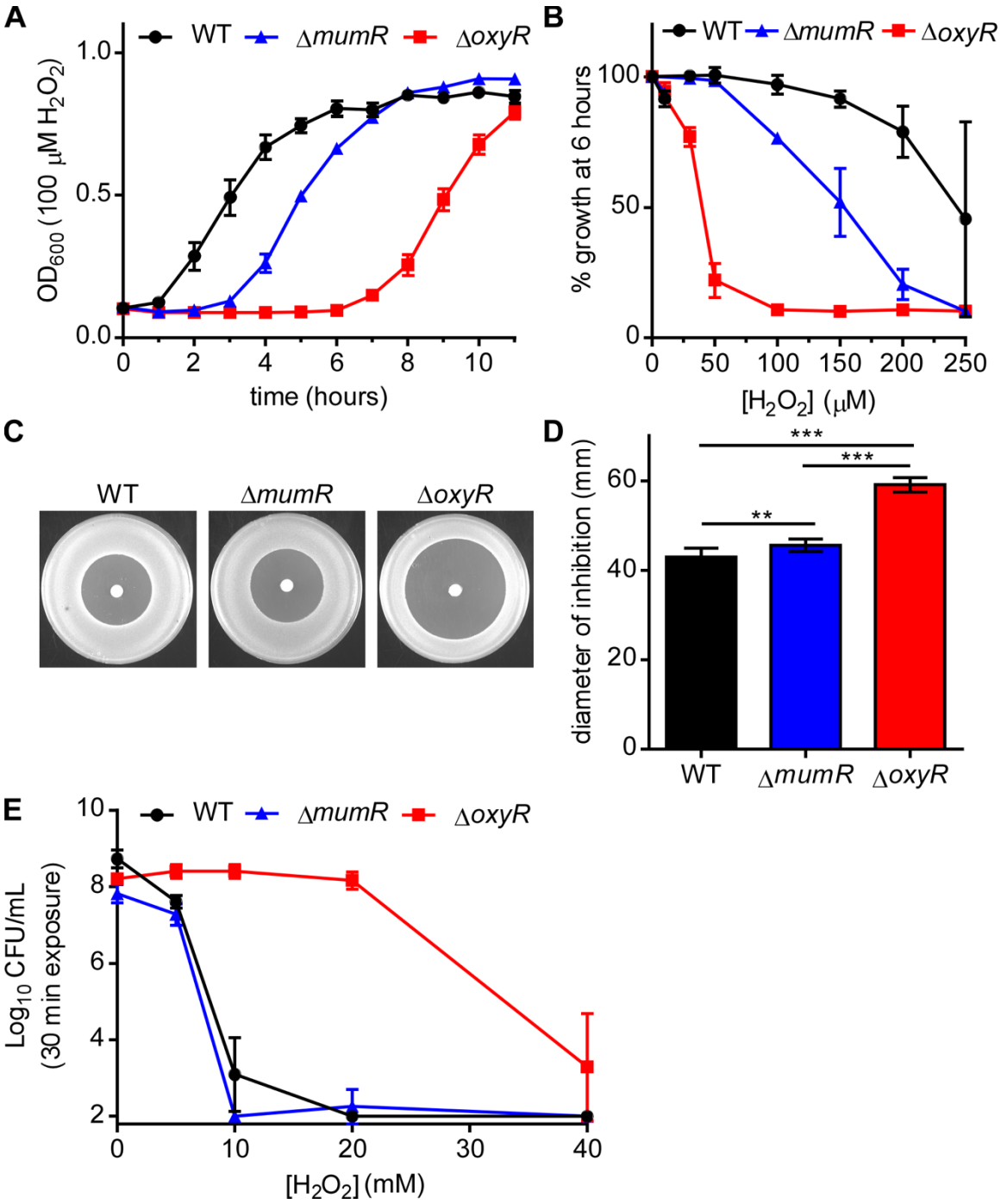

Figure 18. *oxyR* and *mumR* contribute to hydrogen peroxide stress resistance. Growth of *A. baumannii* WT, Δ*oxyR,* and Δ*mumR* was monitored under various conditions (**A-D**). (**A**) Growth of *A. baumannii* in 100 μM H_2O_2 was monitored by OD_{600}. (**B**) Inhibition by a dose-range of H_2O_2 after six hours of growth. Growth as a percent of untreated was calculated by OD_{600}. For (A) and (B), growth curves are from a single experiment performed in biological triplicate and are representative of three independent experiments. (**C**) Zone of inhibition by H_2O_2 spotted onto discs placed on solid medium. Representative plates are shown. after overnight growth. (**D**) Quantification of the diameter of inhibition

by H_2O_2. Data are combined from three independent experiments. **, $P < 0.01$; ***, $P < 0.001$ by one-way analysis of variance (ANOVA) with Tukey's multiple comparison's test. (**E**) Killing of exponential phase *A. baumannii* cultures following a 30 minute exposure to various concentrations of H_2O_2. Colony forming units (CFU) are shown on a $\log_{10}$ scale. The limit of detection was 2-$\log_{10}$. Results are shown from a single experiment performed in biological triplicate and are representative of three independent experiments.

Complementation of Δ*mumR* and Δ*oxyR* growth with hydrogen peroxide

Both Δ*mumR* and Δ*oxyR* display growth lags in the presence of hydrogen peroxide. To ensure that these phenotypes are due to the loss of *oxyR* and *mumR*, the genes were expressed *in trans* under the control of a constitutive promoter and growth curves were performed. Δ*mumR* and Δ*oxyR* harboring the empty vector control had increased lag relative to WT *A. baumannii* harboring empty vector, but this growth lag was complemented by expression of *oxyR* or *mumR in trans* (**Figure 19A&B**).

***A. baumannii* Δ*oxyR* is pre-adapted to hydrogen peroxide stress**

The result that Δ*oxyR* is resistant to killing by hydrogen peroxide was intriguing. I hypothesized that *A. baumannii* may adapt to low-dose hydrogen peroxide exposure in a manner that protects against toxic levels of hydrogen peroxide. I further posited that Δ*oxyR* may be protected from hydrogen peroxide killing because this strain is pre-adapted to hydrogen peroxide stress during logarithmic growth. Indeed, pre-treatment with 1 mM hydrogen peroxide enhanced survival of WT *A. baumannii* in high dose hydrogen peroxide stress, even showing protection from 80 mM bolus hydrogen peroxide (**Figure 20).** *A. baumannii* inactivated for *mumR* remained capable of adapting to hydrogen peroxide, although the protection was less pronounced at 80 mM (**Figure 20**). However, Δ*oxyR* was resistant to hydrogen peroxide exposure even at 80 mM, making it impossible to assess if pre-treatment altered survival of this strain (**Figure 20**). This result suggests to us that Δ*oxyR* is pre-adapted to hydrogen peroxide stress, as the Δ*oxyR* strain that was not pre-treated with hydrogen peroxide survived similarly to WT pre-treated with hydrogen peroxide.

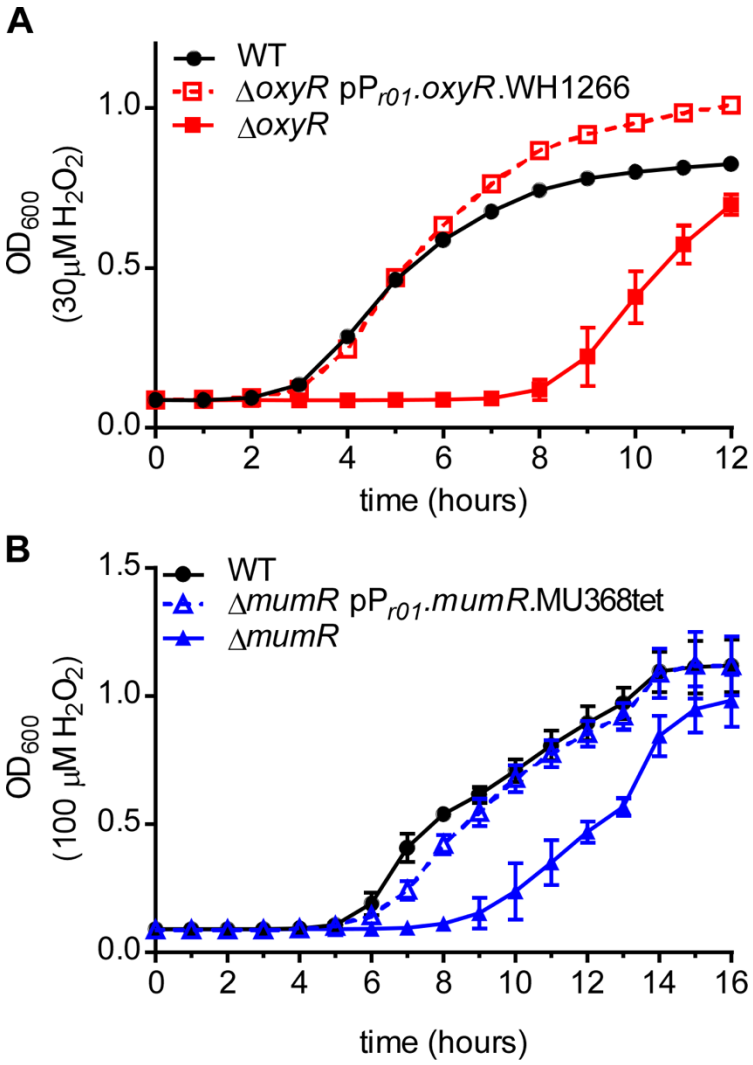

Figure 19. Complementation of Δ*oxyR* and Δ*mumR* in hydrogen peroxide. (**A**) Growth in 30 μM H_2O_2 of *A. baumannii* WT with empty vector, Δ*oxyR* with empty vector, or Δ*oxyR* expressing *oxyR* under the control of the *r01* promoter on a plasmid. (**B**) Growth in 30 μM H_2O_2 of *A. baumannii* WT with empty vector, Δ*oxyR* with empty vector, or Δ*oxyR* expressing *oxyR* under the control of the *r01* promoter on a plasmid.

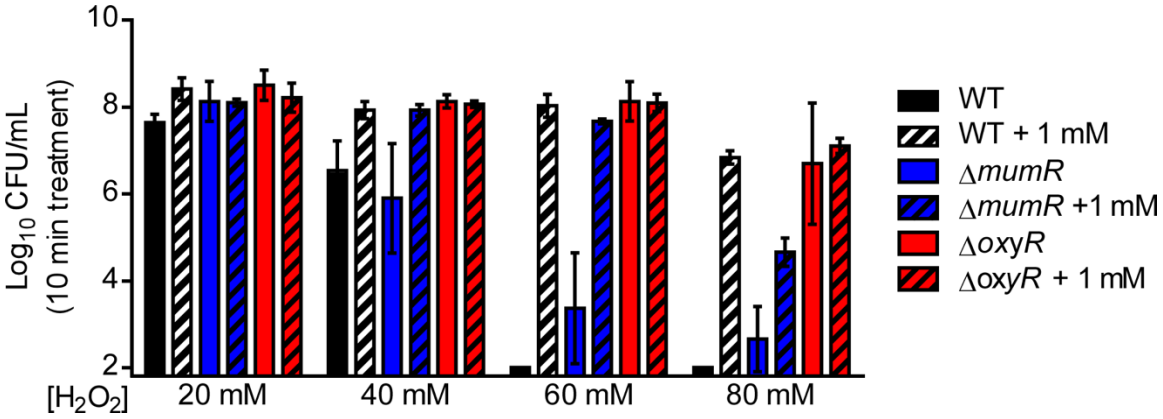

Figure 20. *A. baumannii* Δ*oxyR* is pre-adapted to hydrogen peroxide stress. *A. baumannii* mid-exponential phase cultures were treated pre-treated with 1 mM H_2O_2 for 30 minutes and exposed to a bolus of H_2O_2 at the indicated concentrations for 10 minutes. CFU enumerated following bolus exposure are shown on a $\log_{10}$ scale, and the limit of detection was 2-$\log_{10}$. Cultures that were not pre-treated are included as a control. Data are from a single experiment performed in biological triplicate and are representative of three independent experiments.

Hydrogen peroxide exposure up-regulates *oxyR*-regulated genes

In many Gram-negative organisms, OxyR activates or de-represses transcription of the OxyR regulon when the organism is exposed to hydrogen peroxide (Tao et al., 1991; Tartaglia et al., 1989). I hypothesized that OxyR functions in a similar manner in *A. baumannii.* To test this hypothesis, a panel of genes were identified in *A. baumannii* based on sequence similarity to genes regulated by OxyR in *Pseudomonas aeruginosa* and included to encode alkyl hydroperoxidase (*ahp*), catalases (*katG, A1S_3382, A1S_1386, A1S_1351*) and glutathione peroxidase (*gpx*) (Wei et al., 2012). These genes are canonical members of the OxyR regulon (Tartaglia et al., 1989). Transcription of these genes was then assessed in *A. baumannii* WT and Δ*oxyR* during exponential growth (**Figure 21A**). No significant differences in expression were observed between the two strains, suggesting that transcription of these genes is not altered by *oxyR* in the absence of hydrogen peroxide. Intriguingly, transcription of *mumL* was significantly reduced in Δ*oxyR, mumL* is a member of the *mum* operon, which is transcriptionally upregulated by *mumR* (Chapter II). Following a 10 minute exposure to 1 mM hydrogen peroxide, transcription of *ahp, katG,* and *A1S_3382* was increased in WT *A. baumannii,* but transcription of these genes was not upregulated by hydrogen peroxide exposure in Δ*oxyR* (**Figure 21B**). These results demonstrate that *oxyR* is required for upregulation of genes involved in hydrogen peroxide detoxification.

Because the Δ*mumR* exhibited decreased growth in the presence of hydrogen peroxide, I considered the possibility that MumR may also be important for transcription of genes involved in hydrogen peroxide detoxification. To assess this, transcription of *ahp, katG, A1S_3382, A1S_1386, A1S_1351,* and *gpx* was assessed in Δ*mumR* during

exponential growth (**Figure 21C**). Interestingly, *A1S_1351, gpx,* and *katG* were downregulated in Δ*mumR*. *mumL* was included as a control and was significantly downregulated as expected. Following treatment with hydrogen peroxide, WT and Δ*mumR* displayed similar transcriptional changes (**Figure 21D**). Taken together, these results reveal that *mumR* is not required for upregulation of the subset of hydrogen peroxide detoxification genes tested. However, *mumR* appears to be important for transcription of these genes in the absence of exogenous hydrogen peroxide, which provides a potential explanation for the decreased growth Δ*mumR* displays in the presence of hydrogen peroxide.

OxyR binds the promoters of genes involved in hydrogen peroxide detoxification

Based on the transcriptional data presented above, I expected that OxyR is a direct regulator of the genes *ahp, katG,* and *A1S_3382.* Electromobility shift assays were carried out to determine direct binding by OxyR to the *ahp, katG,* and *A1S_3382* promoters. Recombinantly expressed and purified OxyR with a hexahistidine N-terminal tag was capable to binding to the promoter of all three genes (**Figure 22A-C**). Interestingly, supershifts were present at the highest concentrations, consistent with multiple OxyR molecules binding to a single DNA molecule. This is unsurprising, given that LysR-family regulators typically bind at multiple locations within promoters and also often oligomerize when bound to DNA (Maddocks and Oyston, 2008).

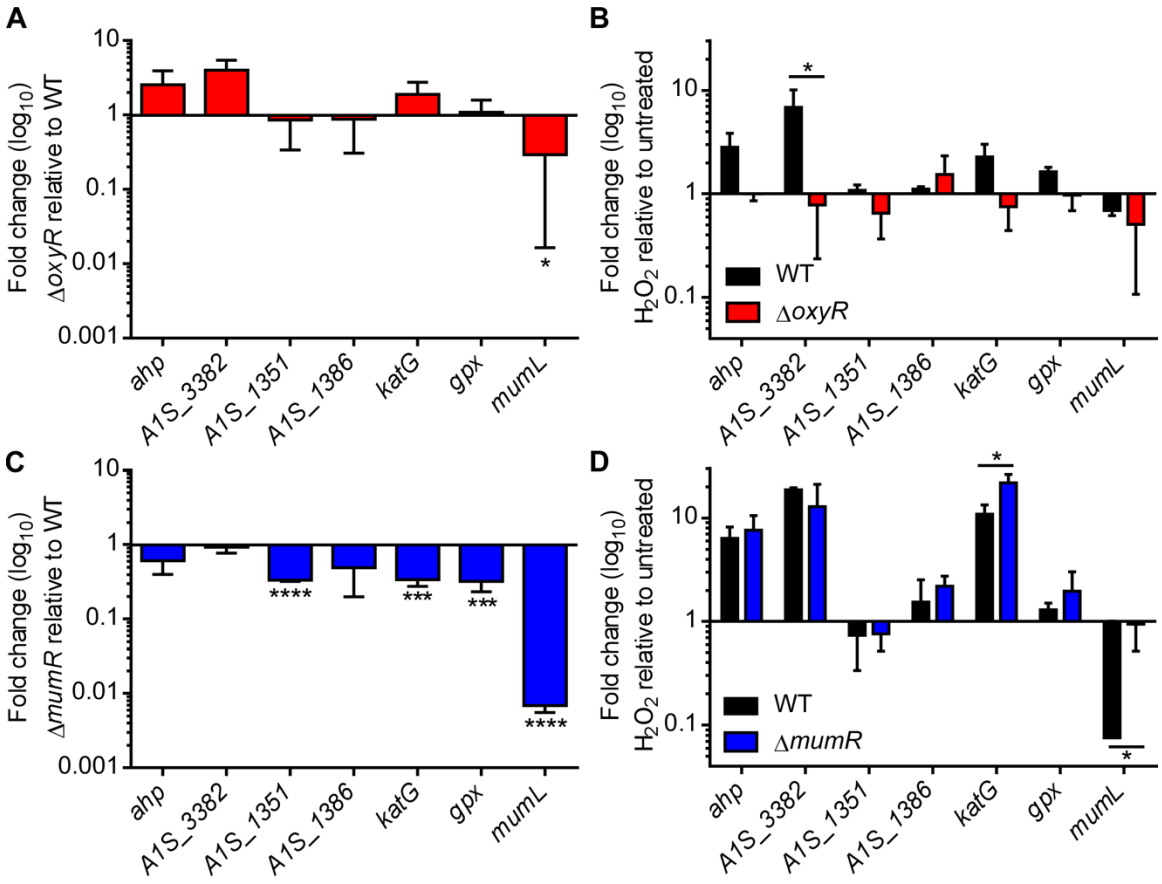

Figure 21. Transcriptional regulation of genes involved in hydrogen peroxide detoxification. Transcription of genes predicted to be involved in hydrogen peroxide detoxification was assessed by quantitative real-time polymerase chain reaction (qRT-PCR) using the ΔΔCT method. (**A**) Fold change of gene targets in Δ*oxyR* compared to WT during growth in LB. Significance was calculated compared to a theoretical value of 1. (**B**) Fold change of gene targets in WT and Δ*oxyR* following a 10 minute exposure to 1 mM H_2O_2 relative to untreated cells. Significance was calculated by *t*-test comparing WT and Δ*oxyR*. (**C**) Fold change of gene targets in Δ*mumR* compared to WT during growth in LB. Significance was calculated compared to a theoretical value of 1. (**D**) Fold change of gene targets in WT and Δ*mumR* following a 10 minute exposure to 1 mM H_2O_2 relative to untreated cells. Significance was calculated by *t*-test comparing WT and Δ*mumR*. For (**A-D**), data are from a single experiment performed in biological triplicate and are representative of three independent experiments. *, $P < 0.05$; ***, $P < 0.001$; ****, $P < 0.0001$.

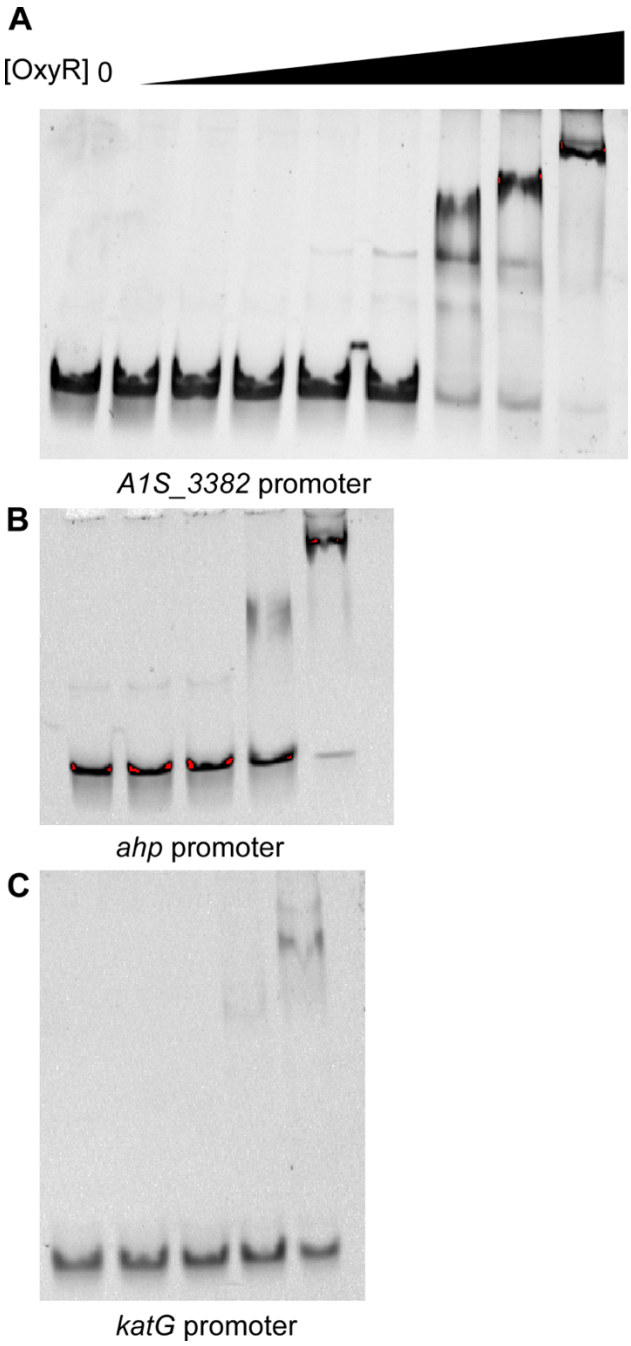

Figure 22. OxyR directly binds promoters involved in hydrogen peroxide detoxification. Binding of recombinant, hexahistidine-tagged OxyR to promoters was determined by electromobility shift assays. DNA was detected by SYBR green staining. The following promoters were assessed: (**A**) *A1S_3382,* (**B**) *ahp,* and (**C**) *katG.* The concentrations of OxyR in B and C correspond with every other lane in (**A**).

Hydrogen peroxide is produced in response to *A. baumannii* lung infection

Hydrogen peroxide is produced during the oxidative burst that is generated by neutrophils (Hampton et al., 1998). Neutrophils are recruited in response to *A. baumannii* infection (van Faassen et al., 2007). However, the production of hydrogen peroxide in response to *A. baumannii* infection has not been studied. To interrogate hydrogen peroxide production *in vivo*, we utilized a recently developed hydrogen peroxide reactive probe (Van de Bittner et al., 2013). This caged probe specifically reacts with hydrogen peroxide to release D-luciferin. In mice expressing luciferase constitutively, D-luciferin serves as the substrate for this reaction and bioluminescence is produced. Mice mock-infected with PBS did not have substantial bioluminescence, indicating that hydrogen peroxide is not generated in these mice (**Figure 23A**). As a control, we injected mice that were mock-infected with PBS or infected with *A. baumannii* with D-luciferin, the direct substrate for light generation. Bioluminescence was similar between mock-infected and infected animals (**Figure 23A**). Next, we assessed whether hydrogen peroxide was produced in response to *A. baumannii* infection. Indeed, mice that were infected intranasally with *A. baumannii* had substantial bioluminescence from the hydrogen peroxide specific probe, and this luminescence localized to the lower lobes of the lung (**Figure 23B&C**). Therefore, hydrogen peroxide is produced in the lung as part of the response to *A. baumannii* infection.

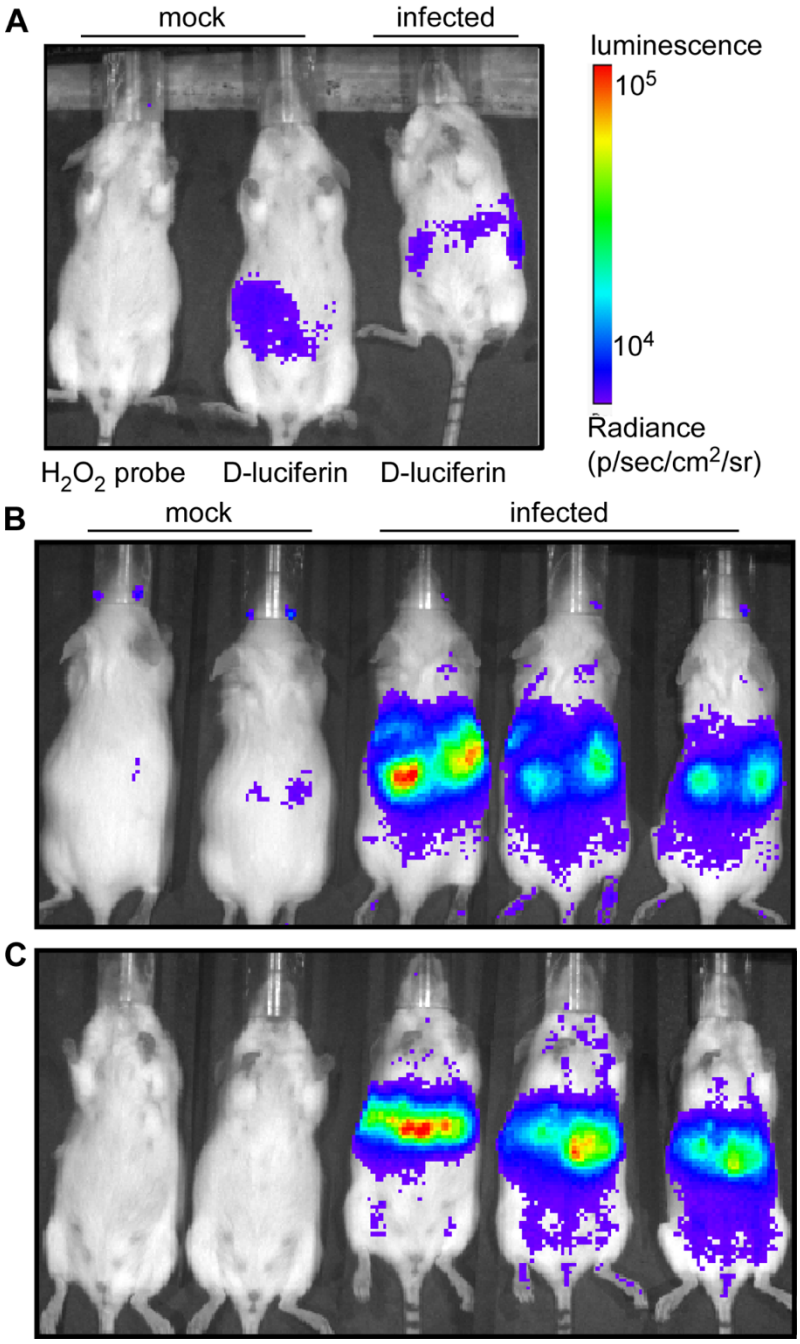

Figure 23. Hydrogen peroxide stress is produced in response to *A. baumannii* lung infection. Production of H_2O_2 was monitored *in vivo* by activation of a caged luciferin probe (PCL-2) that specifically reacts with H_2O_2 (Van de Bittner et al., 2013) to generate bioluminescence. Mice were infected with *A. baumannii* WT or mock-infected with PBS and imaging was performed 36 hours post infection. (**A**) The H_2O_2 probe does not produce light in the absence of infection, but providing D-luciferin leads to light production both in the mock-infected and infected animals. (**B-C**) PCL-2 was utilized to image H_2O_2 production in mock-infected or *A. baumannii* infected mice. Mice were placed (**B**) in the prone position and (**C**) in the supine position.

oxyR and *mumR* promote the fitness of *A. baumannii* in a murine model of pneumonia

As hydrogen peroxide is produced in the lung during *A. baumannii* pneumonia and *oxyR* and *mumR* orchestra the transcriptional response to hydrogen peroxide *in vitro*, I hypothesized that *oxyR* and *mumR* enable *A. baumannii* to respond to hydrogen peroxide during infection of the murine lung. To determine whether *mumR* enhances *A. baumannii* fitness in the lung, mice were co-infected intransally with *A. baumannii* WT and Δ*mumR* and bacterial burdens were enumerated 36 hours post infection. *A. baumannii* Δ*mumR* was recovered at significantly lower numbers than WT *A. baumannii* in the lung as well as in the liver, the primary site of dissemination in this mouse model (**Figure 24A&B**). Similarly, Δ*oxyR* colonized the lungs and livers of mice to significantly lower burdens than WT *A. baumannii* 36 hours after co-infection (**Figure 24C&D**). Therefore, *mumR* and *oxyR* both promote the fitness of *A. baumannii* during infection.

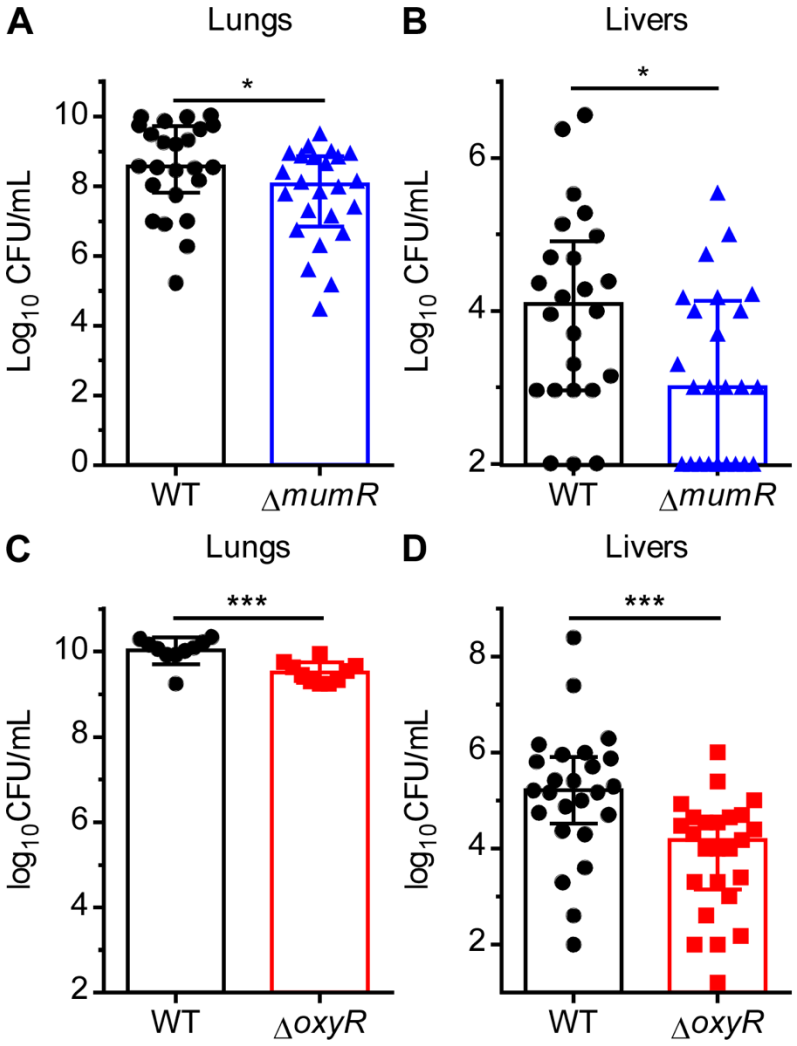

Figure 24. *oxyR* and *mumR* promote the fitness of *A. baumannii* in a murine model of pneumonia. (**A-D**) Bacterial burdens were enumerated from the lungs and livers of mice 36 hours following intranasal inoculation of a 1:1 mixture of WT *A. baumannii* and a kanamycin-marked mutant. (**A-B**) Mice were coinfected with WT and Δ*mumR*. (**C-D**) Mice were coinfected with WT and Δ*oxyR*. (**A-B**) Data are combined from three independent experiments. (**C**) Data are from one experiments. (**D**) Data are combined from two independent experiments. *, $P < 0.05$; ***, $P < 0.001$ by Mann-Whitney.

Discussion

Here, *A. baumannii oxyR* and *mumR* are demonstrated to confer resistance to hydrogen peroxide in multiple growth assays, whereas cells lacking *oxyR* are resistant to hydrogen peroxide killing when cells are treated during logarithmic growth. The transcription of some canonical *oxyR* regulon genes is induced by hydrogen peroxide in an *oxyR*-dependent manner, whereas other genes predicted to be involved in hydrogen peroxide response are regulated by *mumR* in the absence of hydrogen peroxide. Hydrogen peroxide was produced in the lung in response to *A. baumannii* infection, and in keeping with this *A. baumannii* Δ*oxyR* and Δ*mumR* both confer a fitness advantage in this infection model.

This is the first report of a functional role for *A. baumannii* MumR. Inactivation of *mumR* led to mild growth defects in liquid culture containing hydrogen peroxide liquid and in disc diffusion assays when compared to *A. baumannii* Δ*oxyR.* This suggests that *oxyR* is more critical for the hydrogen peroxide detoxification response. In fact, the lack of a phenotype in both killing and adaptation assays suggest that *mumR* is not important for the transcriptional response to bolus hydrogen peroxide stress, but instead may be important in controlling some other aspect of physiology that is required for growth in the presence of hydrogen peroxide, such as repair of damaged proteins or DNA. Interestingly, Δ*mumR* was similarly attenuated to Δ*oxyR* in the lung despite exhibiting milder deficits *in vitro*, suggesting that *mumR* has additional functions beyond hydrogen peroxide stress resistance.

As expected, some canonical OxyR regulon members are upregulated in *A. baumannii* exposed to hydrogen peroxide in an *oxyR*-dependent fashion. However, *A1S_1351, A1S_1386,* and *gpx* were not upregulated under the conditions used in this

study. Perhaps not coincidentally, transcription of these three genes was not altered in Δ*oxyR* but was significantly decreased in Δ*mumR.* These results suggest a model whereby OxyR upregulates target genes *A1S_3382, katG,* and *ahp* following activation by hydrogen peroxide, presumably in a mechanism involving oxidation of cysteine 202. The remaining catalase-like genes and *gpx* are expressed in a *mumR*-dependent manner in the absence of exogenous hydrogen peroxide stress perhaps as a means of detoxifying hydrogen peroxide that is produced as a byproduct of aerobic metabolism (Imlay, 2013). This model is consistent with the larger growth defect for Δ*oxyR* and Δ*mumR* in the presence of hydrogen peroxide, as *ahp, katG,* and *A1S_3382* expression is likely important for growth in hydrogen peroxide. If this model is correct, we anticipate that close inspection of the promoters will reveal binding sites for OxyR upstream of *A1S_3382, katG,* and *ahp*, and binding sites for MumR upstream of *gpx, A1S_1351,* and *A1S_1386.* Interestingly, *katG* appears to be regulated by both OxyR and MumR; this suggests that *katG* is important for detoxifying both hydrogen peroxide produced during aerobic growth and bolus, high dose hydrogen peroxide.

Transcription of *mumL* is surprisingly decreased in Δ*oxyR,* Δ*mumR,* and hydrogen peroxide treatment. We presume that *mumL* transcription represents expression of the entire *mum* operon based on previous results (Chapter II), which means that *mumT* expression is also decreased in the presence of hydrogen peroxide. This contrasts with *E. coli,* in which *mntH* is overexpressed presumably so Mn can populate Fe-dependent enzymes following oxidation of Fe^{2+} to Fe^{3+} (Anjem et al., 2009; Sobota and Imlay, 2011). Perhaps Mn is not utilized by *A. baumannii* in a similar mechanism, or *mumT* in *A.*

baumannii is decreased because it may increase cellular Fe levels, which is undesirable in the presence of hydrogen peroxide.

A. baumannii Δ*oxyR* shares characteristics with *oxyR* mutants in multiple organisms. Amongst others, inactivaction of *oxyR* in *B. abortis, P. aeruginosa, Moraxella catarrhalis,* and *E. coli*, increases the zone of inhibition by hydrogen peroxide in a disc diffusion assay (Hoopman et al., 2011; Kim and Mayfield, 2000; Ochsner et al., 2000; Zheng et al., 2001). *Shewanella oneidensis, P. aeruginosa, Xanthomonas campestris* and *M. catarrhalis* lacking *oxyR* also have a viability defect when plated onto LB agar, a phenotype that we also observed (Hassett et al., 2000; Hoopman et al., 2011; Mongkolsuk et al., 1998; Shi et al., 2015). This phenotype is due to the generation of hydrogen peroxide in the solid medium and can be rescued with exogenous catalase (Hoopman et al., 2011; Mongkolsuk et al., 1998; Shi et al., 2015). There are more discrepancies regarding sensitivity of *oxyR* mutants to hydrogen peroxide killing during log phase growth, as *X. campestris* lacking *oxyR* is sensitive to hydrogen peroxide during log phase growth but *N. meningitidis* and *B. abortus* inactivated for *oxyR* are resistant to hydrogen peroxide killing in exponential growth (Ieva et al., 2008; Kim and Mayfield, 2000; Mongkolsuk et al., 1998). Similar to the latter organisms, *A. baumannii* Δ*oxyR* in exponential phase growth is resistant to hydrogen peroxide. In sum, OxyR seems to function similarly in *A. baumannii* as it does in many other organisms.

Previously, *oxyR* mutants have been shown to have decreased recovery in multiple mouse models, including *P. aeruginosa* pneumonia and burn wound-derived sepsis, *E. coli* urinary tract infection, *Francisella tularensis* pneumonia, *K. pneumoniae* gastrointestinal tract colonization, and *Bacteroides fragilis* intraabdominal infection (Hennequin and

Forestier, 2009; Johnson et al., 2006; Lau et al., 2005; Ma et al., 2016; Sund et al., 2008). This work presents data that demonstrates that *oxyR* and *mumR* increase the fitness of *A. baumannii* in a murine pneumonia model. The modest phenotypes observed are similar to the fitness deficits for *oxyR* in other organisms. These results add to the current knowledge of infection models where *oxyR* enhances infection and define *mumR* as a new factor in *A. baumannii* that is important for fitness during infection.

References

Anjem, A., Varghese, S., and Imlay, J.A. (2009). Manganese import is a key element of the OxyR response to hydrogen peroxide in *Escherichia coli*. Mol. Microbiol. *72*, 844-858.

Antunes, L.C., Visca, P., and Towner, K.J. (2014). *Acinetobacter baumannii:* evolution of a global pathogen. Pathog. Dis. *71*, 292-301.

Becker, K.W., and Skaar, E.P. (2014). Metal limitation and toxicity at the interface between host and pathogen. FEMS Microbiol. Rev. *38*, 1235-1249.

Chiang, S.M., and Schellhorn, H.E. (2012). Regulators of oxidative stress response genes in *Escherichia coli* and their functional conservation in bacteria. Arch. Biochem. Biophys. *525*, 161-169.

Choi, H., Kim, S., Mukhopadhyay, P., Cho, S., Woo, J., Storz, G., and Ryu, S.E. (2001). Structural basis of the redox switch in the OxyR transcription factor. Cell *105*, 103-113.

Christman, M.F., Morgan, R.W., Jacobson, F.S., and Ames, B.N. (1985). Positive control of a regulon for defenses against oxidative stress and some heat-shock proteins in *Salmonella typhimurium*. Cell *41*, 753-762.

Christman, M.F., Storz, G., and Ames, B.N. (1989). OxyR, a positive regulator of hydrogen peroxide-inducible genes in *Escherichia coli* and *Salmonella typhimurium*, is homologous to a family of bacterial regulatory proteins. Proc. Natl. Acad. Sci. *86*, 3484-3488.

Demple, B. (1991). Regulation of bacterial oxidative stress genes. Annu. Rev. Genet. *25*, 315-337.

Dexter, C., Murray, G.L., Paulsen, I.T., and Peleg, A.Y. (2015). Community-acquired *Acinetobacter baumannii*: clinical characteristics, epidemiology and pathogenesis. Expert Rev. Anti. Infect. Ther. *13*, 567-573.

Dijkshoorn, L., Nemec, A., and Seifert, H. (2007). An increasing threat in hospitals: multidrug-resistant *Acinetobacter baumannii*. Nat. Rev. Microbiol. *5*, 939-951.

Geissdorfer, W., Kok, R.G., Ratajczak, A., Hellingwerf, K.J., and Hillen, W. (1999). The genes *rubA* and *rubB* for alkane degradation in *Acinetobacter* sp. strain ADP1 are in an operon with *estB*, encoding an esterase, and *oxyR*. J. Bacteriol. *181*, 4292-4298.

Hampton, M.B., Kettle, A.J., and Winterbourn, C.C. (1998). Inside the neutrophil phagosome: oxidants, myeloperoxidase, and bacterial killing. Blood *92*, 3007-3017.

Hassett, D.J., Alsabbagh, E., Parvatiyar, K., Howell, M.L., Wilmott, R.W., and Ochsner, U.A. (2000). A protease-resistant catalase, KatA, released upon cell lysis during stationary phase is essential for aerobic survival of a *Pseudomonas aeruginosa oxyR* mutant at low cell densities. J. Bacteriol. *182*, 4557-4563.

Hennequin, C., and Forestier, C. (2009). *oxyR*, a LysR-type regulator involved in *Klebsiella pneumoniae* mucosal and abiotic colonization. Infect. Immun. *77*, 5449-5457.

Hillion, M., and Antelmann, H. (2015). Thiol-based redox switches in prokaryotes. Biol. Chem. *396*, 415-444.

Hood, M.I., Mortensen, B.L., Moore, J.L., Zhang, Y., Kehl-Fie, T.E., Sugitani, N., Chazin, W.J., Caprioli, R.M., and Skaar, E.P. (2012). Identification of an *Acinetobacter baumannii* zinc acquisition system that facilitates resistance to calprotectin-mediated zinc sequestration. PLOS Pathog. *8*, e1003068.

Hoopman, T.C., Liu, W., Joslin, S.N., Pybus, C., Brautigam, C.A., and Hansen, E.J. (2011). Identification of gene products involved in the oxidative stress response of *Moraxella catarrhalis*. Infect. Immun. *79*, 745-755.

Ieva, R., Roncarati, D., Metruccio, M.M., Seib, K.L., Scarlato, V., and Delany, I. (2008). OxyR tightly regulates catalase expression in *Neisseria meningitidis* through both repression and activation mechanisms. Mol. Microbiol. *70*, 1152-1165.

Imlay, J.A. (2013). The molecular mechanisms and physiological consequences of oxidative stress: lessons from a model bacterium. Nat. Rev. Microbiol. *11*, 443-454.

Jo, I., Chung, I.Y., Bae, H.W., Kim, J.S., Song, S., Cho, Y.H., and Ha, N.C. (2015). Structural details of the OxyR peroxide-sensing mechanism. Proc. Natl. Acad. Sci. *112*, 6443-6448.

Johnson, J.R., Clabots, C., and Rosen, H. (2006). Effect of inactivation of the global oxidative stress regulator *oxyR* on the colonization ability of *Escherichia coli* O1:K1:H7 in a mouse model of ascending urinary tract infection. Infect. Immun. *74*, 461-468.

Juttukonda, L.J., Chazin, W.J., and Skaar, E.P. (2016). *Acinetobacter baumannii* coordinates urea metabolism with metal import to resist host-mediated metal limitation. mBio *7*.

Kehres, D.G., Janakiraman, A., Slauch, J.M., and Maguire, M.E. (2002). Regulation of *Salmonella enterica* serovar Typhimurium *mntH* transcription by H(2)O(2), Fe(2+), and Mn(2+). J. Bacteriol. *184*, 3151-3158.

Kim, J.A., and Mayfield, J. (2000). Identification of *Brucella abortus* OxyR and its role in control of catalase expression. J. Bacteriol. *182*, 5631-5633.

Lau, G.W., Britigan, B.E., and Hassett, D.J. (2005). *Pseudomonas aeruginosa* OxyR is required for full virulence in rodent and insect models of infection and for resistance to human neutrophils. Infect. Immun. *73*, 2550-2553.

LeBlanc, J.J., Brassinga, A.K., Ewann, F., Davidson, R.J., and Hoffman, P.S. (2008). An ortholog of OxyR in *Legionella pneumophila* is expressed postexponentially and negatively regulates the alkyl hydroperoxide reductase (*ahpC2D*) operon. J. Bacteriol. *190*, 3444-3455.

Longkumer, T., Parthasarathy, S., Vemuri, S.G., and Siddavattam, D. (2014). OxyR-dependent expression of a novel glutathione S-transferase (*Abgst01*) gene in *Acinetobacter baumannii* DS002 and its role in biotransformation of organophosphate insecticides. Microbiology *160*, 102-112.

Ma, Z., Russo, V.C., Rabadi, S.M., Jen, Y., Catlett, S.V., Bakshi, C.S., and Malik, M. (2016). Elucidation of a mechanism of oxidative stress regulation in *Francisella tularensis* live vaccine strain. Mol. Microbiol. *101*, 856-878.

Maddocks, S.E., and Oyston, P.C. (2008). Structure and function of the LysR-type transcriptional regulator (LTTR) family proteins. Microbiology *154*, 3609-3623.

McConnell, M.J., Actis, L., and Pachon, J. (2013). *Acinetobacter baumannii:* human infections, factors contributing to pathogenesis and animal models. FEMS Microbiol. Rev. *37*, 130-155.

Milse, J., Petri, K., Ruckert, C., and Kalinowski, J. (2014). Transcriptional response of *Corynebacterium glutamicum* ATCC 13032 to hydrogen peroxide stress and characterization of the OxyR regulon. J. Biotechnol. *190*, 40-54.

Mongkolsuk, S., Sukchawalit, R., Loprasert, S., Praituan, W., and Upaichit, A. (1998). Construction and physiological analysis of a *Xanthomonas* mutant to examine the

role of the *oxyR* gene in oxidant-induced protection against peroxide killing. J. Bacteriol. *180*, 3988-3991.

Ochsner, U.A., Vasil, M.L., Alsabbagh, E., Parvatiyar, K., and Hassett, D.J. (2000). Role of the *Pseudomonas aeruginosa oxyR-recG* operon in oxidative stress defense and DNA repair: OxyR-dependent regulation of *katB-ankB, ahpB,* and *ahpC-ahpF*. J. Bacteriol. *182*, 4533-4544.

Peleg, A.Y., Seifert, H., and Paterson, D.L. (2008). *Acinetobacter baumannii*: emergence of a successful pathogen. Clin. Microbiol. Rev. *21*, 538-582.

Perez, F., Hujer, A.M., Hujer, K.M., Decker, B.K., Rather, P.N., and Bonomo, R.A. (2007). Global challenge of multidrug-resistant *Acinetobacter baumannii*. Antimicrob. Agents Chemother. *51*, 3471-3484.

Potron, A., Poirel, L., and Nordmann, P. (2015). Emerging broad-spectrum resistance in *Pseudomonas aeruginosa* and *Acinetobacter baumannii*: Mechanisms and epidemiology. Int. J. Antimicrob. Agents. *45*, 568-585.

Roca, I., Espinal, P., Vila-Farres, X., and Vila, J. (2012). The *Acinetobacter baumannii* oxymoron: commensal hospital dweller turned pan-drug-resistant menace. Front. Microbiol. *3*, 148.

Schell, M.A. (1993). Molecular biology of the LysR family of transcriptional regulators. Annu. Rev. Microbiol. *47*, 597-626.

Shi, M., Wan, F., Mao, Y., and Gao, H. (2015). Unraveling the mechanism for the viability deficiency of *Shewanella oneidensis oxyR* null mutant. J. Bacteriol. *197*, 2179-2189.

Sobota, J.M., and Imlay, J.A. (2011). Iron enzyme ribulose-5-phosphate 3-epimerase in *Escherichia coli* is rapidly damaged by hydrogen peroxide but can be protected by manganese. Proc. Natl. Acad. Sci. *108*, 5402-5407.

Storz, G., Tartaglia, L.A., and Ames, B.N. (1990). Transcriptional regulator of oxidative stress-inducible genes: direct activation by oxidation. Science *248*, 189-194.

Sund, C.J., Rocha, E.R., Tzianabos, A.O., Wells, W.G., Gee, J.M., Reott, M.A., O'Rourke, D.P., and Smith, C.J. (2008). The *Bacteroides fragilis* transcriptome response to oxygen and H2O2: the role of OxyR and its effect on survival and virulence. Mol. Microbiol. *67*, 129-142.

Tao, K., Makino, K., Yonei, S., Nakata, A., and Shinagawa, H. (1991). Purification and characterization of the *Escherichia coli* OxyR protein, the positive regulator for a hydrogen peroxide-inducible regulon. J. Biochem. *109*, 262-266.

Tartaglia, L.A., Gimeno, C.J., Storz, G., and Ames, B.N. (1992). Multidegenerate DNA recognition by the OxyR transcriptional regulator. J. Biol. Chem. *267*, 2038-2045.

Tartaglia, L.A., Storz, G., and Ames, B.N. (1989). Identification and molecular analysis of *oxyR*-regulated promoters important for the bacterial adaptation to oxidative stress. J. Mol. Biol. *210*, 709-719.

Tucker, A.T., Nowicki, E.M., Boll, J.M., Knauf, G.A., Burdis, N.C., Trent, M.S., and Davies, B.W. (2014). Defining gene-phenotype relationships in *Acinetobacter baumannii* through one-step chromosomal gene inactivation. mBio *5*, e01313-01314.

Van de Bittner, G.C., Bertozzi, C.R., and Chang, C.J. (2013). Strategy for dual-analyte luciferin imaging: *in vivo* bioluminescence detection of hydrogen peroxide and caspase activity in a murine model of acute inflammation. J. Am. Chem. Soc. *135*, 1783-1795.

van Faassen, H., KuoLee, R., Harris, G., Zhao, X., Conlan, J.W., and Chen, W. (2007). Neutrophils play an important role in host resistance to respiratory infection with *Acinetobacter baumannii* in mice. Infect. Immun. *75*, 5597-5608.

Wei, Q., Minh, P.N., Dotsch, A., Hildebrand, F., Panmanee, W., Elfarash, A., Schulz, S., Plaisance, S., Charlier, D., Hassett, D.*, et al.* (2012). Global regulation of gene expression by OxyR in an important human opportunistic pathogen. Nucleic Acids Res. *40*, 4320-4333.

WHO (2017). Global priority list of antibiotic-resistant bacteria to guide research, discovery, and development of new antibiotics. http://www.who.int/medicines/publications/WHO-PPL-Short_Summary_25Feb-ET_NM_WHO.pdf.

Zheng, M., Aslund, F., and Storz, G. (1998). Activation of the OxyR transcription factor by reversible disulfide bond formation. Science *279*, 1718-1721.

Zheng, M., Wang, X., Templeton, L.J., Smulski, D.R., LaRossa, R.A., and Storz, G. (2001). DNA microarray-mediated transcriptional profiling of the *Escherichia coli* response to hydrogen peroxide. J. Bacteriol. *183*, 4562-4570.

A version of the following section (*Chapter IV, Dietary manganese promotes staphylococcal infection of the heart*) has been submitted for publication.

CHAPTER IV

DIETARY MANGANESE PROMOTES STAPHYLOCOCCAL INFECTION OF THE HEART

Introduction

During infection, pathogens obtain essential nutrient metals from the host (Cerasi et al., 2013; Diaz-Ochoa et al., 2014; Hood and Skaar, 2012; Palmer and Skaar, 2016; Weinberg, 2009; Weiss and Carver, 2017). Alterations in metal homeostasis, including increased dietary iron (Fe) and decreased dietary zinc (Zn), are associated with increased infectious disease risk (Jonker and Boele van Hensbroek, 2014; Katona and Katona-Apte, 2008). However, the current understanding of how dietary metals influence the host-pathogen relationship remains limited. Mn is a common dietary supplement (Greger, 1998), and tissue levels of Mn vary based on exposure (Greger, 1998). Furthermore, Mn is required by many bacterial pathogens for virulence (Juttukonda and Skaar, 2015). For instance, bacterial Mn import systems are required for fitness in multiple animal models of infection (Kelliher and Kehl-Fie, 2016), and some Mn-dependent enzymes are required for full virulence (Juttukonda and Skaar, 2015). Despite the importance of Mn to bacterial fitness during infection and the known variation in host Mn levels, the impact of dietary variation in Mn levels on infection outcomes has not been studied.

S. aureus is the leading cause of bacterial endocarditis (Fowler and Gupta, 2005; Klein and Wang, 2016; Slipczuk et al., 2013), the second most frequent agent of bloodstream infections (Anderson et al., 2014; Laupland, 2013; Laupland and Church,

2014), and the basis of nearly 500,000 hospitalizations each year in the United States (Klein et al., 2007). During infection, *S. aureus* must acquire Mn for full virulence. *S. aureus* encodes two Mn acquisition systems, *mntH* and *mntABC* (Horsburgh et al., 2002a), and genetic inactivation of both Mn transporters impairs *S. aureus* infection of the liver and the kidney (Kehl-Fie et al., 2013). *S. aureus* also encodes two superoxide dismutase enzymes, *sodA* and *sodM* (Clements et al., 1999; Valderas and Hart, 2001) that are important for surviving neutrophil-mediated killing *ex vivo* and colonization of the liver (Kehl-Fie et al., 2011). SodA is a strict Mn-requiring enzyme and SodM can utilize Mn or Fe (Garcia et al., 2017; Kehl-Fie et al., 2011), underscoring the importance of Mn for *S. aureus* pathogenesis. Intriguingly, several risk factors for *S. aureus* infection, including intravenous drug use and liver disease, can increase tissue Mn levels by up to 20-fold (Btaiche et al., 2011; Sikk et al., 2011). However, the impact of dietary Mn on *S. aureus* infection is unknown.

The host possesses mechanisms to restrict essential metals from microbes during infection, collectively termed 'nutritional immunity' (Hood and Skaar, 2012; Weinberg, 1975). Nutritional immunity encompasses an array of small molecule- and protein-metal chelators and metal transporters that combine to minimize metal availability as part of the inflammatory response. Nutritional immunity may be sufficient to restrict dietary metal bioavailability, limiting the impact that dietary metal has on pathogenesis. However, there is evidence that nutritional immunity can be overwhelmed by dietary metal intake. Dietary iron supplementation enhances *Mycobacterium avium* infection in mice (Dhople et al., 1996), and (Gomes and Appelberg, 1998)a recent report demonstrates that excess dietary Zn allows *C. difficile* to overcome host Zn sequestration (Zackular et al., 2016). These

studies suggest that nutritional immunity is limited in its capacity to sequester dietary metals and altering Mn in the diet may affect the outcome of infection.

The only known Mn sequestering protein in vertebrates is calprotectin, a heterodimer of the S100 family proteins S100A8 and S100A9 (MRP8/14). Calprotectin constitutes the majority of the cytoplasmic protein pool of the neutrophil and is also expressed by other cells that respond to inflammatory signals (Frosch et al., 2005; Lagasse and Clerc, 1988; Odink et al., 1987; Zenz et al., 2005; Zwadlo et al., 1988). Chelation of the divalent cations Mn (II), Zn (II), and Fe (II) by calprotectin inhibits bacterial growth *in vitro* (Damo et al., 2013; Nakashige et al., 2015), and calprotectin-deficient mice exhibit altered sensitivity to multiple bacterial pathogens (Achouiti et al., 2014; Achouiti et al., 2012; Corbin et al., 2008; Gaddy et al., 2014; Hood et al., 2012; Zackular et al., 2016). In the liver and the kidney, calprotectin competes with bacterial Mn and Zn importers for access to Mn and Zn, demonstrating that calprotectin restricts bacterial access to metals in these tissues during infection (Hood et al., 2012; Juttukonda et al., 2016; Kehl-Fie et al., 2013). Consistent with this, calprotectin-deficient mice systemically infected with *S. aureus* have increased Mn levels in liver lesions (Corbin et al., 2008). However, calprotectin-deficiency does not have a significant impact on the fitness of *Salmonella* strains lacking Mn import systems in a gastrointestinal infection model (Diaz-Ochoa et al., 2016), raising the possibility that calprotectin-dependent Mn sequestration may be restricted to certain tissues.

Here I set out to investigate the contribution of dietary Mn to murine Mn homeostasis, to determine how alterations in dietary Mn levels impact the outcome of systemic *S. aureus* infection, and to define the ability of calprotectin-mediated nutritional

immunity to limit the impact of high Mn diet on infection. I show that high dietary Mn elevates Mn levels in the heart and calprotectin does not restrict *S. aureus* access to Mn in this organ. Excess dietary Mn enhances *S. aureus* growth and virulence in the heart by protecting *S. aureus* from reactive oxygen species and neutrophil killing. These results suggest that host Mn sequestration is limited in the heart and demonstrate that excess dietary Mn favors *S. aureus* in the host-pathogen battle for this essential nutrient.

Materials and Methods

Ethics Statement. All animal experiments were reviewed and approved by the Institutional Animal Care and Use Committee of Vanderbilt University and performed according to NIH guidelines, the Animal Welfare Act, and US Federal law. *S. aureus* clinical isolates were obtained under a protocol approved by the Vanderbilt Institutional Review Board. Blood was obtained from healthy, de-identified, consenting adult donors as buffy coats from the New York Blood Center.

Animals. C57BL/6 mice were purchased from The Jackson Laboratory. *S100a9*$^{-/-}$ mice (on a C57BL/6 background) were maintained in our animal colony.

Bacterial strains. Experiments utilized the *S. aureus* strain Newman and derivatives, including Δ*mntH/C* (Kehl-Fie et al., 2013) and Δ*sodAM* (Kehl-Fie et al., 2011), unless otherwise noted. Clinical isolates of *S. aureus* isolates were provided by the VUMC Clinical Microbiology Laboratory from blood and/or valve cultures of diagnosed cases of bacterial endocarditis; these isolates were identified by multiple FDA-approved phenotypic methodologies.

Dietary Manipulation. Diets were synthesized by Dyets Inc. using the AIN-93M standardized diet (Reeves et al., 1993). The base diet was formulated as a Mn and Zn-free diet, with Mn and Zn added as carbonate salts to the follow specified concentrations: Control: 10 mg/kg Mn, 29 mg/kg Zn; low Mn: 0 mg/kg Mn, 29 mg/kg Zn; high Mn: 500 mg/kg Mn, 29 mg/kg Zn; low Zn: 10 mg/kg Mn, 0 mg/kg Zn; high Zn: 10 mg/kg Mn, 1000 mg/kg Zn. Six-week old female mice were placed on custom-synthesized diets for 6-8 weeks prior to infection and throughout infection.

Growth curves. Bacterial strains were freshly streaked onto TSA two days prior to growth curves. Overnight cultures were grown in 5 mL of TSB overnight until the cultures reached stationary phase. These overnight cultures were subsequently diluted 1/100 into 96-well round-bottom plates containing tryptic soy broth (BD, Franklin Lakes NJ) with or without 1 mM or 5 mM paraquat (Sigma, St. Louis MO) and 1 mM $MnCl_2$, as indicated in the figure legend. The 96-well plates were incubated at 37°C with shaking. Growth was monitored by absorbance at OD_{600} every hour utilizing a plate reader (BioTek, Winooski VT). Bacterial growth curves were replicated three times. Each experiment utilized biological triplicate cultures.

Murine model of *S. aureus* systemic infection. Mice were 12-14 weeks old at the time of infection, except Figure 2D in which mice were 8-9 weeks old and not placed on diet prior to infection. Mice were inoculated by intravenous injection of the retroorbital sinus with *S. aureus* grown to mid-exponential phase, washed, and resuspended in 100 μL ice-cold PBS. The inoculum utilized was 2 x 10^7 C.F.U. unless otherwise noted. Survival experiments utilized an inoculum of 5 x 10^7 CFU. An inoculum of 1 x 10^7 CFU was used for Figure 4A. Mice were monitored for four days prior to humane euthanasia by inhalation of CO_2.

Livers, hearts, and blood were removed and processed as indicated in the figure legends. To determine bacterial load, organs were homogenized in sterile PBS and serial dilutions were spot-plated onto TSA. For imaging analysis, organs were flash-frozen in liquid nitrogen and stored at -80°C. For histopathological analysis, organs were fixed in 10% formalin, paraffin-embedded and sectioned.

Murine model of *C. difficile* infection. Studies were conducted on adult (8 to 12 week old) age-matched male C57BL/6 (Jackson Laboratories) mice. Mice were subjected to a previously described model of *C. difficile* infection (Theriot et al., 2011). Briefly, mice were given cefoperazone in their drinking water (0.5 mg/ml) for five days. Mice were then given two days of recovery prior to administration of 10^5 spores of *C. difficile* strain 630 in PBS via oral gavage. Prior to infection, each mouse was confirmed to be *C. difficile* culture negative. Following infection mice were monitored for signs of severe disease, including inappetence, diarrhea, hunching, and weight loss. Mice that exhibited severe disease or weight loss in excess of 20% were humanely euthanized. All animal experiments were approved and performed in compliance with the Institutional Animal Care and Use Committee (IACUC). At necropsy, ceca and colons were harvested, fixed in 10% formalin solution, and embedded in paraffin. Sections were stained with hemotoxylin and eosin. Each section was given a disease score by a pathologist in a blinded fashion based on previously described criteria (Theriot et al., 2011). Histological scores were reported as a cumulative score of three independent scoring criteria: inflammation, edema, and epithelial cell damage.

Murine model of *A. baumannii* infection. A mouse pneumonia model of *A. baumannii* infection was employed as previously described (Hood et al., 2012). Briefly, *A. baumannii*

ATCC 17978 was freshly streaked from frozen stocks onto LB agar two days prior to infection. Overnight cultures were grown in LB. On the day of the infection, overnight cultures were sub-cultured 1:1,000 in 10 mL of LB and grown to mid-exponential phase. Cells were then harvested by centrifugation, washed twice in PBS, and resuspended in PBS to a final concentration of 1 x 10^{10} CFU mL^{-1}. Mice were anesthetized with intraperitoneal injection of 2,2,2-tribromoethanol diluted in PBS. Anesthetized mice were inoculated intranasally with 3 x 10^{8} CFU in 30 µL volume. Infection proceeded for 36 hours. Mice were then euthanized with CO_2 and lungs and livers removed and placed on ice. Organs were homogenized in 1 mL PBS, serially diluted in PBS, and dilutions were spot-plated onto LB agar. Infections were performed at the Vanderbilt University Medical Center and were approved and performed in compliance with the Institutional Animal Care and Use Committee (IACUC).

16S rRNA gene sequencing and gut microbiota analysis. Fresh fecal samples were collected from individual mice ($N = 3$) during a four-week time-course of diet manipulation and immediately frozen for storage at -20°C. DNA was isolated from fecal samples using the PowerSoil DNA isolation kit (MO BIO Laboratories). For each sample, the V4 region of the 16S rRNA gene was amplified and sequenced using the Illumina MiSeq Personal Sequencing platform and sequences were curated using the mothur software package, as previously described (Schloss et al., 2009; Zackular et al., 2016). After curation, we obtained between 8,297 and 23,327 sequences per sample (median=13,015), with a median length of 253 bp. Sequences were clustered into operational taxonomic units (OTUs) based on a 3% distance cutoff calculated using the average-neighbor algorithm. The dataset was rarefied to 8,297 sequences per sample to limit the effects of uneven sampling. All

sequences were classified using the RDP training set (version 9) and OTUs were given a consensus classification using a naïve Bayesian classifier (Wang et al., 2007). Microbial biodiversity (alpha-diversity) was calculated using the inverse Simpson's index, species richness was calculated using Sobs (observed OTUs), and structure (beta-diversity) was calculated using the θ_{YC} distance metric with OTU frequency data (Magurran and Henderson, 2010; Schloss et al., 2009; Yue and Clayton, 2005). Analysis of molecular variance (AMOVA) was performed to determine significance between the community structures of different groups of samples based on θ_{YC} distance matrices (Martin, 2002). All FASTQ sequence data obtained in this study has been deposited to the Sequence Read Archive (SRA) at NCBI with the accession number SRP097779.

Tissue Sectioning. Hearts were sectioned at -20°C using a Thermo Fisher Scientific CryoStar NX70 Cryostat (Thermo Fisher Scientific, Waltham, MA.) For MALDI IMS, hearts were sectioned at 10 μm thickness and thaw-mounted onto chilled Indium-tin-oxide float coated glass slides with a resistance of 30-60 Ω (Delta Technologies, Loveland, CO, USA). Sections for histological analysis were collected onto microscope slides, hematoxylin and eosin stained, and scanned at 20x magnification using a Leica SCN400 Brightfield Slide Scanner (Leica Microsystems, Buffalo Grove, IL, USA.) Sections for LA-ICP MS were sectioned at 30 μm thickness and thaw-mounted onto nitric-acid washed poly(L)lysine-coated vinyl slides (Electron Microscopy Sciences, Hatfield, PA.)

MALDI IMS. Heart sections for MALDI IMS analysis were washed to remove interfering lipids and salts similarly to previously described (Spraggins et al., 2015). Briefly, slides were subjected to sequential washes of 70% ethanol for 30 s, 100% ethanol for 30 seconds, Carnoy fluid (6:3:1 ethanol:chloroform:acetic acid) for 120 seconds, 70% ethanol for 30

seconds, and 100% ethanol for 30 seconds. 2,5-dihydroxyacetophenone (DHA) was used as a matrix and prepared to a concentration of 15 mg/mL in 90% acetonitrile with 0.1% trifluoroacetic acid. Matrix was applied to tissue sections using a TM Sprayer (HTX Technologies, Carrboro, NC). The instrument was operated at a flow rate of 0.15 ml/minute with 90% acetonitrile as a pushing solvent. Six passes of matrix were sprayed in a criss-cross pattern at a speed of 1100 mm/minute with a 2 mm spacing between sprays. The matrix coating was rehydrated immediately before analysis in a rehydration chamber (Yang and Caprioli, 2011) in a 55° oven for 3 minutes using 50 mM acetic acid. IMS was performed using a rapifleX MALDI Tissuetyper (Bruker Daltonics, Billerica, MA, USA) equipped with a Smartbeam 3D 10 kHz Nd:YAG laser (355 nm). The laser was operated in 2 mod 5 mode with a pixel scan of 40 μm in both x and y directions. Data were collected from *m/z* 2000-20,000 with 500 laser shots collected at each pixel.

LA ICP MS. Elemental imaging was performed using LSX-213 laser ablation system (*LA*, CETAC, Omaha, USA) online coupled with ELEMENT 2™ inductively coupled plasma mass spectrometry (*HR-ICPMS*, Thermo Fisher Scientific, Bremen, Germany). Slide-mounted slices of mouse heart were placed in sealed ablation cell and ablated in multi-parallel-line mode with a focused Nd:YAG laser beam at a round-shaped spot size of 100 μm diameter. The ablated sample particles were then transferred to ICP-MS for the detection under medium resolution (R=4200).

Digestion of tissues for ICP MS. Whole organs were homogenized in 1 mL PBS in Whirl Paks (Nasco, Fort Atkinson, WA) and digested in 2 mL HNO_3 and 500 μL H_2O_2 (Optima grade metal-free; Fisher, Waltham, MA) at 90 °C overnight in metal-free Teflon jars. Digested samples were then transferred to metal-free 15 mL conical tubes and diluted with

9 mL MilliQ deionized water and submitted for inductively coupled plasma mass spectrometry (ICP-MS) analysis at the Vanderbilt Mass Spectrometry Research Center.

ICP MS. Element quantification analysis on liquid digested samples was performed using ELEMENT 2™ high resolution inductively coupled plasma mass spectrometry (*HR-ICPMS*, Thermo Fisher Scientific, Bremen, Germany) coupled with ESI auto sampler (Elemental Scientific, Omaha, NE). The ICPMS is equipped with a PFA microflow nebulizer (Elemental Scientific, Omaha, NE), a Scott double-pass spray chamber (at room temperature), a magnetic sector followed by an electric sector, and a second electron multiplier. Liquid sample was up-taken by self-aspiration via 0.50 mm ID sample probe and sample capillary. Trace metals of interest were measured under medium resolution (R=4200).

Cytokine Analysis. Infected whole hearts were harvested 24 hours post infection, immediately frozen on dry ice, and stored at -80°C prior to analysis. Hearts were spiked with protease inhibitor cocktail (Sigma, St. Louis MO), thawed, and placed in Navy Bullet Blender tubes (Next Advance, Averill Park NY) in 200 µL PBS (Sigma). Hearts were homogenized at 4°C using setting 8 for 4 min and setting 10 for 2 min in the Bullet Blender (Next Advance, Averill Park NY). Beads and cells were pelleted at 4000 x *g* for 10 minutes at 4°C for 10 min and supernatants were collected. Protein concentrations in the supernatants was quantified by BCA assay kit (Thermo Fisher Scientific, Waltham, MA) and normalized to 10 mg/mL. Cytokines were assayed in supernatants using MILLIPLEX MAP Mouse Cytokine/Chemokine Magnetic Bead Panel (Millipore, Darmstadt, Germany; catalog number: MCYTOMAG-70K) according to the manufacturer's instructions. Samples were run on the Luminex Flexmap 3D platform (Luminex, Austin TX).

Western Blotting. Whole hearts were placed in individual Navy Bullet Blender tubes (Next Advance) with 400 μL PBS containing 1% SDS and 1% mammalian protease inhibitor cocktail (Sigma). Hearts were homogenized and lysed twice at 4°C and setting 12 for 5 min each on the Bullet Blender (Next Advance). Debris and beads were pelleted at 16,000 x *g* and 4°C for 10 min. Protein in the supernatants was quantified by BCA assay kit (Thermo). Lysate samples were diluted to 1 mg/mL, combined with 1% 2-mercaptoethanol and loading buffer to 1X, and incubated 15 min at 90°C. Protein, 18 μg per sample, was separated at constant voltage by SDS-PAGE on a 4-20% gel (Bio-Rad). Gels were transferred to nitrocellulose as described by the manufacturer using a Trans-Blot Turbo (Bio-Rad). The blot was blocked rocking at 25°C for 30 min in 4 mL Odyssey blocking buffer (LI-COR), and rocked overnight at 4°C in primary antibodies diluted in 4 mL Odyssey blocking buffer. Primary antibodies, anti-S100A8 from rabbit host (Abcam, ab92331) and anti-Sod1 from goat host (Abcam, ab62800) were both diluted 1:1000. Blots were washed thrice at 25°C in 5 mL PBST, then 1 h at 25°C in secondary antibody diluted in 4 mL Odyssey blocking buffer, then thrice again at 25°C in 5 mL PBST. Secondary antibodies, anti-goat IRDye 680LT (LI-COR, 926-68024) and anti-rabbit IRDye 800CW (LI-COR, 926-32213) were both diluted 1:4000. The blot was developed on the Odyssey system scanning at 700 nm for goat and 800 nm for rabbit.

Flow cytometry. Freshly harvested hearts were dissected in DMEM (Corning, Corning NY) containing 10% FBS (Atlanta Biologicals, Flowery Branch GA) and digested in 10 mg/mL collagenase Type II (Worthington, Lakewood NJ), 2.5 mM $CaCl_2$, 2.4 U/mL dispase II (Sigma, St. Louis MO) for 7 minutes at 37°C. Digested tissue was passed through a 100 μM cell strainer, red blood cells were lysed, and the cell suspension was treated with

Fc block (BD Pharmingen, Franklin Lakes NJ). Cells were strained with combinations of the following fluorophore conjugated antibodies: CD11c PE (BD Pharmingen, Franklin Lakes NJ), Ly6G FITC (BD Pharmingen, Franklin Lakes NJ), F4/80 APC (Invitrogen, Waltham MA), and CD11b PE-Cy7 (Biolegend, San Diego CA). Live/dead was detected using LIVE/DEAD Fixable Violet Dead Cell Stain Kit (ThermoFisher, Waltham MA). Flow cytometry was conducted on an LSR II (BD, Franklin Lakes NJ).

Calprotectin growth assay on solid medium. Solid medium was prepared from Roswell Park Memorial Institute (RPMI) 1640 (Gibco, Thermo Fisher Scientific, Waltham, MA) containing 1% casamino acids (BD Pharmingen, Franklin Lakes NJ), 2% bacto agar (BD Pharmingen, Franklin Lakes NJ), and 10 μM N,N,N',N'-tetrakis(2-pyridinylmethyl)-1,2-ethanediamine (TPEN, Sigma, St. Louis, MO). RPMI agar plates were overlaid with soft agar (0.8%) containing 10 μM TPEN and 200 μL (approximately 2 x 10^7 C.F.U.) or 20 μL (approximately 2 x 10^8 C.F.U.) of *S. aureus* Newman overnight culture. Subsequently, the soft agar was spotted with 1 μL $MnCl_2$ (100 mM), 5 μL CP + Mn (4 mg/mL), 5 μL CP ΔS1/S2 + Mn (4 mg/mL), or 5 μL CP WT (4 mg/mL). CP was prepared as previously described (Damo et al., 2013), except that CP + Mn was dialyzed with excess Mn in dialysis buffer. Plates were incubated at 37°C for 16 hours.

Human neutrophil killing assays. Human neutrophils (hPMN) were isolated from buffy coats from anonymous, healthy donors (New York Blood Center) as previously described (Reyes-Robles et al., 2016). Neutrophils were suspended in RPMI (Corning) supplemented with 10 mM 4-(2-hydroxyethyl)-1-piperazineethanesulfonic acid (HEPES) (Corning) and 0.05% human serum albumin (SeraCare), medium in which this assay was performed. Flat-bottom 96-well tissue culture treated plates were pre-treated with 20% human serum

(SeraCare) at 37°C and 5% CO_2 for 30 minutes after which hPMNs were seeded at 5 x 10^5 cells per well. Bacteria were grown to mid-logarithmic phase in TSB +/- 1 mM $MnCl_2$ and pre-opsonized with 20% freshly isolated human serum, prepared as described (Berends et al., 2013), for 30 minutes at 37°C under shaking conditions. After incubation, bacteria were washed twice and then added to the neutrophils at multiplicity of infection (MOI) of 10 in the absence or presence of 1 mM $MnCl_2$. The plates were centrifuged at 1500 rpm for 5 minutes at 4°C (synchronization) and then incubated at 37°C and 5% CO_2 for 1h. After incubation, the hPMNs were lysed with 0.1% saponin on ice for 15 minutes, then serially diluted in PBS and plated onto TSA for enumeration of surviving colony-forming units (CFU) after overnight incubation. Data are represented as the percentage of input CFU (determined at T=0).

Experimental Design.

Sample size determination. Sample sizes were not determined a priori by power analysis.

Rules for stopping data collection. Endpoints were defined prior to experiment initiation. Except otherwise noted, animal infections were terminated four days post-infection. Mice that were defined as moribund by veterinary staff blinded to the experimental groups were humanely euthanized and considered to meet the mortality endpoint.

Data inclusion/exclusion criteria. All data collected were included in analyses; animals that did not survive to the endpoint were not assayed.

Outliers. Outliers were included in analyses, except for rare outliers that resulted from documented experimental error (i.e. infectious inoculum was not properly introduced into the bloodstream).

Replicates. Animal experiments were performed a minimum of two times and data were pooled. Growth curves were performed a minimum of three times; independent biological replicates were sampled in technical triplicate.

Randomization. All animals were randomly assigned to diet and treatment groups using random list generator at random.org. Samples from all groups were processed at the same time and using identical techniques. For all animal experiments, groups were labeled by number for analyses and were only decoded after data analysis.

Blinding. Initial diet studies, including survival studies, were performed with the investigator blinded until the completion of the study and data analyses. Subsequent studies were not blinded.

Statistical Analysis. Statistical significance between two groups was examined by a two-tailed Student's *t*-test or the Mann-Whitney test as indicated in the figure legend. Statistical significance between survival curves was determined by the log-rank test. Statistical significance between multiple groups was examined by the one-way analysis of variance (ANOVA) with Dunnett's or Tukey's multiple comparisons test. Statistical significance between neutrophil killing with or without Mn was determined using a repeated measures ANOVA with Sidak's multiple comparisons test. Statistical work was performed using Prism 6 software (GraphPad) and a *P* value of less than 0.05 was considered significant.

Results

Dietary Mn alters tissue levels and distribution of Mn in infected hearts

To interrogate the impact of dietary Mn on systemic *S. aureus* infection, C57BL/6 (WT) mice were fed custom-synthesized diets containing the minimum recommended

concentration of Mn (Control: 10 mg/kg diet), no Mn (Low Mn: 0 mg/kg diet), or excess Mn (High Mn: 500 mg/kg diet; 3x the concentration in standard chow LabDiet® 5K67). Mice eating each of the three diets exhibited no differences in weight gain (**Figure 25A**), consumed similar amounts of food (**Figure 25B**), and displayed no histopathological changes in hearts, livers, kidneys, or the gastrointestinal tract (**Figure 25C** and data not shown).

We next investigated the impact of dietary Mn on the levels of Mn in tissues infected by *S. aureus* in a murine systemic infection model. Mn concentrations were measured in whole heart and liver homogenates by inductively coupled plasma mass spectrometry (ICP-MS). For all tissues studied, organs from mice provided a high Mn diet harbored significantly higher Mn levels compared to hearts from mice fed control diet, while other metals were unchanged (**Figure 26A-G & Figure 27A-B**). Mice fed low Mn diet also exhibited lower Mn levels than mice fed control diet in the heart (**Figure 27A**). From this, we conclude that tissue Mn levels are altered by dietary Mn intake.

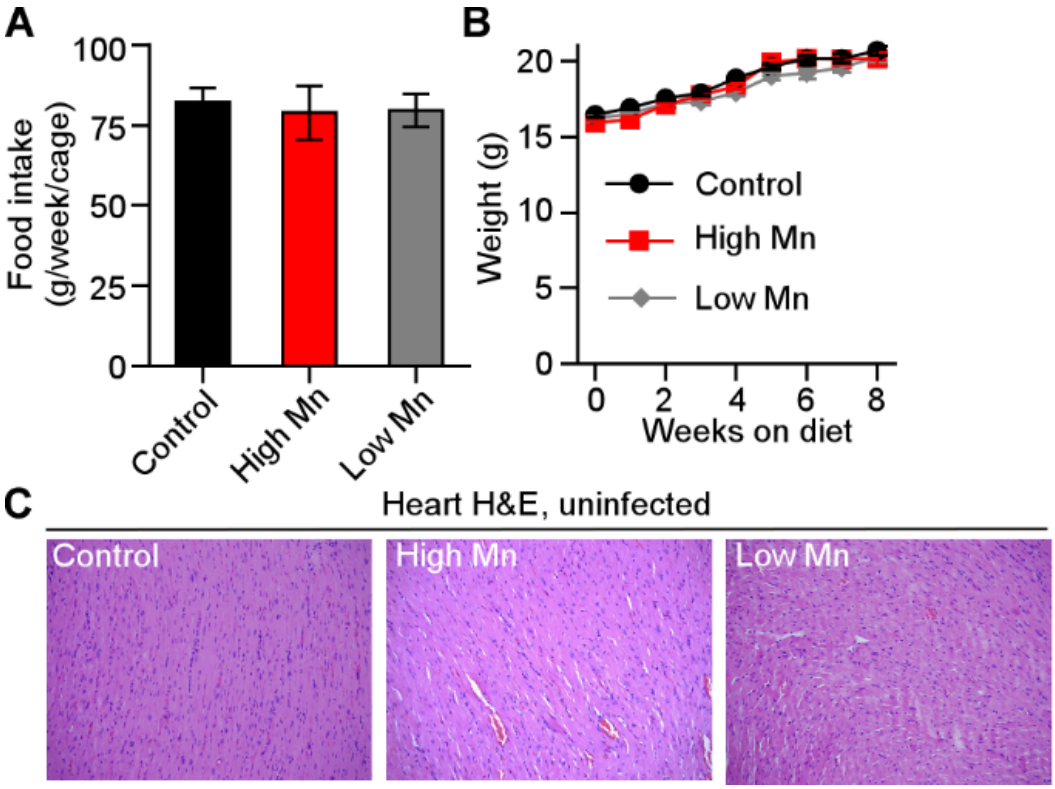

Figure 25. Variation in dietary Mn does not alter food consumption, weight gain or uninfected cardiac pathology. C57BL/6 (WT) mice were fed control, high Mn, or low Mn diet for eight weeks. **(A)** Average food intake (grams consumed/cage/week) over the diet timecourse. $N = 2$ cages per diet with diet weight measured once a week for eight weeks. Bars indicate mean and standard deviation. **(B)** Weight of mice over the diet timecourse. $N = 10$. Bars indicate mean and standard deviation. **(C)** Hematoxylin and eosin stained heart sections from uninfected mice fed control, high Mn, or low Mn diet for eight weeks. No histopathologic differences between groups were noted by a pathologist. Representative images are shown. These findings were replicated in three separate experiments.

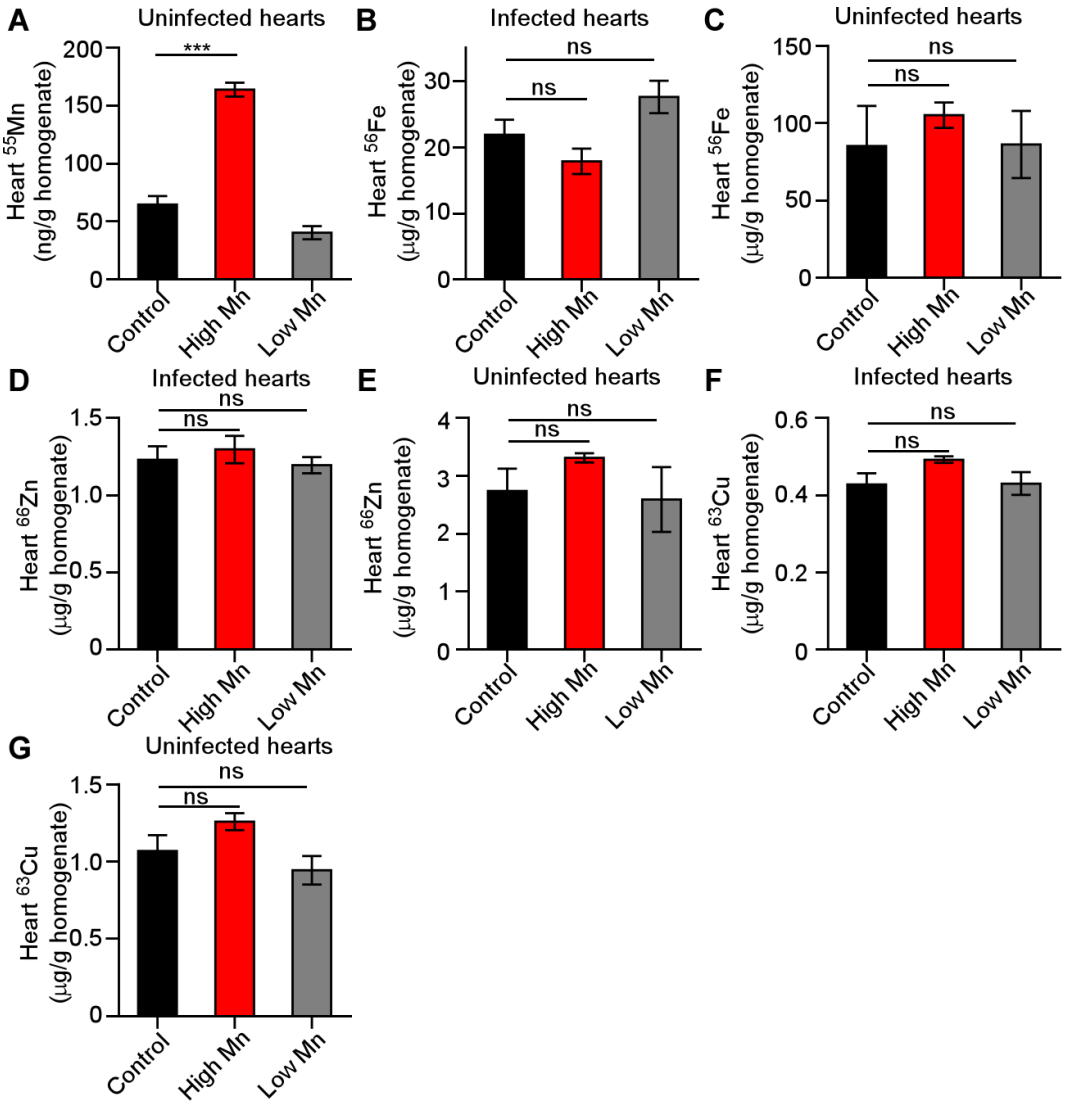

Figure 26. Effect of dietary Mn variation on tissue metal levels. C57BL/6 mice (WT) were fed high Mn, control, or low Mn diet for six weeks. Metals were assayed in heart homogenates by ICP-MS in uninfected mice or mice infected with *S. aureus*. **(A)** Mn concentrations in uninfected hearts. **(B)** Fe levels in infected hearts. **(C)** Fe levels in uninfected hearts. **(D)** Zn levels in infected hearts. **(E)** Zn levels in uninfected hearts. **(F)** Copper (Cu) levels in infected hearts. **(G)** Cu levels in uninfected hearts. (**A-G**) $N = 3$. Bars depict mean and SEM. *** $P < 0.001$. ns = not significant by ANOVA with Dunnet's multiple comparisons test.

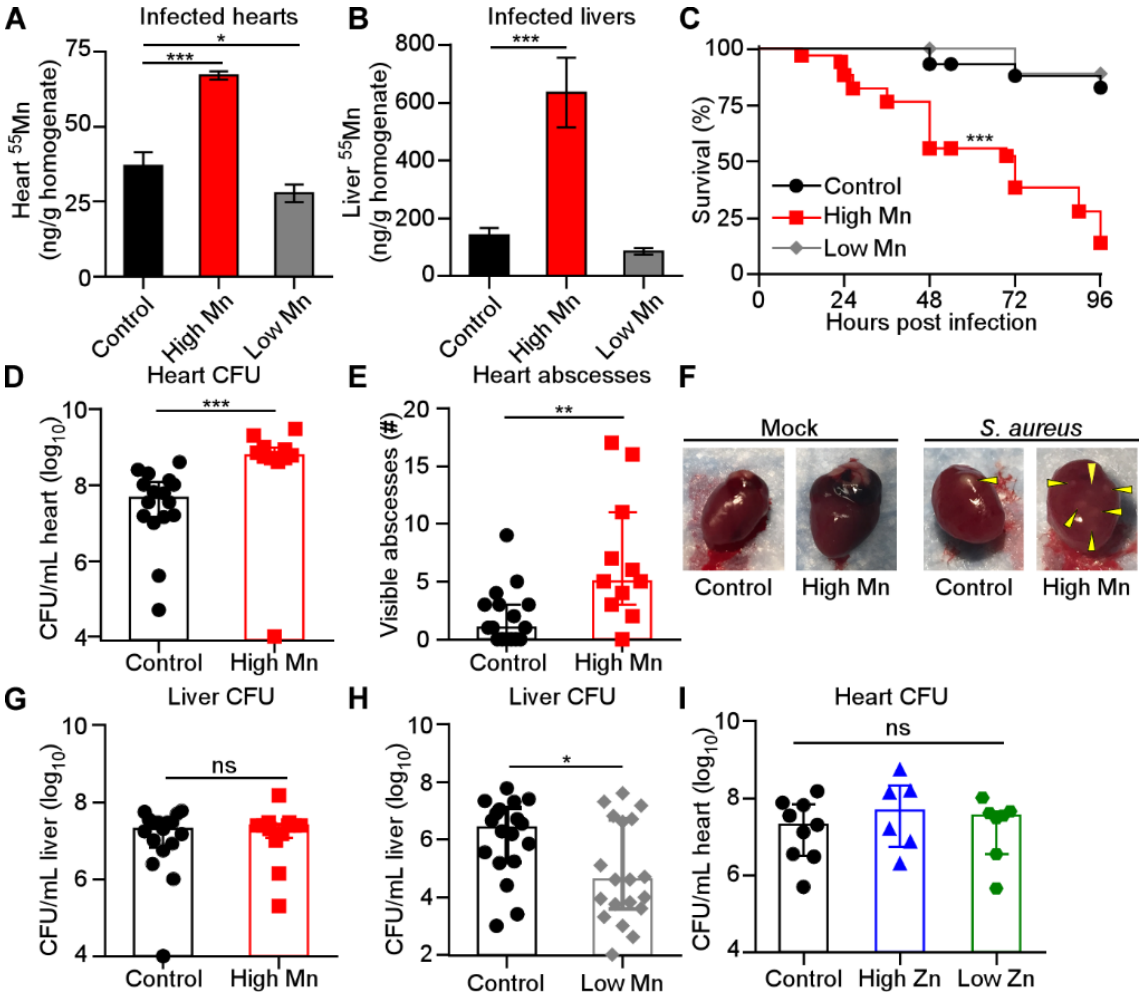

Figure 27. High Mn diet increases lethality and heart bacterial burdens from *S. aureus* systemic infection. (**A-H**) C57BL/6 mice (WT) were fed high Mn, control, or low Mn diet and infected with *S. aureus* for four days. (**A-B**) Mn concentrations in (**A**) heart homogenates and (**B**) liver homogenates were measured by ICP-MS. $N = 3$. **(C)** Survival was monitored. Low Mn $N = 10$; control $N = 29$; high Mn $N = 34$. **(D)** CFU present in heart homogenates. For **D**, **E** and **G,** $N = 16$ (control), 11 (high Mn). **(E)** Enumeration of heart abscesses. (**F**) Heart appearance. Arrowheads indicate abscesses. (**G**) CFU present in liver homogenates. (**H**) CFU present in liver homogenates. $N = 18$ (control); $N = 19$ (low Mn). (**I**) CFU present in heart homogenates from WT mice fed high Zn, control, or low Zn diet and infected with *S. aureus* for four days. $N = 7$ (high Zn), 9 (control), 7 (low Zn). (**A-B**) Bars depict mean and SEM. (**D-E, G-I**) Bars depict median and interquartile range. ns = not significant. $*P < 0.05$. $**P < 0.01$. $***P < 0.001$ by log-rank test (**B**), Mann-Whitney test (**D, E, G, H**) or one-way analysis of variance (ANOVA) with Dunnett's multiple comparisons test (**A-B**) or Tukey's multiple comparisons test (**I**).

Dietary Mn levels govern the severity of *S. aureus* infection of the heart

I hypothesized that Mn levels in infected tissues could alter *S. aureus* infection. To test this hypothesis, I infected mice fed high Mn, control, or low Mn diet. Following intravenous challenge with *S. aureus,* mice provided a high Mn diet displayed significantly increased mortality (**Figure 27C**), with a decrease in survival from 80% of mice fed control diet surviving to fewer than 20% of mice fed high Mn diet. Mice fed high Mn diet also exhibited ten-fold higher bacterial burdens in the heart (**Figure 27D**) and significantly more staphylococcal abscesses in the heart (**Figure 27E & F**). In contrast to the heart, high Mn diet did not alter bacterial burdens in the liver **(Figure 27G)**. However, feeding mice a low Mn diet resulted in a reduction in bacterial burdens in the liver **(Figure 27H**), suggesting that Mn levels in the control diet but not the low Mn diet can support staphylococcal growth in the liver. To determine whether the effects of dietary metal on *S. aureus* virulence in the heart are Mn-specific, mice were fed diets containing altered levels of zinc (Control: 29 mg/kg; High Zn: 1000 mg/kg; Low Zn: 0 mg/kg) and infected with *S. aureus*. Heart bacterial burdens were unchanged by the level of dietary Zn (**Figure 27I**). These results demonstrate that excess dietary Mn enhances *S. aureus* virulence and promotes growth of *S. aureus* specifically in the murine heart.

Dietary Mn does not drastically alter the gut microbiota or the innate immune response

I next interrogated whether dietary Mn alters the gut microbiota, broadly impacts microbial fitness within the murine host, or modifies the innate immune response. Providing mice with low or high Mn diets did not significantly alter the structure or diversity of the gut microbiota (**Figure 28A-C**). Furthermore, mice that were placed on

high or low Mn diet did not exhibit differential pathology following oral challenge with the gastrointestinal pathogen *C. difficile* (**Figure 28D)**. Finally, *A. baumannii* infection of the murine lung was not affected by placing mice on high or low Mn diet (**Figure 28E)**. Together, these findings indicate that not all microbes have amplified fitness in a host fed a high Mn diet; furthermore, these results demonstrate that mice fed a high Mn diet have intact immune responses to extracellular bacterial pathogens.

I hypothesized that dietary Mn may impact the *S. aureus*-specific immune response. *S. aureus* infection typically leads to robust recruitment of neutrophils, which are a critical effector cell in controlling *S. aureus* infection (Rigby and DeLeo, 2012). Phagocyte recruitment to infected hearts was unchanged by providing mice a high Mn diet (**Figure 28F**). Additionally, analysis of a panel of cytokines and chemokines did not detect significant differences in the immune response between mice fed control and high Mn diet (**Table 5-Table 7**). These findings indicate that high dietary Mn does not dramatically impair the innate immune response to *S. aureus* infection in a WT mouse.

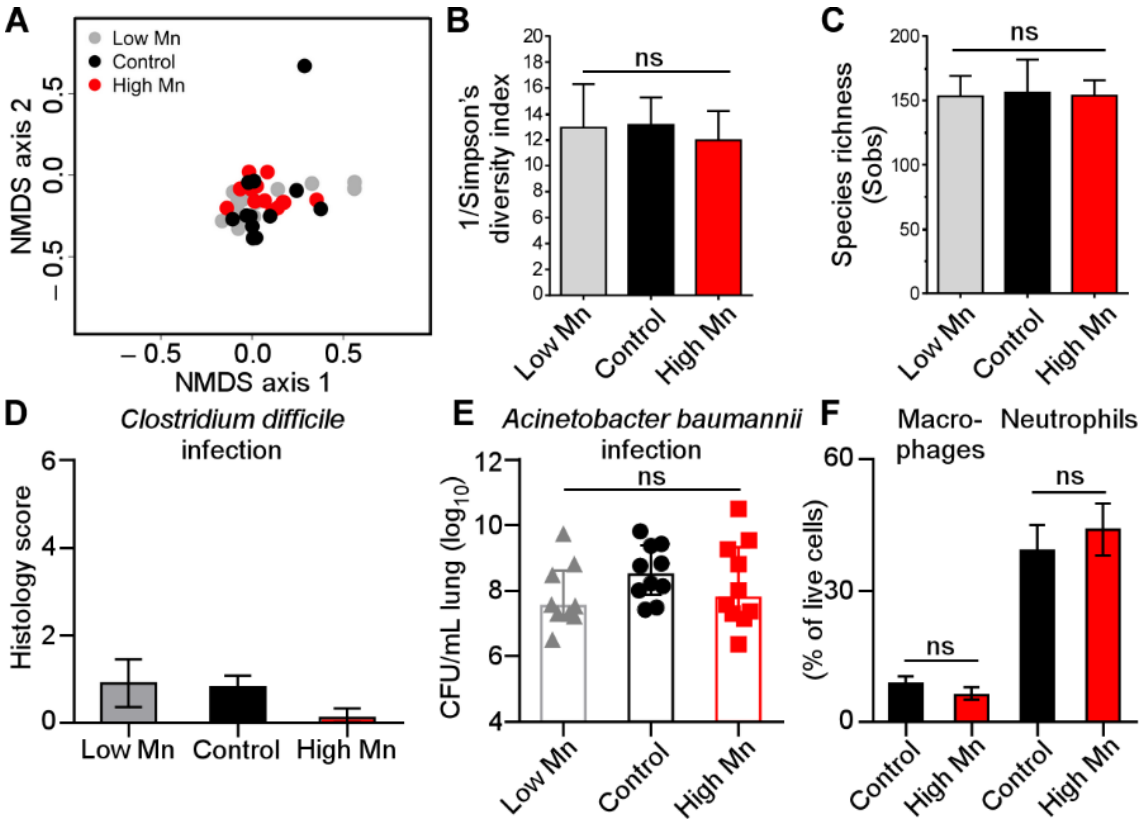

Figure 28. Dietary Mn does not alter the gut microbiota or impact infection with *Clostridium difficile* or *Acinetobacter baumannii*. (**A-F**) WT C57BL/6 mice were placed on control, low Mn, or high Mn diet for all experiments. (**A**) Nonmetric multidimensional scaling (NMDS) ordination showing gut microbiota β-diversity during a 4-week time course of dietary Mn manipulation. Distances were measured using the Yue and Clayton index of dissimilarity (θ_{YC}). No significant differences were observed between groups over the 4-week time-course (Analysis of Molecular Variance; AMOVA) ($P > 0.05$). (**B**) Inverse Simpson's diversity for mice fed low Mn, control, or high Mn diets over a four-week time-course (**C**) Species richness measured by Sobs (number of observed OTUs) for each diet. (**D**) Blinded histological scores from ceca were determined 4 days post-infection with *C. difficile*. Error bars represent standard deviation. (**E**) CFU recovered from lungs 36 hours following intranasal inoculation with *A. baumannii*. (**F**) Flow cytometry quantification of $Ly6G^+CD11b^+$ cells (neutrophils) and F4/80+ (macrophages) cells from *S. aureus*-infected hearts. Previous gate: live cells. $N = 4$ (high Mn), 3 (control). ns = not significant by ANOVA with Tukey's multiple comparison's test (**E**), student's *t*-test (**F**).

Table 5. Cytokine and chemokine analysis of infected heart tissue harvested from mice fed control or high Mn diet 2 hours post infection.

Analyte	Control (pg/mL)	Standard deviation	High Mn (pg/mL)	Standard deviation
G-CSF	2.93[1]	1.93[1]	1.77	0.51
Eotaxin	87.13	9.10	58.70	6.09
GM-CSF	n.d.[2]		n.d.	
INFγ	0.52	0.00[3]	0.40	0.00
IL-1α	8.00	4.35	7.36	5.02
IL-1β	n.d.		n.d.	
IL-2	17.32	6.02	15.18	3.73
IL-4	0.63	0.04	0.83	0.21
IL-3	n.d.		n.d.	
IL-5	n.d.		n.d.	
IL-6	0.81	0.50	1.14	0.81
IL-7	0.41	0.00	0.95	0.26
IL-9	583.67	151.10	444.33	116.26
IL-10	0.50	0.09	0.41	0.00
IL-12 (p40)	4.18	0.51	2.75	1.58
IL-12 (p70)	n.d.		n.d.	
LIF	n.d.		n.d.	
IL-13	15.45	4.26	8.71	6.95
LIX	64.22	18.02	17.37	1.97
IL-15	19.69	3.96	26.28	11.09
IL-17	0.80	0.12	1.52	0.38
IP-10	22.92	2.38	24.77	5.38
KC	10.56	1.04	10.07	2.29
MCP-1	131.00	16.51	97.45	14.62
MIP-1α	7.85	4.12	2.14	0.00
MIP-1β	n.d.		n.d.	
M-CSF	2.40	0.84	2.45	2.12
MIP-2	n.d.		n.d.	
MIG	77.00	2.76	97.69	13.39
RANTES	3.04	1.72	4.64	4.81
VEGF	17.08	1.43	10.33	1.50
TNFα	n.d.		n.d.	

[1] Values are mean +/- standard deviation

[2] n.d. = not detected.

[3] Standard deviation of zero indicates the analyte was only detected in one sample.

Table 6. Cytokine and chemokine analysis of infected heart tissue harvested from mice fed control or high Mn diet 6 hours post infection.

Analyte	Control (pg/mL)	Standard deviation	High Mn (pg/mL)	Standard deviation
G-CSF	45.07[1]	53.15[1]	604.82	611.76
Eotaxin	81.67	5.73	85.68	29.90
GM-CSF	n.d.[2]		n.d.	
INFγ	1.14	0.48	0.86	0.00[3]
IL-1α	56.56	19.28	87.35	29.99
IL-1β	n.d.		n.d.	
IL-2	23.92	4.08	25.98	3.66
IL-4	0.84	0.17	0.93	0.26
IL-3	n.d.		n.d.	
IL-5	n.d.		1.10	0.00
IL-6	11.21	12.47	149.02	182.17
IL-7	n.d.		0.55	0.14
IL-9	508.00	92.12	581.25	42.52
IL-10	1.07	0.71	0.85	0.29
IL-12 (p40)	5.12	4.06	5.46	2.15
IL-12 (p70)	n.d.		n.d.	
LIF	n.d.		3.12	2.57
IL-13	5.05	1.72	11.79	4.47
LIX	66.42	22.05	21.26	0.00
IL-15	17.12	5.59	23.85	3.78
IL-17	0.64	0.09	0.95	0.35
IP-10	27.35	2.85	54.18	21.29
KC	44.01	54.03	284.37	231.13
MCP-1	104.61	20.54	148.85	35.63
MIP-1α	n.d.		3.73	0.54
MIP-1β	n.d.		n.d.	
M-CSF	1.24	0.35	1.98	0.42
MIP-2	n.d.		n.d.	
MIG	71.50	8.81	71.66	16.59
RANTES	1.08	0.34	1.12	0.24
VEGF	10.72	1.71	9.17	1.24
TNFα	n.d.		n.d.	

[1] Values are mean +/- standard deviation

[2] n.d. = not detected.

[3] Standard deviation of zero indicates the analyte was only detected in one sample.

Table 7. Cytokine and chemokine analysis of infected heart tissue harvested from mice fed control or high Mn diet 24 hours post infection.

Analyte	Control (pg/mL)	Standard deviation	High Mn (pg/mL)	Standard deviation
G-CSF	5880.33[1]	2542.68[1]	2020.00	47.00
Eotaxin	74.53	10.57	91.43	29.15
GM-CSF	14.41	0.00[2]	32.04	18.55
INFγ	1.16	0.00	0.86	0.50
IL-1α	31.57	24.88	51.30	21.30
IL-1β	6.27	0.00	25.66	6.26
IL-2	18.56	1.70	26.39	5.91
IL-4	0.72	0.08	1.00	0.18
IL-3	n.d.[3]		0.13	0.00
IL-5	n.d.		n.d.	
IL-6	500.64	424.82	2980.25	2557.78
IL-7	0.45	0.00	1.85	0.00
IL-9	393.67	60.36	624.00	225.72
IL-10	0.85	0.55	2.30	1.44
IL-12 (p40)	6.24	4.88	17.55	9.29
IL-12 (p70)	n.d.		n.d.	
LIF	11.36	11.10	43.13	26.33
IL-13	7.19	1.70	8.82	4.55
LIX	48.96	33.57	143.33	15.76
IL-15	17.55	9.75	36.27	15.20
IL-17	0.99	0.36	2.84	2.20
IP-10	228.33	70.24	245.50	102.64
KC	778.33	679.88	3436.00	2679.96
MCP-1	340.33	171.41	578.50	238.35
MIP-1α	79.06	46.15	126.32	63.24
MIP-1β	5.31	3.03	62.16	31.35
M-CSF	5.89	5.30	14.22	11.11
MIP-2	18.77	4.79	26.62	11.77
MIG	874.00	336.93	549.50	267.31
RANTES	0.93	0.31	1.96	0.59
VEGF	9.68	1.52	10.65	1.71
TNFα	0.81	0.00	6.43	0.99

[1] Values are mean +/- standard deviation
[2] Standard deviation of zero indicates the analyte was only detected in one sample.
[3] n.d. = not detected.

Calprotectin promotes *S. aureus* infection of the heart

Essential metals are withheld from invading pathogens by a metal-sequestration response, collectively termed 'nutritional immunity' (Hood and Skaar, 2012; Palmer and Skaar, 2016; Weinberg, 1975). Because excess dietary Mn enhances *S. aureus* growth in the heart, I hypothesized that the host does not effectively sequester Mn in this organ. Calprotectin, a heterodimer formed by S100A8 and S100A9, is the only identified Mn-sequestering immune protein in vertebrates (Corbin et al., 2008). In the livers of mice, calprotectin sequesters Mn (Corbin et al., 2008; Kehl-Fie et al., 2013), and *S100a9*$^{-/-}$ mice, which are calprotectin-deficient, exhibit higher bacterial burdens in the liver (**Figure 29**) (Corbin et al., 2008; Kehl-Fie et al., 2011; Kehl-Fie et al., 2013). First, we assessed whether calprotectin is effectively recruited to *S. aureus*-infected hearts by imaging mass spectrometry and immunoblot. Indeed, calprotectin was present surrounding staphylococcal abscesses when mice were provided high Mn diet, but calprotectin was not present in mock-infected mice or *S100a9*$^{-/-}$ infected mice (**Figure 30A**). Of note, calprotectin was present surrounding the staphylococcal abscess but not in the abscess center, which contrasts with previous findings in the liver (Corbin et al., 2008) and the kidney (Kehl-Fie et al., 2013), where calprotectin localizes with the staphylococcal abscess. Interestingly, significantly fewer bacteria were recovered from the hearts of *S100a9*$^{-/-}$ mice than WT mice for each diet (**Figure 30B**), with a 6-$\log_{10}$ reduction in bacterial burdens in *S100a9*$^{-/-}$ mice fed a low Mn diet. Moreover, *S100a9*$^{-/-}$ mice were protected from infection mortality when fed high Mn diet (**Figure 30C**). These findings demonstrate that calprotectin is present in infected hearts and supports bacterial growth in this organ.

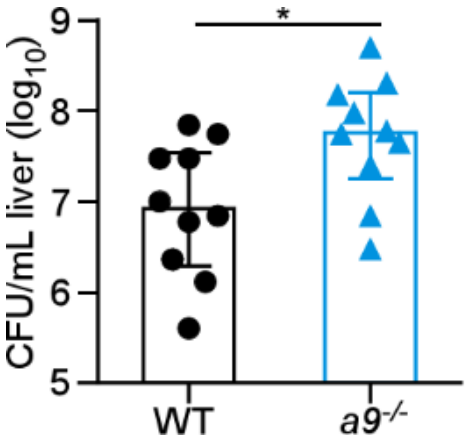

Figure 29. *S100a9*$^{-/-}$ mice harbor higher bacterial burdens in the liver. *S100a9*$^{-/-}$ mice were infected with *S. aureus* and liver bacterial burdens were enumerated 4 days post infection. $N = 10$. $P < 0.05$ by Student's *t*-test.

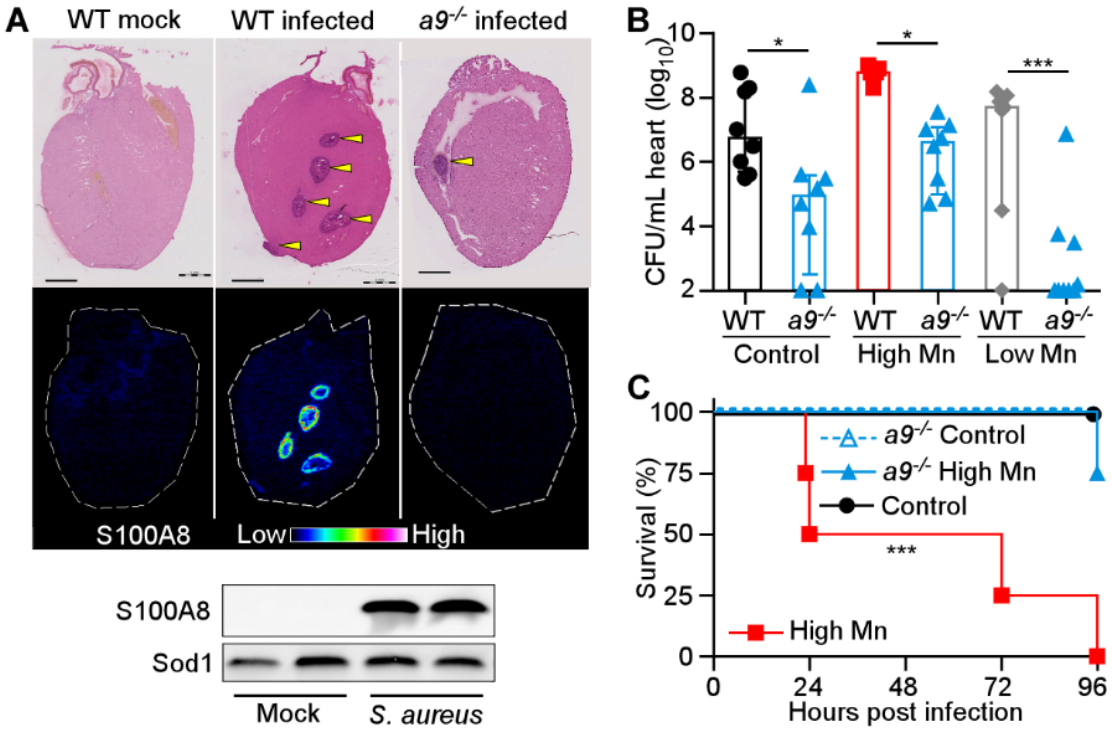

Figure 30. In the heart, calprotectin enhances *S. aureus* infection. (**A-C**) WT or *S100a9*$^{-/-}$ (*a9*$^{-/-}$) mice were fed high Mn, control, or low Mn diet and mock-infected or infected with *S. aureus* for 4 days. **(A)** MALDI-MS images of S100A8 from hearts of mice fed high Mn diet. H&E staining is shown for comparison. Arrowheads indicate abscesses. Scale bar is 1 mm. Below, immunoblot for Sod1 (loading control) and S100A8 in hearts from WT mice. Images and blots are representative of three independent experiments. **(B)** Heart bacterial burdens recovered from WT and *S100a9*$^{-/-}$ mice. $N = 8$ (control WT, control *a9*$^{-/-}$, high Mn *a9*$^{-/-}$), 5 (high Mn WT), 7 (low Mn WT), 9 (low Mn *a9*$^{-/-}$). Bars depict median and interquartile range. **(C)** Survival of WT and *S100a9*$^{-/-}$ mice following infection. $N = 4$. Survival is representative of three independent experiments. *$P < 0.05$. *** $P < 0.001$, by ANOVA with Tukey's multiple comparisons test **(B)** or log-rank test **(C).**

Calprotectin does not restrict Mn availability in the heart

S. aureus possesses two Mn importers, MntH and MntABC (Kehl-Fie et al., 2013). *S. aureus* inactivated for both importers (Δ*mntH/C*) displayed a growth deficit that could be rescued with excess Mn, suggesting that growth of this strain can be used as a biological readout for Mn availability (**Figure 31**). To assess whether loss of calprotectin alters bioavailability of Mn in the heart, mice were infected with *S. aureus* WT or Δ*mntH/C*. Heart bacterial burdens of the Δ*mntH/C* strain were not different in WT or *S100a9*$^{-/-}$ mice (**Figure 32A**), indicating that loss of calprotectin does not affect Mn bioavailability in the heart. In contrast, *S. aureus* Δ *mntH/C* colonizes to higher bacterial burdens in the livers of *S100a9*$^{-/-}$ mice compared to WT mice (Kehl-Fie et al., 2013). This finding indicates that the ability of calprotectin to sequester Mn is tissue-limited.

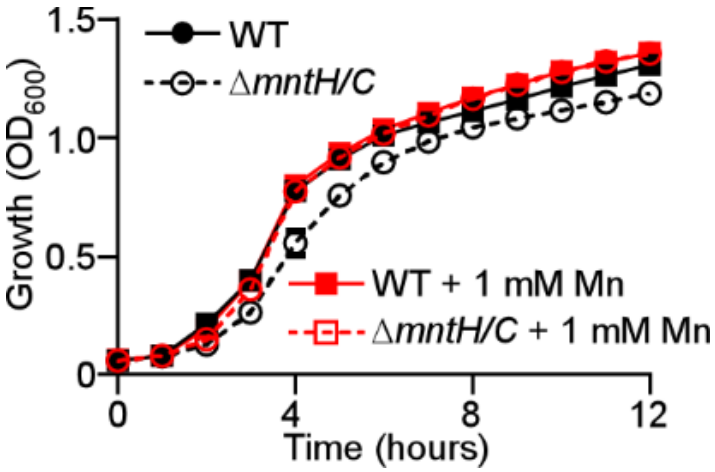

Figure 31. Improved growth of Δ*mntH/C* strain with the addition of Mn to the medium. Growth of *S. aureus* WT or Δ*mntH/C* with or without the addition of 1 mM $MnCl_2$. Growth was measured by OD_{600} over time. Data are combined from three independent experiments and depict the mean and S.E.M.

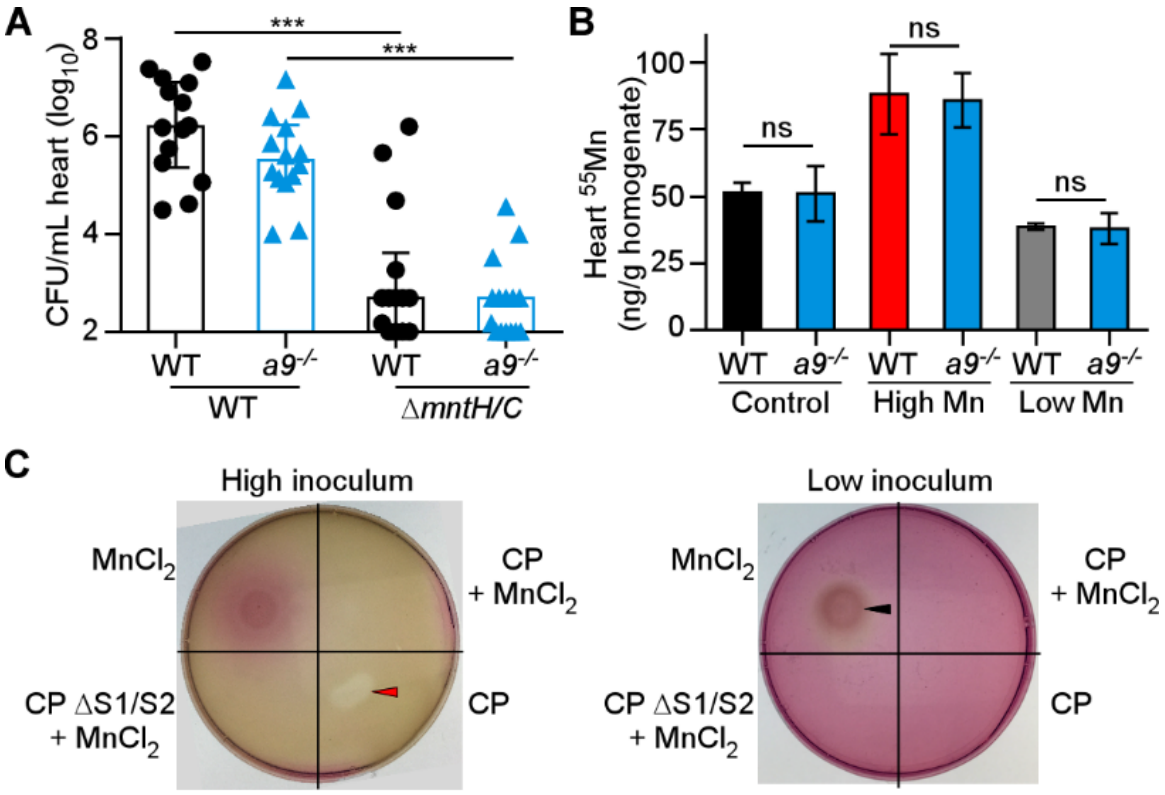

Figure 32. Loss of calprotectin does not impact Mn bioavailability in the heart. (**A**) Heart bacterial burdens from WT and *S100a9*$^{-/-}$ mice provided normal chow and infected for 4 days with *S. aureus* WT or Δ*mntH/C*. N = 15 (*S100a9*$^{-/-}$ Δ*mntH/C*), N = 14 (all other groups). (**B**) Mn concentrations in infected heart homogenates were measured by ICP-MS. Hearts were harvested from WT or *S100a9*$^{-/-}$ (*a9*$^{-/-}$) mice fed high Mn, control, or low Mn diet and infected with *S. aureus* for 4 days. N = 3. (**C**) *S. aureus* growth on RPMI agar containing 10 μM TPEN spotted CP or $MnCl_2$ sources as labeled. High inoculum = 2 x 10^8 CFU, Low inoculum = 2 x 10^7 CFU. Red arrow points to area of growth inhibition and black arrow indicates area of growth enhancement. **(A)** Bars depict median and interquartile range. **(B)** Bars depict mean and SEM. *** $P < 0.001$, ns = not significant by ANOVA with Tukey's multiple comparisons test.

Since calprotectin-deficient mice have lower bacterial burdens than WT mice when fed low Mn diet, I postulated that calprotectin may have a role in cardiac Mn homeostasis. Indeed, calprotectin is present in circulating cells and is capable of binding Mn with high affinity, suggesting the possibility that calprotectin is required for delivery of Mn to the heart. However, the absence of calprotectin had little impact on Mn levels in *S. aureus* infected hearts (**Figure 32B**). These results suggest that the absence of calprotectin does not alter Mn delivery to the heart.

I considered the possibility that Mn-bound calprotectin serves as a nutrient source for *S. aureus,* as calprotectin supports staphylococcal growth in the heart. *Neisseria* species scavenge Zn from calprotectin *in vitro,* a process termed 'Zinc piracy' (Jean et al., 2016; Stork et al., 2013). I assessed whether *S. aureus* is capable of utilizing calprotectin as a nutrient Mn source by a disc diffusion assay. In this assay, RPMI agar containing the chemical chelator N,N,N',N'-tetrakis(2-pyridylmethyl)ethane-1,2-diamine (TPEN) was overlaid with soft agar containing two different bacterial densities of *S. aureus,* and the soft agar was then spotted with Mn chelators and sources. When *S. aureus* was plated at high density, the bacteria grew in a lawn and calprotectin inhibited growth of *S. aureus* whereas calprotectin that was previously loaded with Mn (calprotectin + Mn) did not inhibit *S. aureus* growth (**Figure 32C**). Similarly, calprotectin that lacks the Mn and Zn binding sites (ΔS1/ΔS2) did not inhibit growth (**Figure 32C**). When *S. aureus* was plated at a low density, TPEN inhibited growth. In this condition, calprotectin + Mn could not support growth of *S. aureus*, but free $MnCl_2$ could support growth (**Figure 32C**). Based on these findings, I conclude that *S. aureus* does not possess mechanisms to scavenge Mn from

calprotectin. Taken as a whole, these data suggest that calprotectin does not have a major role in Mn nutritional immunity during *S. aureus* infection of the heart.

Excess dietary Mn is bioavailable to *S. aureus* in the heart

The finding that calprotectin deficiency does not alter Mn bioavailability in the heart suggests that the host may have a limited ability to sequester excess Mn in this tissue. To determine if excess Mn in the heart is in proximity to staphylococcal abscesses and available for bacterial capture, the spatial localization of Mn was examined using laser ablation coupled to ICP-MS (LA-ICP-MS). Uninfected hearts displayed relatively homogeneous Mn and calcium (Ca) concentrations throughout the myocardium (**Figure 33A**). When mice were provided control diet, Mn was depleted in the staphylococcal abscess relative to the adjacent myocardium (**Figure 33B**), similar to the Mn-deplete staphylococcal abscesses observed in livers and kidneys (Corbin et al., 2008; Kehl-Fie et al., 2013). In contrast, mice fed high Mn diet displayed high concentrations of Mn surrounding the staphylococcal abscesses (**Figure 33B**). Ca accumulated within abscesses of mice on both control and high Mn diet (**Figure 33B**). Similar LA-ICP-MS results were obtained in calprotectin-deficient mice (**Figure 34)**. These findings suggest that excess dietary Mn may accumulate in the heart in a location available for acquisition by *S. aureus*. To test this hypothesis, mice were infected with *S. aureus* WT or Δ*mntH/C*. When mice were fed control diet, 6-$\log_{10}$ fewer CFUs were recovered from Δ*mntH/C* infection than WT infection (**Figure 33C**), implying that hearts are Mn deplete at baseline. However, the fitness deficit for Δ*mntH/C* was significantly and profoundly reversed in mice fed high Mn diet (**Figure 33C**). These results indicate that excess dietary Mn is bioavailable to *S. aureus* in the heart.

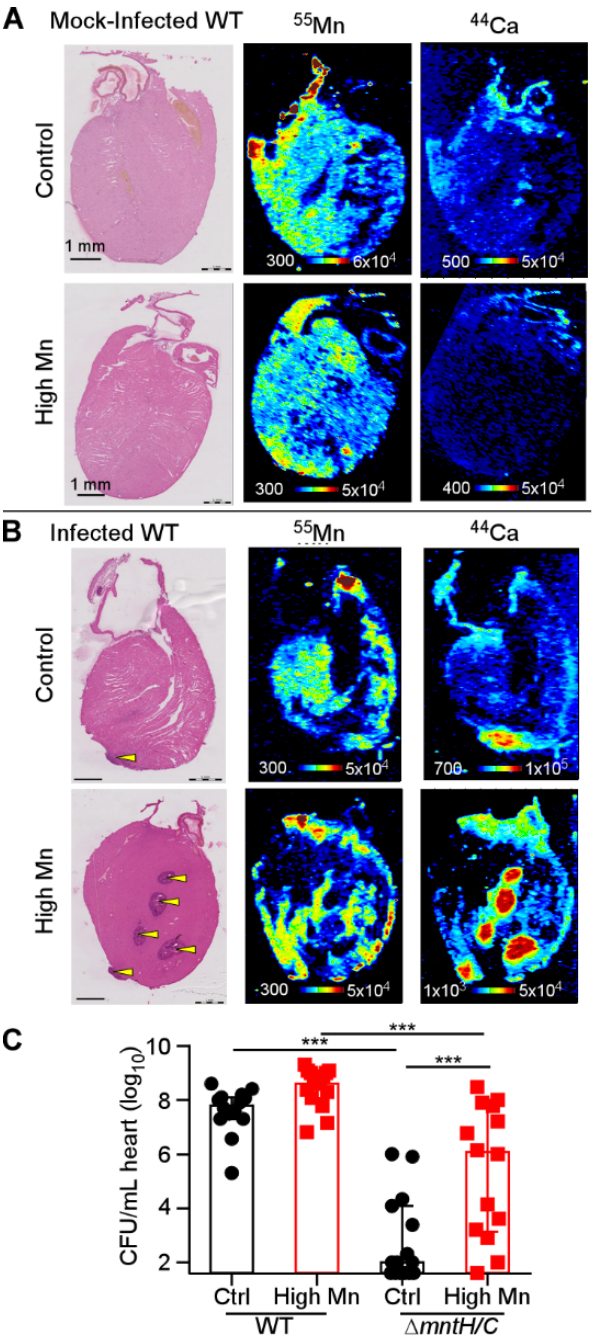

Figure 33. Excess dietary Mn is bioavailable to *S. aureus* in the heart. C57BL/6 mice (WT) were fed high Mn or control diet and infected mock-infected with PBS (**A**) or infected with *S. aureus* WT (**B**) for 4 days. The arrangement and relative concentrations of Mn and Ca in heart sections was assessed by LA-ICP-MS. H&E stained serial sections are shown to the left. Scale bar is 1 mm. (**C**) Heart bacterial burdens recovered following infection with WT or Δ*mntH/C*. $N = 14$ (Control WT, high Mn Δ*mntH/C*); 15 (control Δ*mntH/C*, high Mn WT). Bars depict median and interquartile range. *** $P < 0.001$ by ANOVA with Tukey's multiple comparisons test.

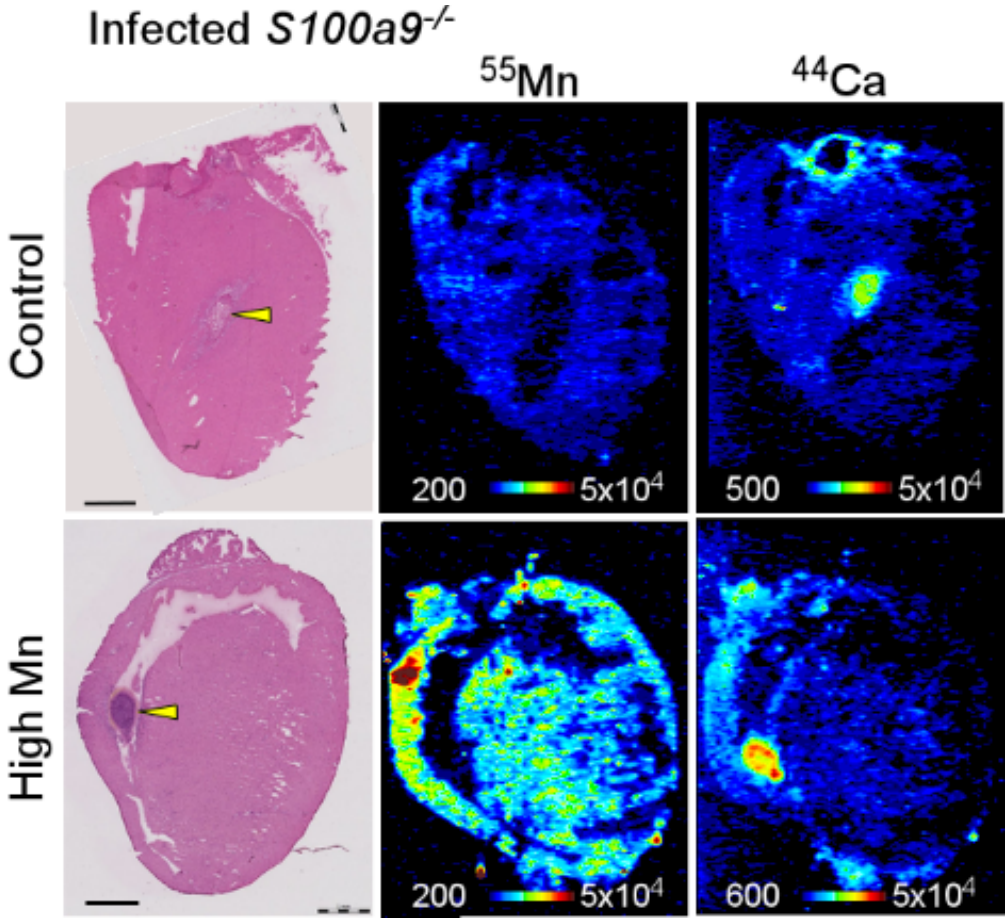

Figure 34. LA-ICP-MS images from *S100a9*$^{-/-}$ mice. *S100a9*$^{-/-}$ mice were fed high Mn or control diet and infected with *S. aureus* WT for 4 days and relative concentrations of Mn and Ca in infected heart sections was assessed by LA-ICP-MS. H&E stained serial sections are shown to the left. Scale bar is 1 mm.

Dietary manganese protects *S. aureus* from superoxide stress

I hypothesized that high Mn diet may protect *S. aureus* from reactive oxygen species (ROS) produced during the host immune response. Mn has multi-faceted roles in bacterial defense against ROS (Horsburgh et al., 2002b; Lisher and Giedroc, 2013). Neutrophils, which are essential for clearance of *S. aureus,* are capable of killing *S. aureus* through the production of ROS (Rigby and DeLeo, 2012). Therefore, I posited that *S. aureus* may utilize Mn to detoxify ROS and therefore escape neutrophil-mediated killing.

S. aureus expresses superoxide dismutase enzymes, SodA and SodM, which can use Mn to detoxify superoxide (Clements et al., 1999; Garcia et al., 2017; Kehl-Fie et al., 2011; Valderas and Hart, 2001). SodA and SodM confer resistance to neutrophil killing, and function of SodA and SodM are impaired by Mn-chelation (Kehl-Fie et al., 2011). To assess the contribution of superoxide dismutase activity to infection of the heart, mice fed control and high Mn diet were infected with WT *S. aureus* and Δ*sodAM*. While *S. aureus* Δ*sodAM* was attenuated approximately 5-$\log_{10}$ in mice fed control diet, Δ*sodAM* had no fitness defect in mice fed the high Mn diet, similar to the rescue seen in neutrophil-depleted mice (**Figure 35A & B**). *S. aureus* Sod enzymes are therefore dispensable in the setting of excess dietary Mn, suggesting that molecular Mn detoxifies ROS independent of Sod (Lisher and Giedroc, 2013). To test this hypothesis, *S. aureus* was grown in the presence of the superoxide donor paraquat with or without added Mn (**Figure 35C**). As expected, Δ*sodAM* was highly susceptible to superoxide stress. However, the addition of Mn to the medium significantly improved the growth of Δ*sodAM* in paraquat. In fact, the rescue of WT and Δ*sodAM* in paraquat by Mn *in vitro* mirrored the bacterial burdens recovered from

hearts of mice on control or high Mn diet (**Figure 35A**). Hence, we propose that Mn serves as an antioxidant independent of superoxide dismutase.

Finally, we investigated a role for Mn in protecting *S. aureus* from superoxide stress in human-derived isolates and human cells. To this end, methicillin-resistant and methicillin-sensitive *S. aureus* isolates from human endocarditis cases were assayed for Mn rescue of growth in paraquat (**Figure 35D & Figure 36A-K**). Mn rescued all isolates from superoxide growth inhibition, suggesting that Mn can serve as an antioxidant for superoxide in endocarditis-causing isolates of *S. aureus*. Next, the ability of Mn to modulate human neutrophil antimicrobial activity was interrogated. Mn protected *S. aureus* from killing by human neutrophils *ex vivo* (**Figure 35E**). Taken together, these results suggest that dietary Mn serves as an antioxidant in the heart, protecting *S. aureus* from ROS-dependent killing by neutrophils. Therefore, modulation of a single dietary element can effectively inactivate one of the most potent activities of the vertebrate innate immune system.

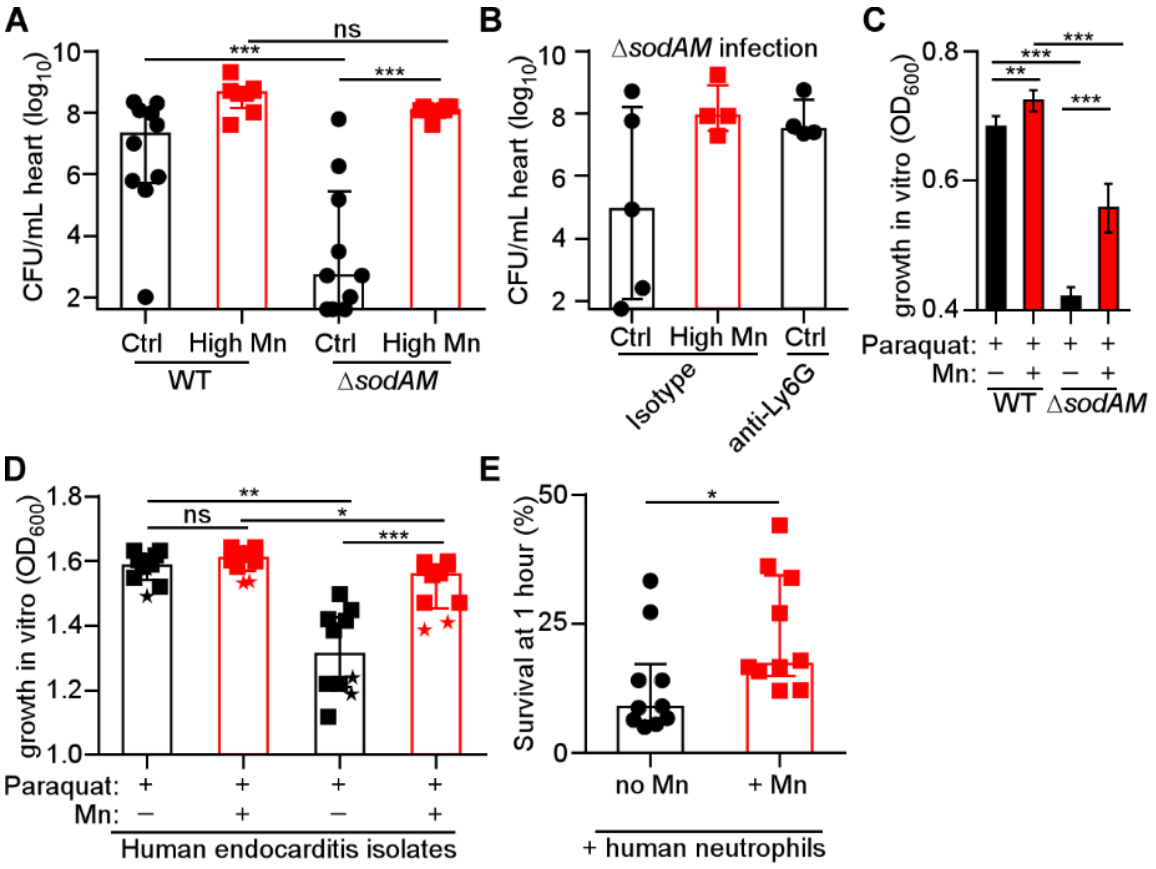

Figure 35. Excess dietary Mn protects against reactive oxygen species *in vivo*. C57BL/6 mice (WT) were fed high Mn or control diet and infected with *S. aureus* or isogenic derivatives for four days. (**A**) Heart bacterial burdens recovered following infection with WT or Δ*sodAM*. $N = 10$ (control diet groups), 8 (high Mn diet groups). (**B**) Heart bacterial burdens recovered from mice treated with anti-Ly6G antibody or isotype control and infected with Δ*sodAM*. $N = 5$ (control diet, isotype group) or 4 (other groups). (**C**) Growth of *S. aureus* WT or Δ*sodAM* in 1 mM paraquat and 1 mM $MnCl_2$. OD_{600} was measured at 8 hours. Data are combined from three independent experiments. (**D**) Growth of 10 clinical endocarditis isolates in paraquat and 1 mM $MnCl_2$. Inhibitory concentrations of paraquat were used and were either 5 mM (square symbols) or 1 mM (star symbols). Each symbol represents an independent bacterial isolate. OD_{600} was measured at 21 hours. (**E**) Bacterial survival (% initial inoculum) after 1 hour incubation of *S. aureus* WT with human neutrophils +/- 1 mM $MnCl_2$. $N = 10$ donors. **(A-B, D-E)** Bars depict median and interquartile range. (**C**) Bars depict mean and SEM. *$P < 0.05$. ** $P < 0.01$. *** $P < 0.001$ by ANOVA with Tukey's multiple comparisons (**A-C**), repeated measures ANOVA with Tukey's multiple comparisons test (**D**), or Mann-Whitney test (**E**).

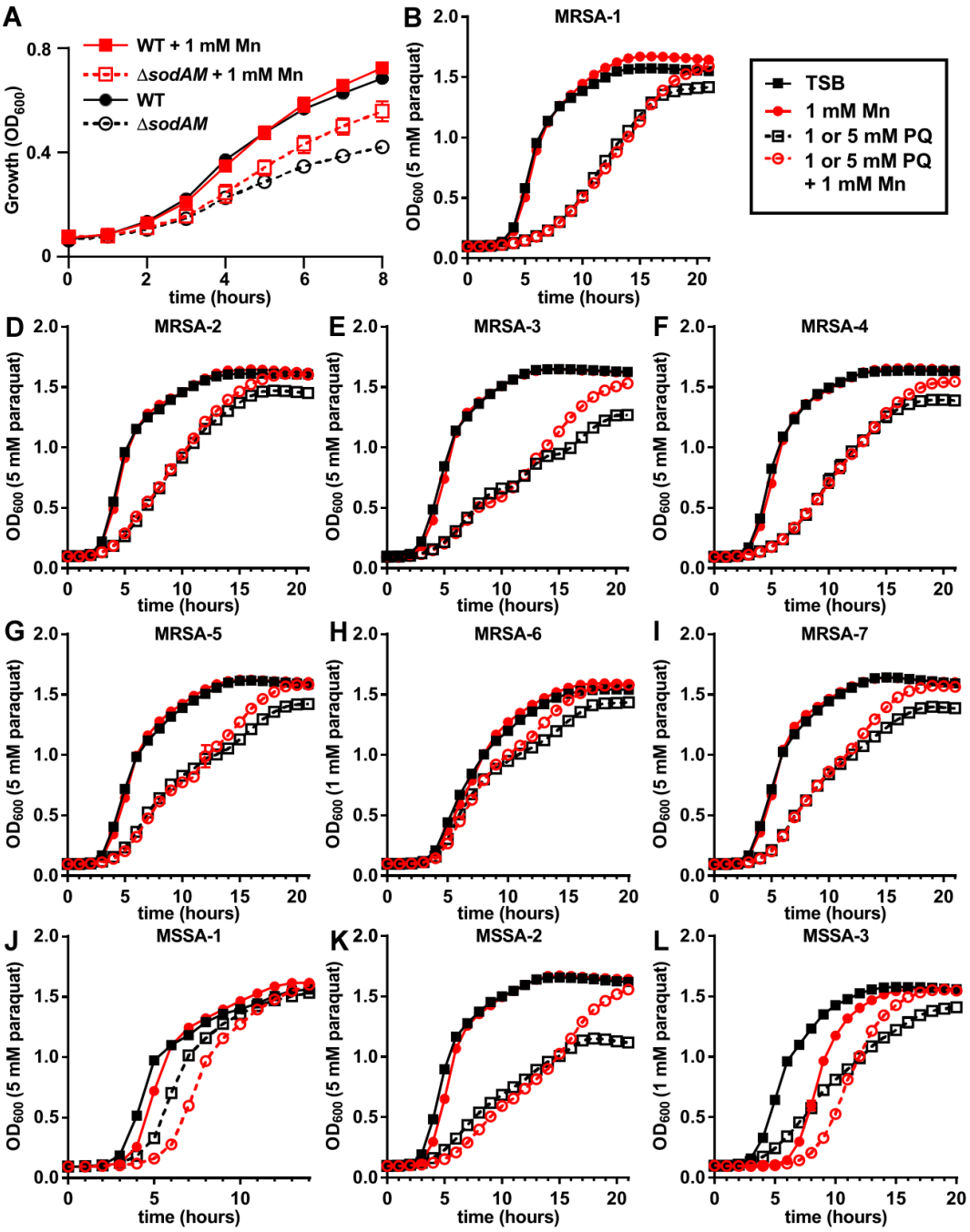

Figure 36. Growth curves in paraquat. (**A**) Growth of *S. aureus* WT or Δ*sodAM* in 1 mM paraquat with or without the addition of 1 mM $MnCl_2$. Growth was measured by OD_{600} over time. Data are combined from three independent experiments and depict the mean and S.E.M. (**B-K**). Growth of individual *S. aureus* clinical isolates as measured by OD_{600}. Strains were grown in TSB with or without paraquat or 1 mM $MnCl_2$ addition. Paraquat concentrations were either 1 mM (**G, K**) or 5 mM (**B-F, H-J**). Symbols represent the mean and error is shown as standard deviation. A single representative experiment of three is shown.

Discussion

I report here that excess dietary Mn enhances *S. aureus* infection of the heart. Altering Mn concentrations in the diet results in significant changes in Mn homeostasis within infected tissue, both in regards to Mn architecture and total Mn concentration. Moreover, *S. aureus* inactivated for the high-affinity Mn transporters MntH and MntABC are rescued by feeding mice a high Mn diet, indicating that excess dietary Mn is bioavailable to *S. aureus*. Treatment with excess Mn *in vitro* protects *S. aureus* from superoxide stress and neutrophil killing, suggesting that improved Mn bioavailability during infection may protect against ROS-mediated killing. Indeed, *S. aureus* inactivated for superoxide dismutase exhibits a virulence defect in the heart that can be fully complemented by excess dietary Mn. We further report that host calprotectin deficiency does not alter Mn bioavailability or increase fitness of *S. aureus* in the heart, even in the setting of dietary Mn manipulation. Compared with previous results demonstrating that calprotectin sequesters Mn in the liver during *S. aureus* infection (Corbin et al., 2008; Kehl-Fie et al., 2011; Kehl-Fie et al., 2013; Radin et al., 2016), our findings suggest that dietary Mn alters *S. aureus* infection in an organ-specific manner. In sum, these results indicate that excess dietary Mn is bioavailable to *S. aureus* in the heart and is utilized by *S. aureus* to escape neutrophil killing.

I propose that calprotectin-mediated Mn sequestration is tissue restricted, and that the limited ability of calprotectin to sequester Mn in the heart contributes to the heart-specific impact of dietary Mn. Calprotectin has a well-studied role in antimicrobial metal chelation *in vitro* (Kelliher and Kehl-Fie, 2016), and calprotectin decreases Mn levels in staphylococcal liver lesions and inhibits *S. aureus* growth in this organ (Corbin et al.,

2008). In contrast, I report here that calprotectin supports *S. aureus* infection of the heart. In *S. aureus* infection of the heart, I found no evidence that calprotectin participates in metal sequestration or alterations of Mn homeostasis. In line with the hypothesis that calprotectin-dependent Mn sequestration is tissue-specific, a recent report demonstrates that loss of calprotectin does not have a major impact on Mn bioavailability to *Salmonella* during gastrointestinal infection (Diaz-Ochoa et al., 2016). These striking findings raise the possibility that additional mechanisms exist to regulate the metal-sequestering properties of antimicrobial proteins in a tissue- or context- dependent fashion.

I propose that baseline differences in Mn concentrations contribute to the phenotypic differences observed between the heart and the liver. In our murine model, Mn concentrations are higher in liver homogenates than heart homogenates, and similar results have been reported for human tissue (Rahil-Khazen et al., 2002). Moreover, *S. aureus* Δ*mntH/C*, which is impaired for growth when Mn is limited, is more highly attenuated in the heart (~6 logs) than in the liver (~one-half log) (Kehl-Fie et al., 2013). These results suggest that the liver has more available Mn than the heart. Interestingly, high Mn diet did not alter bacterial burdens in the liver, despite the liver exhibiting an increase in Mn from ~150 ng/g to ~600 ng/g. High Mn diet did increase bacterial burdens in the heart, which increased Mn levels from ~60 ng/g for control diet to ~160 ng/g for high Mn diet. These results suggest that Mn has a threshold impact on bacterial growth, with concentrations in homogenates around 100 ng/g sufficient for full virulence. Consistent with this hypothesis, feeding mice a low Mn diet decreased Mn levels in the liver to ~80 ng/g and also resulted in a decrease in bacterial burden.

I found that *S. aureus* can counteract ROS and neutrophil killing through a Mn-dependent mechanism. Mn has been reported to serve as an antioxidant through several mechanisms, including serving as a cofactor for Sod enzymes, substituting for Fe in mononuclear enzymes to protect from hydrogen peroxide stress, and by scavenging superoxide via small molecular weight complexes (Lisher and Giedroc, 2013). The finding that *S. aureus* Δ*sodAM* is rescued by Mn in culture suggests that low molecular weight complexes of Mn and phosphate and/or carbonate are contributing significantly to superoxide detoxification (Barnese et al., 2012). Importantly, Δ*sodAM* rescue by high Mn diet in the heart provides evidence that these low molecular weight Mn complexes can serve as an antioxidant during infection. This provides significant relevance for future studies into the production of Mn low molecular weight complexes and their importance during infection.

This work provides proof-of-principle that dietary Mn in excess can alter the virulence of pathogens by protecting these invading organisms from the host immune response. However, the clinical relevance of this finding remains to be assessed. *S. aureus* is the leading cause of bacterial endocarditis (Fowler et al., 2005; Klein and Wang, 2016; Slipczuk et al., 2013) and the second leading cause of bloodstream infections worldwide (Anderson et al., 2014; Laupland, 2013; Laupland and Church, 2014). Notably, there are some shared risk factors for the development of these infections and increased Mn levels. A significant risk factor for *S. aureus* endocarditis is intravenous drug use (Tong et al., 2015), even comparing amongst a cohort of individuals with *S. aureus* bacteremia (Le Moing et al., 2015). A Mn-containing intravenous drug can elevate tissue Mn levels, and heroin is sometimes cut with Mn (Sikk et al., 2013; Sikk et al., 2011; Infante et al., 1999).

In addition, intravenous catheters are a significant risk factor for *S. aureus* bacteremia and endocarditis (Tong et al., 2015); serum levels of Mn are 2-4 times higher in people on long-term intravenous diets (Btaiche et al., 2011). Finally, chronic liver disease is a risk factor for *S. aureus* endocarditis, and impaired Mn excretion caused by liver disease can drastically elevate Mn levels (Hauser et al., 1994; Hung et al., 2013; Reimund et al., 2000; Seminari et al., 2016). Potential links between Mn levels and infection susceptibility or severity warrant further study in clinical trials. Limiting Mn exposure, such as by avoiding nutritional supplements that contain high amounts of Mn, may be an avenue to decrease risk of *S. aureus* infection.

References

Achouiti, A., Vogl, T., Endeman, H., Mortensen, B.L., Laterre, P.F., Wittebole, X., van Zoelen, M.A., Zhang, Y., Hoogerwerf, J.J., Florquin, S.*, et al.* (2014). Myeloid-related protein-8/14 facilitates bacterial growth during pneumococcal pneumonia. Thorax *69*, 1034-1042.

Achouiti, A., Vogl, T., Urban, C.F., Rohm, M., Hommes, T.J., van Zoelen, M.A., Florquin, S., Roth, J., van 't Veer, C., de Vos, A.F.*, et al.* (2012). Myeloid-related protein-14 contributes to protective immunity in gram-negative pneumonia derived sepsis. PLOS Pathog. *8*, e1002987.

Anderson, D.J., Moehring, R.W., Sloane, R., Schmader, K.E., Weber, D.J., Fowler, V.G., Jr., Smathers, E., and Sexton, D.J. (2014). Bloodstream infections in community hospitals in the 21st century: a multicenter cohort study. PLOS one *9*, e91713.

Berends, E.T., Dekkers, J.F., Nijland, R., Kuipers, A., Soppe, J.A., van Strijp, J.A., and Rooijakkers, S.H. (2013). Distinct localization of the complement C5b-9 complex on Gram-positive bacteria. Cell. Microbiol. *15*, 1955-1968.

Btaiche, I.F., Carver, P.L., and Welch, K.B. (2011). Dosing and monitoring of trace elements in long-term home parenteral nutrition patients. J. Parenter. Enteral. Nutr. *35*, 736-747.

Cerasi, M., Ammendola, S., and Battistoni, A. (2013). Competition for zinc binding in the host-pathogen interaction. Front. Cell. Infect. Microbiol. *3*, 108.

Clements, M.O., Watson, S.P., and Foster, S.J. (1999). Characterization of the major superoxide dismutase of *Staphylococcus aureus* and its role in starvation survival, stress resistance, and pathogenicity. J. Bacteriol. *181*, 3898-3903.

Corbin, B.D., Seeley, E.H., Raab, A., Feldmann, J., Miller, M.R., Torres, V.J., Anderson, K.L., Dattilo, B.M., Dunman, P.M., Gerads, R.*, et al.* (2008). Metal chelation and inhibition of bacterial growth in tissue abscesses. Science *319*, 962-965.

Damo, S.M., Kehl-Fie, T.E., Sugitani, N., Holt, M.E., Rathi, S., Murphy, W.J., Zhang, Y., Betz, C., Hench, L., Fritz, G.*, et al.* (2013). Molecular basis for manganese sequestration by calprotectin and roles in the innate immune response to invading bacterial pathogens. Proc. Natl. Acad. Sci. U.S.A. *110*, 3841-3846.

Deguine, J., and Barton, G.M. (2014). MyD88: a central player in innate immune signaling. F1000Prime Rep. *6*, 97.

Dhople, A.M., Ibanez, M.A., and Poirier, T.C. (1996). Role of iron in the pathogenesis of *Mycobacterium avium* infection in mice. Microbios *87*, 77-87.

Diaz-Ochoa, V.E., Jellbauer, S., Klaus, S., and Raffatellu, M. (2014). Transition metal ions at the crossroads of mucosal immunity and microbial pathogenesis. Front. Cell. Infect. Microbiol. *4*, 2.

Diaz-Ochoa, V.E., Lam, D., Lee, C.S., Klaus, S., Behnsen, J., Liu, J.Z., Chim, N., Nuccio, S.P., Rathi, S.G., Mastroianni, J.R.*, et al.* (2016). *Salmonella* mitigates oxidative stress and thrives in the inflamed gut by evading calprotectin-mediated manganese sequestration. Cell Host Microbe *19*, 814-825.

Fowler, R.A., and Gupta, S. (2005). Subacute and acute infective endocarditis. Lancet *366*, 1964.

Fowler, V.G., Jr., Miro, J.M., Hoen, B., Cabell, C.H., Abrutyn, E., Rubinstein, E., Corey, G.R., Spelman, D., Bradley, S.F., Barsic, B.*, et al.* (2005). *Staphylococcus aureus* endocarditis: a consequence of medical progress. JAMA *293*, 3012-3021.

Frosch, M., Metze, D., Foell, D., Vogl, T., Sorg, C., Sunderkotter, C., and Roth, J. (2005). Early activation of cutaneous vessels and epithelial cells is characteristic of acute systemic onset juvenile idiopathic arthritis. Exp. Dermatol. *14*, 259-265.

Gaddy, J.A., Radin, J.N., Loh, J.T., Piazuelo, M.B., Kehl-Fie, T.E., Delgado, A.G., Ilca, F.T., Peek, R.M., Cover, T.L., Chazin, W.J.*, et al.* (2014). The host protein calprotectin modulates the *Helicobacter pylori cag* type IV secretion system via zinc sequestration. PLOS Pathog. *10*, e1004450.

Garcia, Y.M., Barwinska-Sendra, A., Tarrant, E., Skaar, E.P., Waldron, K.J., and Kehl-Fie, T.E. (2017). A superoxide dismutase capable of functioning with iron or manganese promotes the resistance of *Staphylococcus aureus* to calprotectin and nutritional immunity. PLOS Pathog. *13*, e1006125.

Gomes, M.S., and Appelberg, R. (1998). Evidence for a link between iron metabolism and Nramp1 gene function in innate resistance against *Mycobacterium avium*. Immunology *95*, 165-168.

Greger, J.L. (1998). Dietary standards for manganese: overlap between nutritional and toxicological studies. J. Nutr. *128*, 368S-371S.

Hauser, R.A., Zesiewicz, T.A., Rosemurgy, A.S., Martinez, C., and Olanow, C.W. (1994). Manganese intoxication and chronic liver failure. Ann. Neurol. *36*, 871-875.

Hood, M.I., Mortensen, B.L., Moore, J.L., Zhang, Y., Kehl-Fie, T.E., Sugitani, N., Chazin, W.J., Caprioli, R.M., and Skaar, E.P. (2012). Identification of an *Acinetobacter baumannii* zinc acquisition system that facilitates resistance to calprotectin-mediated zinc sequestration. PLOS Pathog. *8*, e1003068.

Hood, M.I., and Skaar, E.P. (2012). Nutritional immunity: transition metals at the pathogen-host interface. Nat. Rev. Microbiol. *10*, 525-537.

Horsburgh, M.J., Wharton, S.J., Cox, A.G., Ingham, E., Peacock, S., and Foster, S.J. (2002a). MntR modulates expression of the PerR regulon and superoxide resistance in *Staphylococcus aureus* through control of manganese uptake. Mol. Microbiol. *44*, 1269-1286.

Horsburgh, M.J., Wharton, S.J., Karavolos, M., and Foster, S.J. (2002b). Manganese: elemental defence for a life with oxygen. Trends Microbiol. *10*, 496-501.

Hung, T.H., Hsieh, Y.H., Tseng, K.C., Tsai, C.C., and Tsai, C.C. (2013). The risk for bacterial endocarditis in cirrhotic patients: a population-based 3-year follow-up study. Int. J. Infect. Dis. *17*, e391-393.

Infante, F., Dominguez, E., Trujillo, D. and Luna, A. (1999). Metal contamination in illicit samples of heroin. J. Forensic Sci. *44*, 110-113

Jean, S., Juneau, R.A., Criss, A.K., and Cornelissen, C.N. (2016). *Neisseria gonorrhoeae* evades calprotectin-mediated nutritional immunity and survives neutrophil extracellular traps by production of TdfH. Infect. Immun. *84*, 2982-2994.

Jonker, F.A., and Boele van Hensbroek, M. (2014). Anaemia, iron deficiency and susceptibility to infections. J. Infect. *69 Suppl 1*, S23-27.

Juttukonda, L.J., Chazin, W.J., and Skaar, E.P. (2016). *Acinetobacter baumannii* coordinates urea metabolism with metal import to resist host-mediated metal limitation. mBio *7*.

Juttukonda, L.J., and Skaar, E.P. (2015). Manganese homeostasis and utilization in pathogenic bacteria. Mol. Microbiol. *97*, 216-228.

Katona, P., and Katona-Apte, J. (2008). The interaction between nutrition and infection. Clin. Infect. Dis. *46*, 1582-1588.

Kehl-Fie, T.E., Chitayat, S., Hood, M.I., Damo, S., Restrepo, N., Garcia, C., Munro, K.A., Chazin, W.J., and Skaar, E.P. (2011). Nutrient metal sequestration by calprotectin inhibits bacterial superoxide defense, enhancing neutrophil killing of *Staphylococcus aureus*. Cell Host Microbe *10*, 158-164.

Kehl-Fie, T.E., Zhang, Y., Moore, J.L., Farrand, A.J., Hood, M.I., Rathi, S., Chazin, W.J., Caprioli, R.M., and Skaar, E.P. (2013). MntABC and MntH contribute to systemic *Staphylococcus aureus* infection by competing with calprotectin for nutrient manganese. Infect. Immun. *81*, 3395-3405.

Kelliher, J.L., and Kehl-Fie, T.E. (2016). Competition for manganese at the host-pathogen interface. Prog. Mol. Biol. Transl. Sci. *142*, 1-25.

Klein, E., Smith, D.L., and Laxminarayan, R. (2007). Hospitalizations and deaths caused by methicillin-resistant *Staphylococcus aureus*, United States, 1999-2005. Emerging Infect. Dis. *13*, 1840-1846.

Klein, M., and Wang, A. (2016). Infective Endocarditis. J. Intensive Care Med. *31*, 151-163.

Lagasse, E., and Clerc, R.G. (1988). Cloning and expression of two human genes encoding calcium-binding proteins that are regulated during myeloid differentiation. Mol. Cell. Bio. *8*, 2402-2410.

Laupland, K.B. (2013). Defining the epidemiology of bloodstream infections: the 'gold standard' of population-based assessment. Epidemiol. Infect. *141*, 2149-2157.

Laupland, K.B., and Church, D.L. (2014). Population-based epidemiology and microbiology of community-onset bloodstream infections. Clin. Microbiol. Rev. *27*, 647-664.

Le Moing, V., Alla, F., Doco-Lecompte, T., Delahaye, F., Piroth, L., Chirouze, C., Tattevin, P., Lavigne, J.P., Erpelding, M.L., Hoen, B*., et al.* (2015). *Staphylococcus aureus* bloodstream infection and endocarditis--a prospective cohort study. PLOS One *10*, e0127385.

Lisher, J.P., and Giedroc, D.P. (2013). Manganese acquisition and homeostasis at the host-pathogen interface. Front. Cell. Infect. Microbiol. *3*, 91.

Magurran, A.E., and Henderson, P.A. (2010). Temporal turnover and the maintenance of diversity in ecological assemblages. Philos. Trans. R. Soc. Lond. B. Biol. Sci. *365*, 3611-3620.

Martin, A.P. (2002). Phylogenetic approaches for describing and comparing the diversity of microbial communities. Appl. Environ. Microbiol. *68*, 3673-3682.

Nakashige, T.G., Zhang, B., Krebs, C., and Nolan, E.M. (2015). Human calprotectin is an iron-sequestering host-defense protein. Nat. Chem. Biol. *11*, 765-771.

Odink, K., Cerletti, N., Bruggen, J., Clerc, R.G., Tarcsay, L., Zwadlo, G., Gerhards, G., Schlegel, R., and Sorg, C. (1987). Two calcium-binding proteins in infiltrate macrophages of rheumatoid arthritis. Nature *330*, 80-82.

Palmer, L.D., and Skaar, E.P. (2016). Transition metals and virulence in bacteria. Ann. Rev. Genet. *50,* 67-91.

Pietrocola, G., Arciola, C.R., Rindi, S., Di Poto, A., Missineo, A., Montanaro, L., and Speziale, P. (2011). Toll-like receptors (TLRs) in innate immune defense against *Staphylococcus aureus*. Int. J. Artif. Organs *34*, 799-810.

Radin, J.N., Kelliher, J.L., Parraga Solorzano, P.K., and Kehl-Fie, T.E. (2016). The two-component system ArlRS and alterations in metabolism enable *Staphylococcus aureus* to resist calprotectin-induced manganese starvation. PLOS Pathog. *12*, e1006040.

Rahil-Khazen, R., Bolann, B.J., Myking, A., and Ulvik, R.J. (2002). Multi-element analysis of trace element levels in human autopsy tissues by using inductively coupled atomic emission spectrometry technique (ICP-AES). J. Trace Elem. Med. Biol. *16*, 15-25.

Reeves, P.G., Nielsen, F.H., and Fahey, G.C., Jr. (1993). AIN-93 purified diets for laboratory rodents: final report of the American Institute of Nutrition ad hoc writing committee on the reformulation of the AIN-76A rodent diet. J. Nutr. *123*, 1939-1951.

Reimund, J.M., Dietemann, J.L., Warter, J.M., Baumann, R., and Duclos, B. (2000). Factors associated to hypermanganesemia in patients receiving home parenteral nutrition. Clin. Nutr. *19*, 343-348.

Reyes-Robles, T., Lubkin, A., Alonzo, F., 3rd, Lacy, D.B., and Torres, V.J. (2016). Exploiting dominant-negative toxins to combat Staphylococcus aureus pathogenesis. EMBO Rep. *17*, 780.

Rigby, K.M., and DeLeo, F.R. (2012). Neutrophils in innate host defense against *Staphylococcus aureus* infections. Semin. Immunopathol. *34*, 237-259.

Schloss, P.D., Westcott, S.L., Ryabin, T., Hall, J.R., Hartmann, M., Hollister, E.B., Lesniewski, R.A., Oakley, B.B., Parks, D.H., Robinson, C.J.*, et al.* (2009). Introducing mothur: open-source, platform-independent, community-supported software for describing and comparing microbial communities. Appl. Environ. Microbiol. *75*, 7537-7541.

Seminari, E., De Silvestri, A., Ravasio, V., Ludovisi, S., Utili, R., Petrosillo, N., Castelli, F., Bassetti, M., Barbaro, F., Grossi, P.*, et al.* (2016). Infective endocarditis in patients with hepatic diseases. Eur. J. Clin. Microbiol. Infect. Dis. *35*, 279-284.

Sikk, K., Haldre, S., Aquilonius, S.M., Asser, A., Paris, M., Roose, A., Petterson, J., Eriksson, S.L., Bergquist, J., and Taba, P. (2013). Manganese-induced parkinsonism in methcathinone abusers: bio-markers of exposure and follow-up. Eur. J. Neurol. *20*, 915-920.

Sikk, K., Haldre, S., Aquilonius, S.M., and Taba, P. (2011). Manganese-induced parkinsonism due to ephedrone abuse. Parkinsons Dis. *2011*, 865319.

Slipczuk, L., Codolosa, J.N., Davila, C.D., Romero-Corral, A., Yun, J., Pressman, G.S., and Figueredo, V.M. (2013). Infective endocarditis epidemiology over five decades: a systematic review. PLOS One *8*, e82665.

Spraggins, J.M., Rizzo, D.G., Moore, J.L., Rose, K.L., Hammer, N.D., Skaar, E.P., and Caprioli, R.M. (2015). MALDI FTICR IMS of Intact Proteins: Using Mass Accuracy to Link Protein Images with Proteomics Data. Journal Am. Soc. Mass Spec. *26*, 974-985.

Stork, M., Grijpstra, J., Bos, M.P., Manas Torres, C., Devos, N., Poolman, J.T., Chazin, W.J., and Tommassen, J. (2013). Zinc piracy as a mechanism of *Neisseria meningitidis* for evasion of nutritional immunity. PLOS Pathog. *9*, e1003733.

Takeuchi, O., Hoshino, K., and Akira, S. (2000). Cutting edge: TLR2-deficient and MyD88-deficient mice are highly susceptible to *Staphylococcus aureus* infection. J. Immunol. *165*, 5392-5396.

Theriot, C.M., Koumpouras, C.C., Carlson, P.E., Bergin, II, Aronoff, D.M., and Young, V.B. (2011). Cefoperazone-treated mice as an experimental platform to assess differential virulence of *Clostridium difficile* strains. Gut Microbes *2*, 326-334.

Tong, S.Y., Davis, J.S., Eichenberger, E., Holland, T.L., and Fowler, V.G., Jr. (2015). *Staphylococcus aureus* infections: epidemiology, pathophysiology, clinical manifestations, and management. Clin. Microbiol. Rev. *28*, 603-661.

Valderas, M.W., and Hart, M.E. (2001). Identification and characterization of a second superoxide dismutase gene (*sodM*) from *Staphylococcus aureus*. J. Bacteriol. *183*, 3399-3407.

Wang, Q., Garrity, G.M., Tiedje, J.M., and Cole, J.R. (2007). Naive Bayesian classifier for rapid assignment of rRNA sequences into the new bacterial taxonomy. Appl. Environ. Microbiol. *73*, 5261-5267.

Weinberg, E.D. (1975). Nutritional immunity. Host's attempt to withold iron from microbial invaders. JAMA *231*, 39-41.

Weinberg, E.D. (2009). Iron availability and infection. Biochim. et Biophysica Acta. *1790*, 600-605.

Weiss, G., and Carver, P.L. (2017). Role of divalent metals in infectious disease susceptibility and outcome. Clin. Microbiol. Infect. In Press, 10.1016/j.cmi. Available online January 18, 2017.

Yang, J., and Caprioli, R.M. (2011). Matrix sublimation/recrystallization for imaging proteins by mass spectrometry at high spatial resolution. Anal. Chem. *83*, 5728-5734.

Yue, J.C., and Clayton, M.K. (2005). A similarity measure based on species proportions. Commun. Stat-Theor. M. *34*, 2123-2131.

Zackular, J.P., Moore, J.L., Jordan, A.T., Juttukonda, L.J., Noto, M.J., Nicholson, M.R., Crews, J.D., Semler, M.W., Zhang, Y., Ware, L.B.*, et al.* (2016). Dietary zinc alters the microbiota and decreases resistance to *Clostridium difficile* infection. Nat. Med. *22*, 1330-1334.

Zenz, R., Eferl, R., Kenner, L., Florin, L., Hummerich, L., Mehic, D., Scheuch, H., Angel, P., Tschachler, E., and Wagner, E.F. (2005). Psoriasis-like skin disease and arthritis caused by inducible epidermal deletion of Jun proteins. Nature *437*, 369-375.

Zwadlo, G., Bruggen, J., Gerhards, G., Schlegel, R., and Sorg, C. (1988). Two calcium-binding proteins associated with specific stages of myeloid cell differentiation are expressed by subsets of macrophages in inflammatory tissues. Clin. Exp. Immunol. *72*, 510-515.

CHAPTER V

S100A9 DRIVES EXCESSIVE NEUTROPHIL RECRUITMENT TO PROMOTE *STAPHYLOCOCCUS AUREUS* INFECTION OF THE HEART

Introduction

S. aureus is an important human pathogen and a significant cause of morbidity and mortality in the United States and worldwide (Tong et al., 2015). Studies investigating the immune response to *S. aureus* infections in mouse models previously revealed that the S100 protein is recruited to staphylococcal liver abscesses, where metal chelation by calprotectin is antimicrobial to *S. aureus* (Corbin et al., 2008). In Chapter IV, I reported the surprising finding that calprotectin does not sequester Mn in the heart in response to *S. aureus* infection. Moreover, calprotectin promoted *S. aureus* heart infection in this model. This is not entirely surprising, as calprotectin is known to both promote and inhibit bacterial control in murine models of infection. The role of calprotectin has been predominantly studied in constitutive *S100a9* knockout mice (*S100a9*$^{-/-}$), as S100A8 does not form a stable homodimer and *S100a9*$^{-/-}$ mice have no detectable S100A8 protein (Hobbs et al., 2003). Specifically, calprotectin has been found to be protective in *K. pneumoniae* pneumonia-derived sepsis, *A. fumigatus* corneal infection, *A. baumannii* intranasal infection, and subcutaneous *C. albicans* infection (Achouiti et al., 2012; Clark et al., 2016; Hood et al., 2012; Urban et al., 2009). On the other hand, calprotectin is detrimental in mouse models of *S.* Typhimurium infection, *S. pneumoniae* pneumonia, *H. pylori* gastric infection, and pneumococcal meningitis (Achouiti et al., 2014; Gaddy et al., 2014; Liu et al., 2012). Therefore, calprotectin has pleiotropic roles in infection control.

In this Chapter, I consider the possibility that calprotectin is promoting *S. aureus* infection by modulating inflammation. Recognized as a clinical biomarker of inflammatory pathologies, calprotectin appears to both be present at sites of inflammation and have proinflammatory properties (Foell et al., 2004; van Zoelen et al., 2009; Viemann et al., 2005). In the context of bacterial infection, calprotectin has been shown to enhance inflammation and cytokine production in response to *S. aureus* intraperitoneal infection, and *E. coli* intraabdominal sepsis (Cho et al., 2015; Vogl et al., 2007). The proinflammatory cytokine production results in mortality from *S. aureus* and *E. coli* intraperitoneal infection (Cho et al., 2015; Vogl et al., 2007). Calprotectin also promotes inflammation in murine tuberculosis without altering bacterial burdens (Gopal et al., 2013). Calprotectin upregulation of cytokines has been attributed to its role as a ligand for the receptor for advanced glycation end products (RAGE) and toll-like receptor 4 (TLR-4) (Bjork et al., 2009; Boyd et al., 2008; Fassl et al., 2015; Ghavami et al., 2008; Narumi et al., 2015; Vogl et al., 2007; Volz et al., 2012; Yonekawa et al., 2011).

Calprotectin and S100A9 have also been shown to induce neutrophil chemotaxis. Extracellular calprotectin has been reported to serve as a chemokine, altering expression or affinity of L-selectin and Mac-1 (receptor consisting of CD11b/integrin α_M and CD18/integrin β_2) and inducing neutrophil chemotaxis in air pouch models (Anceriz et al., 2007; Ryckman et al., 2003a; Ryckman et al., 2003b; Vandal et al., 2003). Supporting this role for extracellular calprotectin, upregulation of CD11b in response to IL-8 stimulation was diminished in neutrophils from *S100a9*$^{-/-}$ mice (Manitz et al., 2003). Additional studies demonstrate that upregulation of CD11b is dependent on TLR4 (Pruenster et al., 2015). Finally, anti-S100A8 or anti-S100A9 antibody blockade decreased neutrophil migration to

the lungs of mice infected with *S. pneumoniae* (Raquil et al., 2008). Taken together, these studies define a role for extracellular calprotectin in neutrophil chemotaxis mediated via TLR-4 stimulation and upregulation of CD11b. In addition to this effect, there is also a report that *S100a9*$^{-/-}$ neutrophils also contain significantly less polymerized tubulin and reduced transendothelial migration (Vogl et al., 2004).

In this Chapter we report that *S100a9*$^{-/-}$ mice are protected from *S. aureus* infection of the heart and have decreased inflammation and neutrophils in the heart four days post infection. Investigations into the mechanism of protection revealed that *Tlr-4*$^{-/-}$ and *Ager*$^{-/-}$ mice were not protected from infection and inflammatory cytokines were not changed in *S100a9*$^{-/-}$ mice, suggesting that previously characterized proinflammatory mechanisms for extracellular calprotectin are not involved in promoting heart infection. Instead, we identify *S100a9* as a cell-intrinsic factor promoting neutrophil accumulation and detrimental heart inflammation from *S. aureus* infection.

Materials and Methods

Ethics Statement

All animal experiments were reviewed and approved by the Institutional Animal Care and Use Committee of Vanderbilt University and performed according to NIH guidelines, the Animal Welfare Act, and US Federal law.

Animals

C57BL/6, CD45.1 (Ly5.1)-congenic, *Tlr-4*$^{-/-}$, and *Myd88*$^{-/-}$ (all on a C57BL/6 background) were purchased from The Jackson Laboratory. *S100a9*$^{-/-}$ and *Ager*$^{-/-}$ (on a C57BL/6

background) were maintained in our animal colony. Studies were all performed in female mice.

Model of *S. aureus* infection

Experiments utilized the *S. aureus* strain Newman. Two days prior to infection, *S. aureus* was streaked to isolated colonies onto tryptic soy agar plates from the -80°C freezer stock. Overnight cultures were grown for 15 hours in a roller drum at 37°C in 5 mL tryptic soy broth (TSB) in 15 mL conical tubes. Infection cultures were prepared by diluting overnight cultures 1:100 into 5 mL TSB in 15 mL conical tubes, which were grown 3 hours in a roller drum at 37°C. Cultures were pelleted at 5,000 x *g* for 10 minutes, resuspended in 10 mL ice-cold, sterile phosphate buffered saline (PBS, Corning, Corning, NY), pelleted a second time, and resuspended in PBS to an optical absorbance at 600 nm of 0.4 or 0.8. An inoculum of 2 x 10^7 colony forming units (CFU) was utilized for all experiments, except for infection of mice following bone marrow transplant or neutrophil depletion, for which the inoculum was 1 x 10^7 CFU. Mice were inoculated by intravenous injection of the retroorbital sinus with *S. aureus* cultures or PBS as mock-infection control. Mice were 12-14 weeks old at the time of infection. WT mice and knockout mice were always age-matched in individual experiments, and data were combined from multiple experiments, each containing 3-5 mice per group per experiment. Mice were monitored for four days prior to humane euthanasia by inhalation of CO_2. Livers and hearts were removed for gross inspection and downstream analyses. To determine bacterial load, organs were homogenized in sterile PBS and serial dilutions were spot-plated onto TSA. For cytokine analysis, organs were flash-frozen in liquid nitrogen and stored at -80°C. For histopathological analysis, organs were fixed in 10% formalin, paraffin-embedded and

sectioned by the Vanderbilt Translational Pathology Shared Resource. Preparation of single cell suspensions for flow cytometry is described below.

Dietary Manipulation

Diets were synthesized by Dyets Inc. using the AIN-93M standardized diet (Reeves et al., 1993). The control diet included 10 mg/kg Mn, whereas the high Mn diet included 500 mg/kg Mn and the low Mn diet included 0 mg/kg Mn. Six-week old female mice were placed on custom-synthesized diets for 6-8 weeks prior to infection and throughout infection. Mice in Figure 1 and Figure 7 were maintained on standard laboratory chow. Mice in Figure 2 and Figure 3A were maintained on high Mn diet. Mice in Figure 3B, Figure 4, Figure 5, and Figure 8 were maintained on control diet.

Hematopoietic stem cell transplants

Recipient mice were lethally irradiated via Cesium-137 exposure (11 Grays, split dose) and adoptively transferred with 10 million donor cells. The bone marrow was reconstituted for at least seven weeks following transplant and chimerism was found to be >95% donor cells. For mixed donor transplants, a one-to-one ratio of donors was confirmed by flow cytometry analysis of CD45.1 and CD45.2.

Neutrophil depletion experiments

Mice were intraperitoneally injected with 250 μg anti-Ly6G monoclonal antibody, clone 1A8, or isotype control antibody, clone 2A3 (BioLegend, San Diego CA). Antibodies were diluted in sterile PBS (Corning, Corning NY) and administered 24 hours prior to infection and daily throughout infection.

Cytokine Analysis

Infected whole hearts were harvested 24 hours post infection, immediately frozen on dry ice, and stored at -80°C prior to analysis. Hearts were spiked with protease inhibitor cocktail (Sigma, St. Louis MO), thawed, and placed in Navy Bullet Blender tubes (Next Advance, Averill Park NY) in 200 μL PBS (Sigma). Hearts were homogenized at 4°C using setting 8 for 4 min and setting 10 for 2 min in the Bullet Blender (Next Advance, Averill Park NY). Beads and cells were pelleted at 4000 g for 10 minutes at 4°C for 10 min and supernatants were collected. Protein concentrations in the supernatants was quantified by BCA assay kit (Thermo Fisher Scientific, Waltham, MA) and normalized to 10 mg/mL. Cytokines were assayed in supernatants using MILLIPLEX MAP Mouse Cytokine/Chemokine Magnetic Bead Panel (Millipore, Darmstadt, Germany; catalog number: MCYTOMAG-70K) according to the manufacturer's instructions. Samples were run on the Luminex Flexmap 3D platform (Luminex, Austin TX).

Flow cytometry

Freshly harvested hearts were dissected in DMEM (Corning, Corning NY) containing 10% FBS (Atlanta Biologicals, Flowery Branch GA) and dissected in 10 mg/mL collagenase Type II (Worthington, Lakewood NJ), 2.5 mM $CaCl_2$, 2.4 U/mL dispase II (Sigma, St. Louis MO) for 7 minutes at 37°C. Digested tissue was passed through a 100 μM cell strainer, red blood cells were lysed, and the cell suspension was treated with Fc block (BD Pharmingen, Franklin Lakes NJ). Cells were strained with combinations of the following fluorophore conjugated antibodies: CD45.2 brilliant violet 421 (Biolegend, San Diego CA), CD45.1 brilliant violet 510 (Biolegend, San Diego CA), CD11c PE (BD Pharmingen, Franklin Lakes NJ), Ly6G FITC (BD Pharmingen, Franklin Lakes NJ), F4/80 APC (Invitrogen, Waltham MA), and CD11b PE-Cy7 (Biolegend, San Diego CA). Live/dead

was detected using propidium iodide or LIVE/DEAD Fixable Violet Dead Cell Stain Kit (ThermoFisher, Waltham MA). Flow cytometry was conducted on an LSR II (BD, Franklin Lakes NJ).

Statistical Analysis

Statistical significance between two groups was examined by the Mann-Whitney test, which does not require normally distributed data. Statistical significance between multiple groups was examined by the one-way analysis of variance (ANOVA) with Dunnett's or Tukey's multiple comparisons test. Statistical work was performed using Prism 6 software (GraphPad) and a *P* value of less than 0.05 was considered significant.

Results

Calprotectin-deficient mice exhibit enhanced protection against *S. aureus* growth within the heart

Calprotectin is a metal-chelating protein that inhibits the growth of *S. aureus* in liquid culture conditions, but the role of calprotectin in defense against *S. aureus* mouse infection was recently reported to be dependent upon the organ that was assessed. In this study, heart bacterial burdens following systemic *S. aureus* infection were decreased in *S100a9*$^{-/-}$ mice, which do not express S100A8 or S100A9 at the protein level (Hobbs et al., 2003). However, this study was carried out in the context of dietary manipulation, which may narrow the generalizability of the conclusions. Thus, we first sought to determine whether *S100a9*$^{-/-}$ knockout mice have lower heart bacterial burdens in the setting of normal laboratory mouse chow. Indeed, mice lacking calprotectin expression are protected

from *S. aureus* infection of the heart, while they maintain higher bacterial burdens in the liver (**Figure 37A**&**B**).

A timecourse of *S. aureus* heart infection was carried out to identify at what stage during infection protection of *S100a9*$^{-/-}$ mice occurs. Bacterial burdens recovered from hearts of WT and *S100a9*$^{-/-}$ mice were similar at 2 and 6 hours post infection, indicating that initial seeding and colonization of the heart is similar for both mouse genotypes (**Figure 38**). At 24 hours post infection, bacterial burdens trend towards being lower in *S100a9*$^{-/-}$ mice, and the difference in CFU is statistically different at 96 hours post infection (**Figure 38**). These results suggest that either *S100a9*$^{-/-}$ mice clear *S. aureus* more efficiently than WT mice or *S. aureus* growth is restricted with *S100a9*$^{-/-}$ mice. Results presented in the previous Chapter demonstrate that *S100a9*$^{-/-}$ mice do not have dramatically altered Mn bioavailability in the heart, suggesting that a mechanism other than metal sequestration is responsible for the protection of *S100a9*$^{-/-}$ mice in the heart.

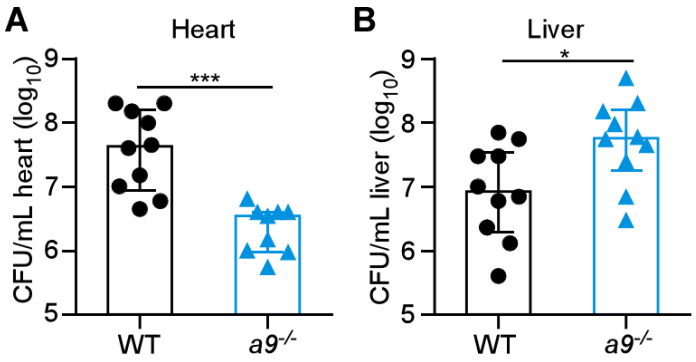

Figure 37. *S100a9*$^{-/-}$ mice are protected from *S. aureus* infection of the heart. Bacterial burdens were enumerated four days post intravenous *S. aureus* infection of 12 week old C57BL/6 (WT) or *S100a9*$^{-/-}$ (*a9*$^{-/-}$) female mice. (**A**) Bacterial burdens recovered from the heart. (**B**) Bacterial burdens recovered from the liver. $N = 10$. Statistical significance was determined by Mann-Whitney. *, $P < 0.05$; ***, $P < 0.001$.

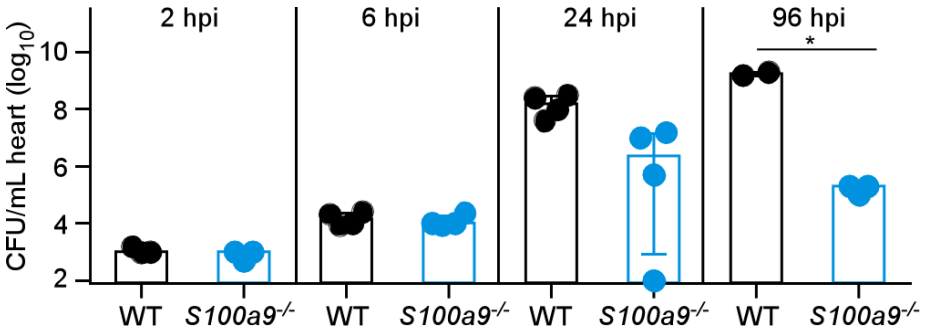

Figure 38. Protection of *S100a9*$^{-/-}$ mice occurs after initial colonization of the heart. A timecourse of heart infection was carried out following intravenous inoculation of *S. aureus*. Mice were female C57BL6 (WT) or *S100a9*$^{-/-}$ mice aged 12 weeks at the time of infection. Bacterial burdens were enumerated 2, 6, 24, and 96 hours post infection. Statistical significance was determined by Mann-Whitney comparing genotypes at each timepoint. *, $P < 0.05$.

Neutrophilic inflammation is decreased in *S. aureus*-infected hearts of *S100a9*$^{-/-}$ mice

Gross inspection of infected hearts during necropsy uncovered that hearts from *S100a9*$^{-/-}$ mice had fewer *S. aureus* abscesses compared to WT controls (**Figure 39A**). This finding prompted us to consider the possibility that *S100a9* is modulating inflammation in the heart. Histopathological analysis of infected hearts revealed that *S100a9*$^{-/-}$ mice exhibit decreased overall inflammation and a poorly formed abscess notable for diminished necrosis, immune cell infiltrate, and the absence of a visible staphylococcal microcolony (**Figure 39B**). To determine which immune cells were decreased in abundance, flow cytometry was performed on heart tissue four days post infection and innate immune cells were quantified. Compared to WT controls, hearts from *S100a9*$^{-/-}$ mice had fewer neutrophils in response to *S. aureus* infection (**Figure 39C**). Macrophage percentages were also different between *S100a9*$^{-/-}$ and WT mice, but only when mice were fed a high Mn diet. This is most likely an artifact of quantifying based on percentage of live cells rather than total cells, as the increase in macrophage percentages in *S100a9*$^{-/-}$ mice corresponds to the decrease in neutrophils. From these results, we conclude that *S100a9*$^{-/-}$ exhibit decreased neutrophilic inflammation.

Mice lacking calprotectin receptors are not protected from infection

Previous studies have identified TLR-4 as a receptor that is engaged by calprotectin (Vogl et al., 2007). We hypothesized that calprotectin stimulation of TLR-4 may be promoting *S. aureus* infection of the heart. To test this hypothesis, *Tlr-4*$^{-/-}$ mice in a C57BL/6 background or C57BL/6 controls were infected with *S. aureus* and bacterial burdens were enumerated four days post infection. There were no significant differences in heart bacterial burdens

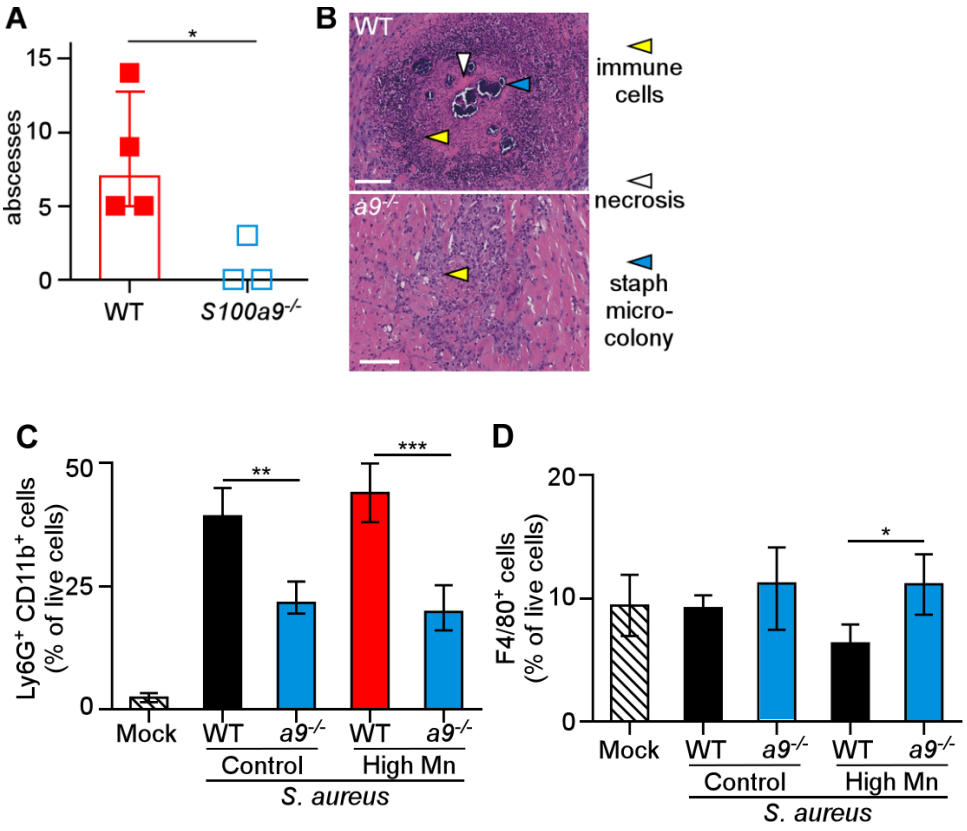

Figure 39. *S100a9*$^{-/-}$ mice exhibit diminished heart neutrophilic inflammation. Twelve week old C57BL/6 (WT) mice and *S100a9*$^{-/-}$ mice (*a9*$^{-/-}$) were intravenously infected with *S. aureus.* Hearts were harvested four days post infection. (**A**) Number of externally visible abscesses. (**B**) Histopathology of infected hearts. Scale bar indicates 100 μM. **(C-D)** Flow cytometry quantification of (**C**) Ly6G^{+}CD11b^{+} cells and (**D**) F4/80^{+} cells. Previous gate, live cells. (**C-D**) $N = 4$ (high Mn groups), 3 (control groups), 2 (mock). Significance was determined by Mann-Whitney. *, $P < 0.05$; **, $P < 0.01$; ***, $P < 0.001$.

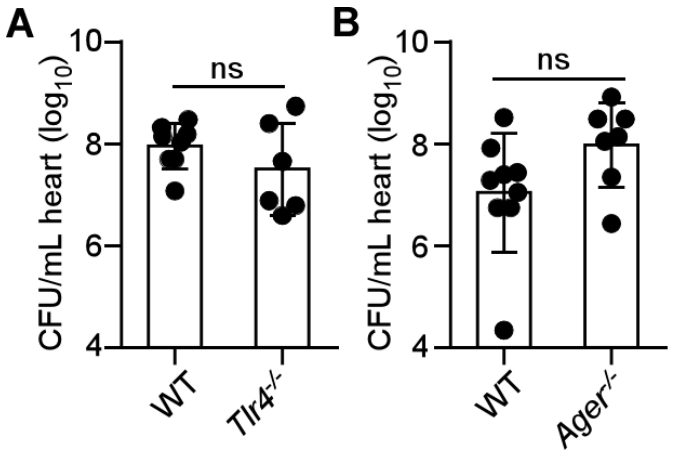

Figure 40. *Tlr4*$^{-/-}$ and *Ager*$^{-/-}$ mice are not protected from *S. aureus* infection of the heart. Heart bacterial burdens from C57BL/6 (WT) mice and *Tlr4*$^{-/-}$ (**A**) or *Ager*$^{-/-}$ (**B**) were enumerated four days post intravenous *S. aureus* infection of 12 week old mice. Differences in bacterial burdens were not significantly different by Mann-Whitney.

between WT and *Tlr-4*$^{-/-}$ mice (**Figure 40A**). S100 family proteins have also been shown to serve as ligands for the Receptor for Advanced Glycation End Products (RAGE), and RAGE has been shown to be expressed in cardiomyosites (Boyd et al., 2008), suggesting that calprotectin may be promoting infection through activation of this receptor. However, *Ager*$^{-/-}$ mice did not have lower heart bacterial burdens following *S. aureus* infection (**Figure 40B**). These experiments demonstrate that loss of signaling through the calprotectin receptors TLR-4 or RAGE do not protect mice from staphylococcal heart infection, suggesting that another mechanism is responsible for the protection of *S100a9*$^{-/-}$ mice.

Inflammatory and chemotactic cytokines are not significantly altered in *S100a9*$^{-/-}$ mice

In a recent study utilizing a *S. aureus* intraperitoneal model, researchers found that *S100a9*$^{-/-}$ mice were protected from infection via the decreased elaboration of the proinflammatory cytokines TNFα and IL-6 (Cho et al., 2015). To assess whether proinflammatory cytokines are different between WT and *S100a9*$^{-/-}$ mice in the heart, WT and *S100a9*$^{-/-}$ mice were infected intravenously with *S. aureus* and hearts were harvested for cytokine analysis 24 hours post infection. This timepoint was chosen because it was the first time point in which bacterial burdens exhibited differences in the timecourse experiment. In this model, local concentrations of the pro-inflammatory cytokines IL-1β, TNFα, and IL-6 were not statistically significantly different between WT and *S100a9*$^{-/-}$ mice, although there was a trend towards increased proinflammatory cytokines in the *S100a9*$^{-/-}$ mice. Therefore, it is unlikely that *S100a9*$^{-/-}$ mice are protected from *S. aureus* heart infection because of a decrease in proinflammatory cytokines.

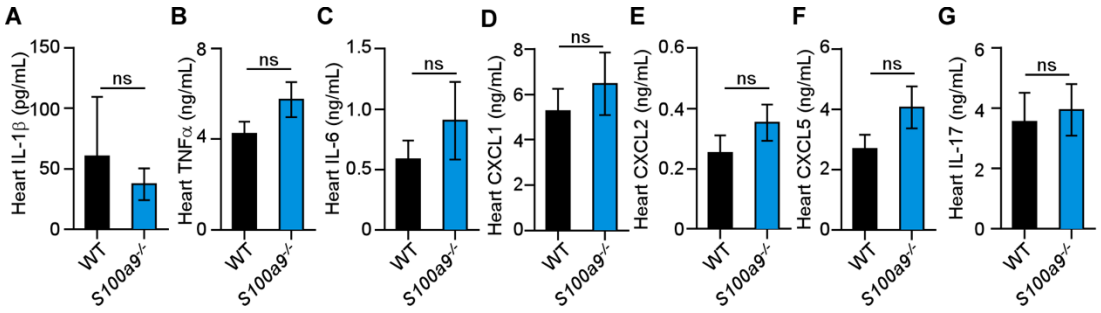

Figure 41. Pro-inflammatory cytokines and neutrophil chemokines are not differentially abundant in *S100a9*$^{-/-}$ mice 24 hours post infection. (**A-G**) WT and *S100a9*$^{-/-}$ mice were infected with *S. aureus,* hearts were harvested 24 hours post-infection, and the indicates cytokines and chemokines were measured in supernatants of heart homogenates. $N = 9$ (*S100a9*$^{-/-}$), 10 (WT) Bars depict mean and SEM. ns = not significant by Mann-Whitney.

S100a9$^{-/-}$ mice have decreased neutrophils in the heart 4 days post infection (**Figure 39C**). Decreased recruitment could be the result of diminished elaboration of neutrophil chemokines. To investigate this possibility, neutrophil chemokines were also measured in the heart tissue harvested 24 hours post infection. There were no significant differences in CXCL1, CXCL2, CXCL5, or IL-17 protein abundance in the heart. These results suggest that early neutrophil chemokines are not responsible for the differences in neutrophil abundance in infected hearts noted in *S100a9*$^{-/-}$ mice.

Neutrophils from *S100a9*$^{-/-}$ mice have an intrinsic deficit in accumulation within *S. aureus*

As calprotectin is produced by hematopoietic and non-hematopoietic cells (Zenz et al., 2005), we interrogated the source of calprotectin that promotes neutrophil accumulation via flow cytometry analysis of neutrophils following reciprocal bone marrow transplants (BMTs) (**Figure 42**, **Figure 43A**). Upon *S100a9*$^{-/-}$ BMT into WT mice, low numbers of neutrophils were present in infected hearts (**Figure 43B**). Conversely, WT BMT into *S100a9*$^{-/-}$ mice resulted in high numbers of neutrophils in infected hearts (**Figure 43B**). These findings indicate that hematopoietic production of calprotectin is the predominant driver of neutrophil accumulation in the heart.

Calprotectin is released from neutrophils and other cells as part of the inflammatory response. We reasoned that if extracellular calprotectin leads to neutrophil accumulation in the heart, WT expression of calprotectin should be sufficient to complement the recruitment of *S100a9*$^{-/-}$ neutrophils to *S. aureus*-infected hearts. To test this, WT mice were transplanted with a 1:1 mixed BMT. Contrary to the hypothesis, nearly twice as many WT neutrophils were present in infected hearts as *S100a9*$^{-/-}$ neutrophils (**Figure 43C**).

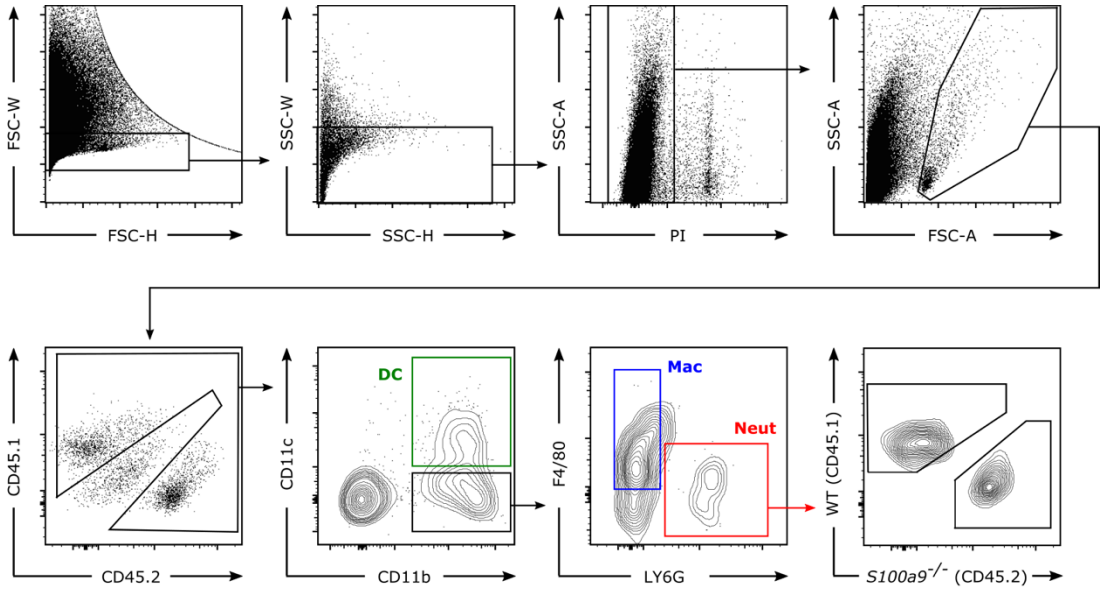

Figure 42. Flow cytometry gating strategy. Gating strategy for distinguishing desired immune cells in heart homogenates. FSC = forward scatter; SSC = side scatter; PI = propidium iodide (live/dead marker). Lineages were distinguished as follows: CD45 for myeloid lineage cells, CD11b and CD11c for dendritic cells (DC), CD11b and F4/80 for macrophages (Mac), and CD11b Ly6G for neutrophils (neut). When appropriate, bone marrow lineages were delineated by CD45.1 or CD45.2.

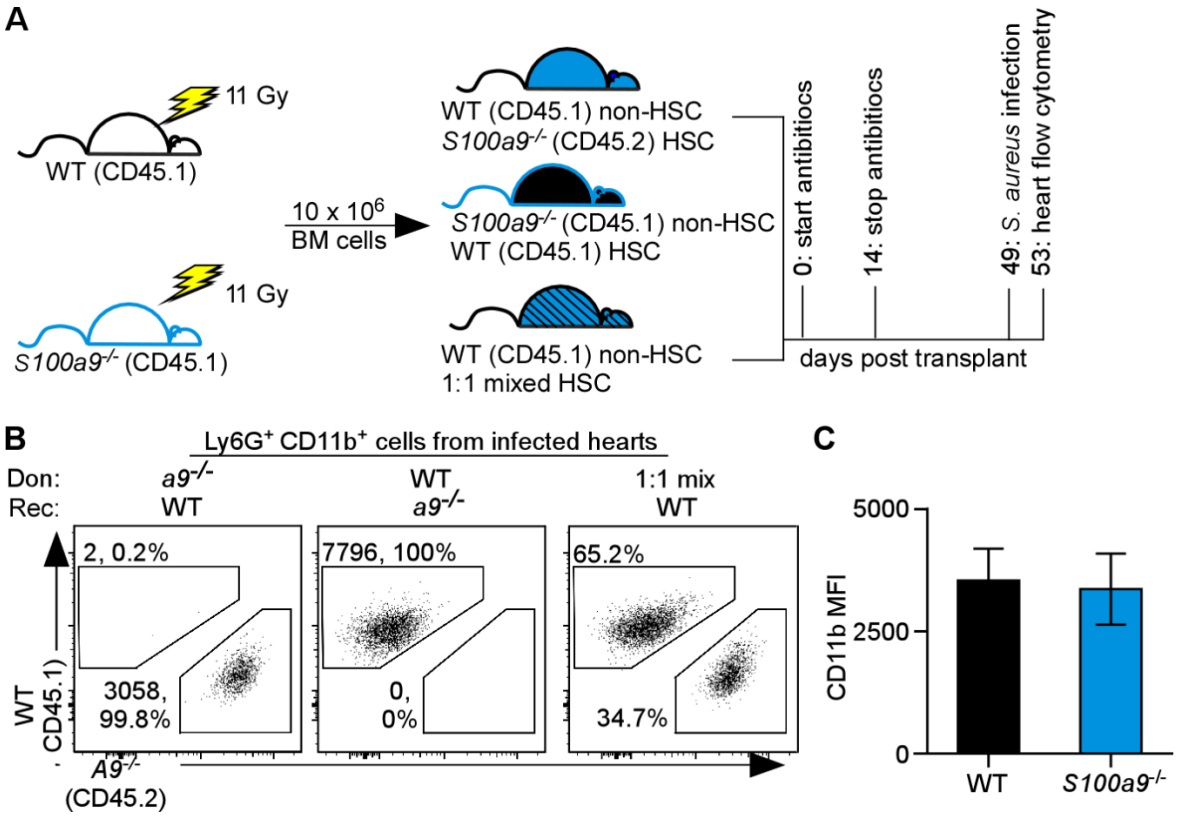

Figure 43. Neutrophils from *S100a9*$^{-/-}$ mice have a cell-intrinsic deficit in accumulation in response to *S. aureus* infection. (**A**) Design of bone marrow transplant experiments. (**B-C**) Mice were infected with *S. aureus* intravenously and hearts were harvested four days post infection. **(B)** Ly6G^{+}CD11b^{+} cells following reciprocal bone marrow transplantation (BMT) between WT congenic mice (CD45.1) and *S100a9*$^{-/-}$ mice (CD45.2) or mixed transplant. Previous gate, CD45^{+} cells. Data are representative of N = 3 (mix), N = 2 (*S100a9*$^{-/-}$ donor), N = 4 (WT donor) from a single experiment. This experiment was repeated twice. (**C**) Mean fluorescence intensity for CD11b on Ly6G^{+} WT and *S100a9*$^{-/-}$ cells. Columns indicate the mean and error bars are standard deviation.

Thus, the inability of calprotectin-deficient neutrophils to accumulate within *S. aureus*-infected hearts is cell-intrinsic, implicating either an impairment in bone marrow production of neutrophils or a cell-intrinsic deficit in neutrophil migration.

Finally, we assessed whether neutrophil expression of CD11b differed between WT and *S100a9*$^{-/-}$ mice. It has been reported that treatment of neutrophils *ex vivo* with recombinant calprotectin stimulates upregulation of CD11b, which is an integrin required for appropriate neutrophil adhesion and migration (Sanchez-Madrid et al., 1983). However, there was no difference in mean fluorescence intensity of CD11b staining between WT and *S100a9*$^{-/-}$ neutrophils, indicating that surface expression of the protein was the same for both genotypes (**Figure 43C**).

***S100a9*$^{-/-}$ neutrophils are necessary and *S100a9*$^{-/-}$ bone marrow sufficient for protection against *S. aureus* heart infection**

To assess whether hematopoietic cells are responsible for the difference in bacterial burdens in the heart, WT and *S100a9*$^{-/-}$ mice that received reciprocal hematopoietic stem-cell transplants were infected with *S. aureus* and bacterial burdens in the heart were assessed. Compared to transplant with *S100a9*$^{-/-}$ BM, *S100a9*$^{-/-}$ mice receiving WT BMT had significantly higher *S. aureus* burdens; reciprocally, burdens in WT mice receiving *S100a9*$^{-/-}$ BMT were decreased compared to WT BMT (**Figure 44A**). However, bacterial burdens in *S100a9*$^{-/-}$ mice receiving *S100a9*$^{-/-}$ BMT were lower than any other group, suggesting that calprotectin production by both hematopoietic and non-hematopoietic cells is sufficient to enhance *S. aureus* growth.

To determine if heart bacterial burden differences are neutrophil-dependent, we treated mice with an anti-Ly6G antibody to deplete neutrophils and found that differences

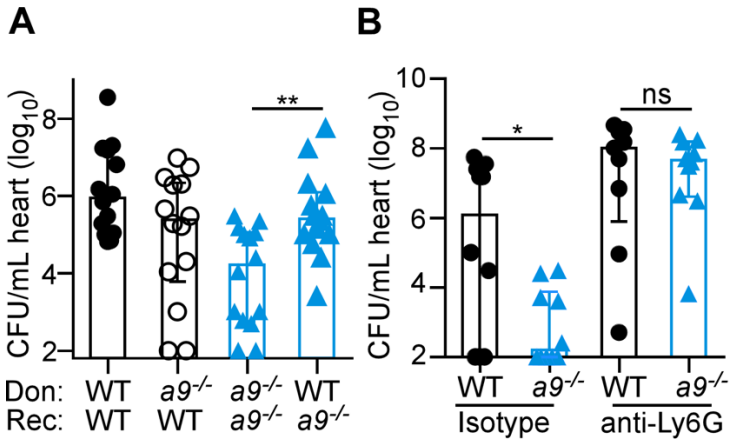

Figure 44. *S100a9*$^{-/-}$ neutrophils are necessary and *S100a9*$^{-/-}$ bone marrow sufficient for protection against *S. aureus* heart infection. Mice were infected with *S. aureus* intravenously, hearts were harvested four days post infection, and bacterial burdens were enumerated. Hearts were harvested four days post infection. **(A)** Heart bacterial burdens following reciprocal BMT between WT and *S100a9*$^{-/-}$ mice. $N = 14$. (**B**) Heart bacterial burdens from WT and *S100a9*$^{-/-}$ mice treated with anti-Ly6G or isotype control antibodies. $N = 9$ (WT depleted), 10 (all other groups). Bars depict median and interquartile range. *$P < 0.05$. ** $P < 0.01$ by Student's *t*-test.

in heart bacterial burdens between WT and *S100a9*$^{-/-}$ mice were completely eliminated when both WT and *S100a9*$^{-/-}$ mice were neutrophil deplete (**Figure 44B**). Thus, neutrophils are required to protect *S100a9*$^{-/-}$ mice from *S. aureus* infection of the heart. These findings suggest a model in which production of calprotectin leads to massive amplification of neutrophil recruitment to the heart, such that calprotectin-deficient mice have sufficient neutrophil recruitment to eradicate staphylococci, while the hearts of WT mice are overwhelmed with neutrophils, which in excess can promote staphylococcal infection (Gresham et al., 2000; Thwaites and Gant, 2011).

Discussion

Here we demonstrate that *S100a9*$^{-/-}$ mice are protected from *S. aureus* infection of the heart, exhibit decreased inflammatory pathology in the heart, and have fewer neutrophils present in the heart following *S. aureus* infection. Protection of *S100a9*$^{-/-}$ mice appears to be independent of TLR-4 and RAGE. Instead, *S100a9*$^{-/-}$ neutrophils have a cell-intrinsic defect in accumulation in the heart, and *S100a9*$^{-/-}$ bone marrow is sufficient to decrease bacterial burdens in WT mice. Finally, neutrophils are essential for protection of *S100a9*$^{-/-}$ mice. Taken together, we have demonstrated a cell-intrinsic role for calprotectin in regulation of neutrophils in response to infection and provided evidence that over-robust neutrophil recruitment can be detrimental in controlling *S. aureus* heart infection.

Previous studies assessing calprotectin function during bacterial infection have generally focused on either metal sequestration or immune modulation. Calprotectin has a well-studied role in antimicrobial metal chelation *in vitro* (Kelliher and Kehl-Fie, 2016). In the context of *S. aureus* infection of the liver, calprotectin decreases staphylococcal

lesion Mn levels and inhibits *S. aureus* growth (Corbin et al., 2008). In contrast, I report here and in Chapter V that calprotectin promotes *S. aureus* infection of the heart. Calprotectin is known to have a pro-bacterial role in other infections, including *Salmonella* infection of the gut and *Streptococcus pneumoniae* lung infection (Achouiti et al., 2014; Liu et al., 2012). However, in both of these cases calprotectin promoted bacterial growth via Zn sequestration. In Chapter V, I presented evidence that calprotectin does not function in nutritional immunity in the heart. In this Chapter, I investigated the cellular mechanism by which calprotectin promotes *S. aureus* infection in the heart.

The findings reported here demonstrate that calprotectin plays a central role in the inflammatory response to *S. aureus* infection of the heart. Calprotectin-deficient mice have previously been found to be protected from intraperitoneal bacterial infections because of decreased TNFα secretion (Cho et al., 2015; Vogl et al., 2007). Calprotectin has also been shown to influence inflammation in response to *S. pneumoniae* lung infection, although there are conflicting reports as to whether calprotectin enhances or dampens lung inflammation (Achouiti et al., 2014; De Filippo et al., 2014). We found that mice lacking calprotectin had decreased heart inflammation and neutrophil migration, consistent with calprotectin having a proinflammatory function in the response to *S. aureus* heart infection.

The findings in this Chapter suggest that calprotectin-mediated host defenses become a liability in the heart by promoting excessive accumulation of neutrophils. Calprotectin has been previously implicated in immune cell migration, but prior studies have predominantly been carried out in cultured cells and the same mechanisms do not appear to be important in our mouse model. Multiple studies have demonstrated that calprotectin stimulates cell migration *ex vivo* in a TLR-4 dependent mechanism (Pruenster

et al., 2015; Wang et al., 2015). However, deficiency in *Tlr-4* does not protect from *S. aureus* infection of the heart. Exposing neutrophils to calprotectin leads to upregulation of β_2-integrins, such as CD11b, which regulate neutrophil adhesion and migration (Newton and Hogg, 1998; Raquil et al., 2008; Ryckman et al., 2003b). This is not the explanation for migration differences to *S. aureus*-infected mice, as CD11b expression was the same between WT and calprotectin-deficient neutrophils. Thus, the cell-intrinsic deficit in *S100a9*$^{-/-}$ neutrophil migration is not due to previously studied mechanisms. The finding that heightened neutrophil accumulation in the heart does not improve host defense against *S. aureus*, and instead promotes bacterial proliferation in this organ, consistent with the fact that this crucial organ cannot tolerate excessive inflammation and remain functional (Corsten et al., 2012; Fontes et al., 2015; Frangogiannis, 2014; Mann, 2002).

We demonstrated that neutrophil recruitment is driven by hematopoietic-produced calprotectin. Switching bone-marrow between WT and calprotectin-deficient mice switched the neutrophil migration phenotypes as well as the bacterial burden phenotypes, which links the two phenotypes and implicates neutrophil migration as the major factor enhancing heart infection of WT mice. Indeed, neutrophils are required for the differences in heart bacterial burdens between WT mice and calprotectin-deficient mice. Moreover, we demonstrate that calprotectin-deficient neutrophils have an intrinsic deficit in migration or proliferation via mixed bone-marrow chimeras. Together, these findings demonstrate an important role for intracellular calprotectin in neutrophil trafficking during infection and define neutrophil behavior as important for controlling *S. aureus* infection of the heart.

Calprotectin may regulate neutrophil accumulation either by altering proliferation of neutrophils in response to infection, regulating neutrophil migration, or altering survival

of neutrophils in infected tissues. Understanding which of these phases of the neutrophil lifespan is altered by calprotectin will require follow-up work, and potential strategies for investigating this are discussed in Chapter IX.

Decreasing neutrophil accumulation may be a potential therapeutic target for staphylococcal abscesses, particularly for multi-drug resistant strains. Calprotectin is a promising target because loss of calprotectin did not completely abolish neutrophil migration, but did dampen neutrophilic inflammation. Our studies suggest that, while neutrophils are required to control bacterial replication, too many neutrophils may provide a niche for bacterial replication. Moreover, staphylococcal abscesses with dense neutrophilic inflammation can damage host tissue and generate zones of decreased antibiotic permeation. Our studies suggest that decreasing this neutrophilic abscess formation may help to control *S. aureus* infection in certain tissues.

References

Achouiti, A., Vogl, T., Endeman, H., Mortensen, B.L., Laterre, P.F., Wittebole, X., van Zoelen, M.A., Zhang, Y., Hoogerwerf, J.J., Florquin, S.*, et al.* (2014). Myeloid-related protein-8/14 facilitates bacterial growth during pneumococcal pneumonia. Thorax *69*, 1034-1042.

Achouiti, A., Vogl, T., Urban, C.F., Rohm, M., Hommes, T.J., van Zoelen, M.A., Florquin, S., Roth, J., van 't Veer, C., de Vos, A.F.*, et al.* (2012). Myeloid-related protein-14 contributes to protective immunity in gram-negative pneumonia derived sepsis. PLOS Pathog. *8*, e1002987.

Anceriz, N., Vandal, K., and Tessier, P.A. (2007). S100A9 mediates neutrophil adhesion to fibronectin through activation of beta2 integrins. Biochem. Biophys. Res. Commun. *354*, 84-89.

Bjork, P., Bjork, A., Vogl, T., Stenstrom, M., Liberg, D., Olsson, A., Roth, J., Ivars, F., and Leanderson, T. (2009). Identification of human S100A9 as a novel target for treatment of autoimmune disease via binding to quinoline-3-carboxamides. PLOS Biol. *7*, e97.

Boyd, J.H., Kan, B., Roberts, H., Wang, Y., and Walley, K.R. (2008). S100A8 and S100A9 mediate endotoxin-induced cardiomyocyte dysfunction via the receptor for advanced glycation end products. Circ. Res. *102*, 1239-1246.

Cho, H., Jeong, D.W., Liu, Q., Yeo, W.S., Vogl, T., Skaar, E.P., Chazin, W.J., and Bae, T. (2015). Calprotectin Increases the Activity of the SaeRS Two Component System and Murine Mortality during *Staphylococcus aureus* Infections. PLOS Pathog. *11*, e1005026.

Clark, H.L., Jhingran, A., Sun, Y., Vareechon, C., de Jesus Carrion, S., Skaar, E.P., Chazin, W.J., Calera, J.A., Hohl, T.M., and Pearlman, E. (2016). Zinc and manganese chelation by neutrophil S100A8/A9 (calprotectin) limits extracellular *Aspergillus fumigatus* hyphal growth and corneal infection. J. Immunol. *196*, 336-344.

Corbin, B.D., Seeley, E.H., Raab, A., Feldmann, J., Miller, M.R., Torres, V.J., Anderson, K.L., Dattilo, B.M., Dunman, P.M., Gerads, R.*, et al.* (2008). Metal chelation and inhibition of bacterial growth in tissue abscesses. Science *319*, 962-965.

Corsten, M.F., Schroen, B., and Heymans, S. (2012). Inflammation in viral myocarditis: friend or foe? Trends Mol. Med. *18*, 426-437.

De Filippo, K., Neill, D.R., Mathies, M., Bangert, M., McNeill, E., Kadioglu, A., and Hogg, N. (2014). A new protective role for S100A9 in regulation of neutrophil recruitment during invasive pneumococcal pneumonia. FASEB J. *28*, 3600-3608.

Fassl, S.K., Austermann, J., Papantonopoulou, O., Riemenschneider, M., Xue, J., Bertheloot, D., Freise, N., Spiekermann, C., Witten, A., Viemann, D.*, et al.* (2015). Transcriptome assessment reveals a dominant role for TLR4 in the activation of human monocytes by the alarmin MRP8. J. Immunol. *194*, 575-583.

Foell, D., Frosch, M., Sorg, C., and Roth, J. (2004). Phagocyte-specific calcium-binding S100 proteins as clinical laboratory markers of inflammation. Clin. Chim. Acta. *344*, 37-51.

Fontes, J.A., Rose, N.R., and Cihakova, D. (2015). The varying faces of IL-6: From cardiac protection to cardiac failure. Cytokine *74*, 62-68.

Frangogiannis, N.G. (2014). The inflammatory response in myocardial injury, repair, and remodelling. Nat. Rev. Cardiol. *11*, 255-265.

Gaddy, J.A., Radin, J.N., Loh, J.T., Piazuelo, M.B., Kehl-Fie, T.E., Delgado, A.G., Ilca, F.T., Peek, R.M., Cover, T.L., Chazin, W.J.*, et al.* (2014). The host protein calprotectin modulates the *Helicobacter pylori cag* type IV secretion system via zinc sequestration. PLOS Pathog. *10*, e1004450.

Ghavami, S., Rashedi, I., Dattilo, B.M., Eshraghi, M., Chazin, W.J., Hashemi, M., Wesselborg, S., Kerkhoff, C., and Los, M. (2008). S100A8/A9 at low concentration

promotes tumor cell growth via RAGE ligation and MAP kinase-dependent pathway. J. Leukoc. Biol. *83*, 1484-1492.

Gopal, R., Monin, L., Torres, D., Slight, S., Mehra, S., McKenna, K.C., Fallert Junecko, B.A., Reinhart, T.A., Kolls, J., Baez-Saldana, R.*, et al.* (2013). S100A8/A9 proteins mediate neutrophilic inflammation and lung pathology during tuberculosis. Am. J. Respir. Crit. Care Med. *188*, 1137-1146.

Gresham, H.D., Lowrance, J.H., Caver, T.E., Wilson, B.S., Cheung, A.L., and Lindberg, F.P. (2000). Survival of *Staphylococcus aureus* inside neutrophils contributes to infection. J. Immunol. *164*, 3713-3722.

Hobbs, J.A., May, R., Tanousis, K., McNeill, E., Mathies, M., Gebhardt, C., Henderson, R., Robinson, M.J., and Hogg, N. (2003). Myeloid cell function in MRP-14 (S100A9) null mice. Mol. Cell. Biol. *23*, 2564-2576.

Hood, M.I., Mortensen, B.L., Moore, J.L., Zhang, Y., Kehl-Fie, T.E., Sugitani, N., Chazin, W.J., Caprioli, R.M., and Skaar, E.P. (2012). Identification of an *Acinetobacter baumannii* zinc acquisition system that facilitates resistance to calprotectin-mediated zinc sequestration. PLOS Pathog. *8*, e1003068.

Kelliher, J.L., and Kehl-Fie, T.E. (2016). Competition for Manganese at the Host-Pathogen Interface. Prog. Mol. Biol. Transl. Sci. *142*, 1-25.

Liu, J.Z., Jellbauer, S., Poe, A.J., Ton, V., Pesciaroli, M., Kehl-Fie, T.E., Restrepo, N.A., Hosking, M.P., Edwards, R.A., Battistoni, A.*, et al.* (2012). Zinc sequestration by the neutrophil protein calprotectin enhances *Salmonella* growth in the inflamed gut. Cell host & microbe *11*, 227-239.

Manitz, M.P., Horst, B., Seeliger, S., Strey, A., Skryabin, B.V., Gunzer, M., Frings, W., Schonlau, F., Roth, J., Sorg, C.*, et al.* (2003). Loss of S100A9 (MRP14) results in reduced interleukin-8-induced CD11b surface expression, a polarized microfilament system, and diminished responsiveness to chemoattractants in vitro. Mol. Cell. Biol. *23*, 1034-1043.

Mann, D.L. (2002). Inflammatory mediators and the failing heart: past, present, and the foreseeable future. Circ. Res. *91*, 988-998.

Narumi, K., Miyakawa, R., Ueda, R., Hashimoto, H., Yamamoto, Y., Yoshida, T., and Aoki, K. (2015). Proinflammatory proteins S100A8/S100A9 activate NK cells via interaction with RAGE. J. Immunol. *194*, 5539-5548.

Newton, R.A., and Hogg, N. (1998). The human S100 protein MRP-14 is a novel activator of the beta 2 integrin Mac-1 on neutrophils. J. Immunol. *160*, 1427-1435.

Pruenster, M., Kurz, A.R., Chung, K.J., Cao-Ehlker, X., Bieber, S., Nussbaum, C.F., Bierschenk, S., Eggersmann, T.K., Rohwedder, I., Heinig, K.*, et al.* (2015).

Extracellular MRP8/14 is a regulator of beta2 integrin-dependent neutrophil slow rolling and adhesion. Nat. Commun. *6*, 6915.

Raquil, M.A., Anceriz, N., Rouleau, P., and Tessier, P.A. (2008). Blockade of antimicrobial proteins S100A8 and S100A9 inhibits phagocyte migration to the alveoli in streptococcal pneumonia. J. Immunol. *180*, 3366-3374.

Reeves, P.G., Nielsen, F.H., and Fahey, G.C., Jr. (1993). AIN-93 purified diets for laboratory rodents: final report of the American Institute of Nutrition ad hoc writing committee on the reformulation of the AIN-76A rodent diet. J. Nutr. *123*, 1939-1951.

Ryckman, C., McColl, S.R., Vandal, K., de Medicis, R., Lussier, A., Poubelle, P.E., and Tessier, P.A. (2003a). Role of S100A8 and S100A9 in neutrophil recruitment in response to monosodium urate monohydrate crystals in the air-pouch model of acute gouty arthritis. Arthritis Rheum. *48*, 2310-2320.

Ryckman, C., Vandal, K., Rouleau, P., Talbot, M., and Tessier, P.A. (2003b). Proinflammatory activities of S100: proteins S100A8, S100A9, and S100A8/A9 induce neutrophil chemotaxis and adhesion. J. Immunol. *170*, 3233-3242.

Sanchez-Madrid, F., Nagy, J.A., Robbins, E., Simon, P., and Springer, T.A. (1983). A human leukocyte differentiation antigen family with distinct alpha-subunits and a common beta-subunit: the lymphocyte function-associated antigen (LFA-1), the C3bi complement receptor (OKM1/Mac-1), and the p150,95 molecule. J. Exp. Med. *158*, 1785-1803.

Thwaites, G.E., and Gant, V. (2011). Are bloodstream leukocytes Trojan Horses for the metastasis of Staphylococcus aureus? Nature reviews. Microbiology *9*, 215-222.

Tong, S.Y., Davis, J.S., Eichenberger, E., Holland, T.L., and Fowler, V.G., Jr. (2015). *Staphylococcus aureus* infections: epidemiology, pathophysiology, clinical manifestations, and management. Clin. Microbiol. Rev. *28*, 603-661.

Urban, C.F., Ermert, D., Schmid, M., Abu-Abed, U., Goosmann, C., Nacken, W., Brinkmann, V., Jungblut, P.R., and Zychlinsky, A. (2009). Neutrophil extracellular traps contain calprotectin, a cytosolic protein complex involved in host defense against *Candida albicans*. PLOS Pathog. *5*, e1000639.

van Zoelen, M.A., Vogl, T., Foell, D., Van Veen, S.Q., van Till, J.W., Florquin, S., Tanck, M.W., Wittebole, X., Laterre, P.F., Boermeester, M.A.*, et al.* (2009). Expression and role of myeloid-related protein-14 in clinical and experimental sepsis. Am. J. Respir. Crit. Care Med. *180*, 1098-1106.

Vandal, K., Rouleau, P., Boivin, A., Ryckman, C., Talbot, M., and Tessier, P.A. (2003). Blockade of S100A8 and S100A9 suppresses neutrophil migration in response to lipopolysaccharide. J. Immunol. *171*, 2602-2609.

Viemann, D., Strey, A., Janning, A., Jurk, K., Klimmek, K., Vogl, T., Hirono, K., Ichida, F., Foell, D., Kehrel, B.*, et al.* (2005). Myeloid-related proteins 8 and 14 induce a specific inflammatory response in human microvascular endothelial cells. Blood *105*, 2955-2962.

Vogl, T., Ludwig, S., Goebeler, M., Strey, A., Thorey, I.S., Reichelt, R., Foell, D., Gerke, V., Manitz, M.P., Nacken, W.*, et al.* (2004). MRP8 and MRP14 control microtubule reorganization during transendothelial migration of phagocytes. Blood *104*, 4260-4268.

Vogl, T., Tenbrock, K., Ludwig, S., Leukert, N., Ehrhardt, C., van Zoelen, M.A., Nacken, W., Foell, D., van der Poll, T., Sorg, C.*, et al.* (2007). Mrp8 and Mrp14 are endogenous activators of Toll-like receptor 4, promoting lethal, endotoxin-induced shock. Nat. Med. *13*, 1042-1049.

Volz, H.C., Laohachewin, D., Seidel, C., Lasitschka, F., Keilbach, K., Wienbrandt, A.R., Andrassy, J., Bierhaus, A., Kaya, Z., Katus, H.A.*, et al.* (2012). S100A8/A9 aggravates post-ischemic heart failure through activation of RAGE-dependent NF-kappaB signaling. Basic Res. Cardiol. *107*, 250.

Wang, J., Vodovotz, Y., Fan, L., Li, Y., Liu, Z., Namas, R., Barclay, D., Zamora, R., Billiar, T.R., Wilson, M.A.*, et al.* (2015). Injury-induced MRP8/MRP14 stimulates IP-10/CXCL10 in monocytes/macrophages. FASEB J. *29*, 250-262.

Yonekawa, K., Neidhart, M., Altwegg, L.A., Wyss, C.A., Corti, R., Vogl, T., Grigorian, M., Gay, S., Luscher, T.F., and Maier, W. (2011). Myeloid related proteins activate Toll-like receptor 4 in human acute coronary syndromes. Atherosclerosis *218*, 486-492.

Zenz, R., Eferl, R., Kenner, L., Florin, L., Hummerich, L., Mehic, D., Scheuch, H., Angel, P., Tschachler, E., and Wagner, E.F. (2005). Psoriasis-like skin disease and arthritis caused by inducible epidermal deletion of Jun proteins. Nature *437*, 369-375.

CHAPTER VI

A SMALL MOLECULE MODULATOR OF METAL HOMEOSTASIS IS TOXIC TO *STAPHYLOCOCCUS AUREUS*

Introduction

S. aureus is a major threat to human health and one of the most common causes of bacterial infection in the United States (Tong et al., 2015). *S. aureus* is the leading source of skin and soft tissue infections, osteomyelitis, and endocarditis and an important agent of bacteremia, pneumonia, and toxin-mediated diseases (Tong et al., 2015). Clearly, having effective antibiotics to treat these infections is vital to prevent morbidity and mortality due to *S. aureus* infections. Alas, *S. aureus* infections in hospitals are now often caused by *S. aureus* resistant to the penicillin class of antibiotics, known as methicillin-resistant *S. aureus* or MRSA (Klevens et al., 2007). MRSA infections are difficult to treat, and surgical site wounds and central line associated bloodstream infections cost the United States more than $1.3 billion per year (Zimlichman and Levin-Scherz, 2013). As these are only two of the dozens of infections caused by *S. aureus*, these numbers only give a small picture of the cost to society. The last line therapy for antibiotic-resistant *S. aureus* is vancomycin, which must be delivered intravenously, requires monitoring to achieve appropriate therapeutic levels, and can cause renal failure (Mergenhagen and Borton, 2014). Moreover, vancomycin-resistant *S. aureus* exist, threatening the function of this last-line therapy (Limbago et al., 2014). New antibiotics or prevention strategies are desperately needed for *S. aureus* infection, leading the CDC to label methicillin-resistant *S. aureus* a 'serious threat' in 2013 (CDC, 2013).

Like all living things, *S. aureus* requires metals for survival. Amongst the most abundant and critical of metals are the divalent cations magnesium (Mg), iron (Fe), manganese (Mn), and zinc (Zn). Metals are used for multiple vital cellular processes. Metals serve as structural elements within macromolecules and as essential cofactors for enzymes. However, metals are also toxic when present in excess, although the level required to meet toxicity depends both on the metal and the organism exposed to the metal. Mechanisms of metal toxicity include competition by non-cognate metals for binding pockets or transport (Hohle and O'Brian, 2014) and generation of hydrogen peroxide through Fenton chemistry (Winterbourn, 1995). It follows logically that bacterial cells strictly maintain metal levels such that metals are available for required processes but never free to cause toxicity. Appropriate metal levels are maintained through a balance of import and efflux proteins as well as metal-sequestering molecules within the cell, and the abundance of metal homeostasis proteins is tightly controlled (Ma et al., 2009). In sum, maintaining optimal metal ratios within cells is essential for bacterial survival and thus represents an intriguing antimicrobial target.

Transition metals are also imperative during infection. Vertebrate hosts limit access to essential metals in a process termed 'nutritional immunity', and a parallel process exists for intoxicating invaders with highly reactive metals (Hood and Skaar, 2012). Therefore, maintaining appropriate metal ratios during infection is a particular challenge for bacteria during infection. Because of this, we predict that metal homeostasis is a weakness that could be exploited by targeted antimicrobial therapy during infection.

The rationale for this study is that altering metal homeostasis may inhibit bacterial growth and thus a potentially novel therapeutic target. However, small molecules that

dysregulate general metal homeostasis have not previously been pursued as potential therapeutics. Therefore, we sought to identify candidate molecules that could be further developed into viable antimicrobials.

In this Chapter I present the identification of small molecule VU0026921 (‘921) as a lead compound for the development of novel antibacterials that interfere with metal homeostasis. A small library of compounds previously identified as modulating Mn levels in neurons was screened for growth inhibition of *S. aureus* lacking Mn import machinery. Along with several potential Mn-chelating compounds, compound ‘921 was identified as a potent inhibitor of *S. aureus* growth. We report that ‘921 is bactericidal to logarithmic *S. aureus* in a manner modulated by extracellular metal concentrations. RNASequencing revealed that treatment with ‘921 upregulated multiple metal exporters, suggesting that ‘921 induces metal toxicity. Indeed, elemental mass spectrometry uncovered massive changes in cellular metal content following ‘921 exposure. In sum, this work reports the discovery of a small molecule that dysregulates metal homeostasis in *S. aureus,* causing substantial toxicity to this organism.

Materials and Methods

Bacterial strains and reagents. The strains used in this study are described in **Table 8**. *S. aureus* and *P. aeruginosa* were routinely grown in tryptic soy broth (TSB), *Micrococcus luteus* was grown in lysogeny broth (LB), and *A. baumannii, K. pneumoniae,* and *Bacillus anthracis* were grown in brain heart infusion broth (BHI). All cultures were grown aerobically at 37°C with 180 rpm shaking. Solid medium contained 1.5% agar. For all

assays, bacterial strains were streaked from -80°C stocks two days prior to the assay. Overnight cultures were grown for 12-15 hours in 5 mL medium in 15 mL conical tubes.

Compound acquisition and storage. The compounds in the 39 compound toolbox were purchased from Chemical Diversity (San Diego, CA) and stored as 10 mM stocks in DMSO at -80°C. Compound '921 was re-purchased three times and confirmed to exert similar similar activity in each batch. Additionally, the structural integrity of purchased '921 was confirmed by NMR. Finally, '921 and '921 analogs were resynthesized by the Vanderbilt Chemical Synthesis Core and used to confirm antimicrobial activity and Mn rescue.

Table 8: Bacterial strains used in Chapter VII.

Strain	Relevant characteristics	Reference or source
S. aureus strain Newman	Wild-type, methicillin-sensitive strain	(Duthie and Lorenz, 1952)
Δ*mntH/C*	In-frame Δ*mntH* and Δ*mntC* mutations in Newman strain background	(Kehl-Fie et al., 2013)
Acinetobacter baumannii	ATCC 17978	ATCC
Klebsiella pneumoniae	ATCC 700721	Maria Hadjifrangiskou
Pseudomonas aeruginosa	PA14	Andrea Battistoni
Bacillus anthracis	Sterne	(Sterne, 1946)
Micrococcus luteus	ATCC 4698	ATCC

Antimicrobial growth assays. All growth curves were carried out in the rich growth medium described for each strain above. For each growth curve, bacterial strains were streaked from -80°C stocks two days prior to the assay. Overnight cultures were grown for 12-15 hours in 5 mL medium in 15 mL conical tubes, and 1 μL of overnight culture was added to 100 μL of medium in a round-bottom 96-well plate (Corning, Corning NY). $MnCl_2$ was prepared as a 100 mM stock in deionized water, sterile filtered, and stored at room temperature. Individual components of the growth assay were added to the 96-well plate in the following order: growth medium, growth medium containing additional Mn, and growth medium containing compound. Immediately after adding compound, cultures were added and optical density absorbance at 600 nm (OD_{600}) at the zero time point was established. 96-well plates were grown at 37°C in a shaking incubator and removed periodically for OD_{600} measurements with a plate reader (BioTek, Winooski, VT). Alternatively, kinetic reads were carried out in the plate reader at 37°C with linear shaking.

Lag phase '921 killing assays. Overnight cultures of *S. aureus* strain Newman were diluted 1:100 into 96 well plates containing TSB, $MnCl_2$, and '921 at the indicated concentrations and grown at 37°C in a shaking incubator. At 0, 2, 4, 6, and 8 hours post inoculation, 5 μL of culture was removed, serially diluted in sterile phosphate buffered saline (PBS; Corning, Corning, NY), and spot plotted onto TSA. Colony forming units (CFU) were calculated by dilution factor per 1 mL of culture.

Exponential phase killing assays. Overnight cultures of *S. aureus* strain Newman were diluted 1:100 into 5 mL TSB in 15 ml conicals and incubated at 37°C in a shaking incubator until cultures reached OD_{600} of 0.4. Mid-exponential cultures were pelleted at 3220 x *g* for

10 minutes and pellets were resuspended in 2.5 mL TSB. TSB, 25 μL of resuspended culture, $MnCl_2$ and '921 were added to a final volume of 100 μL and final concentrations of 1 mM for $MnCl_2$ and 100 μM for '921. After incubation at 37°C for the indicated lengths of time, 5 μL of culture was removed, serially diluted in sterile PBS, and spot plated onto TSA for CFU enumeration.

Growth for RNASeq and RNA isolation. Overnight cultures of *S. aureus* strain Newman were diluted 1:100 into 5 mL TSB in 15 mL conical tubes and grown to mid-exponential phase (OD_{600} = 0.4). Cells were pelleted at 3220 x *g* for 10 minutes at room temperature, supernatants were discarded, and cells were resuspended in 2.5 mL TSB. To a 15 mL conical tube containing TSB and combinations of '921, vehicle control, or Mn was added 2 mL of resuspended bacterial cultures to a final volume of 8 mL and final concentration of 100 μM '921 and 1 mM $MnCl_2$. Following incubation at 37°C with 180 rpm shaking for 30 minutes, 10 μL aliquots were removed for CFU plating and cells were harvested by centrifugation at 6,000 x *g* for 10 minutes at 4°C. Pellets were resuspended in LETS buffer (0.1 M LiCl, 10 mM EDTA, 10 mM Tris HCl pH 7.4, 1% SDS), homogenized in a bead beater (Fastprep-24, MP Biomedical, Santa Ana, CA) with Lysing Matrix B beads (MP Biomedicals, MP Biomedical, Santa Ana, CA) at a speed of 6 m/s for 45 seconds, heated at 55 °C for 5 minutes, and centrifuged for 10 minutes at 15,000 rpm. The upper phase was collected, mixed with 1 mL TRI Reagent (Sigma, St. Louis, MO), and incubated for 5 minutes at room temperature. Chloroform (0.2 mL, Acros Organics, Waltham, MA) was added, samples were vigorously shaken for 15 seconds, and samples were incubated at room temperature for 2 minutes. Following centrifugation at 4 °C for 15 minutes, 600 μL of the upper aqueous phase was collected and RNA was precipitated with 1 mL isopropanol

(Sigma, St. Louis, MO). RNA was washed with 70% ethanol (Sigma, St. Louis, MO) and resuspended in 100 μL DNase-Free, RNase-Free water (ThermoFisher, Waltham, MA). DNA contamination was removed by treatment with 8 μL RQ1 enzyme (Promega, Madison, WI), 12 μL 10X RQ1 buffer, and 2 μL Ribolock RNase inhibitor (ThermoFisher, Waltham, MA) for 2 hours at 37 °C. DNase was removed and samples further purified by the RNEasy kit (Qiagen, Hilden, DE) using the manufacturer's instructions and RNA was stored long-term at -80 °C.

RNA Sequencing. RNA sequencing was performed by Vanderbilt Technologies for Advanced Genomics Core Facility (VANTAGE). RNASequencing was performed on three biological replicates per condition. Total RNA quality was assessed using the 2100 Bioanalyzer (Agilent). At least 200ng of DNase-treated total RNA with a RNA integrity number greater than 6 was used for rRNA depletion and generation of cDNA libraries via the ScriptSeq Complete (Bacterial) kit (Illumina/Epicenter) following the manufacturer's protocol. Library quality was assessed using the 2100 Bioanalyzer (Agilent) and libraries were quantitated using KAPA Library Quantification Kits (KAPA Biosystems). Pooled libraries were subjected to 75 bp paired-end sequencing according to the manufacturer's protocol (Illumina HiSeq3000). Bcl2fastq2 Conversion Software (Illumina) was used to generate de-multiplexed Fastq files.

RNA Sequencing Analysis.

RNAseq data were trimmed to remove all bases below Q3, and had adapter sequence removed, using FaQCs (Lo and Chain, 2014). Trimmed sequence were aligned to the *Staphylococcus aureus* subsp. *aureus* str. Newman reference genome (accession number GCF_000010465.1) using BWA (Li and Durbin, 2009) and default alignment options.

Read counts were generated using HT-Seq v0.6.1p1 (Anders et al., 2015) and default options. The EdgeR (Robinson et al., 2010) package for R was used to analyze count files to identify differential gene expression (DGE). Read counts per gene were also analyzed and visualized using the Degust public server, Version 2.1, degust.erc.monash.edu. Raw read CSV files were uploaded to the server, analysis performed with the built-in Voom/Limma settings, the FDR cut-off modified to <0.01, and the log fold change cut-off changed to 2. COG designations for individual genes were manually curated from microbesonline.org.

Quantitative RT-PCR. Two μg of RNA was reverse transcribed by M-MLV reverse transcriptase (Fisher Scientific, Waltham, MA) in the presence of random hexamers (Promega, Madison, WI) and Ribolock RNase inhibitor (ThermoFisher, Waltham, MA). Reactions containing no reverse transcriptase were used to control for DNA contamination. Resultant cDNA was diluted 1:100 and subjected to qRT-PCR using iQ SYBR green supermix (BIO-RAD, Hercules, CA) with primer pairs listed in **Table 9**. Amplification was performed on a CFX96 qPCR cycler (BIO-RAD, Hercules, CA) using a 3-step melt curve program. CT values for each transcript were normalized by *16s* and fold changes were calculated using the ΔΔCT method.

Inductively-coupled plasma mass spectrometry. Five biological replicate overnight cultures of *S. aureus* strain Newman were diluted 1:100 into 5 mL TSB in 15 mL conical tubes and grown to mid-exponential phase (OD_{600} = 0.4). Cells were pelleted at 3220 x *g* for 10 minutes at room temperature, supernatants were discarded, and cells were resuspended in 2.5 mL TSB. To a 15 mL conical tube containing TSB and combinations of ‘921, vehicle control, or Mn was added 2 mL of resuspended bacterial cultures to a final

volume of 8 mL and final concentration of 100 μM ‘921 and 1 mM $MnCl_2$. Following incubation at 37°C with 180 rpm shaking for 30 minutes, 10 μL aliquots were removed for CFU plating and cells were harvested by centrifugation at 6,000 x *g* for 10 minutes at 4°C. Cells were then washed with 10 mLs of PBS (Corning, Corning NY) and transferred to pre-weighed metal-free 15 mL conical tubes (VWR, Radnor, PA), pelleted at 6,000 x *g* for 10 minutes at 4°C, and air-dried for five hours. The pellet weight was then recorded using an analytical balance (Mettler Toledo, Columbus, OH). Pellets were digested with 3 mL 50% HNO_3 (Optima grade metal-free; Fisher, Waltham, MA) at 50°C for 14 hours, diluted to 10 mL final volume with MilliQ deionized water, weighed using an analytical balance, and subjected to mass spectrometry at the Vanderbilt Mass Spectrometry Research Center. Levels of ^{25}Mg, ^{32}S, ^{59}Co, ^{60}Ni, ^{63}Cu, ^{66}Zn, ^{55}Mn, and ^{56}Fe were measured, concentrations were determined utilizing a standard curve for each metal, and results were normalized by the concentration of ^{32}S.

Statistical analyses. All raw numerical data were saved in Excel files and imported into GraphPad Prism for statistical analysis. All graphs are the result of a single representative experiment performed in biological triplicate, and all experiments were repeated to confirm results.

Table 9: Primers used in Chapter VII.

Primer	Primer Sequence	Primer description
LEJ_265	GCTGCAGCTAACGCATTAAGCACT	*16s* 5' qRT-PCR primer
LEJ_266	TTAAACCACATGCTCCACCGCTTG	*16s* 3' qRT-PCR primer
LEJ_267	taggtcaagaagcgggaatg	*hrtA* 5' qRT-PCR primer
LEJ_268	gcttttcaccgccagataac	*hrtA* 3' qRT-PCR primer
LEJ_269	tagctcaagggcttggtagg	*hrtB* 5' qRT-PCR primer
LEJ_270	tctcaatttgcggctctttc	*hrtB* 3' qRT-PCR primer
LEJ_271	tctagatgagccgtttgtcg	*mntA* 5' qRT-PCR primer
LEJ_272	gcttttgatagatcatggtgga	*mntA* 3' qRT-PCR primer
LEJ_273	atggctctggcgcagaaatag	*NWMN_1451* (glucokinase) 5' qRT-PCR primer
LEJ_274	agttaacaacgcctgtcgctg	*NWMN_1451* (glucokinase) 3' qRT-PCR primer
LEJ_277	ctgcagctgtaagagccgatg	*NWMN_2316* 5' qRT-PCR primer
LEJ_278	aggatgatttcgatcggcagg	*NWMN_2316* 3' qRT-PCR primer
LEJ_279	gaatttgcagtgctcgagttgc	*NWMN_2418* (MarR) 5' qRT-PCR primer
LEJ_280	cacgtgtaatccaacctttgtcc	*NWMN_2418* (MarR) 3' qRT-PCR primer
LEJ_281	tgctgttggtacaagtgcagc	*NWMN_2457* (CopA) 5' qRT-PCR primer
LEJ_282	gccaagcgcattggttgtttg	*NWMN_2457* (CopA) 3' qRT-PCR primer
LEJ_291	cgttaacctcgccacttgcaa	*NWMN_2487* 5' qRT-PCR primer
LEJ_292	ccagtgagtggtggtgatgt	*NWMN_2487* 3' qRT-PCR primer

Results

Identification of compounds that inhibit *S. aureus* growth in a Mn-dependent manner

I hypothesized that compounds that disrupt Mn homeostasis in *S. aureus* could serve as novel antimicrobial agents. To identify such compounds, a 'Mn toolbox' of 39 compounds was chosen to be assessed for antimicrobial activity against *S. aureus.* The Mn toolbox was previously identified in a high throughput screen of 40,167 small molecules as compounds that alter the concentration of Mn in neuronal cell lines (Kumar et al., 2014). I reasoned that such compounds may retain activity as Mn modulators in *S. aureus*, and that altering Mn homeostasis would be antimicrobial to *S. aureus*. Furthermore, the compounds in the Mn toolbox were found to be non-toxic to human primary neuron cell lines at the concentrations tested. Compounds were subjected to a secondary screen to evaluate whether compounds had Mn-dependent antimicrobial activity against *S. aureus* (**Figure 45A**).

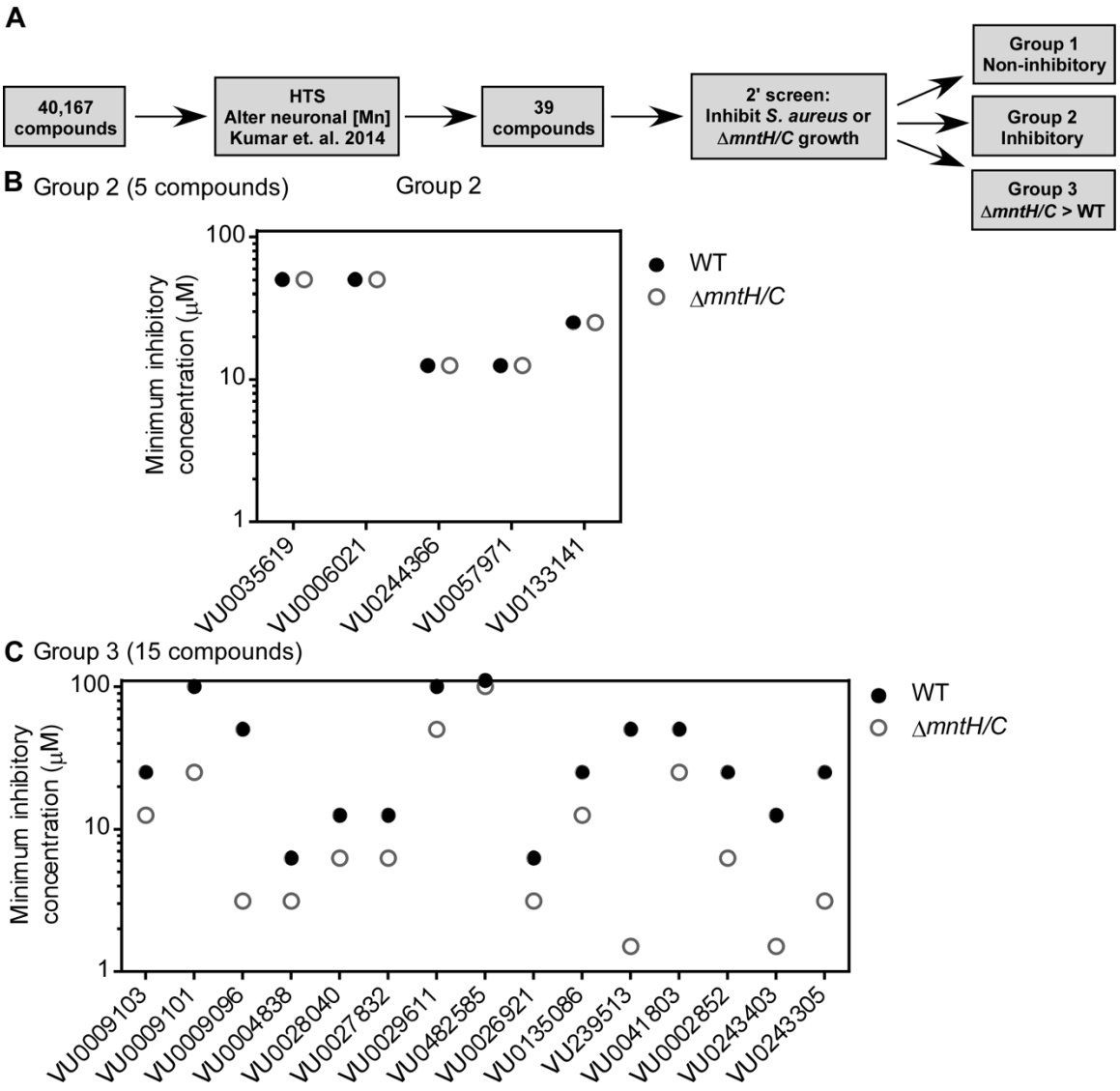

Figure 45. Identifying compounds from Mn toolbox that inhibit *S. aureus* growth in a *mntH/C*-dependent fashion. (**A**) Workflow for identifying compounds of interest. (**B-C**) The minimum inhibitory concentration of compounds, defined as the concentration at which treatment with the indicated compound (X axis) caused 50% decrease in growth at 8 hours, is graphed for WT *S. aureus* (black filled circles) or Δ*mntH/C* (open circles) relative to vehicle control. (**B**) Minimum inhibitory concentration of compounds in Group 2, which inhibited growth equally for both WT *S. aureus* or Δ*mntH/C*. (**C**) Minimum inhibitory concentration of compounds in Group 3, which differentially inhibited growth of WT *S. aureus* or Δ*mntH/C*. For (B-C), growth in the presence of various concentrations of compound is graphed as % of vehicle alone after 8 hours of growth. Growth was measured by OD_{600}.

Table 10. Minimum inhibitory concentrations for compounds in Mn toolbox.

Compound	MIC* for WT (μM)	MIC* for Δ*mntH/C*
VU0243195	>100	>100
VU0035619	50	50
VU0150155	>100	>100
VU0076546	>100	>100
VU0088990	>100	>100
VU0029414	>100	>100
VU0006021	50	50
VU0003610	>100	>100
VU0047355	>100	>100
VU0047375	>100	>100
VU0009103	25	12.5
VU0009101	100	25
VU0009096	50	3.125
VU0025173	>100	>100
VU0004838	6.25	3.125
VU0006712	>100	>100
VU0244366	12.5	12.5
VU0048129	>100	>100
VU0028040	12.5	6.25
VU0027832	12.5	6.25
VU0057971	12.5	12.5
VU0025879	>100	100
VU0133141	25	25
VU0028386	100	>100
VU0029611	100	50
VU0482585	>100	100
VU0063088	>100	>100
VU0050661	>100	>100
VU0026395	>100	>100
VU0026977	>100	>100
VU0135086	25	12.5
VU0026921	6.25	3.125
VU239513	50	1.5
VU0046776	>100	>100
VU0041803	50	25
VU0003765	>100	>100
VU0002852	25	6.25
VU0243403	12.5	1.5
VU0243305	25	3.125

*Defined as minimum concentration of compound that inhibited growth by at least 50% at 8 hours.

Each compound was tested for the ability to inhibit *S. aureus* growth in the rich growth medium TSB. In order to evaluate whether growth inhibition was related to Mn levels in the cell, compounds were also assessed for the ability to inhibit the growth of *S. aureus* Δ*mntH/C*, a strain of *S. aureus* that lacks high-affinity Mn import and therefore exhibits decreased growth in extracellular Mn availability is decreased or intracellular Mn demand is increased (Kehl-Fie et al., 2013). The 39 compounds could be divided into three groups based on their antimicrobial profiles (**Figure 45A, Table 8**). Group 1 consisted of 19 compounds with no antimicrobial activity or low-potency antimicrobial activity, with no inhibition of *S. aureus* growth at 50 μM. Group 2 included 5 compounds that inhibited *S. aureus* growth at concentrations of 50 μM or lower, but inhibited WT and Δ*mntH/C* to a similar degree (**Figure 45B**). Group 3 contained fifteen compounds that exhibited lower minimum inhibitory concentrations (MIC) towards *S. aureus* Δ*mntH/C* than WT *S. aureus*. As I reasoned these compounds may inhibit *S. aureus* growth by altering Mn homeostasis in some manner, compounds in Group 3 were considered for further analysis.

Compounds in Group 3 were first narrowed by potency, and only compounds that inhibit *S. aureus* growth at 5 μM were carried forward (**Figure 46A**). Compound in Group 3 inhibit growth of *S. aureus* Δ*mntH/C* more potently than WT *S. aureus,* suggesting that *S. aureus* with decreased intracellular Mn is more sensitive to these compounds. To complement these findings, *S. aureus* growth in the presence of Group 3 compounds was complimented by the addition of $MnCl_2$. Compounds that inhibit growth by directly chelating Mn would be expected to exhibit dose-dependent decrease in growth inhibition with increasing Mn in a stoichiometric fashion (**Figure 46A**). Indeed, the majority of the compounds exhibited stoichiometric reversal of growth inhibition by Mn (**Figure 46B**).

More specifically, *S. aureus* growth in the presence of 5 μM compounds was substantially improved by the addition of 5 μM $MnCl_2$, and 25 μM $MnCl_2$ completely rescued growth (**Table 11**). Therefore, I concluded that the compounds in Group 3A may function as chelators of Mn. However, compound VU0026921 (‘921) did not exhibit stoichiometric rescue by $MnCl_2$ (**Figure 46C**). Growth inhibition by ’921 could be improved by the addition of Mn, but only at very high concentrations. At eight hours, substantial rescue was only observed with 500 μM $MnCl_2$, or 100-fold excess Mn to ‘921. This result suggests that ‘921 may interfere with *S. aureus* Mn homeostasis or disrupt a process that can be rescued by excess Mn, both exciting possibilities for a novel antimicrobial.

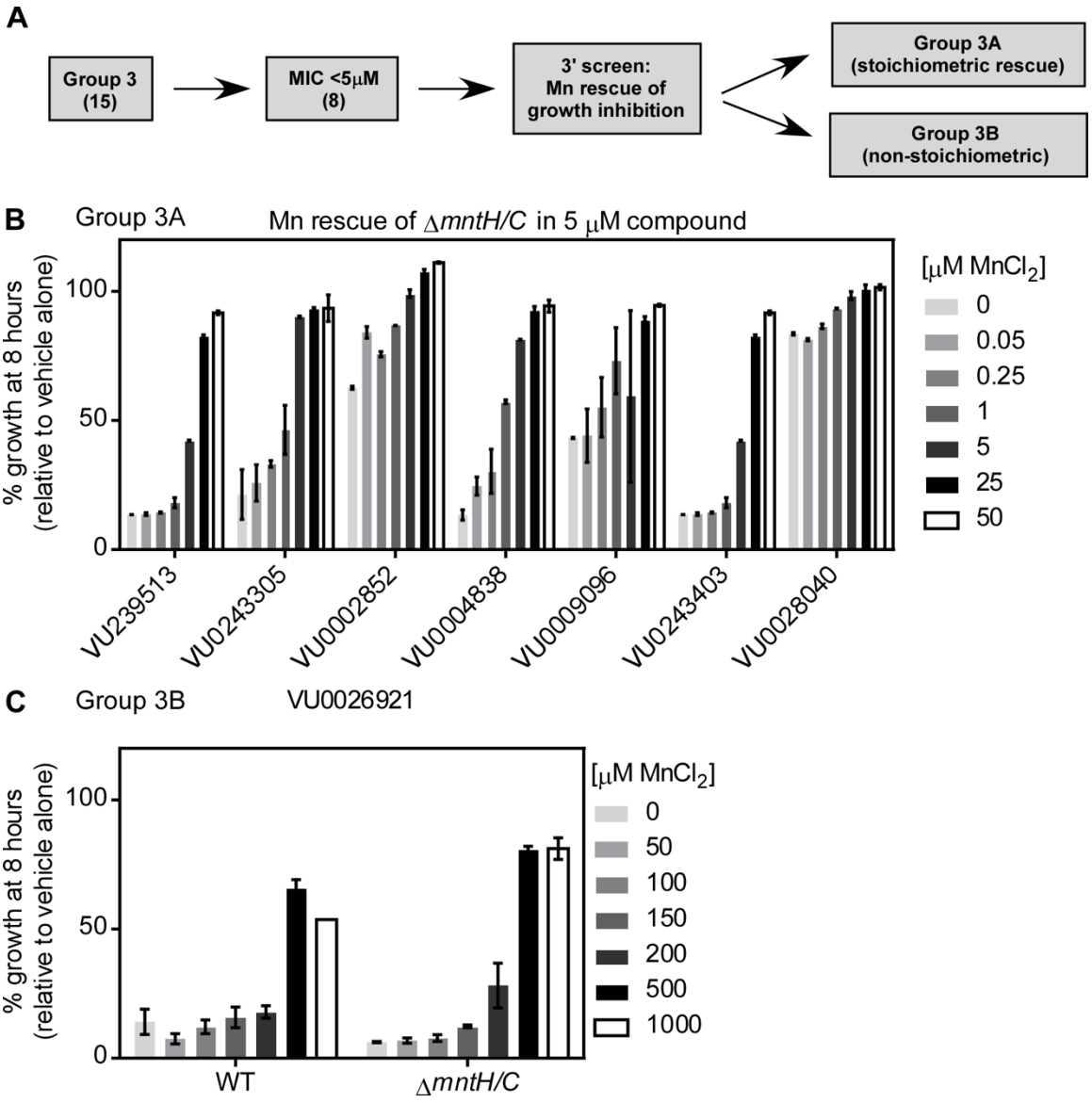

Figure 46. Determining the impact of Mn concentrations on compound activity. (**A**) Schematic for selection of compounds for Mn rescue experiments. (**B**) Dose-dependent Mn rescue of compounds in Group 3A. *S. aureus* was grown in the presence of 5 μM of the indicated compounds with or without the addition of $MnCl_2$ at the indicated concentrations. (**C**) Inhibition of WT *S. aureus* or Δ*mntH/C* growth in the presence of 5 μM VU0026921 with or without the addition of $MnCl_2$ at various concentrations. (B & C) Growth in the presence of various concentrations of compound is graphed as % of vehicle alone after 8 hours of growth. Growth was measured by OD_{600}. Bars or symbols indicate the mean ± standard deviation.

Table 11. Mn rescue of compound growth inhibition at 5 μM

Compound	Mn rescue for WT*	Mn rescue for Δ*mntH/C**
VU0009096	N/A#	1 μM
VU0004838	N/A	1 μM
VU0026921	500 μM	500 μM
VU239513	N/A	50 μM
VU0002852	N/A	5 μM
VU0243403	N/A	50 μM
VU0243305	N/A	5 μM

*Rescue defined by 50% increase in growth at 8 hours.
#N/A indicates compound is not inhibitory to WT at 5 μM.

Characterization of the growth inhibitory properties of ‘921

Compound ‘921 inhibits *S. aureus* growth in a manner modulated by Mn (**Figure 47**). In the presence of 5 μM ‘921, *S. aureus* lag phase is lengthened, increasing the time before *S. aureus* enters exponential growth. Interestingly, the growth rate during exponential growth and the final optical density reached are not altered by ‘921. Mn diminishes the length of lag phase in the presence of ‘921 in a concentration-dependent fashion but also does not alter the growth rate or final optical density (**Figure 47**).

This rapid growth in the presence of ‘921 after a long lag phase suggested the hypothesis that exposure to ‘921 or Mn leads to upregulation of a resistance factor, and expression of this resistance factor permits *S. aureus* to overcome ‘921 and grow at a normal rate. To test this hypothesis, *S. aureus* was grown in a low concentration of ‘921 overnight to determine if exposure to ‘921 increased *S. aureus* resistance to ‘921. In fact, pre-treatment with 2 μM ‘921 did not alter *S. aureus* growth in 5 μM ‘921, and pre-treatment with 4 μM ‘921 decreased growth (**Figure 48**). Therefore, *S. aureus* does not up-regulate a resistance factor following exposure to low-dose ‘921.

An analog of ‘921 was synthesized and assayed for growth inhibitory properties. This analog substitutes the trifluoromethyl group with a methyl group (**Figure 49A**). The ‘921 analog did not inhibit *S. aureus* growth (**Figure 49B**).

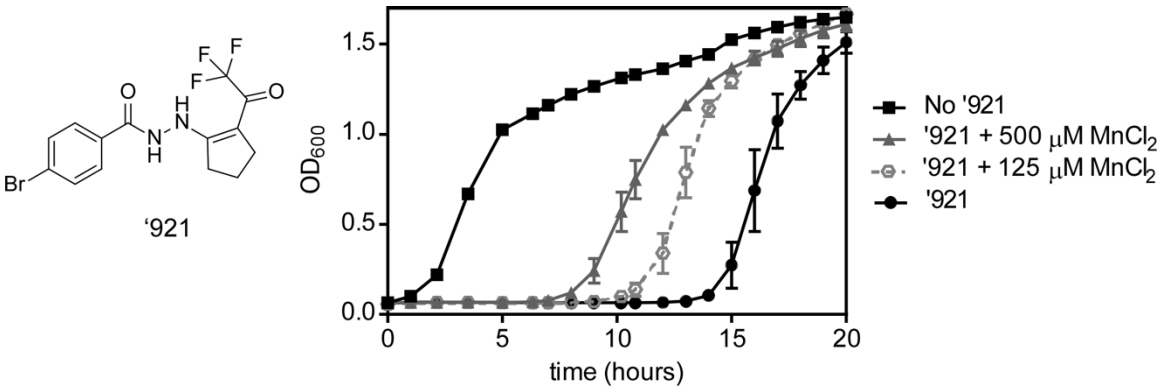

Figure 47. VU0026921 growth inhibition is modulated by Mn. Left, chemical structure of VU0026921 (‘921). Right, *S. aureus* WT was grown in TSB with or without 5 μM ‘921. $MnCl_2$ was added to cultures containing ‘921 at 500 μM, 125 μM, or not added. Growth was monitored as OD_{600} over time. Symbols indicate the mean ± standard deviation.

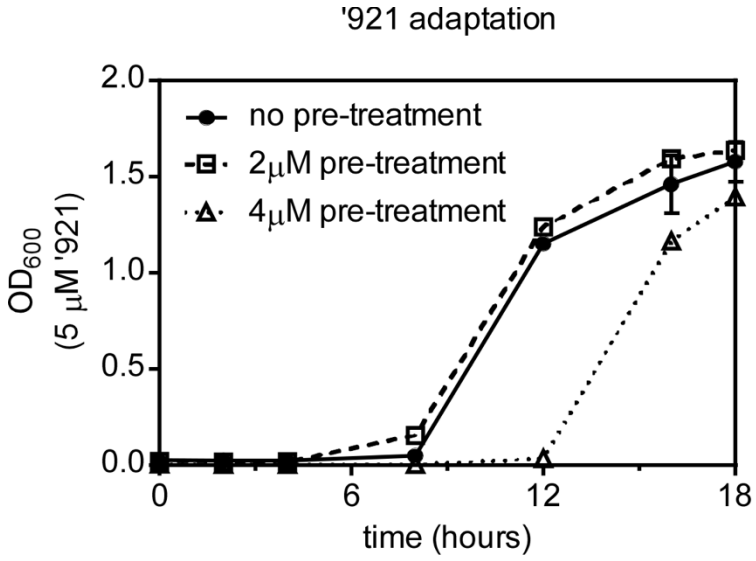

Figure 48. *S. aureus* does not adapt to VU0026921 growth inhibition with low-dose VU0026921 exposure. *S. aureus* WT Newman overnight cultures containing 0, 2, or 4 μM '921 were diluted 1:100 into fresh medium including 5 μM '921 and growth was monitored by OD_{600}.

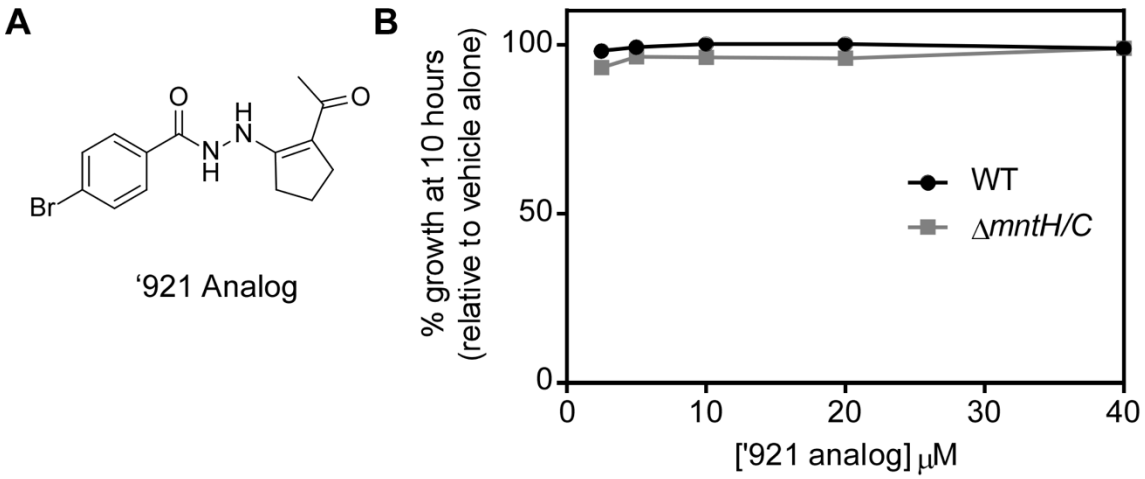

Figure 49. Activity of VU0026921 analog. (A) Chemical structure of '921 analog. (**B**) Growth of WT *S. aureus* Newman or Δ*mntH/C* in the presence of '921 analog at the indicated concentrations. Growth is shown as percent relative to vehicle alone as measured by OD_{600} at 10 hours.

Next, I attempted to identify ‘921-resistant suppressor strains that could be utilized to identify the target of ‘921 within *S. aureus*. However, despite numerous efforts and methods, stable ‘921-resistant strains could not be generated. This result implies that the target of ‘921 toxicity may be essential, or that ‘921 has multiple targets of toxicity within *S. aureus*. The inability of *S. aureus* to generate spontaneous resistance to ‘921 is a therapeutically promising finding.

Bactericidal activity of ‘921

Compound ‘921 has been demonstrated to increase the lag phase of *S. aureus,* but whether growth inhibition was due to bacteriostatic or bactericidal activity was unclear. To address this question, bacterial CFU counts were obtained using antimicrobial growth curve conditions. Under these conditions, bacteria are inoculated from stationary phase cultures into fresh medium containing ‘921. Strikingly, ‘921 exposure caused a substantial decrease in CFU over time, with bacteria at or below the limit of detection after four hours of treatment (**Figure 50A**). Consistent with the finding that Mn decreases the lag phase in cells treated with ‘921, the number of CFU recovered from Mn and ‘921 co-treated cells remained stable across the timepoints tested (**Figure 50A**). Both ‘921 and ‘921/Mn co-treatment appeared in contrast with the vehicle treated cells, which increased by 2 $\log_{10}$ by the four hour timepoint. Thus, ‘921 is bactericidal to *S. aureus* when cells are treated in early lag phase, and the bactericidal activity of ‘921 can be rendered merely bacteriostatic by the addition of 1 mM $MnCl_2$.

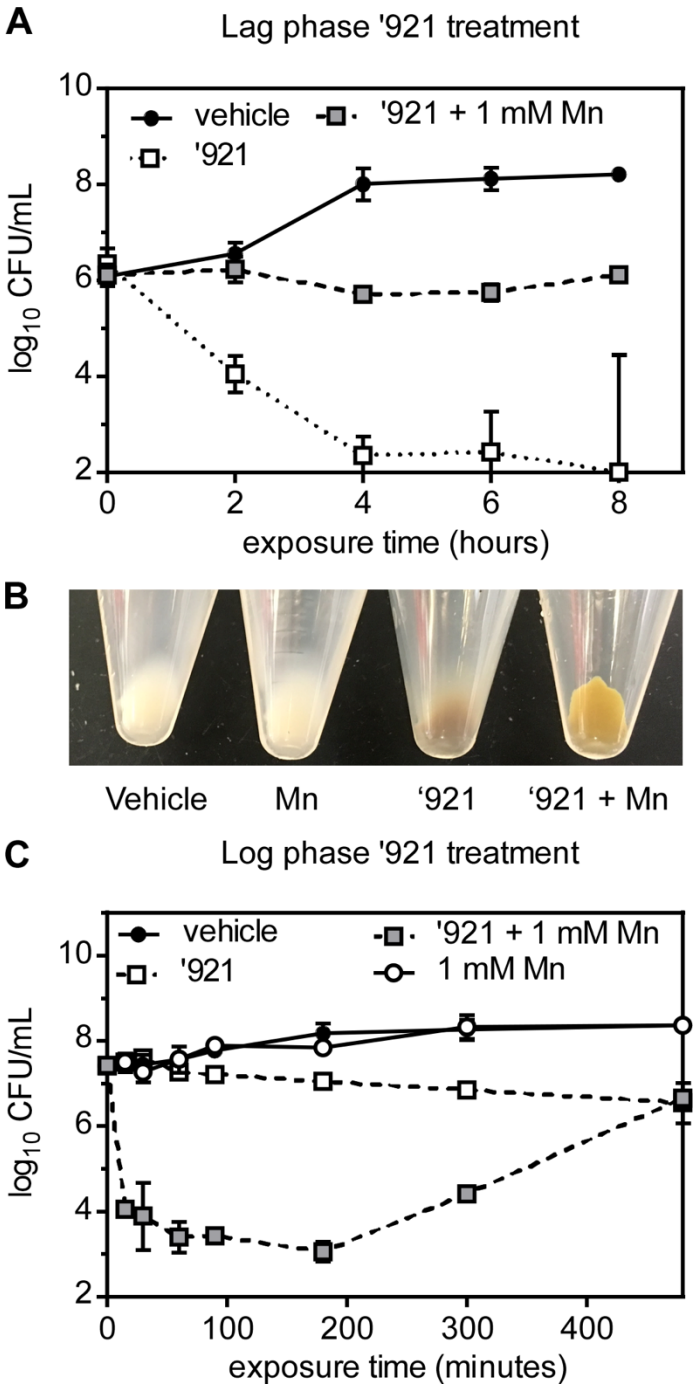

Figure 50. The antimicrobial activity of VU0026921 is modulated by growth phase and exogenous Mn. (**A**) Colony forming unites (CFU) recovered following treatment of lag-phase WT *S. aureus* Newman with vehicle, 5 μM '921, or 5 μM '921 + 1 mM $MnCl_2$. (**B**) Pellet appearance following treatment of WT *S. aureus* Newman grown to mid-exponential phase and treated with vehicle, 100 μM '921, or 100 μM '921 + 1 mM $MnCl_2$ for 30 minutes. (**C**) CFU recovered following treatment of mid-exponential phase cultures of WT *S. aureus* Newman with vehicle, 1 mM $MnCl_2$, 100 μM '921, or 100 μM '921 + 1 mM $MnCl_2$ for the indicated lengths of time.

Because *S. aureus* may not be in lag phase during all stages of infection, I assessed whether ‘921 retained activity in rapidly dividing *S. aureus* in the logarithmic phase of growth. To test this, killing activity of ‘921 was assessed in *S. aureus* cultures in the exponential phase of growth. Of note, pellets from exponential phase cultures that were treated with ‘921 exhibited a striking color change to dark brown and co-treatment turned the pellet to yellow-brown, while vehicle or Mn treated cultures were a very pale gold (**Figure 50B**). *S. aureus* produces a gold-colored pigment, staphyloxanthin, and accumulation of heme turns pellets brown. Surprisingly, ‘921 demonstrated bacteriostatic activity on log phase cultures, whereas co-treatment with ‘921 and Mn was bactericidal (**Figure 50C**). In fact, ‘921 activity in log phase revealed an opposite pattern compared to the lag phase experiments previously discussed. These intriguing results suggest that ‘921 activity may be controlled by growth-phase-dependent expression of genes.

‘921 treatment induces a substantial transcriptional response

Because ‘921 spontaneously resistant suppressor strains could not be identified, a transcriptomic approach was taken to characterize the cellular processes affected by ‘921. To characterize transcriptional changes induced by ‘921 treatment in a Mn-dependent fashion, RNA Sequencing was performed on RNA harvested from log-phase *S. aureus* exposed to 100 μM ‘921 alone or in combination with 1 mM $MnCl_2$, as well as vehicle and 1 mM $MnCl_2$ controls. Treatment with 1 mM $MnCl_2$ alone resulted in 4 significantly changed transcripts, including decreased abundance of the high-affinity *mntABC* operon, known to be repressed by Mn (Horsburgh et al., 2002) (**Table 13, Appendix A, Figure 51A**). These expected transcriptional changes served as internal controls to validate the experimental design.

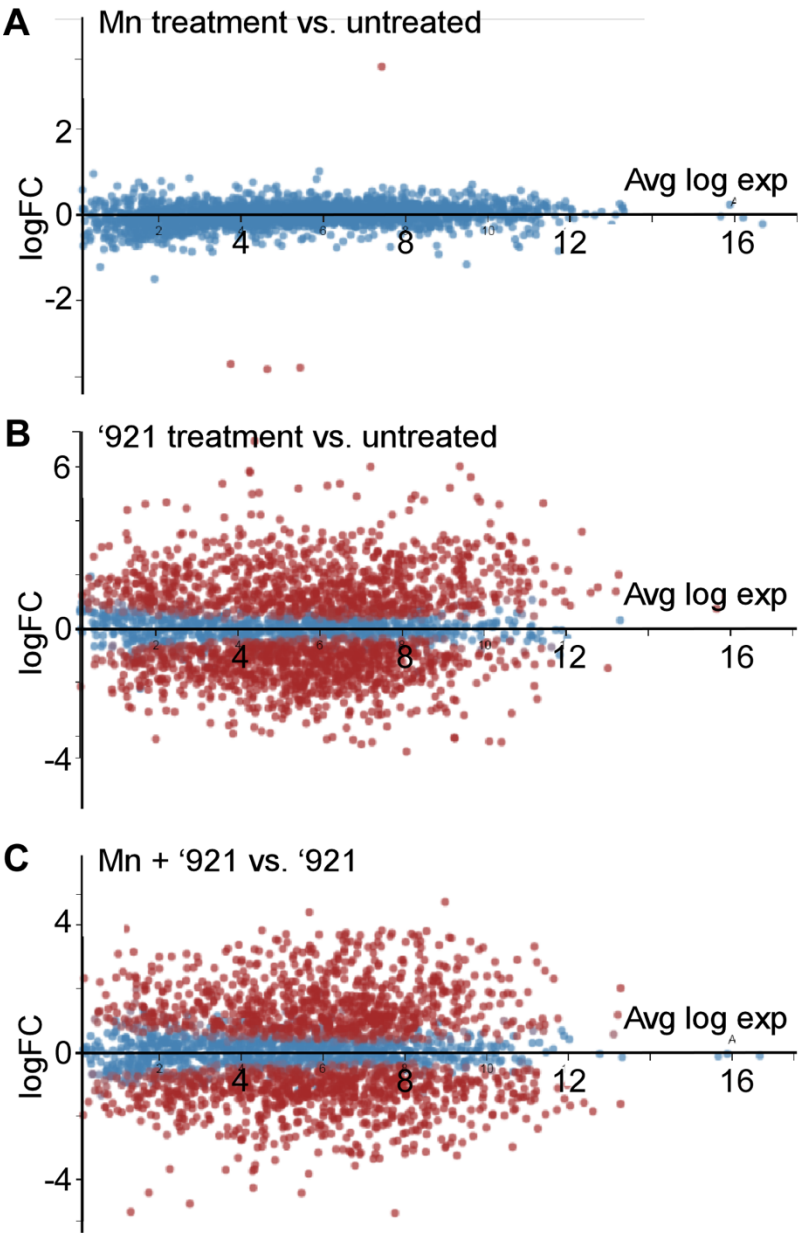

Figure 51. MA plots for RNASequencing results. (**A-C**) MA plots for transcripts identified by high throughput RNA Sequencing of WT *S. aureus* Newman cultures exposed to vehicle, 1 mM $MnCl_2$, 100 μM '921, or 100 μM '921 + 1 mM $MnCl_2$ for 30 minutes.

Exposure to the antimicrobial compound ‘921 resulted in 298 up-regulated and 220 down-regulated genes whose transcripts changed in abundance greater than 2 $\log_2$ (**Table 14, Appendix A, Figure 51B**). Furthermore, 216 genes were up-regulated and 147 genes were down-regulated by co-treatment with ‘921 and Mn compared to ‘921 alone (**Table 15, Appendix A, Figure 51C**). These results demonstrate that ‘921 dramatically alters the transcriptional profile of *S. aureus* in a manner that is further modified by co-treatment with Mn.

Inspection of the RNASeq results revealed that ‘921 and ‘921/Mn co-treatment expression patterns were distinctly different both from each other and from the control groups (**Figure 52A&B**). Multiple dimensional scaling visualization of the biological replicates revealed that vehicle treated and Mn-treated replicates cluster together, whereas ‘921 and ‘921/Mn-treated replicates cluster into individual groups that are both substantially different from the controls (**Figure 52B**). The differences in the transcriptional response are also apparent in a Venn Diagram visualization (**Figure 52C**). In order to narrow the focus to the Mn-dependent transcriptional response, our attention was focused first on transcriptional differences between ‘921 and ‘921/Mn co-treated samples. Genes that were differentially regulated between these conditions were analyzed by Clusters of Orthologous Groups designation to unveil any potential pathways of interest (**Figure 52D**). Notably, most categories had only a handful of hits by this analysis and the majority of changes were uncharacterized. The categories with the most substantial changes were toxin production, amino acid metabolism and transport, and genes involved in transcription. Together, these changes did not suggest a single target by which Mn alters ‘921 toxicity.

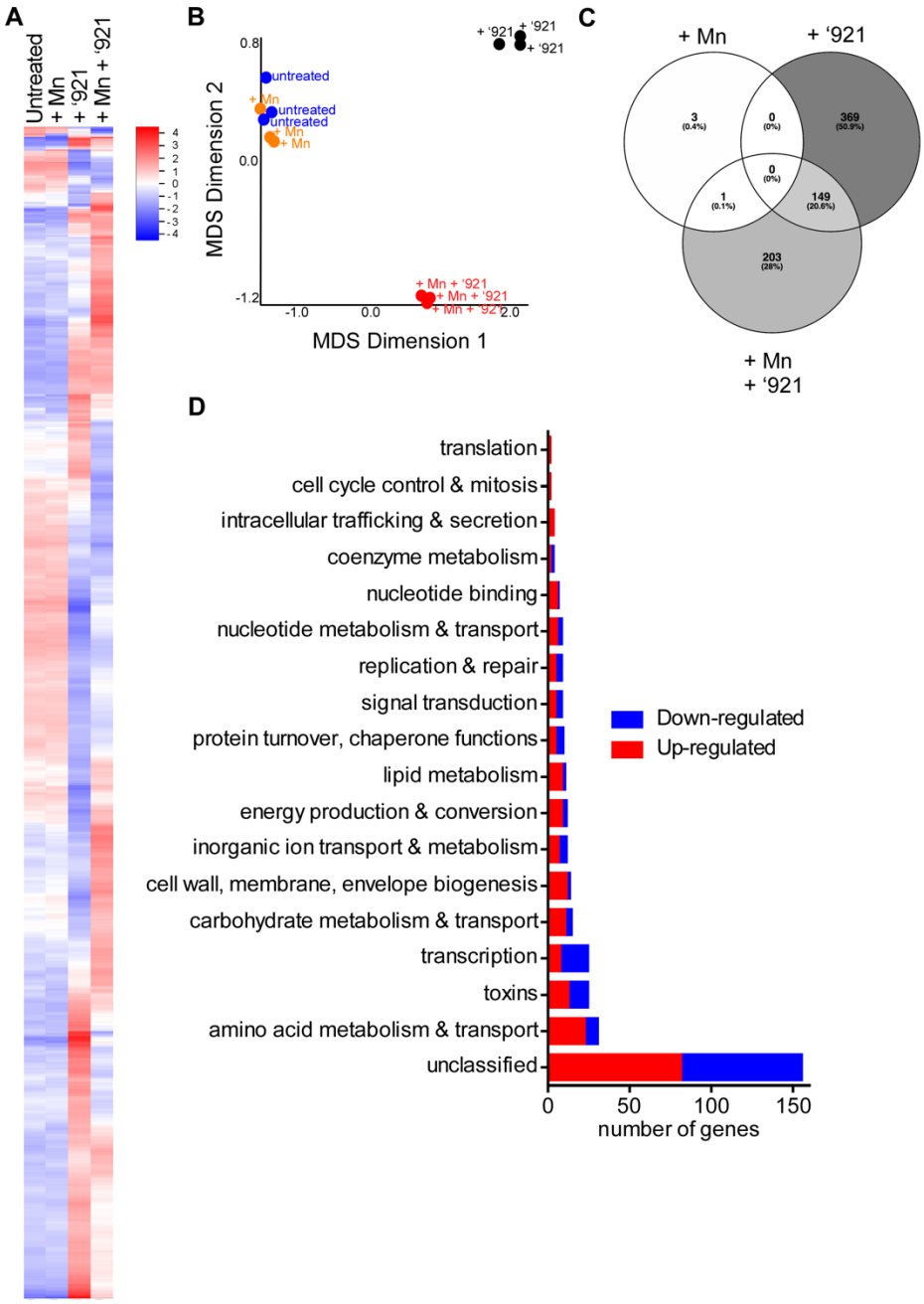

Figure 52. RNASequencing reveals significant transcriptional changes following exposure to VU0026921 that are modulated by Mn. (A-C) RNA Sequencing was performed on mid-exponential cultures of WT *S. aureus* Newman exposed to vehicle, 1 mM $MnCl_2$, 100 μM '921, or 100 μM '921 + 1 mM $MnCl_2$ for 30 minutes. **(A)** Heat map of fold changes for all four conditions relative to mean transcript abundance across all four conditions. (**B**) Multi-dimensional scaling visualization of RNASequencing biological replicates. (**C**) Venn diagram of genes significantly changed relative to untreated cells. (**D**) Categories of genes whose transcription was significantly different between 100 μM '921 treatment and 100 μM '921 + 1 mM $MnCl_2$ treatment. The bar indicates the number of up or down-regulated genes in '921 + 1 mM Mn in each category.

Next, the RNASeq dataset was interrogated for genes with a connection to metal homeostasis. Strikingly, genes associated with metal toxicity were significantly upregulated following ‘921 treatment (**Table 14, Appendix A**), including the heme detoxification system *hrtAB,* a predicted cation transporter, and a copper-exporting P-type ATPase A. Furthermore, genes involved in detoxification of reactive oxygen species, including theoredoxins, non-heme ferritin, and alkyl hydroperoxide reductase, were also upregulated with ‘921 treatment. Together, these findings suggest that ‘921 may cause a metal toxicity response. To confirm the RNASeq results, qRT-PCR was performed on a subset of genes, including transcripts changed by Mn alone, transcripts that were altered by ‘921, and transcripts that were altered by ‘921 + Mn (**Figure 53**). The results of qRT-PCR demonstrated transcriptional up- or down-regulation in the same pattern as the RNASeq, validating the RNASeq findings.

‘921 causes accumulation of cellular metals

Based on the RNASequencing gene expression profile, I hypothesized that ‘921 may be altering metal levels within *S. aureus*. To test this hypothesis, *S. aureus* metal levels were assessed by inductively coupled plasma mass spectrometry (ICP-MS) after exposure to ‘921 for 30 minutes. Following ‘921 treatment, Mn levels in the cell did not change (**Figure 54A**). Similarly, treatment with Mn alone did not alter Mn levels (**Figure 54A**). However, Mn and ‘921 co-treatment caused a massive increase in cellular Mn (**Figure 54A**). In contrast to Mn, Mg levels were decreased by co-treatment with ‘921 and Mn (**Figure 54B**). These results suggests that ‘921 induces the cell to uptake Mn, but that significant differences in levels can only be achieved when extracellular Mn levels are high, and that Mg levels are inversely correlated with Mn levels in these conditions.

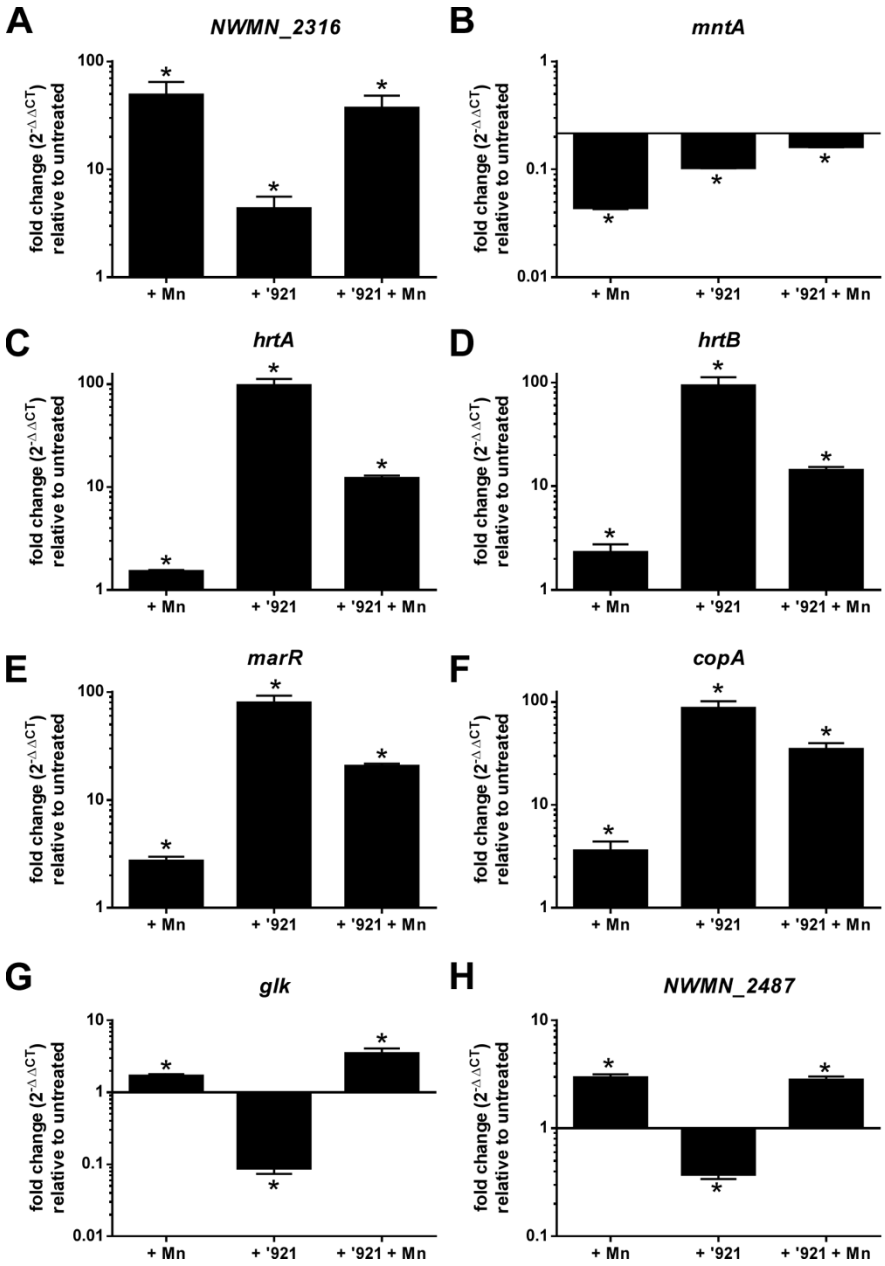

Figure 53. Confirmation of RNASeq transcriptional changes by qRT-PCR. (A-H) qRT-PCR for genes differentially expressed in RNASeq data. RNA was harvested from mid-exponential cultures of WT *S. aureus* Newman were exposed to vehicle, 1 mM $MnCl_2$, 100 μM '921, or 100 μM '921 + 1 mM $MnCl_2$ for 30 minutes. A single biological replicate, analyzed in technical triplicate, is graphed. Statistical significance was calculated by one-way ANOVA compared to a theoretical value of 1. *, $P < 0.05$;

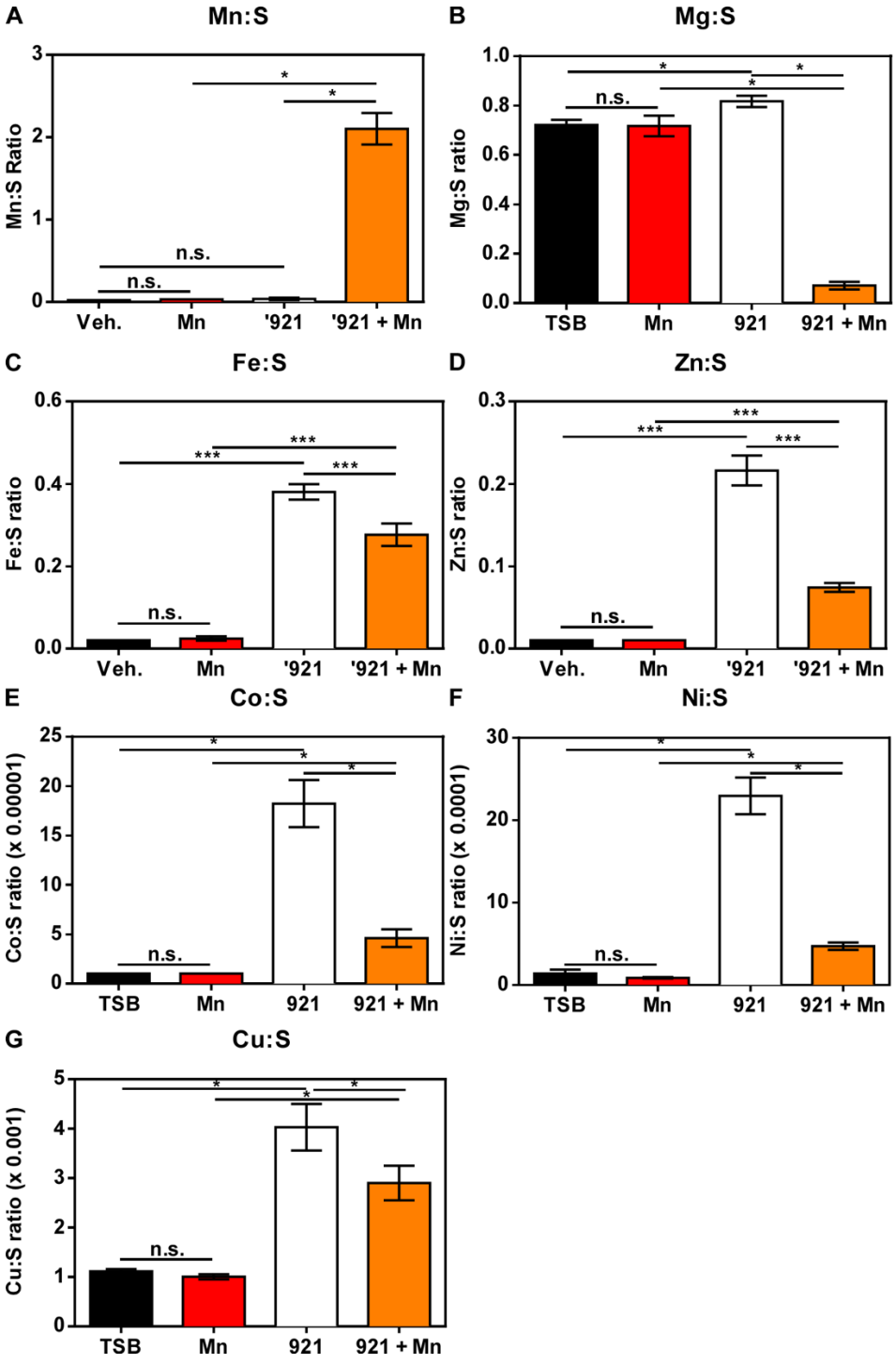

Figure 54. VU0026921 causes accumulation of cellular metals. Inductively coupled plasma mass spectrometry was used to measure concentrations of (**A**) Mn, (**B**) Mg, (**C**) Fe, (**D**) Zn, (**E**) Co, (**F**) Ni, and (**G**) Cu. Metals were measured in lysed *S. aureus* cells treated for 30 minutes with vehicle, vehicle + 1 mM Mn, 100 μM '921, or 100 μM '921 + 1 mM Mn. Values were normalized by calculating the ratio of each metal to sulfur. Bars depict mean +/- standard deviation. Significance was calculated by ANOVA, *, $P < 0.05$.

Treatment with ‘921 alone increased cellular levels of Fe, Zn, Co, Ni, and Cu, whereas co-treatment with ‘921 and Mn also led to increases in these metals, albeit to a lesser extent (**Figure 54C-G**). These results confirm that ‘921 alters *S. aureus* metal homeostasis and imply that ‘921 causes accumulation of metals in a manner that may explain the antimicrobial nature of this compound.

‘921 is antimicrobial against Gram-positive, but not Gram-negative, bacteria

Finally, we assessed the potential for ‘921 to serve as a broad-spectrum antibiotic scaffold. Indeed, we found that ‘921 inhibited the growth of *Micrococcus luteus,* a Gram-positive bacterium often used to screen compounds for antimicrobial activity (Goodwin et al., 2015; Poppel et al., 2015) (**Figure 55A**). The potency of ‘921 against *M. luteus* was similar to the activity seen for *S. aureus. B. anthracis* was also sensitive to ‘921 (**Figure 55A**). *B. anthracis* is a highly virulent organism and anthrax spores have the potential for use as a bioweapon (Sweeney et al., 2011). In contrast to the potent activity of ‘921 against Gram-positive organisms, ‘921 did not inhibit the growth of the Gram-negative pathogens *A. baumannii, P. aeruginosa,* or *K. pneumoniae* (**Figure 55B**), likely because the compound is unable to penetrate the Gram-negative outer membrane. Taken as a whole, ‘921 is a promising scaffold for the development of a novel antibiotic class with activity against multiple Gram-positive bacteria.

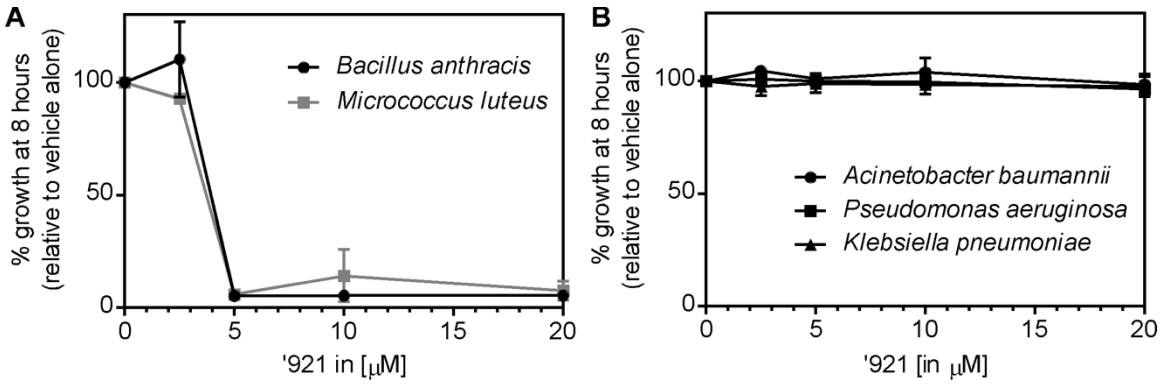

Figure 55. VU0026921 is antimicrobial against Gram-positive, but not Gram-negative, bacteria. (**A**) Percent growth of *B. anthracis* and *M. luteus* grown in the presence of various concentrations of '921 for 8 hours. (**B**) Percent growth of *A. baumannii, P. aeruginosa,* and *K. pneumoniae* grown in the presence of various concentrations of '921 for 8 hours. For (A-B), growth was measured by OD_{600} and is shown relative to treatment with vehicle alone. Symbols and error are mean ± standard deviation.

Discussion

Here we report that small molecule '921 is a potent inhibitor of Gram-positive bacterial growth. Small molecule '921 was identified as a Mn-level-dependent inhibitor of *S. aureus* growth from a library of 29 compounds that were previously reported to enhance or decrease Mn import into neurons (Kumar et al., 2014). Activity of '921 is bacteriostatic or bactericidal, depending on the growth conditions and the concentration of Mn in the medium. *S. aureus* incubated with '921 exhibits massive transcriptional changes, and these changes are further modified by co-treatment with Mn. Consistent with the upregulation of metal efflux genes with '921 treatment, multiple metals accumulated with *S. aureus* following exposure to '921. Taken together, these data identify '921 as a small molecule that amasses metals within *S. aureus* and causes toxicity.

One concern in screening for molecules that alter growth in a metal concentration-dependent fashion is that identified molecules will function as chelators rather than interacting with cellular macromolecules. Several aspects of '921 activity point against '921 chelating Mn. First, although Mn did enhance growth in the presence of '921, it did so in a non-stoichiometric manner. For example, *S. aureus* growth in with 5 μM '921 was only partially rescued by 125 μM Mn, twenty five fold higher than the amount of '921 added. Second, a metal chelator would be expected to inhibit growth broadly, but '921 did not inhibit growth of Gram-negative organisms, suggesting that penetration into the cell or a specific cellular target is required for '921 toxicity.

Activity of '921 is dependent on growth phase or possibly bacterial density, as CFU of lag-phase cultures decrease following '921 treatment whereas exponential phase cultures exhibit growth inhibition by '921, but not killing. Notably, the exponential phase

toxicity of ‘921 occurs only at high concentrations of ‘921 (100 μM), while inhibition in a growth curve is present at lower concentrations (5 μM). The likely explanation for this the increased cell density (10 to 100 fold increased) of exponential phase cultures compared to the initial growth curve conditions, but the difference in concentration may also suggest a different biological activity. Even more complex is the effect of Mn on ‘921 activity. When bacteria were exposed to combination ‘921 and Mn treatment in lag phase, Mn protected *S. aureus* from ‘921-mediated killing. Intriguingly, Mn had the opposite impact on ‘921 treated exponential phase *S. aureus*; in this setting, Mn enhanced killing. I hypothesize that the difference in ‘921 activity is due to differences in ‘921 target expression during lag and exponential phase growth. As an example, lag phase bacteria express metal importers to a different extent than exponential phase bacteria, which could result in differential activity of ’921 (Rolfe et al., 2012).

The most direct evidence that ‘921 dysregulates metal homeostasis comes from ICP-MS measurements of cellular metal levels. *S. aureus* metal levels were essentially unaltered with 1 mM Mn treatment, but treatment with ‘921 or ‘921 + Mn led to dramatic accumulation of all cellular metals tested except Mg, which was unchanged in ‘921 and decreased in ‘921 + Mn. The decrease in Mg in the ‘921 + Mn treated cells could be due to the massive influx of Mn under these conditions, as Mn can block Mg uptake (Hohle and O'Brian, 2014). The accumulation of the metals occurs via an unknown mechanism and presumably accounts for the toxicity of ‘921.

I propose that ‘921 interacts with multiple cellular targets that lead to nonspecific metal influx. Because ‘921 activity occurs within minutes, this is not due to a transcriptional change. One potential mechanism is that ‘921 locks metal porins in an open

conformation. Metals are rapidly influxed from the medium, and if any metal is present in high abundance in the medium, that metal becomes concentrated within the cell, leading to metal toxicity and cell death. Because of the influx of metals, *S. aureus* responds by upregulating metal efflux genes and downregulating metal binding genes in an attempt to return to equilibrium. Because of the massive stress experienced by the cell, additional transcriptional changes occur as secondary effects.

One major drawback to this study is that we have not identified the cellular target or targets of '921. This may be due to the instability of the compound in solution, which complicates selection for resistant mutants. Another potential confounding issue is that '921 has already been identified as a compound that has activity in mammalian cells (Kumar et al., 2014). Therefore, the antimicrobial potential may be limited by side effects. Both of these issues will be addressed in proposed future studies to investigate structure activity relationships of this lead antimicrobial compound.

References

Anders, S., Pyl, P.T., and Huber, W. (2015). HTSeq--a Python framework to work with high-throughput sequencing data. Bioinformatics *31*, 166-169.

CDC (2013). Antibiotic resistance threats in the United States, 2013. https://www.cdc.gov/drugresistance/pdf/ar-threats-2013-508.pdf.

Duthie, E.S., and Lorenz, L.L. (1952). Staphylococcal coagulase; mode of action and antigenicity. J. Gen. Microbiol. *6*, 95-107.

Goodwin, C.R., Covington, B.C., Derewacz, D.K., McNees, C.R., Wikswo, J.P., McLean, J.A., and Bachmann, B.O. (2015). Structuring microbial metabolic responses to multiplexed stimuli via self-organizing metabolomics maps. Chem. Biol. *22*, 661-670.

Hohle, T.H., and O'Brian, M.R. (2014). Magnesium-dependent processes are targets of bacterial manganese toxicity. Mol. Microbiol. *93*, 736-747.

Hood, M.I., and Skaar, E.P. (2012). Nutritional immunity: transition metals at the pathogen-host interface. Nat. Rev. Microbiol. *10*, 525-537.

Horsburgh, M.J., Wharton, S.J., Cox, A.G., Ingham, E., Peacock, S., and Foster, S.J. (2002). MntR modulates expression of the PerR regulon and superoxide resistance in *Staphylococcus aureus* through control of manganese uptake. Mol. Microbiol. *44*, 1269-1286.

Kehl-Fie, T.E., Zhang, Y., Moore, J.L., Farrand, A.J., Hood, M.I., Rathi, S., Chazin, W.J., Caprioli, R.M., and Skaar, E.P. (2013). MntABC and MntH contribute to systemic *Staphylococcus aureus* infection by competing with calprotectin for nutrient manganese. Infect. Immun. *81*, 3395-3405.

Klevens, R.M., Morrison, M.A., Nadle, J., Petit, S., Gershman, K., Ray, S., Harrison, L.H., Lynfield, R., Dumyati, G., Townes, J.M.*, et al.* (2007). Invasive methicillin-resistant *Staphylococcus aureus* infections in the United States. Jama *298*, 1763-1771.

Kumar, K.K., Lowe, E.W., Jr., Aboud, A.A., Neely, M.D., Redha, R., Bauer, J.A., Odak, M., Weaver, C.D., Meiler, J., Aschner, M.*, et al.* (2014). Cellular manganese content is developmentally regulated in human dopaminergic neurons. Sci. Rep. *4*, 6801.

Li, H., and Durbin, R. (2009). Fast and accurate short read alignment with Burrows-Wheeler transform. Bioinformatics *25*, 1754-1760.

Limbago, B.M., Kallen, A.J., Zhu, W., Eggers, P., McDougal, L.K., and Albrecht, V.S. (2014). Report of the 13th vancomycin-resistant *Staphylococcus aureus* isolate from the United States. J. Clin. Microbiol. *52*, 998-1002.

Lo, C.C., and Chain, P.S. (2014). Rapid evaluation and quality control of next generation sequencing data with FaQCs. BMC bioinformatics *15*, 366.

Ma, Z., Jacobsen, F.E., and Giedroc, D.P. (2009). Coordination chemistry of bacterial metal transport and sensing. Chem. Rev. *109*, 4644-4681.

Mergenhagen, K.A., and Borton, A.R. (2014). Vancomycin nephrotoxicity: a review. J. Pharm. Pract. *27*, 545-553.

Poppel, A.K., Vogel, H., Wiesner, J., and Vilcinskas, A. (2015). Antimicrobial peptides expressed in medicinal maggots of the blow fly *Lucilia sericata* show combinatorial activity against bacteria. Antimicrob. Agents Chemother. *59*, 2508-2514.

Robinson, M.D., McCarthy, D.J., and Smyth, G.K. (2010). edgeR: a Bioconductor package for differential expression analysis of digital gene expression data. Bioinformatics *26*, 139-140.

Rolfe, M.D., Rice, C.J., Lucchini, S., Pin, C., Thompson, A., Cameron, A.D., Alston, M., Stringer, M.F., Betts, R.P., Baranyi, J.*, et al.* (2012). Lag phase is a distinct growth phase that prepares bacteria for exponential growth and involves transient metal accumulation. J. Bacteriol. *194*, 686-701.

Sterne, M. (1946). Avirulent anthrax vaccine. Onderstepoort J. Vet. Sci. Anim. Ind. *21*, 41-43.

Sweeney, D.A., Hicks, C.W., Cui, X., Li, Y., and Eichacker, P.Q. (2011). Anthrax infection. Am. J. Respir. Crit. Care Med. *184*, 1333-1341.

Tong, S.Y., Davis, J.S., Eichenberger, E., Holland, T.L., and Fowler, V.G., Jr. (2015). *Staphylococcus aureus* infections: epidemiology, pathophysiology, clinical manifestations, and management. Clin. Microbiol. Rev. *28*, 603-661.

Winterbourn, C.C. (1995). Toxicity of iron and hydrogen peroxide: the Fenton reaction. Toxicol. Lett. *82-83*, 969-974.

Zimlichman, E., and Levin-Scherz, J. (2013). The coming golden age of disruptive innovation in health care. J. Gen. Intern. Med. *28*, 865-867.

CHAPTER VII

SUMMARY AND SIGNIFICANCE

Bacterial infections remain a top ten cause of death worldwide, and yet development of novel classes of antimicrobial agents has stagnated (Luepke et al., 2017). Certain pathogens have been highlighted by the WHO and CDC as high priority organisms for identification of new therapies and antibiotic stewardship practices due to their threat to human health (CDC, 2013; WHO, 2017). *A. baumannii* was named as the top 'critical threat' organism requiring antibiotic development by the World Health Organization in 2017 because of extensive antibiotic resistance (WHO, 2017). *A. baumannii* triggers hospital outbreaks and multi-drug *Acinetobacter* infections cost more than $1.6 billion per year in the United States alone (Nelson et al., 2016). *S. aureus* has been a leading cause of infection in the United States for several decades (Uhlemann et al., 2014). As a result, the CDC has named methicillin-resistant *S. aureus* a 'serious threat' (CDC, 2013). These facts highlight the importance of studying the mechanisms by which *A. baumannii* and *S. aureus* overcome vertebrate immunity to persist in the host and cause infection. Thus, my research has focused on interrogating critical nutrient acquisition and utilization during infection with the goal of identifying novel strategies for developing antimicrobial small molecules and preventing infections.

We posit that manganese is a conserved requirement for bacteria to cause infection. Mn transport machinery promotes fitness of multiple bacterial species in murine models of infection (reviewed in Chapter I). The bacterial species shown to use Mn transport proteins

during infection are quite diverse, ranging from a requirement for Mn import for *S.* Typhimurium virulence to a role for Mn export in infection by Group A *Streptococcus* (Turner et al., 2015; Zaharik et al., 2004). Thus, mechanisms for maintaining Mn levels within the cell may represent conserved processes to target via antimicrobial agents. However, these examples also highlight that the requirement for Mn varies based on the organism and, possibly, the site of infection. Moreover, the cellular processes for which bacteria require Mn continue to be relatively obscure, with some knowledge of Mn-dependent enzymes in model organisms *E. coli* and *B. subtilis*, but a poor understanding of Mn-dependent enzymes in *S. aureus* and essentially no identified Mn-dependent enzymes in *A. baumannii.* Additionally, it is unknown whether Mn levels within the host alter the pathogenesis of infection or infection outcomes. Finally, there are no previously identified strategies to manipulate Mn levels within a bacterium by drugs, and it is unclear whether metal level manipulation is a viable antimicrobial strategy. To address these gaps in knowledge, my thesis research has focused on (1) defining bacterial strategies for acquiring and utilizing Mn during infection, (2) understanding host factors related to Mn homeostasis during infection, and (3) investigating a novel small molecule modulator of bacterial metal homeostasis.

Defining bacterial factors involved in Mn homeostasis and utilization

The role of Mn import in *A. baumannii* infection

The data presented in Chapter II defines *mumT* as an Nramp-family transporter important for maintaining cellular Mn levels *in vitro* and demonstrates that *mumT* contributes to fitness of *A. baumannii* in the lung and ability of *A. baumannii* to disseminate

to the liver. This work establishes that Mn is important for *A. baumannii* during infection, and that *mumT* is a critical factor for Mn homeostasis. Interestingly, deletion of *mumT* alone leads to an increase in growth lag for *A. baumannii.* This is in contrast to other pathogens which often express multiple semi-redundant Mn transporters, leading to very subtle deficits if only one transporter is genetically inactivated (Zaharik et al., 2004). Because deletion of *mumT* imparts a growth defect, I hypothesize that either *mumT* is the dominant Mn transporter in our growth conditions or *A. baumannii* does not encode additional Mn import systems. Therefore, Mn import represents a potential weakness of *A. baumannii.* This is useful information for attempts to target multiple metal import systems via combination therapy, as Mn import could be targeted via a single transporter.

Investigating bacterial Mn-requiring processes

While the importance of Mn to *A. baumannii* and *S. aureus* was implied by studies demonstrating that calprotectin-mediated Mn chelation inhibited growth, the specific cellular processes that require Mn remain obscure. Throughout this work, multiple different strategies were pursued to identify potential Mn-dependent processes and the role of Mn during infection. Similar strategies could be employed in other bacteria to identify processes reliant on cellular Mn.

The first strategy utilized genomic context as a clue for Mn-requiring processes (Chapters II-III). After *mumT* was identified as a Mn transporter in *A. baumannii,* the genomic context of *mumT* was queried in all sequenced *A. baumannii* genomes. This search revealed that *mumT* is encoded within an operon containing genes predicted to function in urea metabolism, suggesting that one or more of the protein products may require Mn for function. Indeed, MumC is predicted to encode a urea carboxylase enzyme whose activity

requires a divalent metal. While specific enzymatic characterization of MumC and its metal-binding properties has not been completed because of time limitations, it has been shown that *A. baumannii* can utilize urea as a sole nitrogen source in a *mumC*-dependent fashion, and that *A. baumannii* cannot grow on urea when the medium is chelated of Mn by calprotectin. Together, these results suggest that urea metabolism via MumC is a Mn-requiring process that requires activity in *A. baumannii.*

The strategy of investigating genomic context also revealed that a LysR-family transcriptional regulator is encoded adjacent to the *mum* operon in all sequenced *A. baumannii* species, suggesting that this regulator may be involved in genetic regulation of this operon. Indeed, *mumR* activates transcription of the *mum* operon. I posited that *mumR* may be involved in the regulation of multiple Mn-dependent processes or a mechanism to upregulate Mn uptake when the cell requires additional Mn. Data presented in Chapter III demonstrate that *mumR* is important for growing in the presence of hydrogen peroxide, although it is not as essential under these conditions as the canonical hydrogen peroxide stress regulator OxyR. I hypothesize that *mumR* regulates multiple Mn dependent processes, and that some of these are important for replication in the presence of hydrogen peroxide. Studies to identify these targets are ongoing.

A candidate approach was taken to identify Mn-requiring processes in *S. aureus* that are important for infection of the murine heart. By manipulating the Mn levels in the heart through alterations in dietary Mn, an environment that enhanced *S. aureus* virulence in a Mn-dependent manner was created. Previous studies identified reactive oxygen species as a stressor that can be detoxified by Mn (Lisher and Giedroc, 2013). Data presented in Chapter IV demonstrates that Mn enhances the infection by *S. aureus* Δ*sodA*/*sodM* a

thousand fold in the heart, demonstrating that Mn is a rate-limiting reagent for superoxide-sensitive *S. aureus in vivo*. These findings reveal that *S. aureus* utilizes a Mn-dependent method for surviving reactive oxygen species during infection independent of the previously identified superoxide dismutase enzymes. The mechanism of protection remains to be identified. Regardless, these results demonstrate that therapeutic Mn limitation may sensitize *S. aureus* to killing by components of the vertebrate immune system.

Finally, the transcriptomics approach employed in Chapter VI may reveal Mn-dependent processes in *S. aureus*. RNAsequencing was performed on *S. aureus* that was treated with the compound '921, which alters metal homeostasis in the cell. A number of genes that were downregulated by '921 treatment are homologs to Mn-dependent processes in eukaryotes, including glutamine amidotransferase, pyruvate carboxylase, and fructose bisphosphatase (Holmes et al., 1973; Kirtley and Dix, 1971; Mildvan et al., 1966). I hypothesize that these enzymes are downregulated because non-cognate metal efflux causes mis-metallation of these enzymes and toxicity. Further investigation of the genes down-regulated by '921 treatment, especially those whose expression is rescued by Mn co-treatment, may reveal multiple Mn-dependent processes in *S. aureus*.

Understanding host factors related to Mn and immune defense against infection

Considering dietary Mn intake as an infection risk factor

The findings reported in Chapter IV reveal that high intake of dietary Mn increases *S. aureus* virulence. *S. aureus* colonized the hearts of mice fed excess dietary Mn to higher CFU than mice fed control diet, while dietary Mn did not alter bacterial burdens in the

liver. This result is intriguing because intravenous drug use is a major risk factor for *S. aureus* heart infection in humans, which almost exclusively manifests as endocarditis of the heart valves (Tong et al., 2015). A Mn-containing intravenous drug can elevate tissue Mn levels, and heroin is sometimes cut with Mn (Sikk et al., 2013; Sikk et al., 2011; Infante et al, 1999). It is possible that the increased risk of endocarditis in IV drug users could be solely due to bacteria gaining access to the bloodstream; however, a study investigating the development of endocarditis in hospitalized patients with bacteremia observed higher rates of endocarditis in IV drug users compared to other patients with bacteremia (Le Moing et al., 2015; Tong et al., 2015). Perhaps the preferential involvement of the heart in IV drug users is related to enhanced Mn availability.

It is premature to state without equivalence that foods with high levels of Mn should be avoided, as many foods high in Mn are nutritious plant-based foods. Mn is also a cofactor for many important enzymes in humans, such as arginase and enzymes involved in sugar metabolism (Aschner and Aschner, 2005). The fact that Mn strongly enhances *S. aureus* infection warrants follow-up studies in groups that consume more than the recommended daily value of Mn. For example, nearly every source of dietary Mn is plant-based, including grains such as oats, fruits such as raspberries, greens such as kale, and legumes such as garbanzo beans (Price et al., 2012). While the recommended daily value of Mn is 2 mg for an adult, those consuming a vegetarian diet may consume significantly more per day (Trumbo et al., 2001). Mn consumption is even in vegan diets, likely because most plant-derived protein sources have greater than 2 mg of Mn in a single serving and plant-based for dairy products are high in Mn, whereas dairy is essentially Mn-free (Haddad et al., 1999; Price et al., 2012). The fact that these diets certainly promote health

in most individual do not contradict the finding that dietary Mn enhances *S. aureus* heart infection. Rather, there are two distinct possibilities; one, that in the setting of a well-balanced diet with diverse natural sources of mineral uptake, perhaps excessive Mn intake does not have detrimental effects. The second possibility is that high levels of Mn intake may alter the course of infection after *S. aureus* has established infection without changing the risk of developing infection.

This is to my knowledge the first study investigating the role of dietary Mn on infection outcomes, and the results caution against Mn supplementation, particularly in at-risk groups. One example of an at-risk group where there is an opportunity to modify clinical procedure is in long-term parenteral nutrition. Mn levels rise during long-term parenteral nutrition and patients receiving this type of therapy often have concomitant medical conditions that increase their risk of infection (Btaiche et al., 2011). Our results suggest that Mn should not be included at a high concentration in intravenous feeding formulas because of the possibility of poor infection outcomes.

Mn sequestration by calprotectin is tissue dependent

Calprotectin was previously identified as a metal-sequestering protein that is broadly antimicrobial *in vitro* (Damo et al., 2013). Work presented in this Thesis demonstrate that the contribution of calprotectin Mn restriction is tissue-specific. For instance, data from Chapter II demonstrate that *A. baumannii* Δ*mumT* is attenuated in both the liver and the lung of wild-type mice. In calprotectin-deficient mice, *A. baumannii* Δ*mumT* is no longer attenuated in the liver, suggesting that Mn is available to *A. baumannii* in these conditions. In contrast, *A. baumannii* Δ*mumT* is still attenuated in the lungs of calprotectin-deficient mice; thus, loss of calprotectin is not sufficient to increase Mn

bioavailability in the lung. A parallel phenotype was observed in *S. aureus* infection. Specifically, increasing dietary Mn levels enhanced *S. aureus* infection in the heart, where chelation of Mn by calprotectin is not effective, but dietary Mn did not alter infection in the liver, where calprotectin successfully chelates Mn. This work adds to previous evidence that calprotectin is capable of sequestering Zn in the liver and in the gut, but calprotectin-deficient mice do not have enhanced Mn bioavailability in the gut (Diaz-Ochoa et al., 2016). Taken as a whole, I propose that the ability of calprotectin to sequester metals is altered by the tissue microenvironment.

Designing therapies that manipulate metal homeostasis as an antimicrobial strategy

Metal homeostasis has been previously targeted for antibacterial therapy through several avenues with little success. Fe chelators were tested in animal infection models as an attempt to limit Fe availability to pathogens. Morosely, in some attempts Fe chelators enhanced infection (Jones et al., 1977; Marx, 2002; Robins-Browne and Prpic, 1985). It is believed this failure occurred because the chelators prevented mammalian cells from importing Fe as a means to sequester this metal. Recent attempts to develop a *S. aureus* vaccine have included metal import systems as antigens, including the proteins required for heme import and MntC, although no vaccine has yet been found to be protective (Fowler et al., 2013; Nissen et al., 2015). I suspect that this vaccine was not protective in part because metal transport proteins are not constitutively expressed by *S. aureus* during infection, permitting some cells to escape antibodies that bind specifically intermittently expressed antigens. In sum, previous attempts to target metal homeostasis as an antimicrobial strategy have not resulted in viable therapies.

The data presented in Chapter VI establish compound ‘921 as a lead compound for developing antimicrobials that target metal homeostasis. While this compound was identified by its ability to modulate Mn in neurons (Kumar et al., 2014), our results demonstrate that ‘921 more broadly impacts metal homeostasis, at least at high concentrations in exponential phase cells. This may be a reasonable therapeutic platform for a number of reasons. First, ‘921 boasts both bactericidal and bacteriostatic activity depending on the physiological state of the cell. The beta-lactam classes of antibiotics similarly exhibit bactericidal or bacteriostatic activity and these antibiotics have been extremely successful for many infections (Satta et al., 1995). Second, ‘921 was antimicrobial to multiple Gram-positive species, indicating that the mechanism of action is conserved. Third, despite many efforts, we were unable to generate spontaneously resistant strains. While this does not mean that resistance could not occur with therapeutic use, it does suggest that there is not a straightforward, monogenic path to resistance. Finally, ‘921 has synergistic activity with metal levels such that activity is enhanced by both low or high concentrations of metal in the growth medium. From this we predict that ‘921 would have antimicrobial activity at multiple sites of infection throughout the body and act in synergy with nutritional immunity. Thus we propose that ‘921 is a useful lead compound for antibiotic development.

However, there are several concerns regarding ‘921 as a potential therapeutic that will have to be addressed if it is to be developed into an antibiotic. This compound was first identified in a screen against mammalian neuronal cells, and ‘921 increased intracellular Mn levels in these cells (Kumar et al., 2014). Perhaps ‘921 exerts the same function of enhanced metal import both in eukaryotic cells and mammalian cells, which

could cause unwanted side effects in patients. While no overt toxicity from ‘921 was observed in mammalian cells (data not shown), it is important that future compounds developed using ‘921 as a scaffold consider activity in mammalian cells. It is possible that ‘921 enhancing host cell metal uptake may actually enhance its antimicrobial activity, as decreased extracellular metal levels would presumably inhibit bacterial growth, but this consideration must be carefully balanced with potential toxicity to host cells. Secondly, ‘921 is not stable under certain conditions, including lengthy incubation with bacterial growth medium (Chapter VI). Compound instability is a substantial drawback for bioavailability and duration of activity *in vivo*. Stability may be improved by modifications to the compound or by packaging ‘921 in such a way that it is exposed to the environment only at the site of infection.

References

Aschner, J.L., and Aschner, M. (2005). Nutritional aspects of manganese homeostasis. Mol. Aspects Med. *26*, 353-362.

Btaiche, I.F., Carver, P.L., and Welch, K.B. (2011). Dosing and monitoring of trace elements in long-term home parenteral nutrition patients. J. Parenter. Enteral. Nutr. *35*, 736-747.

CDC (2013). Antibiotic resistance threats in the United States, 2013. https://www.cdc.gov/drugresistance/pdf/ar-threats-2013-508.pdf

Damo, S.M., Kehl-Fie, T.E., Sugitani, N., Holt, M.E., Rathi, S., Murphy, W.J., Zhang, Y., Betz, C., Hench, L., Fritz, G.*, et al.* (2013). Molecular basis for manganese sequestration by calprotectin and roles in the innate immune response to invading bacterial pathogens. Proc. Natl. Acad. Sci. *110*, 3841-3846.

Diaz-Ochoa, V.E., Lam, D., Lee, C.S., Klaus, S., Behnsen, J., Liu, J.Z., Chim, N., Nuccio, S.P., Rathi, S.G., Mastroianni, J.R.*, et al.* (2016). *Salmonella* mitigates oxidative stress and thrives in the inflamed gut by evading calprotectin-mediated manganese sequestration. Cell Host & Microbe *19*, 814-825.

Fowler, V.G., Allen, K.B., Moreira, E.D., Moustafa, M., Isgro, F., Boucher, H.W., Corey, G.R., Carmeli, Y., Betts, R., Hartzel, J.S*., et al.* (2013). Effect of an investigational vaccine for preventing *Staphylococcus aureus* infections after cardiothoracic surgery: a randomized trial. JAMA *309*, 1368-1378.

Haddad, E.H., Berk, L.S., Kettering, J.D., Hubbard, R.W., and Peters, W.R. (1999). Dietary intake and biochemical, hematologic, and immune status of vegans compared with nonvegetarians. Am. J. Clin. Nutr. *70*, 586S-593S.

Holmes, E.W., McDonald, J.A., McCord, J.M., Wyngaarden, J.B., and Kelley, W.N. (1973). Human glutamine phosphoribosylpyrophosphate amidotransferase. Kinetic and regulatory properties. J. Biol. Chem. *248*, 144-150.

Infante, F., Dominguez, E., Trujillo, D. and Luna, A. (1999). Metal contamination in illicit samples of heroin. J. Forensic Sci. *44*, 110-113

Jones, R.L., Peterson, C.M., Grady, R.W., Kumbaraci, T., Cerami, A., and Graziano, J.H. (1977). Effects of iron chelators and iron overload on *Salmonella* infection. Nature *267*, 63-65.

Kirtley, M.E., and Dix, J.C. (1971). Activation of fructose diphosphatase by manganese, magnesium and cobalt. Arch. Biochem. Biophys. *147*, 647-652.

Kumar, K.K., Lowe, E.W., Jr., Aboud, A.A., Neely, M.D., Redha, R., Bauer, J.A., Odak, M., Weaver, C.D., Meiler, J., Aschner, M*., et al.* (2014). Cellular manganese content is developmentally regulated in human dopaminergic neurons. Sci. Rep. *4*, 6801.

Le Moing, V., Alla, F., Doco-Lecompte, T., Delahaye, F., Piroth, L., Chirouze, C., Tattevin, P., Lavigne, J.P., Erpelding, M.L., Hoen, B*., et al.* (2015). *Staphylococcus aureus* Bloodstream Infection and Endocarditis--A Prospective Cohort Study. PloS one *10*, e0127385.

Lisher, J.P., and Giedroc, D.P. (2013). Manganese acquisition and homeostasis at the host-pathogen interface. Front. Cell. Infect. Microbiol. *3*, 91.

Luepke, K.H., Suda, K.J., Boucher, H., Russo, R.L., Bonney, M.W., Hunt, T.D., and Mohr, J.F., 3rd (2017). Past, present, and future of antibacterial economics: increasing bacterial resistance, limited antibiotic pipeline, and societal implications. Pharmacotherapy *37*, 71-84.

Marx, J.J. (2002). Iron and infection: competition between host and microbes for a precious element. Best Pract. Res. Clin. Haematol. *15*, 411-426.

Mildvan, A.S., Scrutton, M.C., and Utter, M.F. (1966). Pyruvate carboxylase. VII. A possible role for tightly bound manganese. J. Biol. Chem. *241*, 3488-3498.

Nelson, R.E., Schweizer, M.L., Perencevich, E.N., Nelson, S.D., Khader, K., Chiang, H.Y., Chorazy, M.L., Blevins, A., Ward, M.A., and Samore, M.H. (2016). Costs and mortality associated with multidrug-resistant healthcare-associated *Acinetobacter* infections. Infect. Control Hosp. Epidemiol. *37*, 1212-1218.

Nissen, M., Marshall, H., Richmond, P., Shakib, S., Jiang, Q., Cooper, D., Rill, D., Baber, J., Eiden, J., Gruber, W.*, et al.* (2015). A randomized phase I study of the safety and immunogenicity of three ascending dose levels of a 3-antigen *Staphylococcus aureus* vaccine (SA3Ag) in healthy adults. Vaccine *33*, 1846-1854.

Price, C.T., Langford, J.R., and Liporace, F.A. (2012). Essential Nutrients for Bone Health and a Review of their Availability in the Average North American Diet. Open Orthop. J. *6*, 143-149.

Robins-Browne, R.M., and Prpic, J.K. (1985). Effects of iron and desferrioxamine on infections with *Yersinia enterocolitica*. Infect. Immun. *47*, 774-779.

Satta, G., Cornaglia, G., Mazzariol, A., Golini, G., Valisena, S., and Fontana, R. (1995). Target for bacteriostatic and bactericidal activities of beta-lactam antibiotics against *Escherichia coli* resides in different penicillin-binding proteins. Antimicrob. Agents Chemother. *39*, 812-818.

Sikk, K., Haldre, S., Aquilonius, S.M., Asser, A., Paris, M., Roose, A., Petterson, J., Eriksson, S.L., Bergquist, J., and Taba, P. (2013). Manganese-induced parkinsonism in methcathinone abusers: bio-markers of exposure and follow-up. Eur. J. Neurol. *20*, 915-920.

Sikk, K., Haldre, S., Aquilonius, S.M., and Taba, P. (2011). Manganese-induced parkinsonism due to ephedrone abuse. Parkinsons Dis. *2011*, 865319.

Tong, S.Y., Davis, J.S., Eichenberger, E., Holland, T.L., and Fowler, V.G., Jr. (2015). *Staphylococcus aureus* infections: epidemiology, pathophysiology, clinical manifestations, and management. Clin. Microbiol. Rev. *28*, 603-661.

Trumbo, P., Yates, A.A., Schlicker, S., and Poos, M. (2001). Dietary reference intakes: vitamin A, vitamin K, arsenic, boron, chromium, copper, iodine, iron, manganese, molybdenum, nickel, silicon, vanadium, and zinc. J. Am. Diet. Assoc. *101*, 294-301.

Turner, A.G., Ong, C.L., Gillen, C.M., Davies, M.R., West, N.P., McEwan, A.G., and Walker, M.J. (2015). Manganese homeostasis in group A *Streptococcus* is critical for resistance to oxidative stress and virulence. mBio *6*.

Uhlemann, A.C., Otto, M., Lowy, F.D., and DeLeo, F.R. (2014). Evolution of community- and healthcare-associated methicillin-resistant *Staphylococcus aureus*. Infect. Genet. Evol. *21*, 563-574.

WHO (2017). Global priority list of antibiotic-resistant bacteria to guide research, discovery, and development of new antibiotics. http://www.who.int/medicines/publications/WHO-PPL-Short_Summary_25Feb-ET_NM_WHO.pdf.

Zaharik, M.L., Cullen, V.L., Fung, A.M., Libby, S.J., Kujat Choy, S.L., Coburn, B., Kehres, D.G., Maguire, M.E., Fang, F.C., and Finlay, B.B. (2004). The *Salmonella enterica* serovar typhimurium divalent cation transport systems MntH and SitABCD are essential for virulence in an Nramp1G169 murine typhoid model. Infect. Immun. *72*, 5522-5525.

CHAPTER VIII

FUTURE DIRECTIONS

Define the role of OxyR and MumR in defense against host-derived oxidants

In Chapter III, I characterize the transcriptional regulators OxyR and MumR and their role in defense against hydrogen peroxide *in vivo* and present data demonstrating that both Δ*mumR* and Δ*oxyR* have decreased fitness in a murine pneumonia model. However, there are still open areas of investigation regarding the role of these regulators during the response to infection of the host.

1. Defining the regulons of OxyR and MumR

Preliminary qRT-PCR analyses (Chapter III) demonstrate that Δ*mumR* may regulate some genes predicted to be involved in hydrogen peroxide detoxification in rich medium, whereas Δ*oxyR* is required for upregulation of a non-overlapping subset of hydrogen peroxide detoxification machinery when exposed to hydrogen peroxide. To define the genes regulated by MumR and OxyR, RNASequencing is being performed on Δ*mumR* and Δ*oxyR* strains exposed to hydrogen peroxide, with WT and non-exposed controls. Examination of the resultant data set will permit identification of genes regulated in response to hydrogen peroxide in an OxyR- or MumR- dependent manner. Electromobility shift assays, such as those performed for OxyR in Chapter III, will be utilized to determine direct promoter binding by recombinant OxyR or MumR. These experiments will define the regulons of OxyR and MumR in hydrogen peroxide exposed conditions.

2. Evaluating functional redundancy of OxyR and MumR

Δ*mumR* and Δ*oxyR* both have growth defects in hydrogen peroxide, but cells lacking *oxyR* are pre-adapted to hydrogen peroxide stress in the logarithmic phase of growth (Chapter III). This result suggests that there is a mechanism for up-regulating detoxification machinery in the absence of *oxyR.* To determine whether *mumR* is required for this result, and whether *oxyR* and *mumR* perform redundant functions, a double knockout of *mumR* and *oxyR* will be generated. This strain (Δ*mumR*Δ*oxyR*) will be evaluated for pre-adaptation to hydrogen peroxide stress, growth in the presence of hydrogen peroxide, and fitness in a murine model of pneumonia. If *oxyR* and *mumR* are functionally redundant, I would anticipate Δ*mumR*Δ*oxyR* to be substantially less fit than either single mutant under conditions of oxidative stress.

3. Genes required for resistance of Δ*oxyR* to log phase killing

Δ*oxyR* is highly resistant to H_2O_2 killing in mid-exponential growth. I hypothesize this is because peroxide stress detoxification machinery is induced in a compensatory and non-OxyR mediated manner during *A. baumannii* aerobic growth, and that this machinery 'primes' Δ*oxyR* to be resistant to H_2O_2 treatment. To identify genes required for the resistance of Δ*oxyR* under these conditions, a mariner transposon library will be made in Δ*oxyR.* This library will be screened for transposon mutants that are more susceptible to killing by H_2O_2 than Δ*oxyR.*

4. Importance of NADPH oxidase derived oxidants on *A. baumannii* host defense

I hypothesize that host-derived oxidants are vital for the defense against *A. baumannii* infection. To test this hypothesis, mice lacking NADPH oxidase (*Phox*$^{-/-}$) will

be infected with *A. baumannii* and evaluated for the ability to control bacterial replication. The relative fitness of Δ*oxyR* and Δ*mumR* will also be defined in this knockout mouse. I anticipate that *oxyR* and *mumR* are more important for infection of WT mice than mice that lack the immune-cell derived oxidative burst.

5. Role of *mumR* and *oxyR* in other *A. baumannii* strains

A. baumannii isolates exhibit tremendous genetic and phenotypic diversity. As such, it is important to confirm findings from one strain in another strain. To determine the role for *oxyR* and *mumR* in other species, AB5075 isolates containing mutations in the genes of interest will be ordered from the University of Washington's defined transposon library (Gallagher et al., 2015). These transposon mutants will be confirmed and fitness in the presence of hydrogen peroxide will be evaluated. These experiments will permit us to determine the conservation of *mumR* function in hydrogen peroxide stress response across *A. baumannii* strains.

Elucidate the function of *A. baumannii* urea carboxylase

In chapter III, I introduced the urea carboxylase MumC. Preliminary evidence suggests that Δ*mumC* is less virulent in a systemic model of *A. baumannii* infection, and that *mumC* contributes to acidic stress resistance in *A. baumannii.* Extensive work remains to characterize the function and role of MumC during infection. First, MumC will be over-expressed and purified from *E. coli* in order to perform enzymatic assays. Published protocols will be utilized to determine if MumC functions as an ATP and biotin-dependent urea carboxylase (Kanamori et al., 2004). The hypothesis that MumC is a Mn-utilizing enzyme will also be tested *in vitro*: Mn, Mg, Co, and Zn will be added and enzymatic

activity will be monitored. Second, I hypothesize that Δ*mumC* is less fit in a systemic model of *A. baumannii* infection because it this mutant is sensitive to acidic stress experienced during infection. Acidic stress is likely experienced by phagocytosed bacteria, as the phagolysosome is acidic (Cech and Lehrer, 1984). To test whether *A. baumannii* lacking *mumC* is sensitive to acidic stress following phagocytosis, intracellular survival of *A. baumannii* will be assayed using a gentamicin-protection assay. Lung epithelial cells and macrophage-like RAW cells will be utilized for this assay. These experiments will elucidate the function of MumC and whether there is a role for MumC in intracellular survival.

Interrogate the function, regulation, and virulence contribution of probable Mn exporter NWMN_2316 in *S. aureus.*

NWMN_2316 was highly upregulated in RNASeq data obtained under conditions of 1 mM Mn. NWMN_2316 was also the only upregulated gene that met our significance cutoffs (Chapter VI). NWMN_2316 is predicted to encode a cation diffusion facilitator protein, a membrane embedded protein involved in metal efflux under toxic conditions (Kolaj-Robin et al., 2015). It appears to be homologous to the recently described MntP in *Bacillus subtilis*, which is described as an MntR-regulated Mn efflux protein that is required for resistance to Mn stress (Huang et al., 2017). We have explored the roles of Mn import proteins in *S. aureus* virulence but until now had not identified a reciprocal system involved in Mn detoxification. I hypothesize that NWMN_2316 is regulated by MntR, mediates Mn resistance, and that NWMN_2316 will contribute to virulence in specific niches within the host – perhaps in niches where MntABC and MntH are less important

(i.e. the liver, in mice fed high Mn diet, etc). To evaluate this, I propose generating an in-frame deletion mutant of *NWMN_2316* using pKOR1-mediated allelic replacement (Bae and Schneewind, 2006). This mutant will be tested for tolerance to Mn toxicity using growth curves and complementation of the gene on the chromosome will be used to determine the specificity of the finding. As we have a *mntR* mutant in hand, the regulation of *NWMN_2316* transcription will be assessed in an MntR mutant under conditions of Mn toxicity. A *NWMN_2316* promoter-driven luciferase reporter system will also be generated to evaluate expression of *NWMN_2316 in vivo.* Finally, the fitness of the *NWMN_2316*-inactivated strain will be evaluated using our systemic model of infection, both in WT mice, calprotectin-deficient mice, and mice fed a high Mn diet.

Define the tissue-specific metal microenvironment experienced by bacterial pathogens

Bacterial fitness in culture is dependent on sufficient availability of essential metals. Infection models have permitted this observation to be extended to fitness of bacteria within the host during infection. In our laboratory, we have both measured the concentrations of essential metals in infected mouse tissue and image the distribution of metal relative to infectious foci. Comparing this information with the fitness of bacterial mutants that are deficient in uptake of metal nutrients has been enlightening, revealing that there are tissue-specific differences in metal bioavailability that is not strictly governed by metal concentrations. For instance, in Chapter IV I present data that high Mn diet only impacts *S. aureus* fitness in specific tissues, i.e. the heart and not the liver, fitting with the hypothesis that the liver and the heart have differential Mn bioavailability in their

environment. Metal restriction in different tissues may be a factor of both concentration of metal and the presence of host metal restricting proteins or small molecule chelators. The results we have gathered so far only paint part of the picture of the metal environment of the tissue that is infected.

Understanding the metal microenvironment of multiple tissues is important from a drug and vaccine development standpoint. Developing therapeutics that target metal transport proteins or vaccines that use metal transport proteins as antigens relies on consistent expression of these targets *in vivo.* However, I hypothesize that some environments in the host will not require the expression of these targets. Therefore, I propose to interrogate the metal bioavailability of infected tissues by measuring the bacterial and host mRNA levels of metal-regulated genes to fully characterize the bioavailability of metal and the response to this bioavailability during infection. Furthermore, I suggest characterizing how diet and the immune response alter the tissue-specific bioavailability of metal in an unbiased and global way.

As a means for testing this, we have designed custom-synthesized libraries for highly specific quantification of transcripts from mixed samples using Nanostring technology (Barczak et al., 2012). Three libraries have been synthesized for the analysis of transcripts of three diverse bacterial pathogens, *A. baumannii, C. difficile,* and *S. aureus.* Each library contains 100 probes that permit quantification of 100 individual genes (see for the *S. aureus* nanostring library). Within each library, we have included host and bacterial transcripts that are regulated by Mn, Fe, or Zn availability or are related to processes that require Mn, Fe, or Zn for function. By comparing the abundance of transcripts related to metal homeostasis with the housekeeping genes included in each

panel, we will define the metalloregulation by both the host and the bacterium at the site of infection. We will interrogate expression of bacterial proteins in heart, liver, kidney, lung, gastrointestinal tract, and skin. It will be fascinating to compare the transcriptional profile between a single organism infecting different tissue and to compare the same tissue across multiple organisms. Finally, the system will be manipulated by the introduction of specific mouse and or bacterial gene knockouts or variation in dietary metal.

Table 12. *S. aureus* nanostring library.

Gene name	Gene identifier	mRNA identifier	Notes
3-OH butyrate dehydrogenase	Bdh2	NM_027208.1:130	Host Fe binding
Ceruloplasmin	Cp	NM_001042611.1:1750	Host Cu binding
Hepcidin	Hamp	NM_032541.1:202	Host Fe binding
Hemoglobin	Hba-a1	NM_008218.2:26	Host Fe binding
Hmox1	Hmox1	NM_010442.2:610	Host heme binding
Lcn2	Lcn2	NM_008491.1:190	Host Fe binding
Ltf	Ltf	NM_008522.3:2545	Host Fe binding
Flvcr1b	Mfsd7b	NM_001081259.1:394	Host heme transport
MT1	Mt1	NM_013602.3:135	Host Zn binding
Mt2a	Mt2	NM_008630.2:105	Host Zn binding
Nitric oxide synthase	Nos2	NM_010927.3:3715	Host ROS
nptA	NWMN_RS00285	NWMN_RS00285.1:618	Metal transporter
sirA	NWMN_RS00335	NWMN_RS00335.1:120	Fe acquisition
sbnA	NWMN_RS00340	NWMN_RS00340.1:335	Fe acquisition
sbnD	NWMN_RS00355	NWMN_RS00355.1:394	Fe acquisition
sodM	NWMN_RS00435	NWMN_RS00435.1:193	ROS
isdI	NWMN_RS00615	NWMN_RS00615.1:5	Fe acquisition
orfX	NWMN_RS00620	NWMN_RS00620.1:21	Fe acquisition
fepA	NWMN_RS01905	NWMN_RS01905.1:428	Fe acquisition
tatA	NWMN_RS01925	NWMN_RS01925.1:114	Fe acquisition
ahpF	NWMN_RS02100	NWMN_RS02100.1:636	ROS
ahpC	NWMN_RS02105	NWMN_RS02105.1:222	ROS
NWMN_0471	NWMN_RS02695	NWMN_RS02695.1:1082	Heme synthesis
pdxR	NWMN_RS02810	NWMN_RS02810.1:690	Heme toxicity
pdxS	NWMN_RS02815	NWMN_RS02815.1:378	Heme toxicity
pdxT	NWMN_RS02820	NWMN_RS02820.1:298	Heme toxicity
gltX	NWMN_RS02865	NWMN_RS02865.1:393	Heme synthesis
NWMN_0543	NWMN_RS03120	NWMN_RS03120.1:211	Heme toxicity
hemQ	NWMN_RS03155	NWMN_RS03155.1:424	Heme synthesis
mntA	NWMN_RS03435	NWMN_RS03435.1:260	Mn acquisition
mntR	NWMN_RS03440	NWMN_RS03440.1:111	Mn regulation
fhuC	NWMN_RS03505	NWMN_RS03505.1:344	Fe acquisition
sstA	NWMN_RS03980	NWMN_RS03980.1:173	Fe acquisition
sstD	NWMN_RS03995	NWMN_RS03995.1:216	Fe acquisition
lgt	NWMN_RS04130	NWMN_RS04130.1:365	Bacterial housekeeping
NWMN_0783	NWMN_RS04430	NWMN_RS04430.1:78	Bacterial housekeeping
NWMN_0815	NWMN_RS04610	NWMN_RS04610.1:705	Zn responsive
mntH	NWMN_RS05440	NWMN_RS05440.1:106	Mn acquisition

isdA	NWMN_RS05890	NWMN_RS05890.1:605	Heme acquisition
isdC	NWMN_RS05895	NWMN_RS05895.1:412	Heme acquisition
srtB	NWMN_RS05915	NWMN_RS05915.1:74	Heme acquisition
isdG	NWMN_RS05920	NWMN_RS05920.1:11	Heme degradation
fur	NWMN_RS07935	NWMN_RS07935.1:53	Fe regulation
sodA	NWMN_RS08215	NWMN_RS08215.1:347	Oxidative stress
zur	NWMN_RS08220	NWMN_RS08220.1:316	Zn regulation
hemL	NWMN_RS08755	NWMN_RS08755.1:767	Heme synthesis
hemX	NWMN_RS08775	NWMN_RS08775.1:340	Heme synthesis
hemA	NWMN_RS08780	NWMN_RS08780.1:450	Heme synthesis
hemY	NWMN_RS09715	NWMN_RS09715.1:558	Heme synthesis
hemH	NWMN_RS09720	NWMN_RS09720.1:301	Heme synthesis
16S rRNA	NWMN_RS10020	NWMN_RS10020.1:516	Bacterial housekeeping
perR	NWMN_RS10025	NWMN_RS10025.1:334	ROS regulation
bacterioferritin comigratory protein	NWMN_RS10035	NWMN_RS10035.1:113	Fe binding
hemL2	NWMN_RS10040	NWMN_RS10040.1:444	Heme synthesis
NWMN_1767	NWMN_RS10105	NWMN_RS10105.1:155	Potentially involved in heme synthesis
fhuD1	NWMN_RS11140	NWMN_RS11140.1:537	Fe acquisition
NWMN_2624	NWMN_RS11205	NWMN_RS11205.1:30	Stress response
NWMN_1953	NWMN_RS11265	NWMN_RS11265.1:224	ROS regulation
ftnA	NWMN_RS11800	NWMN_RS11800.1:167	Fe acquisition
htsC	NWMN_RS12025	NWMN_RS12025.1:430	Fe acquisition
htsA	NWMN_RS12035	NWMN_RS12035.1:221	Fe acquisition
sfaA	NWMN_RS12055	NWMN_RS12055.1:401	Fe acquisition
sfaD	NWMN_RS12060	NWMN_RS12060.1:567	Fe acquisition
fhuD2	NWMN_RS12615	NWMN_RS12615.1:576	Fe acquisition
hrtA	NWMN_RS13020	NWMN_RS13020.1:279	Heme detoxification
hssR	NWMN_RS13030	NWMN_RS13030.1:222	Heme detoxification
hssS	NWMN_RS13035	NWMN_RS13035.1:621	Heme detoxification
cysG	NWMN_RS13215	NWMN_RS13215.1:331	Related to heme synthesis
adcA	NWMN_RS13255	NWMN_RS13255.1:1051	Zn acquisition
CDF family exporter	NWMN_RS13325	NWMN_RS13325.1:387	Mn detoxification
cntA	NWMN_RS13625	NWMN_RS13625.1:650	ROS
cntM	NWMN_RS13630	NWMN_RS13630.1:533	ROS
cntK	NWMN_RS13640	NWMN_RS13640.1:266	ROS
ahpD	NWMN_RS13660	NWMN_RS13660.1:2	ROS
NWMN_2434	NWMN_RS13990	NWMN_RS13990.1:607	Perhaps Fe related
feoB	NWMN_RS14080	NWMN_RS14080.1:885	Fe acquisition
NWMN_2483	NWMN_RS14255	NWMN_RS14255.1:525	Mn regulated

NWMN_2517	NWMN_RS14455	NWMN_RS14455.1:310	Related to heme synthesis
NWMN_2582	NWMN_RS14810	NWMN_RS14810.1:678	Fe acquisition
Rpl19	Rpl19	NM_009078.1:20	Host housekeeping
S100a7	S100a7a	NM_199422.1:99	Host Zn binding
S100a8	S100a8	NM_013650.2:280	Calprotectin
S100a9	S100a9	NM_009114.2:112	Calprotectin
Slc11a1	Slc11a1	NM_013612.2:945	Host Mn/Fe transport
Slc11a2	Slc11a2	NM_008732.2:1610	Host Fe transport
Slc30a1	Slc30a1	NM_009579.3:1018	Host Zn transport
ZNT10	Slc30a10	NM_001033286.2:1975	Host Zn/Mn transport
ZnT2	Slc30a2	NM_001039677.2:580	Host Zn transport
Znt4	Slc30a4	NM_011774.2:290	Host Zn transport
ZnT5	Slc30a5	NM_022885.2:1986	Host Zn transport
Znt7	Slc30a7	NM_023214.7:500	Host Zn transport
ZIP11	Slc39a11	NM_001166503.1:1782	Host Zn transport
ZIP14	Slc39a14	NM_001135151.1:2630	Host Zn transport
ZIP4	Slc39a4	NM_028064.2:2050	Host Zn transport
ZIP7	Slc39a7	NM_001077709.1:816	Host Zn transport
ZIP8	Slc39a8	NM_001135149.1:1044	Host Zn transport
Ferroportin	Slc40a1	NM_016917.2:1716	Host Fe transport
Sod1	Sod1	NM_011434.1:406	Host ROS
Sod2	Sod2	NM_013671.3:1495	Host ROS
Tubb5	Tubb5	NM_011655.4:2260	Host housekeeping

All told, this experimental approach will reveal global differences in metal bioavailability across infection conditions in the vertebrate hosts and provide information on the diversity and consistency of metal transport gene expression, which will aid in the design of vaccine and small molecule therapies targeting these systems by identifying conserved target expression based on universal metal availability in all host tissues.

Determining the cellular and molecular mechanisms by which calprotectin promotes *S. aureus* infection

1. Determine the cellular source of calprotectin that promotes *S. aureus* infection of the heart.

Earlier work has demonstrated that calprotectin that is present in the staphylococcal abscess is predominantly produced in neutrophils (Corbin et al., 2008). However, expression studies have revealed that *S100a9* and *S100a8* are also expressed in monocytes, epithelial cells, and cardiomyocytes (Frosch et al., 2005; Lagasse and Clerc, 1988; Odink et al., 1987; Zenz et al., 2005; Zwadlo et al., 1988). *S100a9*$^{-/-}$ mice are protected from *S. aureus* heart infection and neutrophils are required for differential bacterial burdens between WT and calprotectin-deficient mice in the heart, consistent with two possible models: (1) *S100a9* modulates neutrophil function in a way that promotes *S. aureus* infection, or (2) *S100a9* modulates the function of a different cell type, but neutrophils are required as part of the response initiated by the different cell. While I favor model 1 because *S100a9*$^{-/-}$ neutrophils have an intrinsic deficit in neutrophil accumulation in the heart, reciprocal bone marrow transplant studies in Chapter V suggested that calprotectin production by hematopoietic or non-hematopoietic cells may promote *S. aureus* infection

of the heart. Therefore, the tissue origin of calprotectin that promotes infection in the heart remains unclear, and I hypothesize that non-neutrophil sources of calprotectin are important for promoting *S. aureus* infection of the heart.

To test this hypothesis, we will delete *S100a9* in a cell-type specific manner to determine in which tissue expression of *S100a9* is required to promote infection. A mouse with a floxed *S100a9* exon 3 (*S100a9*$^{fl/fl}$) is being generated by Jackson Laboratories using CRISPR-Cas. By crossing this mouse with a mouse line expressing the Cre recombinase under the control of tissue-specific promoters, tissue-specific deletions in *S100a9* will be created. We will use this technology to create *S100a9* knockouts in epithelial cells, neutrophils, monocytes, and cardiomyocytes and assess the bacterial burdens in multiple tissues following *S. aureus* infection. Furthermore, the expression of calprotectin in *S. aureus* abscesses will be quantified to determine which tissue types are required for the production of calprotectin in the staphylococcal abscess. These results will illuminate whether calprotectin expression in non-neutrophil cell types contributes to promoting *S. aureus* infection of the heart.

2. Define the molecular mechanism by which *S100a9* promotes neutrophil accumulation in the heart.

In Chapter V, I present results that suggest that calprotectin-deficient neutrophils have an inherent deficit in accumulation in *S. aureus*-infected hearts. This could be due to differences in one or more of the following stages of neutrophil accumulation: (a) production of neutrophils within the bone marrow, (b) neutrophil migration during infection, or (c) neutrophil survival within infected hearts.

2a. Interrogating role for *S100a9* in neutrophil production.

Three different experimental approaches will be used to investigate neutrophil production. First, the ability of WT and *S100a9*$^{-/-}$ neutrophils to reconstitute the bone marrow will be assessed following 1:1 mixed bone marrow transplant and reconstitution for 6 weeks. If *S100a9*$^{-/-}$ neutrophils have a deficit in equilibrium replication within the bone marrow, the neutrophil and neutrophil precursor ratios will be different in the bone marrow. This experiment will be repeated in mice infected systemically with *S. aureus,* which should increase bone marrow proliferation and reveal if there is a deficit in neutrophil or neutrophil precursor proliferation in response to an inflammatory stimulus. A second approach will involve treating *S100a9*$^{-/-}$ mice with exogenous G-CSF to stimulate bone marrow production of neutrophils. By comparing the production of neutrophils in response to this stimulus in WT and *S100a9*$^{-/-}$ mice, it will be possible to see if there is a deficit in neutrophil production. Infection of *S100a9*$^{-/-}$ mice treated with G-CSF vs. mock-treated mice will also be informative: if decreased bone-marrow production of neutrophils is responsible for decreased heart neutrophils in mice lacking *S100a9*$^{-/-}$, G-CSF should be able to increase neutrophil numbers in the heart in *S100a9*$^{-/-}$ mice. The third approach will be to label bone marrow-derived neutrophil precursors with dye to establish doubling times following transfer into a new host. Together, these experiments will reveal if *S100a9*$^{-/-}$ mice have decreased neutrophil production either at baseline or in response to proliferative stimuli.

2b. Investigating a role for *S100a9*$^{-/-}$ in neutrophil migration.

Again, a three-pronged approach will be employed to investigate the role of *S100a9*$^{-/-}$ in neutrophil migration. First, a census of relative percentages of *S100a9*$^{-/-}$ and WT neutrophils will be performed in multiple tissues of interest following 1:1 mixed bone

marrow transplant, reconstitution for 6 weeks, and *S. aureus* infection. These tissues will include the heart, blood, liver, kidney, lung, and spleen. Preliminary data testing blood and heart tissue indicates that there is no difference in the percentages of WT and *S100a9*$^{-/-}$ neutrophils in the absence of infection, suggesting that any deficit in neutrophil proliferation that may be present occurs in response to infection. This experiment will reveal whether differences in neutrophil migration are specific to the heart or are present in multiple peripheral tissues. A second approach will be to neutralize extracellular calprotectin with antibodies prior to or during infection. This will determine if neutrophil recruitment differences are due to surface-exposed calprotectin or extracellular calprotectin. Total neutrophil numbers in blood, spleen and heart will be quantified to ensure that treatment with anti-calprotectin antibodies does not result in neutrophil depletion. Finally, to determine a potential mechanism by which *S100a9*$^{-/-}$ neutrophils exhibit differential migration, surface expression and gene expression of chemotactic receptors will be measured in *S100a9*$^{-/-}$ neutrophils. An alternative approach will be to perform RNASeq on neutrophils isolated from WT and *S100a9*$^{-/-}$ mice in an attempt to uncover differentially expressed genes that could be involved in migration.

2c. Evaluating neutrophil survival in infected hearts.

A final possibility to consider is that neutrophil survival is impacted by *S100a9* expression. A time course infection will be performed on WT and *S100a9*$^{-/-}$ mice and neutrophils will be harvested periodically, beginning 12 hours post infection until 96 hours post infection. Total neutrophil numbers will be assessed to see if neutrophils migrate to the hearts but do not remain viable in the tissue in *S100a9*$^{-/-}$ mice. Additionally, neutrophils will be stained with markers for necrosis and apoptosis to evaluate what percentage of the

neutrophil population from WT and *S100a9*$^{-/-}$ mice may be undergoing cell death. Finally, WT and *S100a9*$^{-/-}$ neutrophils will be stimulated ex vivo with *S. aureus* bacterial products to determine if they exhibit differential survival following stimulation with bacterial products.

Taken together, these approaches will define the stage at which *S100a9* regulates neutrophil accumulation within infected hearts and will inform future studies investigating deeper into the mechanism of regulation.

Investigate the antimicrobial nature of calprotectin-mediated Mn chelation *in vivo.*

We have demonstrated previously that Mn is removed from *S. aureus* abscesses in the liver in a calprotectin-dependent manner. However, similar phenotypes have not been observed in *S. aureus* infected hearts or kidneys: Mn is removed from the abscess in both WT and calprotectin-deficient mice (Chapter IV). Similarly, I have observed that Δ*mumT* has a fitness deficit in the liver that is dependent on calprotectin but has a fitness deficit in the lung that is independent of calprotectin (Chapter II). These data suggest that Mn sequestration by calprotectin occurs in some but not all tissues. Furthermore, the removal of Mn from *S. aureus* abscesses in the liver requires mice that express calprotectin, but this does not prove that Mn binding by calprotectin is the mechanism of Mn removal. I hypothesize that Mn binding by calprotectin is required for removal of Mn from liver abscesses and for eliciting a Mn-starvation response in bacteria in the liver, but that Mn binding by calprotectin is dispensable for host defense of other tissues.

To test this hypothesis, a mouse has been created that expresses a mutant form of calprotectin that lacks four histidine resides in the S100A9 tail; these residues are required

to coordinate Mn in transition metal binding site I. This mouse will be referred to as *S100a9*$^{\Delta Mn}$. *S100a9*$^{\Delta Mn}$ will be subjected to various infection models, including *S. aureus* systemic infection and *A. baumannii* pneumonia. Bacterial burdens will be enumerated to determine whether loss of calprotectin Mn binding impairs host defenses against these pathogens. Furthermore, Mn and Zn levels and distribution will be evaluated at sites of infection to determine if Mn binding by calprotectin is required to generate a Mn-deplete site of infection. Finally, bacterial gene transcription of Mn-responsive genes will be assessed to determine if Mn binding by calprotectin is required for Mn starvation *in vivo.* These results will uncover the role of Mn-binding by calprotectin in antibacterial defense against *S. aureus* and *A. baumannii.*

References

Bae, T., and Schneewind, O. (2006). Allelic replacement in *Staphylococcus aureus* with inducible counter-selection. Plasmid *55*, 58-63.

Barczak, A.K., Gomez, J.E., Kaufmann, B.B., Hinson, E.R., Cosimi, L., Borowsky, M.L., Onderdonk, A.B., Stanley, S.A., Kaur, D., Bryant, K.F.*, et al.* (2012). RNA signatures allow rapid identification of pathogens and antibiotic susceptibilities. Proc. Natl. Acad. Sci. *109*, 6217-6222.

Cech, P., and Lehrer, R.I. (1984). Phagolysosomal pH of human neutrophils. Blood *63*, 88-95.

Corbin, B.D., Seeley, E.H., Raab, A., Feldmann, J., Miller, M.R., Torres, V.J., Anderson, K.L., Dattilo, B.M., Dunman, P.M., Gerads, R.*, et al.* (2008). Metal chelation and inhibition of bacterial growth in tissue abscesses. Science *319*, 962-965.

Frosch, M., Metze, D., Foell, D., Vogl, T., Sorg, C., Sunderkotter, C., and Roth, J. (2005). Early activation of cutaneous vessels and epithelial cells is characteristic of acute systemic onset juvenile idiopathic arthritis. Exp. Dermatol. *14*, 259-265.

Gallagher, L.A., Ramage, E., Weiss, E.J., Radey, M., Hayden, H.S., Held, K.G., Huse, H.K., Zurawski, D.V., Brittnacher, M.J., and Manoil, C. (2015). Resources for Genetic and Genomic Analysis of Emerging Pathogen *Acinetobacter baumannii*. J. Bacteriol. *197*, 2027-2035.

Huang, X., Shin, J.H., Pinochet-Barros, A., Su, T.T., and Helmann, J.D. (2017). *Bacillus subtilis* MntR coordinates the transcriptional regulation of manganese uptake and efflux systems. Mol. Microbiol. *103*, 253-268.

Kanamori, T., Kanou, N., Atomi, H., and Imanaka, T. (2004). Enzymatic characterization of a prokaryotic urea carboxylase. J. Bacteriol. *186*, 2532-2539.

Kolaj-Robin, O., Russell, D., Hayes, K.A., Pembroke, J.T., and Soulimane, T. (2015). Cation Diffusion Facilitator family: Structure and function. FEBS Lett. *589*, 1283-1295.

Lagasse, E., and Clerc, R.G. (1988). Cloning and expression of two human genes encoding calcium-binding proteins that are regulated during myeloid differentiation. Mol. Cell. Biol. *8*, 2402-2410.

Odink, K., Cerletti, N., Bruggen, J., Clerc, R.G., Tarcsay, L., Zwadlo, G., Gerhards, G., Schlegel, R., and Sorg, C. (1987). Two calcium-binding proteins in infiltrate macrophages of rheumatoid arthritis. Nature *330*, 80-82.

Zenz, R., Eferl, R., Kenner, L., Florin, L., Hummerich, L., Mehic, D., Scheuch, H., Angel, P., Tschachler, E., and Wagner, E.F. (2005). Psoriasis-like skin disease and arthritis caused by inducible epidermal deletion of Jun proteins. Nature *437*, 369-375.

Zwadlo, G., Bruggen, J., Gerhards, G., Schlegel, R., and Sorg, C. (1988). Two calcium-binding proteins associated with specific stages of myeloid cell differentiation are expressed by subsets of macrophages in inflammatory tissues. Clin. Exp. Immunol. *72*, 510-515.

APPENDIX

Supplementary Tables associated with Chapter VI

Table 13. Transcripts significantly* changed# by treatment with 1 mM $MnCl_2$.

Locus tag	Old locus tag	Annotation	log_2 FC	FDR
Down-regulated				
NWMN_RS03425	NWMN_0601	manganese ABC transporter substrate-binding protein (*mntC*)	-3.61	4.10E-45
NWMN_RS03435	NWMN_0603	phosphonate ABC transporter ATP-binding protein (*mntA*)	-3.57	3.98E-29
NWMN_RS03430	NWMN_0602	membrane protein (*mntB*)	-3.41	2.46E-27
Up-regulated				
NWMN_RS13325	NWMN_2316	CDF family transporter	3.35	7.03E-26

*Significance was defined as FDR <0.001
#Defined as >2 log_2 fold change

Table 14. Transcripts significantly* changed# by treatment with 100 μM VU0026921.

Locus Tag	Annotation	log_2 FC	FDR
Up-regulated			
NWMN_RS11830	transcriptional regulator	6.98	4.57E-79
NWMN_RS08360	HrcA family transcriptional regulator	6.03	6.43E-117
NWMN_RS08705	DUF4930 domain-containing protein	5.98	1.84E-73
NWMN_RS06105	hypothetical protein	5.97	1.97E-53
NWMN_RS13020	hemin ABC transporter ATP-binding protein	5.81	1.87E-67
NWMN_RS08355	nucleotide exchange factor GrpE	5.63	4.64E-102
NWMN_RS11835	cation transporter	5.38	2.82E-75
NWMN_RS13025	hemin ABC transporter permease	5.30	1.14E-36
NWMN_RS14115	hypothetical protein	5.24	8.78E-48
NWMN_RS13905	MarR family transcriptional regulator	5.23	3.03E-80
NWMN_RS14120	copper-exporting P-type ATPase A	5.22	4.67E-94
NWMN_RS08700	hypothetical protein	5.05	1.17E-85
NWMN_RS02200	hypothetical protein	5.01	3.93E-88
NWMN_RS11180	co-chaperone GroES	4.92	2.61E-87
NWMN_RS13105	phage infection protein	4.91	8.42E-67
NWMN_RS11800	DNA starvation/stationary phase protection protein	4.87	1.85E-84
NWMN_RS02835	excinuclease ABC subunit B	4.79	3.23E-85
NWMN_RS02840	protein arginine kinase	4.76	2.00E-90
NWMN_RS03115	protein VraX	4.72	6.69E-49
NWMN_RS07320	phosphate-binding protein	4.69	4.81E-46
NWMN_RS08350		4.67	3.77E-92
NWMN_RS04760	chaperone protein ClpB	4.62	6.31E-85
NWMN_RS12635		4.61	1.75E-32
NWMN_RS13980	membrane protein	4.55	2.35E-36
NWMN_RS12630		4.45	7.87E-36
NWMN_RS02830	transcriptional regulator CtsR	4.39	2.59E-88
NWMN_RS02235	hypothetical protein	4.24	9.19E-52
NWMN_RS14850	PadR family transcriptional regulator	4.24	6.79E-49
NWMN_RS14580	hypothetical protein	4.19	1.69E-34
NWMN_RS02240	hypothetical protein	4.12	1.44E-56
NWMN_RS02195	hypothetical protein	4.07	2.20E-44
NWMN_RS11175		3.88	1.10E-44
NWMN_RS06835	MerR family transcriptional regulator	3.88	1.41E-69
NWMN_RS04105	hydrolase	3.73	1.44E-39
NWMN_RS14220	hypothetical protein	3.69	2.73E-55
NWMN_RS07685	chromosome replication protein DnaD	3.64	7.87E-41

NWMN_RS14880	arylamine N-acetyltransferase	3.62	2.87E-51
NWMN_RS06625	ribosome maturation factor	3.59	1.00E-39
NWMN_RS10770	MAP domain-containing protein	3.58	2.44E-51
NWMN_RS02245	hypothetical protein	3.56	2.93E-38
NWMN_RS06100	hypothetical protein	3.54	1.10E-42
NWMN_RS02215	hypothetical protein	3.52	3.38E-43
NWMN_RS09650	gamma-hemolysin subunit A	3.51	8.39E-18
NWMN_RS00560	capsular polysaccharide biosynthesis protein Cap8F	3.50	7.58E-30
NWMN_RS07680	endonuclease III	3.48	3.54E-44
NWMN_RS12140	galactose-6-phosphate isomerase subunit LacB	3.48	1.89E-24
NWMN_RS10720	thioredoxin	3.47	1.03E-56
NWMN_RS12640	urease subunit alpha	3.47	5.15E-33
NWMN_RS12145	galactose-6-phosphate isomerase subunit LacA	3.45	2.69E-34
NWMN_RS02210	hypothetical protein	3.44	4.43E-45
NWMN_RS02845	ATP-dependent Clp protease ATP-binding subunit ClpC	3.40	1.95E-38
NWMN_RS00400	diacetyl reductase ((S)-acetoin forming)	3.39	1.25E-24
NWMN_RS03110	hypothetical protein	3.38	1.70E-49
NWMN_RS02065	transcriptional regulator	3.38	2.86E-24
NWMN_RS12205	toxin	3.37	1.03E-29
NWMN_RS06940	threonine aldolase	3.33	3.09E-31
NWMN_RS00565	UDP-N-acetyl glucosamine 2-epimerase	3.32	3.45E-23
NWMN_RS12395	30S ribosomal protein S3	3.31	1.17E-22
NWMN_RS12375	50S ribosomal protein L14	3.26	8.19E-33
NWMN_RS09330	riboflavin biosynthesis protein RibD	3.25	1.99E-51
NWMN_RS09325	riboflavin synthase subunit alpha	3.25	1.02E-54
NWMN_RS13995	thiol reductase thioredoxin	3.25	1.56E-40
NWMN_RS14855	DNA damage-inducible protein DinB	3.25	1.83E-45
NWMN_RS02105	alkyl hydroperoxide reductase subunit C	3.25	1.40E-30
NWMN_RS12400	50S ribosomal protein L22	3.24	1.79E-23
NWMN_RS12370	50S ribosomal protein L24	3.24	3.05E-19
NWMN_RS07675	hypothetical protein	3.24	1.09E-27
NWMN_RS12390	50S ribosomal protein L16	3.24	3.23E-29
NWMN_RS05140	serine protease	3.22	5.60E-25
NWMN_RS06630		3.22	1.14E-36
NWMN_RS00015	RNA-binding protein	3.22	8.53E-55
NWMN_RS11170	integrase	3.21	1.04E-24
NWMN_RS00555	UDP-glucose 4-epimerase	3.20	2.93E-21
NWMN_RS01715	hypothetical protein	3.18	2.44E-21
NWMN_RS14890	ABC transporter ATP-binding protein	3.18	1.47E-41
NWMN_RS14205	hypothetical protein	3.18	8.37E-49

NWMN_RS12380	30S ribosomal protein S17	3.16	8.63E-26
NWMN_RS12975	multidrug efflux protein	3.16	3.69E-25
NWMN_RS07035	catalase	3.16	6.17E-34
NWMN_RS12365	50S ribosomal protein L5	3.15	1.35E-33
NWMN_RS06305	orotate phosphoribosyltransferase	3.15	1.84E-26
NWMN_RS08345	molecular chaperone DnaJ	3.14	4.99E-30
NWMN_RS12405	30S ribosomal protein S19	3.12	5.15E-23
NWMN_RS14845	hypothetical protein	3.11	9.08E-48
NWMN_RS10775	hypothetical protein	3.11	7.80E-21
NWMN_RS02120	hypothetical protein	3.07	9.23E-30
NWMN_RS09585	serine protease SplA	3.07	8.28E-15
NWMN_RS02130	hypothetical protein	3.06	7.37E-44
NWMN_RS06850	XRE family transcriptional regulator	3.04	2.45E-19
NWMN_RS10765	MAP domain-containing protein	3.03	2.04E-27
NWMN_RS07315	phosphate ABC transporter permease subunit PstC	3.03	2.99E-22
NWMN_RS12410		3.03	2.53E-24
NWMN_RS04985	membrane protein	3.02	1.04E-36
NWMN_RS00440	hypothetical protein	3.02	5.95E-31
NWMN_RS12355	30S ribosomal protein S8	3.01	8.11E-29
NWMN_RS14410	hypothetical protein	3.01	1.22E-27
NWMN_RS14895	bacitracin ABC transporter permease	3.01	1.20E-34
NWMN_RS05015	competence protein ComK	3.01	1.92E-22
NWMN_RS00665	hypothetical protein	3.00	2.88E-33
NWMN_RS08395	ComE operon protein 2	2.98	6.08E-45
NWMN_RS01710	hypothetical protein	2.98	1.38E-26
NWMN_RS06640	50S ribosomal protein L7ae	2.96	3.30E-32
NWMN_RS09320	riboflavin biosynthesis protein RibBA	2.96	9.49E-47
NWMN_RS04580	hypothetical protein	2.94	9.46E-31
NWMN_RS12350	50S ribosomal protein L6	2.92	9.72E-36
NWMN_RS00550	polysaccharide biosynthesis protein EpsC	2.90	6.84E-15
NWMN_RS01855	multidrug efflux MATE transporter transcriptional repressor MepR	2.89	3.13E-22
NWMN_RS12385	50S ribosomal protein L29	2.88	1.22E-33
NWMN_RS12970	multidrug MFS transporter	2.88	4.35E-26
NWMN_RS06300	orotidine 5'-phosphate decarboxylase	2.88	2.75E-17
NWMN_RS12415	50S ribosomal protein L23	2.87	1.01E-18
NWMN_RS11475	histidine kinase	2.87	2.52E-32
NWMN_RS14200	hypothetical protein	2.87	1.05E-40
NWMN_RS13920	NAD(P)H-dependent oxidoreductase	2.86	5.29E-25
NWMN_RS14225	TetR family transcriptional regulator	2.85	1.08E-32
NWMN_RS01675	hypothetical protein	2.84	7.50E-30

NWMN_RS01735	minor structural protein	2.84	9.18E-25
NWMN_RS04770	2-isopropylmalate synthase	2.83	8.17E-19
NWMN_RS14375	membrane protein	2.83	5.16E-26
NWMN_RS02020	30S ribosomal protein S6	2.81	8.51E-29
NWMN_RS03105	protein VraC	2.81	1.14E-17
NWMN_RS14125	copper chaperone CopZ	2.80	9.11E-24
NWMN_RS12360		2.80	6.41E-33
NWMN_RS01680	major capsid protein	2.79	5.32E-31
NWMN_RS01445	lipase	2.77	3.14E-35
NWMN_RS14215	hypothetical protein	2.76	2.22E-37
NWMN_RS01730	peptidase	2.76	3.50E-30
NWMN_RS06080	alpha-hemolysin	2.75	5.50E-28
NWMN_RS01740	hypothetical protein	2.74	3.44E-24
NWMN_RS09660	hypothetical protein	2.74	1.57E-35
NWMN_RS00020	DNA recombination protein RecF	2.74	1.96E-35
NWMN_RS02030	30S ribosomal protein S18	2.73	1.00E-30
NWMN_RS06645	translation initiation factor IF-2	2.72	3.35E-34
NWMN_RS14015	holin-like protein CidB	2.72	2.37E-30
NWMN_RS12315		2.72	9.09E-21
NWMN_RS07440	hypothetical protein	2.71	4.87E-32
NWMN_RS06635	DNA-binding protein	2.71	2.55E-28
NWMN_RS12425	50S ribosomal protein L3	2.70	2.50E-16
NWMN_RS02055	hypothetical protein	2.70	1.31E-27
NWMN_RS12420	50S ribosomal protein L4	2.69	5.39E-19
NWMN_RS05615	hypothetical protein	2.68	8.88E-22
NWMN_RS01725	phage tail protein	2.68	3.67E-23
NWMN_RS12430	30S ribosomal protein S10	2.68	5.15E-17
NWMN_RS05815	hypothetical protein	2.68	4.72E-18
NWMN_RS03065	hypothetical protein	2.68	1.66E-26
NWMN_RS01670	hypothetical protein	2.68	6.03E-15
NWMN_RS12290	50S ribosomal protein L17	2.68	2.21E-26
NWMN_RS02785		2.67	2.34E-14
NWMN_RS00670	formate dehydrogenase	2.67	3.57E-32
NWMN_RS04240	SsrA-binding protein	2.66	7.89E-39
NWMN_RS05965	endonuclease MutS2	2.66	4.80E-22
NWMN_RS02025	single-stranded DNA-binding protein	2.65	1.61E-30
NWMN_RS12135	tagatose-6-phosphate kinase	2.65	1.76E-14
NWMN_RS12295	DNA-directed RNA polymerase subunit alpha	2.65	4.42E-28
NWMN_RS13345	gamma-hemolysin component A	2.64	1.35E-34
NWMN_RS13535	hypothetical protein	2.64	4.90E-35
NWMN_RS01765	tail protein	2.64	1.33E-23

NWMN_RS01655	terminase	2.61	7.15E-23
NWMN_RS00570	O-acetyltransferase	2.61	2.22E-15
NWMN_RS13900	glyoxalase	2.61	7.34E-25
NWMN_RS14230	short-chain dehydrogenase	2.61	8.35E-36
NWMN_RS08465	hypothetical protein	2.60	3.86E-28
NWMN_RS12340	30S ribosomal protein S5	2.60	2.20E-30
NWMN_RS12345	50S ribosomal protein L18	2.59	5.79E-32
NWMN_RS12300	30S ribosomal protein S11	2.59	2.61E-26
NWMN_RS02225	hypothetical protein	2.57	4.91E-26
NWMN_RS01720	terminase	2.56	2.31E-25
NWMN_RS02050	toxin	2.56	4.24E-15
NWMN_RS13990	esterase	2.56	4.94E-33
NWMN_RS05770	phage capsid protein	2.55	3.45E-22
NWMN_RS13660	alkylhydroperoxidase	2.55	2.96E-14
NWMN_RS06730	ribonuclease Y	2.55	8.45E-29
NWMN_RS10185	hypothetical protein	2.54	5.96E-24
NWMN_RS08340	ribosomal protein L11 methyltransferase	2.54	4.49E-26
NWMN_RS01705	tail protein	2.53	6.96E-26
NWMN_RS05585	transcriptional regulator	2.53	8.68E-19
NWMN_RS13355	gamma-hemolysin component B	2.52	7.42E-33
NWMN_RS12335	50S ribosomal protein L30	2.52	3.60E-26
NWMN_RS14010	pyruvate oxidase	2.51	1.01E-23
NWMN_RS12320	adenylate kinase	2.50	3.65E-23
NWMN_RS13565	peptidase M28	2.50	1.45E-25
NWMN_RS08675	50S ribosomal protein L27	2.49	3.71E-21
NWMN_RS05135	staphopain B	2.49	1.06E-20
NWMN_RS01685	hypothetical protein	2.49	6.06E-26
NWMN_RS12325	protein translocase subunit SecY	2.47	2.12E-18
NWMN_RS10180	hypothetical protein	2.47	3.42E-18
NWMN_RS01690	phage head-tail adapter protein	2.47	7.10E-24
NWMN_RS11160	phage terminase small subunit	2.46	3.05E-19
NWMN_RS01695	hypothetical protein	2.46	1.34E-23
NWMN_RS05975	hypothetical protein	2.45	1.25E-21
NWMN_RS10395	oxidoreductase	2.44	5.28E-24
NWMN_RS10160	hypothetical protein	2.43	2.28E-20
NWMN_RS05110	isochorismate synthase	2.42	1.54E-23
NWMN_RS14530	tributyrin esterase	2.42	2.15E-22
NWMN_RS01700	hypothetical protein	2.42	5.13E-25
NWMN_RS12330	50S ribosomal protein L15	2.41	9.07E-24
NWMN_RS04360	organic hydroperoxide resistance protein-like	2.41	5.23E-16
NWMN_RS12305	30S ribosomal protein S13	2.41	8.31E-22

NWMN_RS03360	transcriptional regulator	2.40	5.79E-18
NWMN_RS01500	hypothetical protein	2.39	5.37E-19
NWMN_RS10405	transcriptional regulator	2.39	4.38E-26
NWMN_RS01650	terminase	2.39	6.04E-24
NWMN_RS05875	phage holin	2.38	8.95E-21
NWMN_RS04270	membrane protein	2.38	3.34E-23
NWMN_RS02520		2.38	2.34E-12
NWMN_RS10165	peptidase	2.38	1.84E-21
NWMN_RS07195	DNA repair protein MucB	2.37	1.80E-31
NWMN_RS01495	hypothetical protein	2.36	2.85E-17
NWMN_RS02365	hypothetical protein	2.35	7.32E-29
NWMN_RS05800	hypothetical protein	2.35	1.19E-21
NWMN_RS01660	phage portal protein	2.35	9.88E-23
NWMN_RS01490	antirepressor	2.35	1.70E-25
NWMN_RS14575	aureolysin	2.33	5.12E-19
NWMN_RS01665	phage head morphogenesis protein	2.33	1.00E-23
NWMN_RS13350	gamma-hemolysin component C	2.31	9.30E-24
NWMN_RS05625	hypothetical protein	2.31	1.17E-26
NWMN_RS05595	hypothetical protein	2.31	5.60E-22
NWMN_RS07310	phosphate ABC transporter permease protein PstA	2.30	1.75E-12
NWMN_RS00575	capsular polysaccharide biosynthesis protein	2.30	1.78E-12
NWMN_RS03060	bacillithiol biosynthesis deacetylase BshB2	2.29	1.89E-24
NWMN_RS08560	cysteine desulfurase	2.29	5.26E-24
NWMN_RS01905	Efem/EfeO family lipoprotein	2.28	2.30E-13
NWMN_RS00035	carbohydrate kinase	2.28	3.53E-21
NWMN_RS07180	peptide-methionine (S)-S-oxide reductase	2.28	2.01E-17
NWMN_RS10520	non-heme ferritin	2.28	6.50E-17
NWMN_RS03355	lysophospholipase	2.28	4.87E-16
NWMN_RS04145	thioredoxin reductase	2.28	2.05E-23
NWMN_RS12310		2.26	1.29E-21
NWMN_RS03825	hypothetical protein	2.26	1.84E-24
NWMN_RS02100	alkyl hydroperoxide reductase subunit F	2.26	7.29E-19
NWMN_RS10005		2.25	5.21E-06
NWMN_RS00435	Superoxide dismutase [Mn/Fe] 2	2.24	1.65E-23
NWMN_RS07435	hypothetical protein	2.24	1.80E-20
NWMN_RS01745	hypothetical protein	2.24	1.20E-15
NWMN_RS13260	addiction module antitoxin RelB	2.23	3.31E-26
NWMN_RS05870	hypothetical protein	2.23	4.28E-18
NWMN_RS14210	glyoxalase	2.23	6.45E-25
NWMN_RS09385	transaldolase	2.22	9.40E-21

NWMN_RS01345	hypothetical protein	2.22	1.61E-15
NWMN_RS05835	minor structural protein	2.22	4.62E-21
NWMN_RS10190	tail protein	2.22	1.10E-23
NWMN_RS10175	hypothetical protein	2.21	2.94E-22
NWMN_RS00545	capsular polysaccharide biosynthesis protein Cap8C	2.21	1.38E-07
NWMN_RS05590	hypothetical protein	2.20	1.94E-19
NWMN_RS01480	hypothetical protein	2.20	1.73E-24
NWMN_RS13485	epimerase	2.19	4.89E-21
NWMN_RS02945	50S ribosomal protein L7/L12	2.18	2.33E-20
NWMN_RS10385	hypothetical protein	2.17	1.22E-22
NWMN_RS05980	excinuclease ABC subunit C	2.17	1.07E-23
NWMN_RS04275	acetyltransferase	2.17	9.87E-16
NWMN_RS03815	two-component sensor histidine kinase	2.17	1.29E-26
NWMN_RS05865	tail protein	2.17	1.61E-18
NWMN_RS05960	DNA polymerase/3'-5' exonuclease PolX	2.16	2.91E-22
NWMN_RS09765	foldase	2.16	3.59E-28
NWMN_RS02430	membrane protein	2.16	1.33E-14
NWMN_RS11200	hydrolase in agr operon	2.15	1.14E-26
NWMN_RS08685	50S ribosomal protein L21	2.14	6.18E-18
NWMN_RS06000	glutamate racemase	2.13	1.42E-17
NWMN_RS03820	DNA-binding response regulator	2.13	5.94E-29
NWMN_RS08670	GTPase ObgE	2.13	1.05E-19
NWMN_RS05040	putative holin-like toxin	2.13	0.000125976
NWMN_RS10195	hypothetical protein	2.12	4.13E-17
NWMN_RS04585	hypothetical protein	2.12	1.54E-17
NWMN_RS13835	hypothetical protein	2.12	3.28E-18
NWMN_RS12560	molybdopterin molybdenumtransferase	2.12	2.02E-19
NWMN_RS07525	peptide-methionine (S)-S-oxide reductase	2.12	3.13E-25
NWMN_RS03830	hypothetical protein	2.11	6.40E-16
NWMN_RS05830	peptidase	2.11	2.13E-17
NWMN_RS12130	Tagatose diphosphate aldolase	2.10	2.24E-10
NWMN_RS10070	metal-dependent hydrolase	2.09	1.40E-24
NWMN_RS10535	DNA polymerase IV	2.09	3.29E-21
NWMN_RS04720	ATP-dependent helicase/deoxyribonuclease subunit B	2.08	9.13E-16
NWMN_RS02300	hypothetical protein	2.08	4.88E-13
NWMN_RS12505	MarR family transcriptional regulator	2.08	4.40E-11
NWMN_RS10170	phage tail protein	2.08	4.09E-16
NWMN_RS01755	hypothetical protein	2.08	5.33E-17
NWMN_RS14235	amidohydrolase	2.07	1.57E-11
NWMN_RS05620	hypothetical protein	2.07	1.26E-15

NWMN_RS00820	peptidase M23	2.07	1.14E-18
NWMN_RS06665	30S ribosomal protein S15	2.06	1.25E-10
NWMN_RS03070	glucosamine-6-phosphate deaminase	2.06	1.08E-17
NWMN_RS12650	urease accessory protein UreF	2.06	8.90E-14
NWMN_RS12645		2.06	6.40E-12
NWMN_RS12665	transcriptional regulator	2.06	2.91E-22
NWMN_RS05955	colicin V production protein CvpA	2.05	1.17E-22
NWMN_RS08680	hypothetical protein	2.05	3.69E-26
NWMN_RS07805	hypothetical protein	2.05	1.06E-08
NWMN_RS00265	hypothetical protein	2.05	1.37E-16
NWMN_RS03055	GTP cyclohydrolase FolE2	2.05	4.29E-24
NWMN_RS03195	transcriptional regulator	2.04	1.61E-09
NWMN_RS06095	hypothetical protein	2.04	1.34E-16
NWMN_RS01340	hypothetical protein	2.03	3.63E-17
NWMN_RS02190	hypothetical protein	2.01	3.88E-22
NWMN_RS05810	hypothetical protein	2.01	1.20E-12
NWMN_RS13160	heat-shock protein Hsp20	2.01	3.89E-15
NWMN_RS07450	hypothetical protein	2.00	8.89E-25
NWMN_RS03640	LysR family transcriptional regulator	2.00	1.48E-25
NWMN_RS04025	glycerate kinase	2.00	1.05E-17

Down-regulated			
NWMN_RS02395	sodium-dependent transporter	-4.57	1.01E-10
NWMN_RS01365	formate/nitrite transporter	-4.45	1.67E-44
NWMN_RS12020	membrane protein	-4.31	1.06E-26
NWMN_RS14920	cold-shock protein	-4.26	1.49E-20
NWMN_RS14345	hypothetical protein	-4.20	3.12E-20
NWMN_RS11875	glutamine-fructose-6-phosphate aminotransferase	-4.13	1.03E-35
NWMN_RS14350	amino acid permease	-4.08	5.40E-18
NWMN_RS08865	glyceraldehyde-3-phosphate dehydrogenase	-4.05	3.79E-33
NWMN_RS14180	transglycosylase IsaA	-4.03	1.86E-37
NWMN_RS14160	glycosyl-diaponeurosporenoate acyltransferase	-4.01	8.56E-29
NWMN_RS09310	proline dehydrogenase	-4.01	1.78E-32
NWMN_RS02475	PTS ascorbate transporter subunit IIA	-3.93	2.05E-33
NWMN_RS06990	hypothetical protein	-3.90	2.60E-36
NWMN_RS14785		-3.87	0.000802674
NWMN_RS04600	sodium:proton antiporter	-3.80	1.96E-08
NWMN_RS07625	sulfite reductase subunit alpha	-3.80	6.93E-33
NWMN_RS12015	hypothetical protein	-3.70	1.46E-33
NWMN_RS03130	hypothetical protein	-3.68	1.35E-58
NWMN_RS07760	nucleoside-diphosphate kinase	-3.58	3.70E-29

NWMN_RS01095	antiholin-like protein LrgA	-3.56	1.04E-33
NWMN_RS13815	gluconate kinase	-3.50	1.17E-21
NWMN_RS10645	prephenate dehydratase	-3.49	1.55E-27
NWMN_RS14175	GNAT family acetyltransferase	-3.48	1.51E-28
NWMN_RS07115	choline transporter	-3.38	8.04E-40
NWMN_RS06270	bifunctional protein PyrR	-3.36	4.02E-07
NWMN_RS14925	transcriptional regulator	-3.35	1.22E-39
NWMN_RS04695	argininosuccinate synthase	-3.32	6.61E-07
NWMN_RS09130	acetate--CoA ligase	-3.28	1.09E-31
NWMN_RS13140	DUF4889 domain-containing protein	-3.28	5.32E-32
NWMN_RS12480	membrane protein	-3.27	6.28E-31
NWMN_RS09100	tyrosine--tRNA ligase	-3.27	5.71E-17
NWMN_RS12695	hypothetical protein	-3.26	7.73E-16
NWMN_RS05480	cell division protein FtsW	-3.23	1.25E-50
NWMN_RS07600	amino acid permease	-3.21	2.92E-33
NWMN_RS00735	PTS glucose EIICBA component	-3.19	1.16E-20
NWMN_RS12215	acetolactate synthase	-3.18	2.73E-36
NWMN_RS02265	hypothetical protein	-3.17	2.74E-27
NWMN_RS11795	purine-nucleoside phosphorylase	-3.15	1.70E-49
NWMN_RS04305	cold-shock protein	-3.15	1.01E-23
NWMN_RS11725	hypothetical protein	-3.14	3.37E-29
NWMN_RS12775	CAAX amino protease	-3.14	6.47E-34
NWMN_RS00045	serine--tRNA ligase	-3.12	1.26E-13
NWMN_RS12465	hypothetical protein	-3.12	1.49E-29
NWMN_RS02270	hypothetical protein	-3.11	2.31E-37
NWMN_RS13820	GntR family transcriptional regulator	-3.10	1.20E-44
NWMN_RS11815	membrane protein	-3.08	4.87E-16
NWMN_RS08055	geranyltranstransferase	-3.08	1.31E-33
NWMN_RS13230	cobalamin biosynthesis protein CbiX	-3.08	8.44E-31
NWMN_RS04650	kinase	-3.07	1.68E-18
NWMN_RS06180	cell division protein FtsL	-3.07	4.92E-41
NWMN_RS06790	glycerol transporter	-3.07	1.76E-36
NWMN_RS11540	protein translocase component YidC	-3.06	1.95E-29
NWMN_RS00625	aldehyde dehydrogenase	-3.03	1.88E-26
NWMN_RS14185	membrane protein	-3.01	1.77E-14
NWMN_RS03135	membrane protein	-2.99	2.14E-38
NWMN_RS14165	CHAP domain-containing protein	-2.99	2.95E-07
NWMN_RS12710	membrane protein	-2.99	2.10E-21
NWMN_RS13240	formate/nitrite transporter	-2.98	9.16E-42
NWMN_RS08090	elongation factor P	-2.97	4.43E-45
NWMN_RS13150	hypothetical protein	-2.97	9.16E-25

NWMN_RS10710	hypothetical protein	-2.95	2.14E-40
NWMN_RS14280	dihydroorotate dehydrogenase 2	-2.94	1.14E-25
NWMN_RS06130	permease	-2.94	4.16E-15
NWMN_RS13145	proton/sodium-glutamate symport protein GltT	-2.93	5.48E-38
NWMN_RS12475	hypothetical protein	-2.93	1.93E-17
NWMN_RS03730	membrane protein	-2.92	4.98E-17
NWMN_RS03725	aldo/keto reductase	-2.90	2.52E-39
NWMN_RS03005	deoxycytidine kinase	-2.88	1.96E-27
NWMN_RS14025	LysR family transcriptional regulator	-2.88	5.15E-33
NWMN_RS14790		-2.86	0.005609394
NWMN_RS14155	diapolycopene oxygenase	-2.86	1.45E-15
NWMN_RS03675	hypothetical protein	-2.81	2.91E-22
NWMN_RS08915	alanine glycine permease	-2.81	1.92E-27
NWMN_RS13555	iron export ABC transporter permease subunit FetB	-2.80	1.30E-12
NWMN_RS14105	1-pyrroline-5-carboxylate dehydrogenase	-2.80	1.18E-20
NWMN_RS07580	ribonuclease H	-2.79	6.38E-12
NWMN_RS10080	membrane protein	-2.77	3.44E-39
NWMN_RS03450	N-acetylmannosaminyltransferase	-2.76	1.01E-33
NWMN_RS11580	hypothetical protein	-2.74	1.14E-29
NWMN_RS02080	phosphoglycerate mutase	-2.74	8.23E-30
NWMN_RS10655	sodium-dependent dicarboxylate transporter SdcS	-2.72	9.00E-32
NWMN_RS11840	lytic regulatory protein	-2.69	1.06E-25
NWMN_RS13790	UTP--glucose-1-phosphate uridylyltransferase	-2.69	5.98E-39
NWMN_RS06140		-2.67	2.12E-18
NWMN_RS06605	phosphatidate cytidylyltransferase	-2.66	1.90E-29
NWMN_RS09800	transcriptional regulator	-2.66	6.56E-21
NWMN_RS12210	alpha-acetolactate decarboxylase	-2.64	1.80E-31
NWMN_RS06020	fibrinogen-binding protein	-2.64	3.40E-16
NWMN_RS13700	hypothetical protein	-2.64	3.56E-26
NWMN_RS14780	histidinol dehydrogenase	-2.63	0.003805299
NWMN_RS00690	hypothetical protein	-2.62	6.96E-26
NWMN_RS00865	hexose phosphate transporter	-2.62	1.31E-13
NWMN_RS07390	cold-shock protein CspA	-2.62	4.72E-18
NWMN_RS06995	aspartate kinase	-2.59	3.31E-24
NWMN_RS03700	undecaprenyl-diphosphatase	-2.57	2.83E-34
NWMN_RS14440	anaerobic ribonucleoside-triphosphate reductase	-2.57	9.35E-08
NWMN_RS14140	dehydrosqualene desaturase	-2.57	5.22E-11
NWMN_RS10600	hypothetical protein	-2.56	2.17E-18
NWMN_RS03765	hypothetical protein	-2.56	1.42E-14

NWMN_RS13440	transcriptional regulator	-2.53	1.20E-13
NWMN_RS03590	hypothetical protein	-2.51	2.08E-34
NWMN_RS12000	hemolysin III	-2.51	2.92E-32
NWMN_RS06690	zinc protease	-2.50	3.96E-24
NWMN_RS03595	anion permease	-2.50	2.30E-31
NWMN_RS01870	glycerol-3-phosphate transporter	-2.50	1.36E-16
NWMN_RS11670	protein-tyrosine-phosphatase	-2.49	2.11E-19
NWMN_RS10640	nitric oxide synthase oxygenase	-2.48	1.79E-19
NWMN_RS14050	hypothetical protein	-2.48	1.32E-16
NWMN_RS09740	multidrug ABC transporter ATP-binding protein	-2.47	2.87E-33
NWMN_RS07635	DUF4889 domain-containing protein	-2.47	1.26E-22
NWMN_RS08845	hypothetical protein	-2.47	4.23E-17
NWMN_RS01845	PTS ascorbate transporter subunit IIA	-2.47	7.28E-09
NWMN_RS05500	membrane protein	-2.46	1.91E-35
NWMN_RS05240	phosphoribosylformylglycinamidine synthase	-2.46	3.54E-19
NWMN_RS00055	membrane protein	-2.46	4.52E-15
NWMN_RS09135	acetoin dehydrogenase	-2.45	5.20E-22
NWMN_RS05300	hypothetical protein	-2.43	7.88E-07
NWMN_RS07640	RNA methyltransferase	-2.42	7.29E-22
NWMN_RS10605	adenylosuccinate lyase	-2.42	3.49E-17
NWMN_RS11820	mannose-6-phosphate isomerase	-2.42	1.87E-32
NWMN_RS04130	prolipoprotein diacylglyceryl transferase	-2.41	5.07E-33
NWMN_RS00120	metallo-hydrolase	-2.39	4.27E-20
NWMN_RS14045	hypothetical protein	-2.38	1.43E-09
NWMN_RS04050	undecaprenyl-phosphate alpha-N-acetylglucosaminyl 1-phosphate transferase	-2.38	3.26E-22
NWMN_RS04605	thioesterase	-2.37	1.22E-08
NWMN_RS01050	hypothetical protein	-2.36	4.72E-25
NWMN_RS00185	hypothetical protein	-2.36	6.71E-13
NWMN_RS14130	lactate dehydrogenase	-2.36	1.37E-20
NWMN_RS13695	hypothetical protein	-2.36	1.04E-17
NWMN_RS13595	hypothetical protein	-2.35	4.03E-25
NWMN_RS01370	branched-chain amino acid transporter II carrier protein	-2.32	3.22E-13
NWMN_RS02975	2-amino-3-ketobutyrate CoA ligase	-2.32	6.69E-28
NWMN_RS12715	CHAP domain-containing protein	-2.31	1.51E-20
NWMN_RS14270	type VII secretion protein	-2.31	1.21E-09
NWMN_RS07135	glycerol-3-phosphate acyltransferase	-2.30	8.90E-13
NWMN_RS02405	cystathionine beta-lyase	-2.29	4.72E-25
NWMN_RS11500	cell division protein FtsW	-2.29	3.44E-28
NWMN_RS03330	enterobactin ABC transporter permease	-2.28	5.63E-19

NWMN_RS03490	nucleoside permease	-2.28	5.32E-32
NWMN_RS03170	mevalonate kinase	-2.28	2.99E-23
NWMN_RS03210	hypothetical protein	-2.28	2.28E-10
NWMN_RS06190	phospho-N-acetylmuramoyl-pentapeptide-transferase	-2.28	1.86E-29
NWMN_RS12870	LysR family transcriptional regulator	-2.27	1.15E-21
NWMN_RS11755	hypothetical protein	-2.27	2.51E-22
NWMN_RS00715	branched-chain amino acid transporter II carrier protein	-2.27	1.12E-23
NWMN_RS06135	DNA-binding protein	-2.27	3.30E-13
NWMN_RS11920	arginase	-2.27	5.20E-25
NWMN_RS05075	glycosyl transferase family 1	-2.26	1.34E-17
NWMN_RS07770	demethylmenaquinone methyltransferase	-2.26	1.10E-16
NWMN_RS04525	protein NagD	-2.26	1.17E-25
NWMN_RS10085	teichoic acid ABC transporter ATP-binding protein	-2.26	4.59E-25
NWMN_RS14355	aspartate aminotransferase family protein	-2.24	1.55E-10
NWMN_RS10485	methionine aminopeptidase	-2.23	1.44E-28
NWMN_RS12980	TetR family transcriptional regulator	-2.23	5.28E-14
NWMN_RS07905	DNA-binding response regulator	-2.23	8.20E-27
NWMN_RS07795		-2.23	4.48E-14
NWMN_RS05495	protoheme IX farnesyltransferase	-2.22	1.14E-26
NWMN_RS09435	transposase	-2.21	9.55E-25
NWMN_RS02400	cysteine synthase	-2.21	1.37E-09
NWMN_RS14275	fructosamine-3-kinase	-2.21	9.26E-08
NWMN_RS02825	pyrimidine nucleoside transporter NupC	-2.21	8.89E-25
NWMN_RS04810	membrane protein	-2.20	5.95E-12
NWMN_RS10500	hypothetical protein	-2.20	5.21E-10
NWMN_RS13075	quinone oxidoreductase	-2.20	2.77E-28
NWMN_RS10715	membrane protein	-2.19	3.59E-18
NWMN_RS03805	glyoxal reductase	-2.18	1.08E-19
NWMN_RS08190	hypothetical protein	-2.18	3.07E-10
NWMN_RS07775	heptaprenyl pyrophosphate synthase subunit A	-2.17	2.72E-12
NWMN_RS07765	heptaprenyl diphosphate synthase subunit II	-2.16	2.47E-18
NWMN_RS14040	hypothetical protein	-2.16	6.90E-13
NWMN_RS14860	2-oxoglutarate translocator	-2.16	2.26E-21
NWMN_RS00755	RpiR family transcriptional regulator	-2.15	4.68E-09
NWMN_RS05335	cytochrome d ubiquinol oxidase subunit I	-2.15	4.55E-21
NWMN_RS01850	hypothetical protein	-2.15	1.20E-14
NWMN_RS03125	uracil-DNA glycosylase	-2.15	1.39E-19
NWMN_RS01795	NADH-dependent flavin oxidoreductase	-2.15	5.55E-22
NWMN_RS11720	fructose-bisphosphate aldolase	-2.14	8.03E-31

NWMN_RS05365	hypothetical protein	-2.14	7.61E-13
NWMN_RS09820	class II fumarate hydratase	-2.14	5.16E-26
NWMN_RS12960	esterase	-2.14	1.12E-19
NWMN_RS12885	lysostaphin resistance protein A	-2.13	2.63E-23
NWMN_RS01380	hypothetical protein	-2.13	1.05E-06
NWMN_RS00750	permease	-2.13	8.30E-12
NWMN_RS08185	glucokinase	-2.12	3.70E-28
NWMN_RS14100	hypothetical protein	-2.12	9.88E-07
NWMN_RS12890	ribose-5-phosphate isomerase	-2.11	1.52E-15
NWMN_RS04785	phosphatidylethanolamine-binding protein	-2.10	9.04E-13
NWMN_RS11995	multidrug MFS transporter	-2.09	5.63E-21
NWMN_RS14170	O-acetyltransferase OatA	-2.09	5.35E-20
NWMN_RS04940	AI-2E family transporter	-2.09	1.61E-22
NWMN_RS07940	ADP-ribose pyrophosphatase	-2.08	5.28E-24
NWMN_RS07605	serine/threonine dehydratase	-2.07	1.83E-15
NWMN_RS05225	5-(carboxyamino)imidazole ribonucleotide mutase	-2.06	6.22E-14
NWMN_RS07610	alanine dehydrogenase	-2.06	1.19E-11
NWMN_RS11615	ATP synthase subunit gamma	-2.06	3.97E-27
NWMN_RS00305	hypothetical protein	-2.06	3.60E-10
NWMN_RS13680	hypothetical protein	-2.05	9.44E-12
NWMN_RS00970	nitric oxide dioxygenase	-2.05	4.10E-16
NWMN_RS13850	alkaline phosphatase	-2.05	1.83E-11
NWMN_RS11690	thymidine kinase	-2.04	4.06E-14
NWMN_RS07030	gamma-aminobutyrate permease	-2.04	1.44E-22
NWMN_RS13220	nitrite reductase NAD(P)H small subunit	-2.04	4.97E-17
NWMN_RS10075	hypothetical protein	-2.04	1.93E-11
NWMN_RS00995	hypothetical protein	-2.03	1.13E-21
NWMN_RS13225	nitrite reductase large subunit	-2.03	1.65E-21
NWMN_RS11675	translation factor Sua5	-2.03	1.21E-18
NWMN_RS06920	hypothetical protein	-2.03	3.02E-13
NWMN_RS11400	anti-sigma B factor RsbW	-2.02	1.75E-13
NWMN_RS03235	hypothetical protein	-2.02	9.92E-09
NWMN_RS02125	hypothetical protein	-2.02	9.23E-20
NWMN_RS09390	hypothetical protein	-2.02	1.35E-06
NWMN_RS13880	fructose bisphosphatase	-2.01	2.32E-23
NWMN_RS09250	NAD(FAD)-utilizing dehydrogenase	-2.01	1.81E-21
NWMN_RS07335	virulence factor B	-2.01	2.61E-18
NWMN_RS06815	RNA-binding protein Hfq	-2.01	2.31E-10
NWMN_RS05485	pyruvate carboxylase	-2.00	8.84E-26
NWMN_RS02090	hypothetical protein	-2.00	2.87E-20

NWMN_RS02695	tRNA(Ile)-lysidine synthase	-2.00	1.44E-22
NWMN_RS01790	alpha/beta hydrolase	-2.00	1.23E-17
NWMN_RS13095	membrane protein	-2.00	3.59E-18

*Significance was defined as FDR <0.001
#Defined as >2 $\log_2$ fold change

Table 15. Transcripts significantly* changed# between 100 μM VU0026921 and 100 μM '921/1 mM $MnCl_2$ combination treatment.

Locus tag	Old locus tag	Annotation	log_2 FC	FDR
Up-regulated				
NWMN_RS10105	NWMN_1767	glutamine amidotransferase	4.72	1.66E-34
NWMN_RS00305	NWMN_0053	hypothetical protein	4.37	1.44E-32
NWMN_RS12705	NWMN_2201	octopine dehydrogenase	3.84	1.15E-32
NWMN_RS03665	NWMN_0645	GNAT family acetyltransferase	3.81	5.53E-35
NWMN_RS09610	NWMN_1711	bacitracin ABC transporter ATP-binding protein	3.80	2.61E-34
NWMN_RS11825	NWMN_2048	oxidoreductase	3.80	1.50E-23
NWMN_RS03170	NWMN_0553	mevalonate kinase	3.73	1.71E-51
NWMN_RS01830	NWMN_0321	hypothetical protein/ oxidoreductase protein	3.72	2.78E-22
NWMN_RS03690	NWMN_0650	hypothetical protein	3.70	1.80E-45
NWMN_RS13255	NWMN_2306	zinc ABC transporter substrate-binding protein	3.70	3.77E-47
NWMN_RS14415	NWMN_2512	MBL fold hydrolase	3.68	9.94E-27
NWMN_RS00180	NWMN_0029	pyridine nucleotide-disulfide oxidoreductase	3.68	6.31E-36
NWMN_RS14275	NWMN_2487	fructosamine-3-kinase	3.67	4.27E-16
NWMN_RS13305	NWMN_2314	drug:proton antiporter	3.67	5.56E-69
NWMN_RS07540	NWMN_1338	thymidylate synthase	3.67	2.78E-73
NWMN_RS04180	NWMN_0737	epimerase	3.65	7.81E-62
NWMN_RS12095	NWMN_2089	glycine/betaine ABC transporter permease	3.64	1.00E-31
NWMN_RS12695	NWMN_RS12695	hypothetical protein	3.63	1.90E-17
NWMN_RS10460	NWMN_1821	hypothetical protein/ ribonuclease	3.62	1.89E-19
NWMN_RS05315	NWMN_0948	hypothetical protein	3.57	6.34E-43
NWMN_RS10660	NWMN_1855	pectate lyase	3.54	5.21E-38
NWMN_RS09605	NWMN_1710	hypothetical protein	3.52	2.29E-24
NWMN_RS12700	NWMN_2200	Na+/H+ antiporter NhaC	3.51	2.35E-43
NWMN_RS03695	NWMN_0651	hypothetical protein	3.48	5.46E-29
NWMN_RS14385	NWMN_2507	antibiotic biosynthesis monooxygenase	3.48	9.98E-24
NWMN_RS00630	NWMN_0114	cation transporter / Co/Zn/Cd efflux CzcD	3.45	1.26E-30
NWMN_RS04020	NWMN_0710	hypothetical protein / bacillithiol YtxJ	3.45	9.04E-37

NWMN_RS08185	NWMN_1451	glucokinase	3.44	7.81E-62
NWMN_RS14140	NWMN_2461	dehydrosqualene desaturase	3.44	4.33E-16
NWMN_RS03180	NWMN_0555	phosphomevalonate kinase	3.44	1.81E-26
NWMN_RS05165	NWMN_0922	mannosyl-glycoprotein endo-beta-N-acetylglucosamidase / atl	3.42	2.57E-43
NWMN_RS13555	NWMN_2352	iron export ABC transporter permease subunit FetB	3.38	1.53E-15
NWMN_RS14155	NWMN_2464	diapolycopene oxygenase / crtI	3.36	6.96E-18
NWMN_RS00625	NWMN_0113	aldehyde dehydrogenase / aldA	3.36	4.56E-28
NWMN_RS14870	NWMN_2594	DNA-binding protein / RNA polymerase	3.35	3.35E-25
NWMN_RS11890	NWMN_2059	mannitol-specific phosphotransferase enzyme IIA component / mtlA	3.33	1.74E-26
NWMN_RS00535	NWMN_0095	capsular polysaccharide type 5 biosynthesis protein cap5A / capA	3.32	8.64E-16
NWMN_RS02060	NWMN_0364	Peptidase / zinc-binding peptidase	3.32	7.19E-15
NWMN_RS13325	NWMN_2316	Transporter / CDF-family transporter	3.32	6.03E-29
NWMN_RS11895	NWMN_2060	mannitol-1-phosphate 5-dehydrogenase / mtlD	3.31	5.28E-25
NWMN_RS10450	NWMN_1819	protein-tyrosine-phosphatase	3.28	5.65E-29
NWMN_RS03175	NWMN_0554	diphosphomevalonate decarboxylase / mvaD	3.28	2.15E-26
NWMN_RS09795	NWMN_1738	hypothetical protein	3.25	7.46E-43
NWMN_RS03930	NWMN_0695	lipid kinase	3.25	4.12E-28
NWMN_RS08180	NWMN_1450	hypothetical protein	3.25	2.51E-33
NWMN_RS13040	NWMN_2265	LytTR family transcriptional regulator	3.25	3.61E-41
NWMN_RS05300	none	hypothetical protein	3.24	3.85E-10
NWMN_RS09190	NWMN_1636	hypothetical protein	3.22	1.02E-41
NWMN_RS08175	NWMN_1449	hydroxyacylglutathione hydrolase / zinc-binding hydrolase	3.20	1.32E-34
NWMN_RS13420	NWMN_2330	hypothetical protein	3.20	3.84E-27
NWMN_RS04735	NWMN_0840	hypothetical protein	3.19	1.15E-53
NWMN_RS09185	NWMN_1635	tRNA-binding protein	3.15	9.16E-54
NWMN_RS03805	NWMN_0672	glyoxal reductase	3.14	7.29E-33

NWMN_RS07495	NWMN_1331	acetyltransferase	3.13	1.75E-30
NWMN_RS13440	NWMN_2334	transcriptional regulator	3.13	5.83E-17
NWMN_RS02635	none	hypothetical protein	3.09	5.99E-18
NWMN_RS11880	NWMN_2057	PTS mannitol transporter subunit IICB	3.09	4.73E-34
NWMN_RS01385	NWMN_0250	peptide ABC transporter permease	3.09	2.24E-29
NWMN_RS06535	NWMN_1159	DNA processing protein DprA	3.08	4.18E-28
NWMN_RS14975	none	membrane protein	3.07	3.78E-12
NWMN_RS05425	NWMN_0968	spermidine/putrescine ABC transporter substrate-binding protein	3.04	6.78E-44
NWMN_RS14360	NWMN_2502	membrane protein	3.04	5.25E-23
NWMN_RS03685	NWMN_0649	Rossman fold protein TIGR00730 family	3.04	1.08E-28
NWMN_RS13310	none	hypothetical protein	3.03	8.48E-18
NWMN_RS05170	NWMN_0923	GNAT family N-acetyltransferase	3.00	1.45E-27
NWMN_RS09830	NWMN_1745	hypothetical protein	2.99	2.15E-27
NWMN_RS01380	none	hypothetical protein	2.96	6.47E-10
NWMN_RS10455	NWMN_1820	hypothetical protein	2.95	1.37E-28
NWMN_RS14685	none	hypothetical protein	2.95	6.33E-29
NWMN_RS00325	NWMN_0057	iron ABC transporter permease / siderophore transport sirC	2.94	6.85E-21
NWMN_RS04695	NWMN_0832	argininosuccinate synthase / argG	2.94	3.51518E-06
NWMN_RS08570	NWMN_1526	hypothetical protein	2.91	1.30E-17
NWMN_RS03145	NWMN_0548	membrane protein	2.90	9.52E-34
NWMN_RS07530	NWMN_1336	hypothetical protein	2.90	2.15E-39
NWMN_RS11395	NWMN_1970	RNA polymerase sigma factor SigB	2.89	1.85E-17
NWMN_RS13835	NWMN_2406	hypothetical protein	2.89	1.34E-25
NWMN_RS00865	NWMN_0158	hexose phosphate transporter / uhpT	2.89	2.16E-14
NWMN_RS04340	NWMN_0767	hypothetical protein	2.87	1.35E-19
NWMN_RS14160	NWMN_2465	glycosy diaponeurosporenoate acyltransferase	2.87	4.42E-14
NWMN_RS06790	NWMN_1207	glycerol transporter / glpF	2.85	7.37E-34
NWMN_RS04335	NWMN_0766	hypothetical protein	2.84	6.15E-17
NWMN_RS07490	NWMN_1330	UDP-N-acetylglucosamine--N-acetylmuramyl-	2.83	2.18E-25

		(pentapeptide) pyrophosphoryl-undecaprenol N-acetylglucosamine transferase / murG		
NWMN_RS12050	NWMN_2080	siderophore synthetase	2.83	1.43E-35
NWMN_RS00220	NWMN_0036	DUF4865 domain-containing protein	2.83	4.78E-24
NWMN_RS00720	NWMN_0131	Isochorismatase / entB	2.82	5.63E-16
NWMN_RS03810	NWMN_0673	glycosyl transferase	2.82	8.34E-22
NWMN_RS09165	NWMN_1631	hypothetical protein	2.82	7.08E-22
NWMN_RS09170	NWMN_1632	hypothetical protein	2.81	3.45E-16
NWMN_RS02395	NWMN_0423	sodium-dependent transporter	2.80	7.85221E-06
NWMN_RS12880	NWMN_2235	Formimidoylglutamase / hutG	2.78	5.65E-15
NWMN_RS00185	none	hypothetical protein	2.78	3.68E-15
NWMN_RS02080	NWMN_0367	phosphoglycerate mutase / pgm	2.77	2.35E-31
NWMN_RS06190	NWMN_1092	phospho-N-acetylmuramoyl-pentapeptide-transferase / mraY	2.77	1.31E-42
NWMN_RS11325	NWMN_1962	ketol-acid reductoisomerase / ilvC	2.76	4.61E-13
NWMN_RS03150	NWMN_0549	hypothetical protein	2.76	4.42E-34
NWMN_RS04445	NWMN_0786	Fe-S cluster assembly protein SufD	2.75	3.27E-36
NWMN_RS13910	NWMN_2419	acetyltransferase	2.73	2.58E-30
NWMN_RS11400	NWMN_1971	anti-sigma B factor RsbW	2.73	6.70E-20
NWMN_RS14105	NWMN_2454	1-pyrroline-5-carboxylate dehydrogenase	2.72	2.55E-17
NWMN_RS08975	NWMN_1601	metal-dependent hydrolase	2.72	1.47E-15
NWMN_RS12850	NWMN_2229	Oxidoreductase / short chain dehydrogenase family	2.72	2.31E-16
NWMN_RS01150	NWMN_0205	LacI family transcriptional regulator /rbsR	2.71	7.31E-22
NWMN_RS14345	none	hypothetical protein	2.71	2.70E-09
NWMN_RS11885	NWMN_2058	PTS lactose transporter subunit IIB	2.70	8.48E-24
NWMN_RS09615	NWMN_1712	peptidase S8 / bsaP	2.70	4.18E-31
NWMN_RS13045	NWMN_2266	membrane protein	2.69	2.26E-30
NWMN_RS12995	NWMN_2257	hypothetical protein / tcaA	2.66	1.09E-25
NWMN_RS00055	none	membrane protein	2.65	5.24E-16
NWMN_RS04070	NWMN_0720	competence protein ComF	2.65	1.24E-27
NWMN_RS06540	NWMN_1160	DNA topoisomerase 1 / topA	2.63	2.88E-28

NWMN_RS08255	NWMN_1464	RNA polymerase sigma factor SigA	2.63	2.19E-34
NWMN_RS08835	NWMN_1575	gamma-aminobutyrate permease / lysP	2.63	2.92E-31
NWMN_RS06120	NWMN_1080	hypothetical protein	2.62	1.69E-21
NWMN_RS09825	NWMN_1744	membrane protein	2.61	3.97E-20
NWMN_RS01390	NWMN_0251	ABC transporter ATP-binding protein	2.58	2.64E-21
NWMN_RS14180	NWMN_2469	transglycosylase IsaA	2.56	1.08E-18
NWMN_RS02075	none	hypothetical protein	2.56	4.27E-16
NWMN_RS11805	NWMN_2044	hypothetical protein / thiol-disulphide oxidoreductase	2.56	7.04E-35
NWMN_RS04310	NWMN_0762	hypothetical protein	2.55	1.13E-18
NWMN_RS08575	NWMN_1527	CsbD family protein	2.54	9.59E-18
NWMN_RS10100	NWMN_1766	monofunctional glycosyltransferase	2.54	3.72E-35
NWMN_RS04315	NWMN_0763	hypothetical protein	2.53	3.13E-15
NWMN_RS04450	NWMN_0787	cysteine desulfurase / sufS	2.52	3.91E-30
NWMN_RS07485	NWMN_1329	phosphatidic acid phosphatase	2.52	6.31E-27
NWMN_RS13560	NWMN_2353	ABC transporter ATP-binding protein	2.51	3.13E-11
NWMN_RS07355	NWMN_1306	4-hydroxy-tetrahydrodipicolinate synthase / dapA	2.50	3.62E-16
NWMN_RS11405	NWMN_1972	anti-sigma B factor antagonist / rsvB	2.49	1.22E-14
NWMN_RS12045	NWMN_2079	alanine racemase	2.48	1.22E-16
NWMN_RS07350	NWMN_1305	aspartate-semialdehyde dehydrogenase / asD	2.48	1.18E-16
NWMN_RS03955	NWMN_0699	protein NrdI	2.48	7.45E-20
NWMN_RS14150	NWMN_2463	diaponeurosporenoate glycosyltransferase	2.47	3.04E-10
NWMN_RS11815	NWMN_2046	membrane protein	2.47	9.53E-09
NWMN_RS07360	NWMN_1307	4-hydroxy-tetrahydrodipicolinate reductase / dapB	2.47	1.04E-15
NWMN_RS14350	NWMN_2500	amino acid permease	2.47	2.70E-09
NWMN_RS05565	NWMN_0992	DNA invertase /int	2.46	3.59E-21
NWMN_RS04405	NWMN_0778	topiosmerase	2.43	4.32E-29
NWMN_RS12875	NWMN_2234	metallothiol transferase FosB	2.42	1.07E-08
NWMN_RS14745	none	hypothetical protein	2.42	1.58E-09
NWMN_RS09835	none	hypothetical protein	2.42	1.18E-13
NWMN_RS09235	NWMN_1645	hypothetical protein	2.41	4.68E-17

NWMN_RS03960	NWMN_0700	ribonucleotide-diphosphate reductase / nrdE	2.41	1.64E-27
NWMN_RS09375	NWMN_1670	membrane protein	2.40	9.98E-16
NWMN_RS11540	NWMN_1994	protein translocase component YidC / oxaA	2.38	4.69E-22
NWMN_RS12750	NWMN_2210	formate dehydrogenase subunit alpha / Fe-S containing enzyme	2.37	4.59E-23
NWMN_RS09560	NWMN_1701	serine protease SplF	2.35	9.27E-13
NWMN_RS13415	none	hypothetical protein	2.35	2.39E-07
NWMN_RS03185	NWMN_0556	hypothetical protein	2.34	3.26E-24
NWMN_RS03965	NWMN_0701	ribonucleotide-diphosphate reductase subunit beta / nrdF	2.34	1.17E-29
NWMN_RS00660	NWMN_0119	hypothetical protein	2.33	9.27E-19
NWMN_RS07365	NWMN_1308	2-2-2-2-5-tetrahydropyridine-2-2C6-dicarboxylate N-acetyltransferase / dapD	2.33	5.27E-16
NWMN_RS03140	NWMN_0547	amino acid permease	2.33	4.12E-15
NWMN_RS11590	NWMN_2004	UDP-N-acetylglucosamine 1-carboxyvinyltransferase / murA	2.33	3.45E-25
NWMN_RS07470	NWMN_1328	DNA-binding response regulator	2.33	2.30E-22
NWMN_RS04455	NWMN_0788	iron-sulfur cluster assembly scaffold protein NifU	2.32	8.93E-26
NWMN_RS11705	NWMN_2026	aldehyde dehydrogenase	2.32	1.42E-10
NWMN_RS07370	NWMN_1309	Hydrolase / hipO	2.30	3.34E-11
NWMN_RS02070	NWMN_0366	membrane protein	2.29	2.30E-14
NWMN_RS12090	NWMN_2088	hypothetical protein	2.29	4.83E-12
NWMN_RS14145	NWMN_2462	dehydrosqualene synthase / crtM	2.29	3.53E-09
NWMN_RS03385	NWMN_0593	cation:proton antiporter / mnhA	2.28	1.87E-15
NWMN_RS11570	NWMN_1999	transglycosylase SceD	2.28	5.80E-16
NWMN_RS14270	NWMN_2486	type VII secretion protein	2.27	1.62E-08
NWMN_RS00310	NWMN_0054	L-lactate permease	2.27	1.58E-09
NWMN_RS03760	NWMN_0664	multidrug efflux MFS transporter NorA	2.27	5.57E-26
NWMN_RS14240	NWMN_2480	hydrolase	2.26	3.91E-08
NWMN_RS03905	NWMN_0690	glycine/betaine ABC transporter ATP-binding protein	2.26	7.28E-27
NWMN_RS06545	none		2.25	4.69E-22
NWMN_RS14265	NWMN_2485	hypothetical protein	2.25	2.45E-12

NWMN_RS04440	NWMN_0785	ABC transporter ATP-binding protein / sufC	2.25	1.28E-24
NWMN_RS14750	NWMN_2570	bifunctional phosphoribosyl-AMP cyclohydrolase/phosphoribosyl-ATP pyrophosphatase / hislE	2.24	1.70E-08
NWMN_RS06115	NWMN_1079	carbamate kinase 1 / arcC	2.24	1.32E-15
NWMN_RS11615	NWMN_2008	ATP synthase subunit gamma / atpG	2.22	1.02E-28
NWMN_RS10655	NWMN_1854	sodium-dependent dicarboxylate transporter SdcS	2.22	4.36E-19
NWMN_RS13065	NWMN_2270	hypothetical protein	2.22	8.19E-17
NWMN_RS02440	NWMN_0432	GNAT family acetyltransferase	2.22	8.71E-28
NWMN_RS07115	NWMN_1261	choline transporter	2.21	5.64E-19
NWMN_RS14630	NWMN_2547	accessory Sec system glycosyltransferase GtfA	2.21	1.40E-19
NWMN_RS03700	NWMN_0652	undecaprenyl-diphosphatase / bacA	2.20	3.45E-25
NWMN_RS12845	NWMN_2228	membrane protein	2.20	1.13E-21
NWMN_RS08250	NWMN_1463	tRNA methyltransferase	2.19	3.51E-19
NWMN_RS11310	NWMN_1960	dihydroxy-acid dehydratase / ilvD	2.17	3.49E-12
NWMN_RS05305	NWMN_0946	hypothetical protein	2.16	1.57E-22
NWMN_RS07250	NWMN_1287	aminoacyltransferase FemB	2.15	3.09E-22
NWMN_RS14100	NWMN_2453	hypothetical protein	2.15	7.85221E-06
NWMN_RS05060	NWMN_0903	ABC transporter ATP-binding protein	2.14	3.88E-09
NWMN_RS11130	NWMN_1929	succinyl-diaminopimelate desuccinylase	2.13	3.70E-09
NWMN_RS03680	NWMN_0648	acetyltransferase	2.13	7.26E-17
NWMN_RS03090	NWMN_0536	proline/betaine transporter	2.13	7.91E-16
NWMN_RS07535	NWMN_1337	dihydrofolate reductase / drfA	2.12	4.47E-25
NWMN_RS03745	NWMN_0661	membrane protein	2.12	4.86E-12
NWMN_RS04270	NWMN_0754	membrane protein	2.12	2.97E-23
NWMN_RS00395	NWMN_0070	membrane protein	2.11	1.32E-13
NWMN_RS03915	NWMN_0692	histidinol-phosphate aminotransferase / hisC	2.11	2.67E-15
NWMN_RS14625	NWMN_2546	accessory Sec system glycosylation chaperone GtfB	2.11	1.81E-14
NWMN_RS04160	NWMN_0734	hypothetical protein	2.10	1.72E-23

NWMN_RS00280	NWMN_0048	quinolone resistance protein NorB	2.10	6.06688E-06
NWMN_RS08190	none	hypothetical protein	2.10	4.50E-08
NWMN_RS14675	NWMN_2556	hypothetical protein	2.09	2.95E-14
NWMN_RS05295	none	hypothetical protein	2.09	2.84E-12
NWMN_RS09180	NWMN_1634	cell division protein FtsK	2.09	2.18E-25
NWMN_RS09755	NWMN_1730	hypothetical protein	2.08	5.23E-16
NWMN_RS14875	NWMN_2595	nickel transporter NixA	2.08	1.07E-16
NWMN_RS03380	NWMN_0592	recombinase	2.07	1.02E-09
NWMN_RS14635	NWMN_2548	accessory Sec system translocase SecA2	2.06	8.32E-18
NWMN_RS12715	NWMN_2203	CHAP domain-containing protein	2.06	4.75E-17
NWMN_RS00735	NWMN_0133	PTS glucose EIICBA component	2.05	8.79E-09
NWMN_RS11730	NWMN_2031	CTP synthetase / pyrG	2.05	1.61E-23
NWMN_RS12745	NWMN_2209	hypothetical protein	2.05	6.32E-17
NWMN_RS04410	NWMN_0779	thiol reductase thioredoxin	2.05	2.73E-20
NWMN_RS04360	NWMN_0771	organic hydroperoxide resistance protein-like	2.05	5.98E-11
NWMN_RS06195	none		2.04	1.94E-29
NWMN_RS11330	NWMN_1963	2-isopropylmalate synthase / leuA	2.04	2.70E-07
NWMN_RS04715	NWMN_0836	signal peptidase IB / spsB	2.04	1.42E-20
NWMN_RS09195	NWMN_1637	thiol reductase thioredoxin	2.03	9.25E-21
NWMN_RS04430	NWMN_0783	CsbD family protein	2.01	2.52E-08
NWMN_RS02490	none	hypothetical protein	2.01	5.43E-16
NWMN_RS09655	NWMN_1720	hypothetical protein	2.00	8.15E-15

Down-regulated				
NWMN_RS14580	NWMN_2537	hypothetical protein / isaB	-4.93	1.19E-42
NWMN_RS13980	NWMN_2432	membrane protein / copper transport	-4.86	7.56E-38
NWMN_RS13905	NWMN_2418	MarR family transcriptional regulator	-4.45	6.85E-77
NWMN_RS13020	NWMN_2261	hemin ABC transporter ATP-binding protein / HrtA	-4.25	4.89E-54
NWMN_RS06105	NWMN_1077	hypothetical protein / superantigen like protein	-3.84	4.49E-31
NWMN_RS04105	NWMN_0725	hydrolase	-3.82	2.07E-53
NWMN_RS07320	NWMN_1300	phosphate-binding protein	-3.67	6.68E-26
NWMN_RS14850	NWMN_2590	PadR family transcriptional regulator	-3.65	2.95E-43

NWMN_RS13025	NWMN_2262	hemin ABC transporter permease / hrtB	-3.63	6.29E-26
NWMN_RS02200	NWMN_0390	hypothetical protein / toxin	-3.54	1.51E-57
NWMN_RS02065	NWMN_0365	transcriptional regulator	-3.54	2.72E-28
NWMN_RS02210	NWMN_0391	hypothetical protein / superantigen like protein	-3.42	4.93E-46
NWMN_RS13755	NWMN_2389	hypothetical protein	-3.40	7.35E-27
NWMN_RS08705	NWMN_1552	DUF4930 domain-containing protein	-3.36	1.12E-34
NWMN_RS12675	NWMN_2196	hypothetical protein	-3.35	3.94E-49
NWMN_RS10410	NWMN_1812	DNA-binding protein / phage repressor	-3.21	1.32E-56
NWMN_RS00015	none	RNA-binding protein	-3.19	1.42E-55
NWMN_RS14000	NWMN_2436	acyl-CoA thioester hydrolase	-3.18	1.47E-31
NWMN_RS06145	NWMN_1084	hemolytic protein	-3.16	1.84E-33
NWMN_RS13260	NWMN_2307	addiction module antitoxin RelB	-3.15	1.68E-44
NWMN_RS06150	NWMN_2620	hemolytic protein	-3.12	2.05E-26
NWMN_RS13920	NWMN_2421	NAD(P)H-dependent oxidoreductase	-3.11	3.00E-28
NWMN_RS05020	NWMN_0896	hypothetical protein	-3.11	3.74E-18
NWMN_RS10775	NWMN_1873	hypothetical protein / truncated beta hemolysin	-3.10	1.04E-20
NWMN_RS04580	NWMN_0810	hypothetical protein	-3.09	5.73E-37
NWMN_RS07400	NWMN_1314	hypothetical protein	-3.09	2.98E-21
NWMN_RS13585	NWMN_2356	hypothetical protein	-3.06	2.04E-46
NWMN_RS11200	NWMN_1942	hydrolase in agr operon	-3.06	6.44E-49
NWMN_RS13995	NWMN_2435	thiol reductase thioredoxin	-3.05	6.75E-41
NWMN_RS00665	NWMN_0120	hypothetical protein	-3.02	4.13E-29
NWMN_RS13990	NWMN_2434	esterase	-2.99	1.36E-42
NWMN_RS08700	NWMN_RS08700	hypothetical protein	-2.97	1.09E-38
NWMN_RS11830	NWMN_2049	transcriptional regulator / Zn and Co transport repressor protein	-2.96	6.28E-28
NWMN_RS07180	NWMN_1273	peptide-methionine (S)-S-oxide reductase / msrA	-2.96	1.11E-26
NWMN_RS10720	none	thioredoxin	-2.93	3.15E-39
NWMN_RS13265	none	prevent-host-death protein	-2.93	2.18E-29
NWMN_RS06940	NWMN_1228	threonine aldolase	-2.92	1.72E-27
NWMN_RS00400	NWMN_0071	diacetyl reductase ((S)-acetoin forming)	-2.90	3.46E-17

NWMN_RS01855	NWMN_0326	multidrug efflux MATE transporter transcriptional repressor MepR / marR	-2.90	9.58E-30
NWMN_RS02835	NWMN_0485	excinuclease ABC subunit B / uvrB/C	-2.89	1.61E-34
NWMN_RS08360	NWMN_1485	HrcA family transcriptional regulator / heat-shock protein	-2.83	8.94E-34
NWMN_RS05450	NWMN_0973	inositol monophosphatase	-2.83	1.40E-37
NWMN_RS01445	none	hypothetical protein	-2.77	7.93E-07
NWMN_RS06910	NWMN_0262	Lipase / geh	-2.76	4.67E-31
NWMN_RS12640	NWMN_2190	urease subunit alpha / ureC	-2.76	8.87E-27
NWMN_RS01090	NWMN_0195	DNA-binding response regulator / lytR	-2.75	5.59E-16
NWMN_RS06080	NWMN_1073	alpha-hemolysin / hla	-2.74	2.69E-26
NWMN_RS08465	NWMN_1504	hypothetical protein	-2.74	9.66E-32
NWMN_RS09285	none	MarR family transcriptional regulator	-2.71	3.10E-26
NWMN_RS02235	NWMN_0395	hypothetical protein / set8nm	-2.71	2.34E-27
NWMN_RS02120	none	hypothetical protein	-2.71	8.87E-24
NWMN_RS12590	NWMN_2179	molybdate ABC transporter substrate-binding protein / modA	-2.69	1.84E-33
NWMN_RS04585	none	hypothetical protein	-2.68	1.34E-26
NWMN_RS14120	NWMN_2457	copper-exporting P-type ATPase A	-2.67	5.56E-28
NWMN_RS08355	NWMN_1484	nucleotide exchange factor GrpE / heat-shock protein	-2.65	4.21E-30
NWMN_RS11475	NWMN_1983	histidine kinase / kdpD, osmosensitive histidine kinase	-2.61	3.55E-30
NWMN_RS14845	NWMN_2589	hypothetical protein	-2.61	4.25E-34
NWMN_RS14200	NWMN_2472	hypothetical protein	-2.61	1.32E-32
NWMN_RS01085	NWMN_0194	sensor protein LytS	-2.61	2.31E-29
NWMN_RS03110	NWMN_0541	hypothetical protein	-2.60	8.96E-33
NWMN_RS14530	NWMN_2528	tributyrin esterase / estA	-2.60	3.99E-28
NWMN_RS05955	NWMN_1054	colicin V production protein CvpA	-2.60	2.16E-32
NWMN_RS12245	NWMN_2117	helicase	-2.59	1.57E-20
NWMN_RS12240	NWMN_2116	hypothetical protein	-2.59	6.55E-37
NWMN_RS02840	NWMN_0486	protein arginine kinase	-2.58	6.89E-33
NWMN_RS09470	none	calcium-binding protein	-2.57	3.92E-24
NWMN_RS00020	NWMN_0003	DNA recombination protein RecF	-2.56	9.57E-38
NWMN_RS13160	NWMN_2287	heat-shock protein Hsp20	-2.54	1.53E-23

NWMN_RS05015	NWMN_0895	competence protein ComK	-2.54	5.27E-16
NWMN_RS01110	NWMN_0199	hypothetical protein / PTS-related	-2.52	3.92E-24
NWMN_RS12435	NWMN_2154	membrane protein	-2.52	5.94E-34
NWMN_RS02185	NWMN_0387	NAD(P)-dependent oxidoreductase	-2.51	1.23E-24
NWMN_RS14205	NWMN_2473	hypothetical protein	-2.48	1.24E-32
NWMN_RS02830	NWMN_0484	transcriptional regulator CtsR	-2.46	1.46E-33
NWMN_RS02180	NWMN_0386	membrane protein	-2.46	6.79E-19
NWMN_RS11180	NWMN_1938	co-chaperone GroES	-2.45	2.11E-24
NWMN_RS14375	NWMN_2505	membrane protein	-2.42	1.51E-21
NWMN_RS13565	NWMN_2354	peptidase M28	-2.41	1.69E-24
NWMN_RS03815	NWMN_0674	two-component sensor histidine kinase / saeS	-2.38	3.84E-25
NWMN_RS06065	NWMN_1071	membrane protein	-2.38	6.40E-09
NWMN_RS11145	NWMN_1932	potassium transporter KtrB	-2.38	2.58E-24
NWMN_RS12595	NWMN_2180	formate dehydrogenase accessory protein FdhD	-2.37	5.12E-33
NWMN_RS12665	NWMN_2195	transcriptional regulator / sarR	-2.37	3.84E-27
NWMN_RS07445	NWMN_1323	hypothetical protein	-2.37	1.35E-26
NWMN_RS12155	NWMN_2101	NAD-dependent protein deacetylase	-2.37	1.00E-21
NWMN_RS02195	NWMN_0389	hypothetical protein / set2nm	-2.35	4.53E-19
NWMN_RS02240	NWMN_0396	hypothetical protein / set9nm	-2.35	1.21E-24
NWMN_RS02245	NWMN_0397	hypothetical protein / set10nm	-2.35	1.03E-20
NWMN_RS05070	NWMN_0905	hypothetical protein	-2.35	7.95E-13
NWMN_RS14880	NWMN_2596	arylamine N-acetyltransferase	-2.34	8.24E-23
NWMN_RS06100	NWMN_1076	hypothetical protein / superantigen like protein	-2.34	8.23E-22
NWMN_RS07805	none	hypothetical protein	-2.33	9.88E-11
NWMN_RS08395	NWMN_1491	ComE operon protein 2	-2.32	1.84E-33
NWMN_RS00215	NWMN_0035	LysR family transcriptional regulator	-2.31	5.18E-25
NWMN_RS07160	NWMN_1270	protein GlcT	-2.30	1.11E-26
NWMN_RS08535	NWMN_1518	hypothetical protein	-2.29	2.20E-35
NWMN_RS08530	NWMN_1517	crossover junction endodeoxyribonuclease RuvA	-2.29	7.76E-32
NWMN_RS10070	NWMN_1761	metal-dependent hydrolase	-2.29	7.80E-27
NWMN_RS06070	none	membrane protein	-2.28	1.61E-12
NWMN_RS09230	NWMN_1644	dipeptidase PepV	-2.27	3.10E-26
NWMN_RS03485	NWMN_0613	antibiotic ABC transporter ATP-binding protein	-2.26	4.55E-26

NWMN_RS10025	NWMN_1753	transcriptional repressor / perR	-2.26	5.54E-22
NWMN_RS08005	NWMN_1418	hypothetical protein	-2.26	7.04E-23
NWMN_RS07685	NWMN_1364	chromosome replication protein DnaD	-2.25	2.02E-24
NWMN_RS06945	none	hypothetical protein	-2.24	6.57E-14
NWMN_RS06985	NWMN_1237	hypothetical protein	-2.24	1.51E-25
NWMN_RS03195	NWMN_0558	transcriptional regulator	-2.23	1.41E-10
NWMN_RS02575	none	hypothetical protein	-2.22	1.29E-19
NWMN_RS00125	NWMN_0022	multifunctional 2'%2C3'-cyclic-nucleotide 2'-phosphodiesterase/5'-nucleotidase/3'-nucleotidase	-2.22	3.96E-12
NWMN_RS13535	NWMN_2348	hypothetical protein	-2.22	7.78E-31
NWMN_RS11195	NWMN_1941	nitroreductase	-2.21	8.86E-29
NWMN_RS04720	NWMN_0837	ATP-dependent helicase/deoxyribonuclease subunit B / rexB	-2.21	1.04E-24
NWMN_RS13685	NWMN_2375	oxidoreductase	-2.20	4.58E-16
NWMN_RS09650	NWMN_1719	gamma-hemolysin subunit A / lukE	-2.20	8.04E-09
NWMN_RS08390	NWMN_1490	DNA internalization-related competence protein ComEC/Rec2	-2.19	5.69E-21
NWMN_RS09660	NWMN_1721	hypothetical protein	-2.19	1.58E-25
NWMN_RS14575	NWMN_2536	aureolysin	-2.18	9.95E-17
NWMN_RS05100	NWMN_0910	acetyltransferase	-2.16	1.96E-16
NWMN_RS06305	NWMN_1116	orotate phosphoribosyltransferase / pyrE	-2.16	1.21E-15
NWMN_RS12835	NWMN_2226	hypothetical protein	-2.16	7.69E-25
NWMN_RS06075	NWMN_1072	hypothetical protein	-2.16	8.56E-18
NWMN_RS05095	none	hypothetical protein	-2.15	1.57E-21
NWMN_RS07385	NWMN_1312	protein msa	-2.15	2.32E-07
NWMN_RS06160	NWMN_1086	hypothetical protein	-2.14	2.96E-21
NWMN_RS01470	none	transcriptional regulator	-2.13	1.85E-15
NWMN_RS00440	NWMN_0078	hypothetical protein	-2.12	4.11E-15
NWMN_RS09060	NWMN_1615	peroxiredoxin	-2.11	7.41E-20
NWMN_RS09585	NWMN_1706	serine protease SplA	-2.11	6.36E-08
NWMN_RS04110	none	hypothetical protein	-2.11	9.04E-12
NWMN_RS12145	NWMN_2099	galactose-6-phosphate isomerase subunit LacA	-2.11	6.40E-13
NWMN_RS03820	NWMN_0675	DNA-binding response regulator / saeR	-2.08	1.38E-22

NWMN_RS07450	NWMN_1324	hypothetical protein	-2.08	1.48E-24
NWMN_RS05140	NWMN_0918	serine protease / sspA	-2.08	6.58E-13
NWMN_RS09210	NWMN_1640	hypothetical protein	-2.08	8.68E-22
NWMN_RS13445	NWMN_2335	hypothetical protein	-2.08	6.16E-21
NWMN_RS00770	NWMN_0140	hypothetical protein	-2.07	1.82E-26
NWMN_RS09475	NWMN_1689	hypothetical protein	-2.07	6.07E-17
NWMN_RS11565	none	hypothetical protein	-2.06	6.56E-11
NWMN_RS07655	NWMN_2233	hypothetical protein	-2.05	9.94E-27
NWMN_RS14570	NWMN_2535	ArgR family transcriptional regulator	-2.05	3.35E-13
NWMN_RS07405	NWMN_1315	acylphosphatase	-2.05	2.42E-24
NWMN_RS08110	NWMN_1437	octanoyltransferase LipM	-2.04	1.13E-21
NWMN_RS02215	NWMN_0392	hypothetical protein / set5nm	-2.04	9.98E-18
NWMN_RS12785	NWMN_2217	RpiR family transcriptional regulator	-2.02	4.86E-19
NWMN_RS05110	NWMN_0912	isochorismate synthase	-2.02	3.90E-21
NWMN_RS02580	NWMN_0452	rRNA (cytidine-2'-O-)-methyltransferase	-2.01	2.30E-15
NWMN_RS04520	NWMN_0799	hypothetical protein	-2.01	4.37E-15

*Significance was defined as FDR <0.001
#Defined as >2 $\log_2$ fold change